

NASA CONTRACTOR REPORT

NASA CR-503



NASA CR

0099499



LOAN COPY: RETURN TO
AFWL (WLIL-2)
KIRTLAND AFB, N MEX

DESIGN STUDIES OF ADVANCED LENTICULAR PASSIVE COMMUNICATION SATELLITES FROM LOW TO SYNCHRONOUS ORBIT

Prepared by
GOODYEAR AEROSPACE CORPORATION
Akron, Ohio
for Langley Research Center



Page 37: In the second row of the first column in this table, the angle θ should be 2θ .

Page 51: In figure 4, the label θ in the ordinate scale and on the lower curve should be 2θ , and the angle $\theta/2$ in the sketch at the top right should be θ .

Page 52: The equation for the diameter D below the large sketch should be corrected to read: $D = 2\rho \sin \theta$, satellite diameter.

Page 128: In the first line, table 1 should be table A4.

Issued July 1966



DESIGN STUDIES OF ADVANCED LENTICULAR
PASSIVE COMMUNICATION SATELLITES
FROM LOW TO SYNCHRONOUS ORBIT

Distribution of this report is provided in the interest of information exchange. Responsibility for the contents resides in the author or organization that prepared it.

Prepared under Contract No. NAS 1-3114 by
Goodyear Aerospace Corporation
Akron, Ohio

for Langley Research Center

NATIONAL AERONAUTICS AND SPACE ADMINISTRATION

For sale by the Clearinghouse for Federal Scientific and Technical Information
Springfield, Virginia 22151 - Price \$6.00

FOREWORD

A parametric study was performed by Goodyear Aerospace Corporation (GAC) of Akron, Ohio to determine the effects of variations in orbital altitude, lens radius of curvature, and lens included angle on the physical characteristics and performance of advanced gravity-gradient stabilized lenticular satellite configurations. The study was accomplished in three parts: design and structural analysis, stabilization analysis, and initial capture analysis. This work was conducted as Amendment No. 8 of Contract NAS 1-3114 from May 15 through September 1965. The technical objective was to provide parametric design and performance information to help define the lenticular satellite system once a payload weight and orbital altitude are established.

The work was administered by the Applied Materials and Physics Division of Langley Research Center with Mr. D.C. Grana from the Spacecraft Applications Section acting as Project Engineer. F.J. Stimler of the Space Systems and Analytics Division was the GAC Project Engineer. The work was conducted as a cooperative effort by personnel from several divisions within GAC for the various specialties listed below:

Design	H.W. Barrett
Structural Analysis	E. Rottmayer and J.D. Marketos
Stabilization Analysis	A.C. Buxton, K. Losch, and J. Nedelk
Computer Program	D. Rohner
Capture Analysis	A.C. Buxton
Planning	H.T. Stewart
Contract Administration	A.F. Tinker

Monthly technical review meetings were held between cognizant LRC and GAC personnel to direct the parametric effort, resolve problem areas, and develop curves and data facilitating prediction of overall satellite design and performance characteristics compatible with future system studies.

SUMMARY

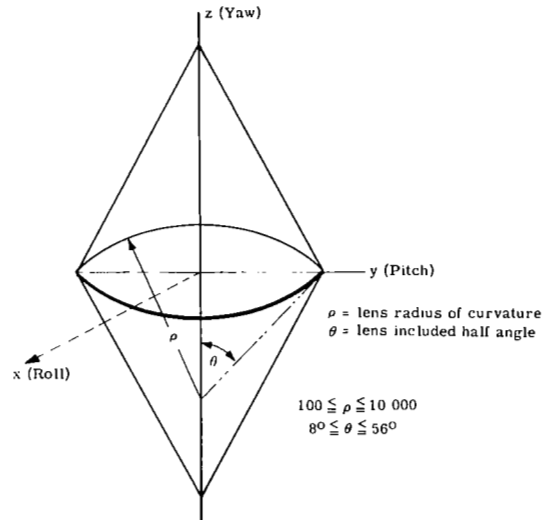
Parametric analyses were conducted on advanced gravity-gradient stabilized lenticular satellite configurations to determine the effects of variations in orbital altitude, radius of curvature of the rf reflecting lens, and lens included angle on satellite physical characteristics and performance. Detailed information is presented on equation development, assumptions, mode, and choice of constants or design factors utilized in the study either in the body of the report or in the appendixes. Summary charts and curves are presented in a form suitable for lenticular satellite system studies.

The program studies were accomplished in three parts: (1) design and structural analysis, (2) stabilization analysis, and (3) initial capture analysis. Physical characteristics of the lenticular lens were determined for four materials considered representative of the various types of lens structural materials. Type I is an aluminum-Mylar sandwich material. Type II is a woven-wire/cast photolyzable film using copper wire. Types III and IV are filament-wound wire/photolyzable film materials using aluminum wire, 96% reflective at 8000 and 800 Mc respectively.

Detailed structural and physical properties determined for these four materials included material definition, minimum gages anticipated, buckling characteristics, material unit weight, rigidization pressure requirements, and microwave frequency requirements of wire spacing, where applicable. For all four materials, summary curves of lens unit weight and lens rigidization pressure are presented as a function of lens radius of curvature, with the effects of minimum gages incorporated. The lens radius of curvature was investigated for a range of 100 to 10 000 feet. The lens included half-angle (see sketch) was investigated for a range of 8° to 56° to simulate complete earth rf coverage from 1000 to 19 300 n.mi. (synchronous) altitudes.

The weights and moments of inertia data of the lens, torus, inflation system, and canister were utilized to predict the total satellite physical characteristics for a constant value of the ratio of roll to yaw moment of inertia ($I_x - x/I_z - z = 5.75$). Five typical configurations were analyzed in detail to illustrate the design procedure, and to verify the scaling parameters. The five configurations analyzed are as follows:

- (1) Configuration A - Orbit altitude, 19 300 n.mi. (synchronous). Lens included angle, $21^\circ 18'$. Lens radius of curvature, 1280 ft.
- (2) Configuration B - Orbit altitude, 19 300 n.mi. (synchronous). Lens included angle, $21^\circ 18'$. Lens radius of curvature, 438 ft.
- (3) Configuration C - Orbit altitude, 2000 n.mi. Lens included angle, 84° . Lens radius of curvature, 438 ft.



- (4) Configuration D - Orbit altitude, 2000 n.mi. Lens included angle, 84° . Lens radius of curvature, 747 ft.
- (5) Configuration E - Orbit altitude, 6000 n.mi. Lens included angle, $47^{\circ} 12'$. Lens radius of curvature, 600 ft.

These configurations represent the lightest and heaviest satellite configurations obtained for the synchronous and 2000 n.mi. orbit altitude conditions. The 6000 n.mi. satellite configuration represents a median point for additional considerations. The satellite total weights are presented in terms of lens radius of curvature and lens included half-angle.

The transient and steady-state performance of the satellite stabilization system was analyzed. An Ames X system, consisting of a damper boom and a fixed boom for effecting satellite yaw position control, was attached to the space-side apex point of the tetrapod boom system. The opposite apex point contained inflation system and miscellaneous control equipment. The equation of motion of the stabilization system was derived and then solved both by analog and digital computer simulation. Parametric studies of the damper system were conducted to effectively establish the fixed boom characteristics and the included angle between these booms for optimum performance. Steady-state performance resulting from the effects of solar pressure and orbital eccentricity derived torques were determined for the five configurations defined earlier.

Program results indicate that the stabilization system provides generally the necessary transient damping capability and steady-state accuracy for a weight allowance of approximately 10 percent of the total satellite weight for the altitudes under consideration in this study.

Several subsystems for ensuring upright capture of the lenticular satellite in the gravity-gradient centrifugal force field were evaluated. It is necessary that the satellite and its stabilization system have sufficient structural integrity to endure the stresses caused by initial tumbling rates which have been estimated to be as high as five times orbital rate. Although no simple passive means are available to counteract the tumbling problem, a "repeated flip system" is recommended as a solution to the initial capture problem. A pair of beacons and a pair of attitude tumbling jets located at the canister positions are utilized to invert the satellite through ground control as the need arises. Continued flip operations are applied until the satellite is right side up. The other systems under consideration were considered too heavy or complex for the passive satellite under study here.

CONTENTS

	Page
FOREWORD	iii
SUMMARY	v
INTRODUCTION	1
SYMBOLS	2
DESIGN AND STRUCTURAL ANALYSIS	4
General	4
Lens Material Considerations	4
Weights and Moments of Inertia	5
Configuration Analysis	10
Summary	16
STABILIZATION ANALYSIS	17
Introduction	17
Transient Response	20
Steady-State Response	26
Summary and Conclusions	30
INITIAL CAPTURE ANALYSIS	32
Introduction	32
Recommended Capture System	32
Alternate Solutions	33
CONCLUSIONS AND RECOMMENDATIONS	34
TABLES	35
ILLUSTRATIONS	49
Appendix A - Materials Definitions	123
Appendix B - Surface Area, Volume, and Mass Moments of Inertia of Lens, Torus, and Rim, and Section Properties of Rim	133
Appendix C - Unit Weights of Lens and Torus Material, Material Volume per Square Inch of Lens Material, and Rigidization Pressures for Four Types of Lens Material	135
Appendix D - Weight and Mass Moments of Inertia of Lens, Torus, Inflation System, and Canister versus Lens Radius of Curvature and Central Half Angle for Various Lens Materials	139
Appendix E - Criteria for the Determination of the Size of Rim and Tetrapod Booms	165
Appendix F - Lenticular Lens Surface Area and Enclosed Volume	169
Appendix G - Derivation of Gravity-Gradient Stabilized Lenticular Satellite Equations of Motion, Orbital Eccentricity Forcing Functions, and Solar Torque Forcing Functions	171
Appendix H - Derivation of Realizable Damper Boom Mass Moment of Inertia	193
<i>References</i>	207

TABLES

Table		Page
1	Lenticular Lens Included Angle for Horizon-to-Horizon Coverage	35
2	Weights and Mass Moments of Inertia of Various Lenticular Satellite Components for Four Types of Lens Material	36
3	Lenticular Satellite Configurations Using Lens Material III	37
4	Results of Damping System Optimization Study	38
5	Opaqueness versus Radius of Curvature for Various Lens Materials	39
6	Worksheet for Configuration A, 0° to Sun Line	40
7	Worksheet for Configuration A, 45° to Sun Line	41
8	Worksheet for Configuration B, 0° to Sun Line	42
9	Worksheet for Configuration B, 45° to Sun Line	43
10	Worksheet for Configuration C, 0° to Sun Line	44
11	Worksheet for Configuration C, 45° to Sun Line	45
12	Worksheet for Configuration E, 0° to Sun Line	46
13	Worksheet for Configuration E, 45° to Sun Line	47
14	Summary of Stabilization Error Analysis and Transient Damping Capability	48

ILLUSTRATIONS

Figure		Page
1	Schematic of lenticular satellite with gravity-gradient stabilization	49
2	Definitions of terms and symbols for the satellite system	50
3	Satellite orbital frequency as a function of orbital altitude	51
4	Lens lenticular angle for horizon-to-horizon coverage and stabilization system error as a function of orbital altitude	51

ILLUSTRATIONS (Continued)

Figure		Page
5	Effect of lens radius of curvature and lenticular angle on satellite size . .	52
6	Lens central half angle versus radius of curvature for various satellite weights - lens material I	53
7	Lens central half angle versus radius of curvature for various satellite weights - lens material III	53
8	Lens central half angle versus radius of curvature for various satellite weights - lens material IV	54
9	Definition of lens half angle and radius of curvature for representative satellite configurations based on material III characteristics and contemplated launch boosters	54
10	Gravity-gradient stabilization system with solar sails and yaw controller	55
11	Weight penalty of oversize lens angle to offset stabilization error	56
12	Stabilization system axes and coordinate system definitions	57
13	Optimum transient response as a function of boom inertias	58
14	Damper system parameters associated with $F = 0.01$	59
15	Damper system parameters associated with $F = 0.02$	59
16	Damper system parameters associated with $F = 0.04$	60
17	Damper system parameters associated with $F = 0.08$	60
18	Damper system parameters associated with $F = 0.12$	61
19	Damper system parameters associated with $F = 0.16$	61
20	Damper system angular parameters and constraints versus optimum configuration values	62
21	Transient response when optimum boom inertias are $F = 0.16$ and $D = 0.143$	63
22	Transient response when optimum boom inertias are $F = 0.12$ and $D = 0.129$	67
23	Transient response when optimum boom inertias are $F = 0.08$ and $D = 0.114$	71
24	Transient response when optimum boom inertias are $F = 0.04$ and $D = 0.10$	75

ILLUSTRATIONS (Continued)

Figure		Page
25	Transient response when optimum boom inertias are $F = 0.04$ and $D = 0.03$	79
26	Transient response when optimum boom inertias are $F = 0.02$ and $D = 0.095$	83
27	Transient response when optimum boom inertias are $F = 0.02$ and $D = 0.0175$	87
28	Transient response when optimum boom inertias are $F = 0.01$ and $D = 0.00875$	91
29	Transient response for configuration A at synchronous orbit	95
30	Transient response for configuration B at synchronous orbit	99
31	Transient response for configuration C at 2000 n.mi. altitude with booms designed for non-tumbling orbital conditions	103
32	Transient response for configuration E at 6000 n.mi. altitude	107
33	Maximum moment of inertia of damper boom about its mid-point for case 1	111
34	Maximum moment of inertia of damper boom about its mid-point for case 2	112
35	Damper boom weight versus boom half-length for maximum mid-point mass moment of inertia for case 1	113
36	Damper boom weight versus boom half-length for maximum mid-point mass moment of inertia for case 2	114
37	Pitch error for one percent eccentricity	115
38	Roll and yaw error for one percent eccentricity	115
39	Frequency response for pitch axis torque corresponding to 0.01 eccentricity - pitch error	116
40	Frequency response for pitch axis torque corresponding to 0.01 eccentricity - roll and yaw error	116
41	Frequency response for pitch axis torque corresponding to 0.01 eccentricity - boom error	117
42	Pitch error for disturbance torque T_y'' about the pitch axis	117
43	Roll error for disturbance torque T_y'' about the pitch axis	118

ILLUSTRATIONS (Continued)

Figure		Page
44	Pitch error for disturbance torque T_x'' about the roll axis	118
45	Roll error for disturbance torque T_x'' about the roll axis	118
46	Yaw error for disturbance torque T_x'' about the roll axis	118
47	Magnitude of constant and sinusoidal forces due to booms	119
48	Pitch error for disturbance torque T_y'' about the pitch axis	119
49	Roll and yaw error for disturbance torque T_y'' about the pitch axis	120
50	Hang-off error for constant torques T_{yB}'' and T_{xB}'' about the pitch and roll axes	120
51	Transient damping capability of gravity-gradient stabilization system . . .	121

62-503

INTRODUCTION

The results of earlier feasibility and design effort on gravity-gradient stabilized lenticular satellites also conducted under Contract NAS 1-3114 were used as a basis and guide in the present parametric study (refs. 1 and 2). The primary components of this lenticular satellite system are shown schematically in figure 1. The expandable satellite is packaged in a canister during payload ascent and orbital placement. During satellite deployment and inflation the canister halves and attached hardware are extended by inflatable booms and serve as fixed weights for the gravity-gradient stabilization system. The torus serves as a deployment mechanism for the rim and lens caps, and also provides system stiffness while the lens caps become rigidized through controlled yielding of the photolyzable film/wire grid surfaces. The rim serves as the attachment point for the two lens caps and booms. The damping system is attached to the space-side canister half. The earth-side canister half provides the mounting interface of the inflation system and miscellaneous controls. Once operational, the torus (shown dotted in fig. 1) and lens film surfaces disappear through photolysis action.

An Ames X-type damper system provides both damping of satellite librations and yaw control for solar sailing. The weights at the apex of the tetrapod booms are positioned to control the satellite pitch and roll moments of inertia, while the yaw moment of inertia is primarily dependent on the lens, rim, and torus components of the satellite.

The lenticular-shaped structure by itself possesses an inappropriate mass distribution in the gravity-gradient field. The mass distribution of the lenticular structure must be augmented so that the resultant mass distribution approaches that of a dumbbell with the optical axis of the lenticule coincident with the principal axis of the dumbbell having the minimum moment of inertia. The dumbbell mass distribution is achieved efficiently by the attachment of the tetrapod booms and canister. An optimum mass distribution provides gravity-gradient restoring torques and moments of inertia axes such that the resultant torque-to-inertia ratios correspond to desirable natural frequencies of all modes of satellite libration. These natural frequencies should preferably be remote from the frequencies associated with the attitude disturbances due to solar pressure and orbital eccentricity. Solar pressure torques have fixed steady components as well as sinusoidally varying components at frequencies of one and two times orbital frequency. Orbital eccentricity effectively produces a perturbing torque which is periodic - once per orbit. The mass distribution must therefore provide sufficient gravity-gradient stiffness to offset steady bias torques with acceptably low resultant hang-off error, as well as a set of natural libration frequencies that are remote from one and two times orbital frequency.

Figure 2 generally defines the key terms and symbols of a typical lenticular satellite system as used in the design and structural analysis effort. Figure 3 is a plot of satellite orbital frequency as a function of orbital altitude above the earth. The synchronous altitude characteristics of 19 300 n.mi. altitude and 7.272×10^{-5} radians/sec orbital frequency are pinpointed.

Table 1 shows the lenticular lens included angle necessary for horizon-to-horizon coverage for altitudes from 1000 n.mi. to synchronous orbit altitude for ground antenna elevation angles of zero and five degrees. All the parametric data of this report consider horizon-to-horizon coverage to mean using five degrees as the minimum ground antenna elevation angle for definition of lens lenticular angle, θ (fig. 4). To ensure complete horizon-to-horizon coverage it becomes necessary to make the lenticular angle larger to account for the stabilization system error. A design objective of stabilization system error as a function of altitude is shown in figure 4. Therefore, to determine the desired lenticular lens angle, all conditions

of coverage and stabilization error must be included. For example, the lenticular angle of the lens must be approximately 84 degrees for a satellite to give full earth coverage at 2000 n.mi. orbit under the conditions just established, while a satellite at synchronous orbit should have a lenticular angle of 19.5 degrees.

For complete communications coverage, the satellite size increases markedly for a given rf capability (function of ρ) at the lower altitudes (see fig. 5). For this reason higher orbit altitudes are recommended as feasible for complete coverage by fewer satellites. At lower altitudes it is quite likely that multiple satellite systems would be required.

The range of radius of curvature (ρ) and lens included angle (θ) chosen for the parametric study are representative. The report is meant to provide basic information for the overall satellite unit, and in no way predicts optimum satellite usage for a communication system.

SYMBOLS

a	with subscripts from 1 to 6 represents various constant coefficients defined in the text	I_{Z-Z}	satellite moment of inertia about yaw axis
B	viscous damper coefficient, lb-sec/rad	I_D	damper boom
B"	normalized viscous damper coefficient, $B/I_D\omega_0^2$	I_F	fixed boom
d	wire diameter	I_{max}	maximum moment of inertia of a damping boom
D	flexural stiffness, $EI/(1 - \mu^2)$; also, in stabilization analysis, I_D/I_{X-X}	I'_Z	combined mass moment of in- ertia of lens and rim about z- axis of satellite
E	modulus of elasticity	k	with a subscript, strength-to- weight ratio; without subscript, a constant
F	I_F/I_{X-X}	K	extensional stiffness, EA; also spring deflection coefficient, lb/rad
h	without subscript, the tetrapod height; with subscript, height in general	K"	normalized spring deflection co- efficient, $K/I_D\omega_0^2$
I	mass moment of inertia, or moment of inertia of a cross section about centroidal axis	ℓ	length
I_{X-X}	satellite moment of inertia about roll axis (including damper boom weights)	L	length of boom measured from tip to tetrapod apex, ft
I_{Y-Y}	satellite moment of inertia about pitch axis (including damper boom weights)	m	gas atomic weight; mass per unit area
-			

p	inflation pressure	θ_D	angular degree of freedom of damping boom
p _{cr}	buckling pressure		
r	without subscript, the radius of the torus meridional section; with subscript, radius in general	θ, ϕ, ψ	Euler angle sequence about pitch (y), roll (x), and yaw (z) axes
r _p	reflective efficiency	μ	Poisson's ratio
R	rim radius	δ	angle locating damping boom with respect to complete damper; satellite principal roll axis
s	wire spacing		
t	thickness		
T	temperature Rankine	γ	angle locating fixed boom with respect to complete damper; satellite principal roll axis
T _x , T _y , T _z	torques acting about the generalized coordinates ϕ, θ, ψ respectively	ψ_D	angle between fixed and damping booms
T _x '', T _y '', T _z ''	normalized torques acting about the generalized coordinates ϕ, θ, ψ respectively	ψ_D, θ_D	Euler angle sequence locating damper system booms with respect to satellite axes
V	volume		
v	volume per unit area	ψ_{SS}	angle between satellite-damper system principal roll axis and orbital velocity vector ($\psi_{SS} = \gamma$)
w	weight per unit area	ω	angular velocity
W	weight in general; also complete weight of one boom, $2(W_t + W_r)$, lb	ω_0	orbital frequency, rad/sec
W _{D+F}	weight of damper system (both booms), lb	<u>Subscripts</u>	
W _r	weight of damper boom rod over length L, lb	B	bottle or tetrapod boom
W _S	weight of complete satellite damper system, lb	C	canister or core (referring to sandwich material)
W _t	weight of each tip mass located at each boom end, lb	F	face (referring to sandwich material)
x, y, z	coordinate axes in general, identified along the roll, pitch, and yaw axes respectively of the satellite	I	inflation system
ρ	lens radius of curvature	L	lens
ϵ	orbital eccentricity	R	rim
γ	density	T	torus
	$\frac{I_{y-y} - I_{x-x}}{I_{x-x}} = F$	TF	entire satellite
θ	lens central half angle	TP	combination of lens, torus, inflation system, and canister
		x, y, z	referring to roll, pitch, and yaw respectively

DESIGN AND STRUCTURAL ANALYSIS

General

The principal objective of this study was to establish the weights, moments of inertia, and major dimensions of the satellite in a manner suitable for use in a communications system study. The two important microwave parameters for a system study are the radius of curvature of the lens (ρ), and the included angle (θ). In view of this, the analysis was developed so that the weights, inertia, and major dimensions can be established once ρ and θ are specified.

The feasibility of accomplishing this was based upon previous lenticular satellite feasibility studies (refs. 1 and 2). It was found that for 2000 n. mi., the major portion of the weight (78.5 percent) consisted of the sum of the weights of the lens, torus, canister, and inflation system components, which can easily be determined once the materials of construction are selected. The remaining weight (21.5 percent) consists of booms, rim, and damping system which are not easily scaled in terms of ρ and θ . The approach selected was to determine the major weight and polar moment of inertia (lens, torus, canister, and inflation system) in a general form and then by specific, detailed designs establish a relationship between the total satellite weight and the major components listed above.

The equations were developed in a general form stating the assumptions used. These were then applied to several lens materials to determine the weights and polar moments of inertia of the pressure-dependent items (lens, torus, canister, and inflation system) which contribute to the major portion of the weight. Curves of weight and polar moment of inertia were plotted as functions of ρ and θ for the four lens materials selected.

Five specific designs were then developed using a filament-wound wire/photolyzable film lens material (material III). A wide range of lens radius of curvature and orbital altitude (or lens angle assuming full coverage) was used in order to determine the ratio of total weight to the pressure-dependent weight, within a more realistic range. This ratio was found to be a function of orbital altitude and satellite diameter that is usually small but increases rapidly for low altitude and large diameter. For lower altitudes, 6000 n. mi. and less, it is recommended that the equations developed herein, rather than the scaling ratio, be used to determine the weight of the rim, booms, and damping system.

Detail formula development, typical calculations, and working data are included in the appendixes so that other satellite materials can be compared with those selected for this study. Complete data is included to enable these comparisons to be made using the same assumptions, factors, and design philosophy as were used in this study. State-of-the-art fabrication techniques and previous test experience were most helpful in presenting a realistic design and structural approach during the study. No attempt was made to optimize the choice of materials for the satellite. However, the four lens materials chosen provide good basic design data and serve as a point of departure for later satellite analyses.

Lens Material Considerations

General. - Representative materials considered for the lens are (1) laminate and (2) wire grid materials. The objective of this design and structural analysis was to determine the unit weight of lens material and rigidization pressure as a function of radius of curvature for the four types of material under consideration, subject to the constraints of buckling pressure, microwave frequency, minimum gages, and material properties. The four types of

materials, which are described in detail in appendix A, are as follows:

Type	Description	Physical Data
I	Aluminum-Mylar sandwich	<p>— Alum. (t, thickness) ~ Mylar (2t, thickness) — Alum. (t, thickness)</p>
II	Woven wire/ cast photolyzable film	Copper wire, 21 x 21 mesh 1/2-mil photolyzable film
III	Filament-wound wire/photolyzable film	Al wire, square grid 96% reflective at 8000 Mc 1/2-mil photolyzable film
IV	Filament-wound wire/photolyzable film	Al wire, square grid 96% reflective at 800 Mc 1/2-mil photolyzable film

Buckling pressure. - For all materials it was assumed that the solar pressure is 1.3×10^{-9} psi and the buckling constant is 0.28 or 23.3 percent of 1.2, which is the classical buckling constant (ref. 3, page 517, eq. 11-31 for $\nu = 0.3$).

Microwave frequency. - The microwave frequency introduces a constraint on the wire spacing, s , and the wire diameter, d , for wire-grid lens materials. This problem was investigated in reference 4, and it was found that the minimum wire weight was obtained at a microwave reflective efficiency of about 96 percent. Therefore, for the present study an efficiency of 96 percent is used. Two microwave frequencies were selected, 800 and 8000 Mc; these are somewhat arbitrary, but do cover the range of microwave frequency of primary interest and demonstrate the effect of this parameter on the satellite weight.

Radius of curvature. - The radius of curvature range was from 100 ft to 10 000 ft.

Minimum gages and material properties. - The material properties and minimum gages for each material are tabulated in appendix A.

Weights and Moments of Inertia

General. - Surface areas, volumes, and moments of inertia of the lens and torus were used in deriving the equations of weights and moments of inertia. General expressions for these quantities are given in tabular form in appendix B. Other quantities employed in the derivation of equations are the unit weight of lens and torus material, rigidization pressure, and material volume of lens and torus. This data is tabulated in appendix C for all four lens materials. The minimum material gages (film and aluminum thickness and wire diameter) were used to establish the necessary modifications in the equations for unit lens weight, etc, as shown in the table in appendix C. However, in the computer program for the numerical calculation of weights and moments of inertia, presented in appendix D, minimum gages were disregarded.

Basic assumptions. - In deriving the weight and moment of inertia equations for the various components of the satellite the following assumptions were employed:

- (1) Factor of safety on torus pressure, $a_1 = 1.25$
- (2) Factor of safety on torus strength, $a_2 = 1.25$
- (3) Ratio of radius of torus cross section to the radius of rim, $r/R = 0.02927$ (the same as in the configuration described in ref. 1)
- (4) Factor applied to the combined gas and bottle weight to account for the total weight of the inflation system, $a_3 = 1.12$
- (5) Gas bottle safety factor, $a_4 = 2.0$
- (6) Gas leak and reserve factor, $a_5 = 2.5$
- (7) Packaging factor, $a_6 = 5.0$ (ratio of canister volume to the molten volume of lens and torus and the anticipated volumes of rim and tetrapod booms)
- (8) Factor applied on the idealized spherical canister weight to account for the actual canister (flanges, bolts, etc), based on Echo I, $a_7 = 2.5$
- (9) Density of canister material, $\gamma_C = 0.065 \text{ lb/in.}^3$ (magnesium)
- (10) Density of torus material, $\gamma_T = 0.038 \text{ lb/in.}^3$ (photolyzable film)
- (11) Strength-to-weight ratio of torus material, $k_T = \frac{F_T}{\gamma_T} = 0.26 \times 10^6 \text{ in.}$
- (12) Strength-to-weight ratio of gas bottle material, $k_B = 1.8 \times 10^6 \text{ in.}$
- (13) Modulus of elasticity of canister material, $E = 6.5 \times 10^6 \text{ psi}$
- (14) Inflation gas atomic weight, $m = 4$ (helium)
- (15) Gas temperature, $T = 530^\circ \text{ Rankine.}$

Lens. -

$$\text{Weight: } W_L = 4\pi\rho^2 (1 - \cos \theta) w_L \text{ lb} \quad (1)$$

Moment of inertia about the roll or pitch axis:

$$\begin{aligned} I_{L, (x \text{ or } y)} &= \frac{2}{3} \pi \rho^4 m_L (1 - \cos \theta)^2 (4 - \cos \theta) \\ &= 0.014544 \rho^4 w_L (1 - \cos \theta)^2 (4 - \cos \theta) \text{ lb-ft}^2 \end{aligned} \quad (2)$$

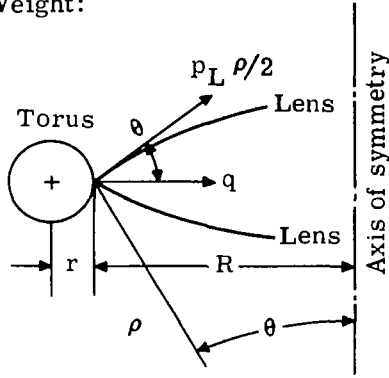
Moment of inertia about the yaw axis:

$$\begin{aligned} I_{L, z} &= \frac{4}{3} \pi \rho^4 m_L (1 - \cos \theta)^2 (2 + \cos \theta) \\ &= 0.029089 \rho^4 w_L (1 - \cos \theta)^2 (2 + \cos \theta) \text{ lb-ft}^2 \end{aligned} \quad (3)$$

In the above equations, ρ is measured in inches and w_L in lb/in².

Torus. -

Weight:



Basic equations:

$$q = 2 \left(\frac{p_L \rho}{2} \right) \cos \theta = p_L \rho \cos \theta \quad (4)$$

$$a_1 q R = p_T \pi r^2 \quad (5)$$

(wrinkling criterion)

$$\frac{p_T r}{2 t_T} \left(2 + \frac{r}{R} \right) = \frac{F_T}{a_2} \quad (6)$$

(strength criterion)

Assume that for all satellite configurations (regardless of absolute sizes of ρ and θ), the radii r and R are related by equation

$$r = 0.02927 R, \quad (7)$$

which corresponds to the 2000 n.mi. configuration described in reference 1. Solving equation (5) for p_T , noting that $R = \rho \sin \theta$, and taking equations (4) and (7) into account, results in

$$p_T = 371.5 a_1 p_L \cot \theta. \quad (8)$$

The torus thickness, t_T , from equation (6), is

$$t_T = 11.033 a_1 a_2 p_L \rho \cos \theta / F_T. \quad (9)$$

Then the weight of the torus is

$$\begin{aligned} W_T &= 2\pi r \cdot 2\pi (R + r) t_T \gamma_T \\ &= \frac{13.123}{k_T} a_1 a_2 p_L \rho^3 \sin^2 \theta \cos \theta \text{ lb.} \end{aligned} \quad (10)$$

It should be noted that the in-plane or out-of-plane buckling criteria for a torus (eq. 3, page 107, ref. 1) has not been considered here, because in all previous tests the torus has showed no signs of collapse, even at lens pressures almost twice that theoretically required to collapse the torus.

Moment of inertia about the roll or pitch axis:

$$\begin{aligned} I_{T, (x \text{ or } y)} &= 2\pi^2 r^3 (R + r) m_T \left[\left(\frac{R}{r} + 1 \right)^2 + \frac{5}{2} \right] \\ &= 0.004384 w_T \rho^4 \sin^4 \theta \text{ lb-ft}^2 \end{aligned} \quad (11)$$

Moment of inertia about the yaw axis:

$$\begin{aligned}
 I_{T,z} &= 4\pi^2 r^3 (R+r) m_T \left[\left(\frac{R}{r} + 1 \right)^2 + \frac{3}{2} \right] \\
 &= 0.008761 w_T \rho^4 \sin^4 \theta \quad \text{lb-ft}^2
 \end{aligned} \tag{12}$$

In equations (11) and (12) the quantities ρ and w_T are measured in inches and lb, in.² respectively. (For values of w_T see appendix C.)

Inflation system. - Deployment is effected by helium gas inflation with the torus and booms inflated first, and then the lens. The torus remains pressurized during lens inflation. The inflation system consists of the inflation gas required to inflate lens and torus, the bottle containing the gas, and some hardware (valves, batteries, and other electronic equipment). The weight of the inflation system can be written in the form

$$W_I = a_3 (W_G + W_B). \tag{13}$$

Noting that $W_G = \frac{mpV}{18540T}$ and $W_B = \frac{3}{2} pV \frac{a_4}{k_B}$,

equation (13) becomes

$$W_I = a_3 pV \left(\frac{m}{18540T} + \frac{3a_4}{2k_B} \right), \tag{14}$$

but

$$pV = a_5 (p_T V_T + p_L V_L),$$

$$V_L = \frac{2}{3} \pi \rho^3 (1 - \cos \theta)^2 (2 + \cos \theta)$$

$$V_T = \pi r^2 \cdot 2\pi (R+r) = 0.01741 \rho^3 \sin^3 \theta.$$

Substituting the last three equations and the numerical values $m = 4$ (for helium) and $T = 530^\circ$ Rankine in equation (14), and simplifying, results in

$$\begin{aligned}
 W_I &= a_3 a_5 (10^{-6}) \left(0.4071 + 1.5 \times 10^6 \frac{a_4}{k_B} \right) p_L \rho^3 \left[6.468 a_1 \cos \theta \sin^2 \theta + \right. \\
 &\quad \left. 2.0944 (1 - \cos \theta)^2 (2 + \cos \theta) \right].
 \end{aligned} \tag{15}$$

Because for the operational satellite the entire weight of the inflation system (minus a negligibly small part corresponding to the inflation gas) is located at the apex of the lower tetrapod, the roll and pitch moments of inertia can be readily determined as a point mass moment of inertia, and the yaw moment of inertia can be neglected.

Canister. -

Weight: The canister must be large enough to contain the lens, torus, rim, and tetrapod booms in the packaged condition. The stabilization system (De Havilland-type damper and fixed booms) and the inflation system are attached on the outside of the canister. The major items contained in the canister are the lens and the torus. Previous packaging experience with structures consisting of wire-film or plain film material shows that the volume of the container must be three to four times the molten volume of the packaged structure. However, in the present parametric analysis, only the lens and torus volumes of the packaged structure are known. The determination of rim and tetrapod boom sizes requires a detailed analysis, as discussed in a later section of this report. For the purpose of determining the volume of the canister in this parametric study, the rim and tetrapod booms have been taken into account by considering a factor $a_6 = 5$ applied to the molten volume of the lens and torus.

The shape of the canister was assumed to be spherical, and its wall thickness was taken to withstand a uniform pressure of five atmospheres, i.e., about 75 psi. With these assumptions the following equations can be written.

$$p_{cr} = 75 = 0.6E \left(\frac{t_C}{a} \right)^2 \quad (16)$$

The coefficient 0.6 in this equation, along with the five-atmospheric values for p_{cr} , is in line with the design of the Echo I canister.

Torus molten volume,

$$V_{m,T} = \frac{W_T}{\gamma_T} = \frac{13.123}{\gamma_T k_T} a_1 a_2 p_L \rho^3 \sin^2 \theta \cos \theta. \quad (17)$$

Lens molten volume,

$$V_{m,L} = 4\pi \rho^2 (1 - \cos \theta) v_L. \quad (18)$$

Combined molten volume of lens and torus material,

$$V_{m,L,T} = \frac{13.123}{\gamma_T k_T} a_1 a_2 p_L \rho^3 \sin^2 \theta \cos \theta + 4\pi \rho^2 (1 - \cos \theta) v_L. \quad (19)$$

Hence, the volume of the canister is $a_6 V_{m,L,T}$, and its radius, a , is given by equation

$$a = \left(\frac{3a_6 V_{m,L,T}}{4\pi} \right)^{1/3} \quad (20)$$

Solving equation (16) for t_C results in

$$t_C = a \sqrt{\frac{125}{E}}. \quad (21)$$

Then the weight of the canister is

$$W_C = 4\pi a^2 t_C \gamma_C a_7. \quad (22)$$

Substituting equations (19), (20), and (21) into equation (22) and simplifying yields

$$W_C = 3a_6 a_7 \gamma_C \sqrt{\frac{125}{E}} \left[\frac{13.123}{k_T \gamma_T} a_1 a_2 p_L \rho^3 \sin^2 \theta \cos \theta + 4\pi \rho^2 (1 - \cos \theta) v_L \right] \quad (23)$$

Volume: The canister volume, $V_C = a_6 V_{m, L, T}$, can be found from equations (19) and (23). Combining these equations results in

$$V_C = \frac{W_C}{3a_7 \gamma_C \sqrt{\frac{125}{E}}} \quad (24)$$

For $a_7 = 2.5$, $\gamma_C = 0.065 \text{ lb/in.}^3$ and $E = 6.5 \times 10^6$ (magnesium), equation (24) yields

$$V_C = 0.2707 W_C \text{ ft}^3 \quad (W_C \text{ in pounds}) \quad (25)$$

Summary. - The results of the preceding discussion have been applied to all four satellite types categorized by lens materials I through IV and summarized in Table 2. For each lens material the following ten quantities were calculated:

- (1) lens weight
- (2) torus weight
- (3) inflation system weight
- (4) canister weight
- (5) combined weight of the previous four components
- (6) canister volume
- (7) combined mass moment of inertia about the yaw axis of unphotolyzed lens and torus
- (8) combined mass moment of inertia about the pitch or roll axis of unphotolyzed lens and torus
- (9) yaw mass moment of inertia of photolyzed lens
- (10) pitch or roll mass moment of inertia of photolyzed lens

The two independent variables were the lens radius of curvature, ρ , and the lens central half-angle, θ . From considerations of altitude, coverage, and information capacity of the satellite, the range for the lens radius of curvature for this parametric study was taken between 100 ft and 10 000 ft, and the central half angle from 8 degrees to 56 degrees. The numerical results are given in tabular form and shown graphically in appendix D.

Configuration Analysis

General. - The combined weight W_{TP} of the lens, torus, inflation system, and canister is a large percent of the total weight, W_{TF} , of the satellite. Additional components are the tetrapod booms, the rim, and the stabilization system. Previous studies (refs.1 and 2) on specific configurations have shown that the weight of the first four components is more than 70 percent of the satellite total weight. Since the weights of these four components have been established parametrically in the previous discussion of weights and moments of inertia, it is

desirable to determine a constant or functional (function of ρ and θ) coefficient by means of which the total weight of the satellite can be found when the combined weight of the lens, torus, inflation system, and canister is known. Figures 6, 7, and 8 plot the weights, W_{TP} , for materials I, III, and IV respectively against the variables ρ and θ . These figures were cross-plotted from data in appendix D (figs. D5, D25, and D35). A cross-plot for material II (see fig. D15 in appendix D) has not been included because weight comparison of the four lens materials (table D1) shows that this material is considerably heavier than the other three materials.

In figure 6 the three lines $t_{Mylar} = 0.05$ mil, etc indicate the lens radii of curvature for which the indicated Mylar thickness would be adequate. These thicknesses are supposedly minimum gages. (However, present state of the art is $t_{Mylar} = 0.15$ mil). To the left of each of the three lines the weight curves should be modified because of the constant material gage up to the particular value of ρ corresponding to this gage. Similar lines are shown in figures 7 and 8, which indicate assumed minimum aluminum wire diameters.

Configuration determination. - Since material III is the lightest of all four lens materials considered in this report, figure 7 was chosen as a typical case to determine the functional coefficient for the ratio W_{TF}/W_{TP} within a practical range of θ and ρ values. To establish such a range, an upper and a lower limit were determined as follows. The payload capability of a typical booster at various altitudes for full coverage was plotted in figure 9 as curve No. 1. Assuming an average ratio of W_{TF}/W_{TP} equal to 1.35, curve No. 2 was plotted, representing the upper weight limit. As a lower limit a minimum wire gage of one mil was selected. The lens radius of curvature was determined from the equation

$$\rho = \left[6.884s/e^{0.22575/s} \right] \times 10^6 \text{ in.},$$

where s , wire spacing, and d , wire diameter, are related by equation

$$d = (s/\pi)/e^{0.1505/s}$$

for a microwave reflective efficiency of 96 percent at a frequency of 8000 Mc. This gives $\rho = 438$ ft, and determines line No. 3 in figure 9. Points A, B, C, and D were then determined from curves No. 1, 2, and 3. Two of these points are at synchronous orbit altitude and two at 2000 n.mi. A fifth point, E, was chosen arbitrarily at about the center of this area. The considered points are as follows:

Point A: $\rho = 1280$ ft, $\theta = 10^\circ 39'$ (19 300 n.mi. - synchronous)

Point B: $\rho = 438$ ft, $\theta = 10^\circ 39'$ (19 300 n.mi. - synchronous)

Point C: $\rho = 438$ ft, $\theta = 42^\circ$ (2000 n.mi.)

Point D: $\rho = 747$ ft, $\theta = 42^\circ$ (2000 n.mi.)

Point E: $\rho = 600$ ft, $\theta = 23^\circ 36'$ (6000 n.mi.)

As has been mentioned, the main satellite components that contribute significantly to the weight and have not yet been considered in this parametric analysis are the rim, the tetrapod booms, and the stabilization system. Because the structural integrity of these components cannot be checked without knowing the final satellite configuration in order to determine gravity gradient and other inertia loads, some criteria must be established in selecting these components. Available weight to be placed at the apices of the tetrapods comes from the canister and almost the entire inflation system (all except the negligibly small weight of the escaping gas). This weight is divided so that the entire inflation system and 55 percent of the

canister are placed at the apex of the lower tetrapod; the remaining 45 percent of the canister is located at the upper tetrapod apex, along with the stabilization system (Ames damper), which for equal tetrapod heights should be equal to the balance; i. e., equal to the inflation system weight plus 10 percent of the canister weight. If more weight is required for the stabilization system, an amount equal to the additional weight could be placed at the lower tetrapod apex as dummy weight, or the tetrapods could be made with unequal heights.

For the rim it was thought that a maximum out-of-plane deflection of 1 percent of the rim diameter would be an adequate design criterion. This, as shown in appendix E, leads to the following equations for the dimensions, weight, and mass moment of inertia of the rim (beryllium-copper with $t_R = 0.00025h_R$).

$$h_R = 0.1461 \sqrt[4]{\omega^2 h^2 R W} \text{ inch} \quad (26)$$

$$W_R = 13.16 R h_R t_R (0.297) = 3.9 R h_R t_R \text{ lb} \quad (27)$$

$$I_{x,R} = \frac{1}{2} I_{z,R} = 10.429 \omega R^3 h \sqrt{W R} \times 10^{-6} \text{ lb-in.}^2 \quad (28)$$

where W is the combined weight of canister, inflation system, and stabilization system (pounds).

Neglecting the mass moments of inertia of the tetrapod booms, and considering the stabilization system as a point mass concentrated at the apex of the upper tetrapod, the height, h , can be determined from the following equation:

$$I_{x-x}/I_{z-z} = \text{constant}$$

where I_x is the combined x-moment of inertia of photolyzed lens, rim (eq. 28), and all point masses at the tetrapod apices (inflation system, canister, and stabilization system); and I_z is the z-moment of inertia of photolyzed lens and rim. The constant on the right-hand side of the above equation is a number large enough to satisfy stabilization considerations. In this report the value 5.75 was used for all configurations.

The criterion for determination of the tetrapod boom size and weight is that the angle of twist should not exceed 5 degrees. The boom radius, r_B , can be determined from the equation

$$r_B = 3.946 \times 10^{-6} \left(\frac{s_B}{d_B} \right)^3 \sqrt[3]{\frac{\ell_B^2 I_z'}{h d_B}} \text{ (ref. appendix E),} \quad (29)$$

where s_B and d_B are respectively the axial wire spacing and wire diameter of the booms, ℓ_B the tetrapod boom length, and I_z' the combined yaw moment of inertia of lens and rim. The spacing of the hoop wires in the booms is $s_B/2$ for equal stress under rigidization pressure, and both sets of wires are sandwiched within two 0.25-mil layers of Mylar.

It should be noted that for a constant s_B/d_B ratio the wire diameter, d_B , can be optimized for minimum boom weight. Thus, the boom weight per unit length (inch) can be written as follows:

$$w_B = 2\pi r_B \left[0.0005 \times 0.05 + \frac{3\pi}{4} \frac{d^2}{s} \times 0.1 \right].$$

or taking equation (29) into account, and letting $s_B/d_B = 50$, the unit weight equation becomes

$$w_B = C \left[25 \times 10^{-6} d_B^{-1/3} + 0.004712 d_B^{2/3} \right]$$

where C is a constant. Solving equation $dw_B/d(d_B) = 0$ for d_B yields $d_B = 2.66$ mils. For the purpose of the present study the wire diameter was taken as $d_B = 2.5$ mils, and the axial wire spacing $s_B = 50 \times 2.5$ mils = 0.125 in. Equation (29) was thus reduced to

$$r_B = 0.0014537 \sqrt[3]{\frac{\ell_B^2 I'_z}{h}} \text{ in.} \quad (30)$$

The preceding discussion was applied to the five configurations indicated in figure 9. The values of W_{TF} , W_{TP} are given below for the corresponding points (configurations) and altitudes.

<u>Configuration</u>	<u>Altitude</u>	<u>W_{TF}/W_{TP}</u>
A	19 300 n.mi. (syn)	1.206
B	19 300 n.mi. (syn)	1.134
C	2 000 n.mi.	1.34
D	2 000 n.mi.	3.50
E	6 000 n.mi.	1.264

The value 3.50 appears to be excessively high, and corresponds to a relatively low altitude and an extremely large satellite. Values of the ratio W_{TF}/W_{TP} for partial coverage can be found by determining the weight of the rim and tetrapod booms by using the derived equations.

Example. - The following example shows how the preceding method can be used to determine the weight and moments of inertia of the various components of the lenticular satellite.

Determine the size, weights, and moments of inertia of the various components of a full-coverage lenticular satellite, orbiting at an altitude of 6000 n.mi., using lens material III, a lens radius of curvature, ρ , of 600 ft, and a central half angle, θ , of 23.6° (including the anticipated stabilization system error).

Solving equations

$$\rho = \frac{6.884 s \times 10^6}{e 0.22575/s} \text{ inch, } d = \frac{s/\pi}{e 0.1505/s}$$

by trial and error for s and d , the following values are obtained:

$$\begin{aligned} s &= 0.0566 \text{ inch} \\ d &= 0.00125 \text{ inch} \\ \sin \theta &= 0.40035 \\ \cos \theta &= 0.91636. \end{aligned}$$

Rim radius: $R = \rho \sin \theta = 600 \times 0.40035 = 240.21 \text{ ft} = 2883 \text{ inches}$

Lens weight (see table 2):

$$\begin{aligned} \text{(a) With film: } W_L &= 12.566 (7200)^2 (1 - 0.91636) \left(0.1571 \times \frac{1.5625}{0.0566} + 19 \right) \times 10^{-6} \\ &= 1271.5 \text{ lb} \end{aligned}$$

$$\text{(b) Without film: } W'_L = 1271.5 \times \frac{4.337}{23.337} = 236.3 \text{ lb}$$

$$\begin{aligned} \text{(c) } I_x \text{ (no film)} &= 0.0022849 (7200)^4 \frac{1.25^2}{0.0566} \times 10^{-6} (0.08364)^2 (3.08364) \\ &= 3.6567 \times 10^6 \text{ lb-ft}^2 \end{aligned}$$

$$\begin{aligned} \text{(d) } I_z \text{ (no film)} &= 0.004570 (7200)^4 \times \frac{1.25^2}{0.0566} \times 10^{-6} (0.08364)^2 (2.91636) \\ &= 6.9167 \times 10^6 \text{ lb-ft}^2 \end{aligned}$$

Torus weight:

$$W_T = 0.49548 \times \frac{(7200)^2 (0.00125)^2}{0.0566} (0.40035)^2 (0.91636) = 104.1 \text{ lb.}$$

Inflation system weight:

$$\begin{aligned} W_I &= 0.21856 \times \frac{(7200)^2 (0.00125)^2}{0.0566} (1 - 0.91636) (0.91636^2 + 0.91636 + 0.69923) \\ &= 64.2 \text{ lb.} \end{aligned}$$

Canister weight:

$$\begin{aligned} W_C &= 0.13432 (7200)^2 \left[1.0376 \times \frac{0.00125^2}{0.0566} \times 0.40035^2 \times 0.91636 + 0.0005 (1 - 0.91636) \right. \\ &\quad \left. + 0.1591 (1 - 0.91636) \frac{0.0566}{0.301/0.0566} \right] = 346.1 \text{ lb.} \end{aligned}$$

Weights at tetrapod apices:

(a) Lower tetrapod	
100 percent of inflation system	64.2 lb
55 percent of canister	<u>190.4</u>
Total	254.6 lb
(b) Upper tetrapod	
45 percent of canister	155.7 lb
Stabilization system (balance)	<u>98.9</u>
Total	254.6 lb

Determination of h:

$$I_x = 3.6567 \times 10^6 + 10.429\omega R^3 h \times 10^{-6} \sqrt{WR}/12 + (2 \times 254.6) h^2 \text{ lb-ft}^2$$

$$I_z = 6.9167 \times 10^6 + 2 \times 10.429\omega R^3 h \sqrt{WR} \times 10^{-6}/12 \text{ lb-ft}^2$$

where R is in inches and h in feet,

$$\omega = 0.00027304 \text{ rad/sec, } W = 2 \times 254.6 = 509.2 \text{ lb.}$$

Substituting numerical values, and solving equation $I_x/I_z = 5.75$ for h yields $h = 346.6 \text{ ft} = 4159 \text{ inches}$.

Rim size, weight, etc: (see eqs. 26, 27, 28)

$$h_R = 0.1461 \sqrt[4]{(0.00027304)^2 (2883) (509.2) (4159)^2} = 5.10 \text{ inches}$$

$$t_R = 0.00025 \times 4.80 = 0.00128 \text{ in.} \approx 1.3 \text{ mils}$$

$$W_R = 3.9 (2883) (5.1) (0.0013) = 74.5 \text{ lb}$$

$$I_{x,R} = \frac{1}{2} I_{z,R} = 74.5 \times (240.21)^2 \left(\frac{1}{2}\right) = 2.1494 \times 10^6 \text{ lb-ft}^2$$

Tetrapod booms (see eq 30):

$$\ell_B = (2883^2 + 4159^2)^{1/2} = 5060.5 \text{ inches}$$

$$I'_z = (6.9167 + 2 \times 2.3877) \times 10^6 = 11.6921 \times 10^6 \text{ lb-ft}^2$$

$$r_B = 0.0014537 \sqrt[3]{\frac{25.609 \times 10^6 \times 11.6921 \times 10^6 \times 144}{4159}} = 14.537 \sqrt[3]{10.367} = 31.7 \text{ in.}$$

Weight of both tetrapods:

$$W_B = 8 (2\pi r_B) \ell_B w_B, \text{ where } w_B \text{ is the boom weight per sq in. or } w_B = 0.0005 \times 0.05$$

$$+ \frac{3\pi}{4 \times 0.175} \times 0.0025^2 (0.1) = 25 \times 10^{-6} + 11.78 \times 10^{-6} = 36.78 \times 10^{-6} \text{ lb/in.}^2 \text{ and}$$

$$W_B = 1.8488 r_B \ell_B \times 10^{-3} \text{ lb} = 243.7 \text{ lb}$$

$$I_{x,B} = \frac{W_B}{12} (R^2 + 2h^2) = \frac{243.7}{12} (2 \times 240.21^2 + 346.6^2) = 4.7833 \times 10^6 \text{ lb-ft}^2$$

$$I_{z,B} = \frac{W_B}{6} R^2 = \frac{243.7}{6} (240.21^2) = 2.3436 \times 10^6 \text{ lb-ft}^2$$

Summary of weights and moments of inertia: To summarize, the calculated values of a full-coverage lenticular satellite orbiting at 6000 n. mi., with a central half angle of 23.6° , lens radius of curvature of 600 ft, rim radius of 240.21 ft, and tetrapod height of 346.6 ft. are as follows:

Component	Launch Weight, lb	Orbital Satellite		
		Weight, lb	I_{x-x} (lb-ft ²)	I_{z-z} (lb-ft ²)
Lens	1271.5	236.3	3.6567×10^6	6.9167×10^6
Torus	104.1	0		
Inflation system	64.2	64.2		
Canister	346.1	346.1		
$W_{TP} =$	1785.9	646.6	61.1710×10^6	0
Stabilization system, $W_S =$	98.9	98.9		
Rim	74.5	74.5	2.1494×10^6	4.2987×10^6
Tetrapod booms	243.7	243.7	4.7833×10^6	2.3436×10^6
Sail (Est) ^a	52.6	52.6	---	---
$W_{TF} =$	2255.6	$W_O = 1116.3$	$I_X = 71.7604 \times 10^6$	$I_Z = 13.5590 \times 10^6$
$W_{TF}/W_{TP} = 2255.6/1785.9 = 1.264$ $W_S/W_O = 98.9/1116.3 = 0.0886 \cong 9 \text{ percent}$				

^aThe sail weight, W_{sail} , was found from equation $W_{sail}/Rh = \text{constant}$, where the value of the constant was taken from the configuration described in reference 2 (page 67), in which $W_{sail} = 22 \text{ lb}$, $R = 133.8 \text{ ft}$, and $h = 260.3 \text{ ft}$.

Summary

The results of the structural design study have indicated that the weights and moments of inertias of the satellite and its components can be predicted with reasonable accuracy for low to synchronous altitude applications. Specific configurations were determined for complete rf ground coverage at the altitudes in question. Configurations giving partial coverage, defined by ρ and θ , can readily be determined.

Table 3 summarizes the physical and mass characteristics of the five configurations depicted in figure 9. These configurations are based on the assumptions that the space-side apex weight consists of 45 percent of the canister weight plus the stabilization system weight; the earth-side apex weight consists of the inflation system weight and 55 percent of the canister weight; and both apex points are equidistant from the plane of the rim. These five configurations were used as the starting point for the transient and steady-state dynamic analyses. The stabilization analysis includes the moment of inertia effect of the Ames X booms thus requiring an adjustment in h (apex height above rim plane) to maintain the desired satellite inertia ratios.

The value $W_{TF}/W_{TP} = 1.264$ seems to be a typical average that can be used as a first approximation on any practical satellite configuration for a quick estimate of the overall weight.

STABILIZATION ANALYSIS

Introduction

General. - A three-axis gravity-gradient stabilization system with an adjustable steady-state yaw reference is required for proper attitude control of the lenticular satellite. Figure 10 depicts the three-axis system and the yaw reference drive. The system is essentially a modified Ames system. Damping of gravity-gradient librations is provided by a single damper boom with a nominally horizontal pivot axis skewed to the orbital plane. Thus pitch and roll librations of the satellite directly excite the damper boom. A fixed boom is skewed to the orbital plane in an opposite sense to that of the damper boom. The two booms provide yaw axis gravity-gradient restoring torques; the null yaw reference position is determined by equilibrium between the yaw restoring torques of the two booms. Both booms are attached to the yaw reference drive, which provides the necessary adjustment capability to accommodate the changing solar sail requirements. The reference drive is extremely slow, so that in no case do the inertial reaction torques overcome the gravity-gradient restoring torques. In order to achieve satisfactory gravity-gradient stiffness about the yaw axis, the pair of booms must have a moment of inertia that is commensurate with the yaw axis moment of inertia of the satellite proper. Adequate pitch and roll gravity-gradient stiffness is ensured by adequate height of the satellite and the weight of the equipment on the canisters.

Good transient stability and low steady-state forced errors are desirable. In general, pitch and roll attitude errors penalize satellite weight, because these errors must be traded off against increased lens angle, as shown in figure 11. If the weight penalty is to be limited to 25 percent, pitch and roll attitude errors should be less than 5 degrees for low-altitude lensats, where lens angles are approximately 85° . For synchronous altitude lensats for which the lens angles are 17 degrees, the pitch and roll errors should perhaps be limited to 2 degrees, if one assumes an acceptable weight penalty of 50 percent. Transient damping time constants may be a few orbits in duration.

Orbital position keeping by means of a solar sail requires yaw axis stability with a steady-state yaw reference adjustment capability to accommodate the effects of orbital precession and annular earth rotation about the sun which slowly alter the inclination of the sun line to the orbital plane. It is not required that the yaw reference adjustment capability be fast enough to offset the relatively short-term effects of orbital velocity in altering the angle of attack of the solar sail. Adjustments in the yaw reference attitude may be made periodically (once per month or less). Yaw accuracy requirements are relatively relaxed because the propulsive forces on the solar sail are relatively insensitive to yaw attitude, and 15 to 20 degree yaw errors appear to be tolerable.

The transient and steady-state performance of the stabilization system was analyzed. Equations of motion of the stabilization system were derived using the LaGrange method. Solutions to the equations of motion were obtained by both analog computer simulation and digital computers. Transient performance was optimized by the method of steepest descent, which maximized the transient damping of the least damped mode of satellite motion by optimizing the damping system spring constants, dashpot constant, and skew angles of the booms for various size damping system booms. Steady-state forced attitude errors due to the effects of orbital eccentricity and solar pressure torques were determined. In general, the results of the study show that the stabilization system provides the necessary transient damping capability and steady-state accuracy, with the weight allowance for the stabilization system held to 10 percent of the total satellite weight for all altitudes from synchronous to 2000 n.mi.

Stabilization System Considerations. - The most significant factors influencing the performance of the gravity gradient stabilization system are:

- (1) The damping capability of the Ames damping system which determines the transient stability of the various modes of satellite libration in the gravity-gradient field.
- (2) The steady-state error sensitivity of the satellite to perturbing torques due to solar pressure and the effects of orbital eccentricity.

The transient stability of the satellite is determined by the effectiveness of the Ames gravity-gradient damping system. Limitations in the damping system are a result of limitations in the realizability of sufficient inertia of the damping boom. The inertia of the damper boom is limited because of the following effects:

- (1) Thermoelastic bending of the De Havilland type booms due to solar heating
- (2) Bending of the booms due to static gravity-gradient moments caused by the booms having to be mounted on the upper canister at great height above the composite center of mass
- (3) A requirement for reserve stiffness in the booms to withstand bending moments caused by centrifugal forces during a possible initial tumbling period when the satellite may tumble as often as five times per orbit.

The transient stability of the satellite has been investigated and optimized within the physical limits of boom inertia. A digital computer was used to optimize transient performance on a parametric basis by employing the analytical method of steepest descent which maximized the transient damping of the least damped mode of satellite libration. Optimum spring constants, dashpot constants, and steady-state skew angles of the booms relative to the orbital plane were determined for various values of fixed and damper boom inertias. This optimization method continually trades damping capability of the more highly damped modes for increased damping capability in the least damped mode until all modes of libration are essentially equally well damped. Analog computer simulations were made of the time histories of the decay of initial condition attitude errors.

The mass distribution of the lenticular structure must provide sufficient gravity-gradient stiffness to offset steady bias torques and a set of natural libration frequencies that are remote from one and two times orbital frequency. The lenticule and canisters provide pitch and roll axis stiffness, but no yaw restoring torques. Yaw axis stiffness, as stated earlier, is provided by the fixed and damper booms attached to the upper canister. Unfortunately, analysis of the total effect on natural frequencies due to the combined set of masses consisting of the lenticule, the upper and lower canisters, the fixed boom, and the damper boom becomes very involved. However, on the basis of rigid body dynamics, which ignore the spring coupling of the damper boom in shifting satellite libration frequencies, it was attempted to keep the ratio of roll axis inertia to yaw axis inertia near the value of 5.75. The effect of the fixed and damper booms in modifying the effective ratio of pitch axis to roll axis inertia is very obscure, due to the complexity of the spring coupling of the damper boom and to the effect of the skew angles of each of the booms to the orbital plane. Nevertheless, it was possible to achieve sets of natural frequencies that resulted in acceptably low steady-state resonant rises in response to orbital eccentricity and solar pressure torques. These natural frequencies of the satellite tended to be close to the following values:

Pitch	1.3 to 1.6 ω_0
Roll	1.8 to 1.9 ω_0
Yaw	0.4 to 0.5 ω_0
Damper	0.7 to 0.9 ω_0

The steady-state attitude errors due to steady sinusoidal perturbing torques were determined by a computer programmed to solve the steady-state equations of motion in responding to unit normalized perturbing torques about each of the three satellite axes. LaPlace transformed equations of motion were employed, and the usual steady-state analytical substitution, $s = j\omega$, was made. Steady-state error sensitivity coefficients were calculated for perturbing torques at zero frequency, orbital frequency, and twice orbital frequency. Cross-coupled error sensitivity coefficients between all axes and direct-coupled coefficients were calculated, so that, for example, the errors resulting from a roll axis perturbing torque could be calculated for the pitch and yaw axes as well. These steady-state error sensitivity coefficients are functions of the natural frequencies of satellite libration, and hence of the mass distribution of the satellite. Because the fixed and damping booms of the Ames stabilization system have a significant effect on the total satellite mass distribution, the satellite natural frequencies vary with the size of these booms. The error sensitivity coefficients are thus functions of the inertia of the fixed and damper booms.

Definition of parameters and equations of motion. - Figure 12 presents the different coordinate systems and the relationship between principal body axes of the satellite and the various coordinate systems. The derivation of the equations of motion from the kinetic and potential energy expressions are given in appendix G. All necessary coordinate system transformations are also shown in appendix G.

The inertial coordinates are the frame of reference from which all motion is measured, and by which motion description is mathematically formulated. However, the inertial system is not a convenient frame for stability analysis. For this reason, the trajectory coordinate system is defined. The trajectory coordinates, as shown in figure 12, are centered at the satellite center of mass. The coordinates are aligned with the nominal satellite orientation, which for a circular orbit is also the local horizontal. Oscillations about the nominal orientation, due to disturbances, can then be conveniently measured from the trajectory system, which is an attitude reference. Satellite attitude is described by attaching a set of body axes to the vehicle and analyzing the Euler angle rotations which relate the body to the attitude reference system. The Euler angle rotational sequence is shown in figure 12.

Note that this approach reduces the satellite motion to a translation and a rotation. The translational component is the motion of the trajectory coordinates (satellite c.m.), while the rotational component is the motion of the satellite relative to the trajectory (attitude reference) coordinates. The stability analysis is the study of the rotational motion of the vehicle about the nominal orientation. Use of the trajectory axis system thus permits a readily grasped description of that rotational motion. This does not imply, however, that stability is completely divorced from translation. The translational motion is the orbital motion of the trajectory coordinates (satellite c.m.). The orbital rate is a rotation in inertial space. This is duly accounted for in the equations of motion (see appendix G).

A damper boom having one rotational degree of freedom relative to the satellite is attached as shown in figure 12. The relative motion of the damper boom is measured in a damper axis system. The damper axes are referenced to the body axes through a coordinate transformation. Complete motion description of the satellite, including the damper, is thus accomplished through these coordinates.

The effect of solar pressure on satellite stability is considered in the dynamics analysis. Solar pressure is a vector quantity, and therefore its effect on stability is a function of the relative orientation between the solar vector and the vehicle attitude. Representation of relative solar pressure-vehicle orientation is handled by introducing a sun line vector, which relates to the inertial coordinate system. The solar pressure vector is then transformed through the defined coordinate to the body axis system. This permits a complete description of solar effects for any satellite attitude or position in space.

Transient Response

The primary parameters determining the transient response performance of the damping system are the moment of inertia ratios F and D , which are the ratios of the fixed and damper boom moments of inertia respectively to the satellite roll moment of inertia. Figure 13 shows transient response performance plotted against D for various fixed values of F . The performance axis is scaled to show both σ , the real part of the complex root of the least-damped mode, and the number of orbits required for a small step disturbance to decay to approximately 5 percent of its initial value. These curves are the results of the optimization of the normalized equations of motion, and are applicable to any satellite similarly equipped with this form of stabilization at any orbital altitude. The parameters defining the relative location of the damping system booms (γ , δ , and ψ_D as shown in fig. 12) and the spring deflection (K'') and viscous damper coefficient (B'') are shown in figures 14 through 19.

It is important to note the relatively narrow range of the normalized spring and viscous damper coefficients over the complete range of variables. Actual hardware coefficients can be calculated using the normalizing relationships. Figure 20 shows the relative angular position of the fixed and damper booms with respect to the overall system principal roll axis, which is normally aligned with the orbital velocity vector. The parameters are plotted here against the ratio D/F to show the effect of the constraint defining the location of the system principal axes due to the booms. The location of the damper boom askew to orbital plane is very important in establishing optimum damping performance. Figure 20 shows that when D is smaller than F , D can be located for optimum performance. However, when D becomes greater than F , the location of D becomes constrained and performance deteriorates rapidly as seen in figure 13. An important consideration not shown herein, but noted and described in reference 5, deals with the sensitivity of the various parameters at or very near the peaks or optimums of the family of performance curves shown in figure 13. In the apparent optimum region of each curve the parameters exhibit a relatively high sensitivity to damper configuration variations and could present stringent design considerations. These effects lead to a conclusion that F should always be selected slightly larger than D , and that D should be located to the left of the optimum peak of the F curve being used.

The parameter data presented above was developed using digital computation. An analog simulation was used to illustrate the performance with time history plots. Following is a list of the computer runs, which are shown in figures 21 through 32:

<u>Run No.</u>	<u>Configuration</u>	<u>Figure No.</u>
1 through 4	Transient Response when Optimum Boom Inertias are $F = 0.16$ and $D = 0.143$	21
5 through 8	Transient Response when Optimum Boom Inertias are $F = 0.12$ and $D = 0.129$	22

<u>Run No.</u>	<u>Configuration</u>	<u>Figure No.</u>
9 through 12	Transient Response when Optimum Boom Inertias are $F = 0.08$ and $D = 0.114$	23
13 through 16	Transient Response when Optimum Boom Inertias are $F = 0.04$ and $D = 0.10$	24
17 through 20	Transient Response when Optimum Boom Inertias are $F = 0.04$ and $D = 0.03$	25
21 through 24	Transient Response when Optimum Boom Inertias are $F = 0.02$ and $D = 0.095$	26
25 through 28	Transient Response when Optimum Boom Inertias are $F = 0.02$ and $D = 0.0175$	27
29 through 32	Transient Response when Optimum Boom Inertias are $F = 0.01$ and $D = 0.00875$	28
33 through 36	Transient Response for Configuration A at Synchronous Orbit	29
37 through 40	Transient Response for Configuration B at Synchronous Orbit	30
41 through 44	Transient Response for Configuration C at 2000 n. mi. altitude with booms designed for non-tumbling orbital conditions	31
45 through 48	Transient Response for Configuration E at 6000 n. mi. altitude.	32

Computer runs 1 through 32 illustrate the transient response associated with the parameter σ for all the peak optimum configurations associated with each fixed value of F shown in figure 13. These time histories show the response to a 5-degree error in each axis separately (sheets 1, 2, and 3 for each run), and then the response for 5-degree errors in all axes (sheet 4 for each run). It is important to note that the response of the yaw axis is relatively well damped, considering that it has the lowest natural frequency. In the analog simulation, data for the yaw angle, ψ , was not linearized to show the performance in this axis, as it is the most difficult to damp. Table 4 contains a tabulation of the data points obtained from the optimization study and includes the natural frequencies of the system as obtained from the roots of the system characteristic equation. Examination of this table and the analog computer runs shows that the natural frequency of the damper boom is always located between the system yaw and pitch natural frequencies, and is usually tuned closely to the yaw mode. The damper mode is extremely well damped. This permits it to be sensitive to a broad spectrum of input disturbing frequencies ranging from yaw to roll, which is always the highest. In order for the damping boom to be sensitive to both roll and pitch disturbances, it may be located askew to the orbital plane.

Referring to the performance curves for $F = 0.04$ and 0.02 in figure 13, there are two apparent optimum peaks for each curve. The lower optimum value appears to occur for the anticipated value of D , i.e., $D \cong 0.8 F$. The second and maximum peak occurs for a relatively large value of D , i.e., $D \cong 2.5 F$. In order to explain this effect, reference is again made to the data shown in table 4. Examining the system natural frequencies, it can be seen that for the higher D the apparent pitch and roll frequencies are nearly equal. In effect, the addition of the booms has changed the system natural frequencies from the initial desired values associated with the inertia ratio of $J = 0.1739$ to a tuned condition between pitch and roll, even though the relative boom angular locations are restricted by the angular constraint

defining the location of the system principal axes. Although this is an optimum, a better optimum can be obtained by reversing these values of F and D , which follows the conclusion reached earlier.

Transient response runs 33 through 48 are also shown for several typical satellite configurations. While all the transient response runs are shown with the time base scaled in orbits, the satellite configuration runs are also scaled in real time, since the orbital period is defined for each configuration.

Since the primary parameters determining the transient response performance of the damping system are F and D , their maximum values should be determined with respect to the weight allocated to the damping system. The common denominator of F and D is the roll moment of inertia of the satellite and is constrained by configuration requirements. The numerators are the moments of inertia of the damper system booms. Appendix H contains an analysis relating the maximum attainable moment of inertia, I_{\max} , of a boom to its weight. The constraint is used that the deflection of the boom tip is less than 10 percent of its length, L , as measured from the tetrapod, while experiencing combined maximum solar heating and gravity-gradient forces. The gravity-gradient force is directly proportional to ω_0^2 , and to the height, h , of the booms above the system center of gravity. This analysis considers two cases; the first is normal orbital flight, where the gravity gradient force coefficient is $3\omega_0^2$; the second considers a tumbling condition of $5\omega_0$, where the coefficient increases to $27\omega_0^2$. Figures 33 and 34 show the results of this analysis with I_{\max} and L plotted against $\omega_0^2 h$ for various constant boom weights. Note that I_{\max} is the moment of inertia for only one boom. Since two booms are required for the damping system, the damping system weight allocation must be divided between the fixed and damper booms. The relationship for determining the boom design parameters are shown in figures 35 and 36.

In the damping system configurations considered, the weights of the boom deployment motor and damper hardware are insignificant. The transient response analysis has shown that F and D should be approximately equal, so I_{\max} can be determined using half the damping system weight allocation.

Stabilization system parameter selection. - The procedure presented here can be used to establish the damping - satellite system configuration. Worksheet No. 1, shown on the following page, can be used as an aid in defining configuration parameters.

- (1) Determine the following necessary input data from the lens configuration:

ω_0 , rad/sec	orbital frequency
I_{z-z} , slug-ft ²	lens structure yaw moment of inertia
$I_{x-x} = A + Bh^2$, slug-ft ²	lens structure pitch or roll moment of inertia. A represents components of I_{x-x} that are independent of h ; B represents lumped masses that are located at the tetrapod apexes. Their contribution to I_{x-x} varies as h^2 .
$W_D + F$, lb	weight allocated to the damping system

WORKSHEET NO.1

Selection of Damper Configuration

Lensat Configuration

Orbital Alt. (n. mi.) = _____
 ω_0 (rad/sec) = _____
 α (deg) = _____
 ρ (ft) = _____
 W_S (lb) = _____
 I_{Z-Z} (slug-ft²) = _____
 I_{X-X} (slug-ft²) = $A_{X-X} + F_{X-X}h^2$
 A_{X-X} = _____
 B_{X-X} = _____
 $*I_{X-X}$ (slug-ft²) = _____
 $*h$ (ft) = _____
 $(W_D + F)/W_S$ = _____

*Damper Configuration

W_{D+F} (lb) = _____
 I_{max} (slug-ft²) = _____
 I_F (slug-ft²) = _____
 I_D (slug-ft²) = _____
 L for I_{max} (ft) = _____
 ψ_D (deg) = _____
 k (lb/rad) = _____
 B (lb-sec/rad) = _____
 F = _____
 D = _____
 K'' = _____
 B'' = _____
 γ = _____
 δ = _____
 $(W_D + F)/2$ = _____

*FINAL VALUE

Estimate					
h					
h^2					
$B_{X-X} h^2$					
A_{X-X}					
I_{X-X}					
ω_0^2 Calculate					
$\omega_0^2 h$					
$\omega_0^2 h \times 12$					
I_{max}					
I_F					
I_{Z-Z}					
$I'_{Z-Z} = I_{Z-Z} + I_F$					
Compare					
$5.75 (I'_{Z-Z})$					
I_{X-X}					
$F = I_{max}/I_{X-X}$					

- (2) Determine a minimum h that satisfies the nominal relation $I_{X-X} = 5.75 I_{Z-Z}$.

$$h = \sqrt{\frac{5.75 I_{X-X} - A}{B}}$$

(This neglects the fact that the fixed boom inertia should be added to I_{Z-Z} .)

- (3) Determine the maximum I_{\max} that can be attained with the given configuration. Using the minimum h from step (2), use $\omega_0^2 h \times 12$ and $(W_D + F)/2$ to determine I_{\max} from the appropriate set of curves in figure 33 or 34.

NOTE: Calculations of steps (2) and (3) are the minimum h and maximum I_{\max} for the given configuration. As h increases, I_{\max} decreases.

- (4) Calculate $I_{X-X} = A + Bh^2$ and $5.75 I'_{Z-Z} = 5.75 (I_{Z-Z} + I_{\max})$

Compare I_{X-X} and $5.75 I'_{Z-Z}$.

- (a) If $I_{X-X} \leq 5.75 I'_{Z-Z}$, the satellite roll moment of inertia is small and h must be increased to increase I_{X-X} . Proceed to step (5).
 - (b) If $I_{X-X} > 5.75 I'_{Z-Z}$, proceed to step (6). In this case I_{\max} is not a constraint on the allowable value of I_F or I_D . A value of F can be chosen from the transient response performance curve, the required h calculated to achieve the necessary inertia ratio of $I_{X-X}/I_{Z-Z} + I_F = 5.75$, and I_{\max} recalculated with the new h to assure that I_F is still less than or equal to I_{\max} .
- (5) Estimate a new h and calculate
- (a) $\omega_0^2 h \times 12$ and determine new I_{\max} .
 - (b) Again compare $I_{X-X} = A + Bh^2$ and $5.75 I'_{Z-Z} = 5.75 (I_{Z-Z} + I_{\max})$, where $I_{\max} = I_F$.
 - (c) If $I_{X-X} \approx 5.75 I'_{Z-Z}$, then the configuration is defined and F can be calculated from $F = I_F/I_{X-X}$.

Refer to the damping performance curves (fig. 13) to select D and finally to the other curves (figs. 14 through 19) defining the damper configuration parameters. ($D \approx 0.8F$ appears to be a satisfactory relationship.) Boom dimensions can now be calculated, using step (7).

- (d) Re-estimate h and repeat step (5) if

$I_{X-X} < 5.75 I'_{Z-Z}$, increasing the previous estimate of h

$I_{X-X} > 5.75 I'_{Z-Z}$, reducing the previous estimate of h

- (6) Select a desired value of F and D , where $D \approx 0.8 F$, from the damping system performance curve (fig. 13).

(a) Calculate $h = \left[\frac{1}{B} \left(\frac{5.75 I_{X-X}}{1 - (F) 5.75} - A \right) \right]^{1/2}$

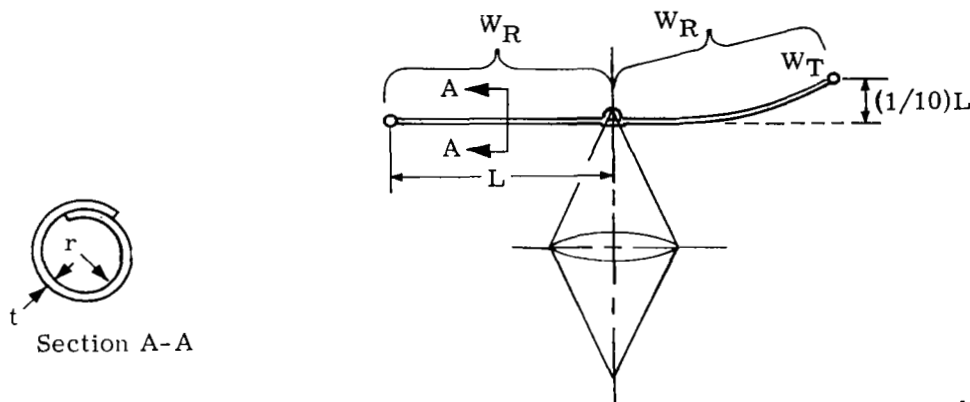
- (b) Recalculate I_{\max} using the new h for $\omega_0^2 h$
- (c) Calculate $I_{x-x} = A + Bh^2$
- (d) Using $I_F = (F)I_{x-x}$, recheck $I_F \leq I_{\max}$

If $I_F > I_{\max}$, the configuration is defined for the selected F and D and reference can be made to the other curves (fig. 14 through 19) for complete configuration parameter definition. Boom dimensions can be calculated according to step (7).

If $I_F > I_{\max}$, the selected value of F cannot be attained for the weight allocation; h must be reduced and the procedure shown in step (5) followed.

(7) Calculation of boom dimensions:

- (a) Boom length, L - half length defined as distance from tip to midpoint where boom is attached to satellite tetrapod apex. See sketch. L is obtained from figure 35 or 36, and is defined by $\omega_0^2 h$ and $(W_D + F)/2$.



- (b) Moment of inertia of boom, I_{\max} , slug-ft²

r = radius of boom tube, inches

t = tube thickness, inches

W_T = weight of concentrated tip masses, lb

W_R = weight of half boom length, lb

$\frac{W_D + F}{4} = W_T + W_R$ weight of boom, lb

$$W_R = 2\pi r \frac{520}{360} L \frac{r}{130} (0.38) (12)$$

$$= 0.02653 r^2 L (12)$$

$$W_T = \frac{W_D + F}{4} - W_R$$

$$t = \frac{r}{130}$$

$$r^2 = \frac{W_D + F}{4L (12)} - \frac{I_{\max} 32.2}{2L^3 (12)} \frac{1}{0.01769} \left. \vphantom{\frac{W_D + F}{4L (12)}} \right\} \text{ see sketch}$$

Steady-State Response

In order to define the steady-state performance of the complete satellite - damper system, it is necessary to (1) define the disturbing torques; and (2) relate the disturbing torques and system parameters to attitude errors.

The torques considered here are those associated with orbital eccentricity and solar pressure. The derivations defining the magnitude and sinusoidal frequency of these torques are presented in appendix G. Attitude errors are shown graphically as functions of the basic configuration parameters, F and D , for a normalized torque magnitude and the frequencies of interest. The computed magnitude of each torque can then be referenced to the normalized torque and, with the aid of the appropriate graph, the associated error can be computed. In order to simplify the analysis, each torque is considered separately. A summation of the absolute value of the various errors for multiple torque inputs results in a "worst case" error. This is due to neglecting the phase shift effects of multiple inputs. An alternate technique is to consider an rms value of the contributing errors. It is important to note that a torque applied to one axis of the satellite can result in attitude errors in the other satellite axes.

The torques that arise from orbital eccentricity have been simplified to the normalized form

$$T_y'' = 2\epsilon(1 + F + D - A) \sin \omega_0 t$$

$$T_x'' = T_z'' = 0$$

where ϵ is the orbital eccentricity, and T_y'' is the normalized torque acting upon the y axis. Since the normalized torque in this case can be defined in terms of the basic parameters F and D , the resultant attitude errors can be related directly to the eccentricity.

Figure 37 shows the pitch error due to an eccentricity of $\epsilon = 0.01$, and figure 38 shows the associated errors in yaw and roll for various values of F . The errors for other eccentricity values would be in direct proportion to the given $\epsilon = 0.01$ and the errors shown in these figures.

The effect of a disturbance into pitch causing errors in roll and yaw can also be seen in figures 39, 40, and 41, which show the response of each axis, including the boom deflection angle, to a sinusoidal pitch disturbance ranging from $0.1\omega_0$ to $2.5\omega_0$. An eccentricity disturbance at $1\omega_0$ would then induce errors in each axis in proportion to the magnitude of amplitudes shown for each response at the frequency $1\omega_0$.

The torques due to solar pressure must consider the geometry of the satellite - damper system and the relative location of the sun. The effect of the geometry of the satellite can be divided into two cases:

- (1) Torques associated with the basic satellite configuration, primarily the lens and the canisters
- (2) Torques associated with the damper configuration, i.e., the booms

In the first case the frequency of the disturbance torque may be either $1\omega_0$ and/or $2\omega_0$, depending upon the angular location of the sun line to the orbital plane.

In the second, the torque may have a frequency component of $1\omega_0$ and/or a constant component, again dependent upon the location of the sun line. In all cases the torques act

about either the pitch or roll axes. There are no torques acting about the yaw axis. Various disturbance torques in terms of their source, the axes they act upon, and the figures that should be used to determine the magnitude of the errors are tabulated in Worksheet No. 2. The top of this worksheet shows the required parameters needed to determine the magnitude of each torque. I_{x-x} and ω_0^2 are the normalizing parameters that are necessary to convert each torque into a normalized value. The other parameters are also associated with the configuration under consideration, and are necessary in computing torque magnitudes.

The normalized torques are subscripted to show that they act about either the pitch (y) or the roll (x) axes, and are related to torques due to the booms (B) or the satellite (S). The normalized torques due to solar pressure acting upon the satellite are T''_{yS} and T''_{xS} . Two cases are considered with respect to the relative location of the sun and the orbital plane. Case 1 considers the sun in line with the orbital plane; Case 2 considers it 45° from the orbital plane.

The torques are:

<u>Case 1</u>	<u>Case 2</u>
$T''_{yS} = \frac{C_1}{I_{x-x}\omega_0^2} \sin 2\omega_0 t$	$T''_{yS} = \left(\frac{C_1}{2}\right) \frac{1}{I_{x-x}\omega_0^2} \sin 2\omega_0 t$
$T''_{xS} = 0$	$T''_{xS} = \frac{C_1}{I_{x-x}\omega_0^2} \cos \omega_0 t$

where C_1 is defined by

$$C_1 = \frac{P_i \pi \mu^2}{4C} \left[-a^3 \sin(2\zeta_{\max}) + 2R_c^2 h \right]$$

and

$$\frac{P_i}{C} = \frac{\text{incident radiation power per unit area}}{\text{speed of light}} = 9.649 \times 10^{-8} \text{ lb/ft}^2$$

$$a = R \sin \zeta_{\max}$$

$$R = \text{radius of curvature of lens, ft}$$

$$\zeta_{\max} = \text{included lens angle}$$

$$R_c = \text{canister radius, ft}$$

$$h = \text{canister moment arm feet from lens}$$

$$\mu_{\text{len}} = \frac{\text{reflecting area of lens}}{\text{total lens area}} \quad (\text{reference table 5})$$

$$\mu_{\text{can}} = \text{reflectance coefficient} = 1$$

The first term in C_1 is the lens component of torque, while the second is due to the canister located at the tetrapod apex. It is important to notice that the torque about the pitch axis, T_{yS} , has a frequency of $2\omega_0$ in both cases while in the roll axis a frequency of $1\omega_0$ appears only in Case 2.

WORKSHEET NO. 2

Steady-State Errors

Configuration _____ [This worksheet applies to Case 1 only.
 T''_{yS} and T''_{xS} equations change for Case 2.]

Conditions

$$I_{x-x} = \text{_____ slug-ft}^2$$

$$\omega_0^2 = \text{_____ rad/sec}^2$$

$$C_1 = \text{_____ ft-lb}$$

$$F = \text{_____}$$

$$D = \text{_____}$$

$$D/F = \text{_____}$$

$$h = \text{_____}$$

$$L = \text{_____}$$

$$r = \text{_____}$$

$$F'_{x0} = \text{_____ lb}$$

$$F'_{x1} = \text{_____}$$

$$F'_{y0} = \text{_____}$$

$$F'_{y1} = \text{_____}$$

Type of Disturbance		Reference Figure	Normalizing Factor ^a	Error, deg ^b		
				θ	ϕ	ψ
1% Eccentricity		37 38	^a Normalizing factor = amplitude of disturbance. ^b In the Error column, the value from the graph (referenced figure number) is shown in parentheses. The second number in each column is the error, calculated as follows: $\text{error} = \frac{(\text{graph value})(\text{normalizing factor})}{10^{-2}}$			
Sinusoidal Torques	Pitch	$T''_{yB} = \frac{h \left(\frac{Lr}{300} \right) F'_{y1} \sin \omega_0 t}{I_{x-x} \omega_0^2}$		48 49		
		$T''_{yS} = \frac{(C_1/2) \sin 2\omega_0 t}{I_{x-x} \omega_0^2}$		42 43		
	Roll	$T''_{xB} = \frac{h \left(\frac{Lr}{300} \right) F'_{x1} \sin \omega_0 t}{I_{x-x} \omega_0^2}$		44 45 46		
		$T''_{xS} = \frac{C_1 \cos \omega_0 t}{I_{x-x} \omega_0^2}$		44 45 46		
Constant Torques		$T''_{yB} = \frac{h \left(\frac{Lr}{300} \right) F'_{y0}}{I_{x-x} \omega_0^2}$		50		
		$T''_{xB} = \frac{h \left(\frac{Lr}{300} \right) F'_{x0}}{I_{x-x} \omega_0^2}$		50		
Summation of Errors						
RMS of Errors						

Figures 42 and 43 show the attitude errors in each axis - pitch, roll, and yaw - for a normalized torque $T_y'' = 10^{-2} \sin 2\omega_0$. Using the F and D values for the configuration and the relative magnitude of T_y'' to T_y' , the error in each axis can be calculated for either Case 1 or Case 2 for the described pitch torque. Figures 44, 45, and 46 are used to determine the errors in the various axes due to the roll torque of $1\omega_0$ for Case 2.

In order to calculate the contribution of the solar torque transmitted by the booms, the simplifying assumption was made that booms are always located in the same relative position for all values of F and D. The actual values assumed were $\gamma = 25^\circ$ and $\delta = 45^\circ$, corresponding to what appears the normal value when $D \approx 0.8 F$. Using this assumption, the solar torque transmitted has the form

$$T_{yB}'' = \frac{h}{I_{x-x} \omega_0^2} \left[\frac{Lr}{300} \right] \left[F_{y0}' + F_{y1}' \sin \omega_0 t \right]$$

$$T_{xB}'' = \frac{h}{I_{x-x} \omega_0^2} \left[\frac{Lr}{300} \right] \left[F_{x0}' + F_{x1}' \sin \omega_0 t \right]$$

The coefficient (hLr, I_{x-x}) depends on size and shape of the boom and the satellite.

F_{y0}' and F_{x0}' are constant torque terms, while F_{y1}' and F_{x1}' determine the magnitude of the sinusoidal terms. The F_x and F_y terms are dependent upon the relative location of the sun line to the orbital plane. Figure 47 illustrates the magnitude of these terms with respect to the sun line. These terms can be handled in a fashion similar to the method used for the torques associated with the satellite. Figures 48 and 49 relate the pitch axis disturbance to the errors for the $1\omega_0$ frequency disturbance, and the same curves that were used for roll disturbances are again applicable. Figure 50 can be used to determine the errors associated with the steady-state torques, but it should be noted that it is applicable with high accuracy only in the region $D \approx 0.8 F$ due to the simplifying assumptions made with respect to the angular location of the booms.

The total steady-state error in each axis can now be determined by summing the errors. If the errors are in excess of acceptable values, a trade-off between steady-state and transient response performance should be made. In the configurations examined, it is apparent that the largest error is caused by solar pressure on the booms and the extremely long lever arm (h, height of tetrapod) producing a large torque. If a smaller I_F is used and transient response can be sacrificed, the lengths and diameters of the booms can be reduced to produce a smaller exposed surface to solar pressure. The height of the boom above the satellite center of mass would also be reduced, because the ratio of effective yaw axis inertia to roll axis inertia is held constant through the parametric relationship

$$J = \frac{I_{z-z} + I_F}{I_{x-x}} = 0.1739.$$

The steady-state error worksheets for four basic satellite - damper configurations are shown in tables 6 through 13 for two locations of the sun relative to the orbital plane. One location has the sun in plane with the satellite orbital plane, while the second has the sun 45° from the orbital plane.

Summary and Conclusions

The results of the study show that acceptable stabilization system performance may be achieved over the entire range of altitude of interest if the stabilization system is allocated up to 10 percent of the launch weight of the satellite. It has been shown that both speed of transient response and sensitivity to effects of orbital eccentricity and solar pressure torques are acceptable. Figure 51 summarizes the theoretical transient damping capability of the gravity-gradient stabilization system as a function of the parameter D , the ratio of damper boom inertia to satellite roll axis inertia. Inspection of figure 51 shows that the damping capability improves with an increase in the relative inertia of the damper boom. The validity of this curve is constrained by certain practical limiting factors such as orbital altitude, height of the damper booms above the center of mass of the satellite, the requirement of the damper booms to withstand tumbling, and thermoelastic deflections of the damper boom due to solar heating. At the lower altitudes the requirement for the booms to withstand a tumble rate of 5 times per orbit limits the parameter to perhaps as low as $D = 0.02$ and 95 percent transient decay times of the order of 30 days. At the higher altitudes the tumbling capability requirement of the booms has less constraining effect, and values of the parameter D as high as $D = 0.12$ are practical.

Table 14 presents a summary of the stabilization error analysis mode of four specific satellite configurations. These configurations do not necessarily reflect optimum performance of the stabilization system. Configuration C provides very low steady-state errors. However, the transient damping capability of this configuration is definitely limited by the low realizable mass moment of inertia of the fixed and damper booms, because of the requirement for the booms to be stiff enough to withstand the effects of the satellite tumbling at the rate of 5 times per orbit. The limitation could be offset to some extent by the allocation of more weight to the stabilization booms, which in this case is 130 lb, or only about 4 percent of the total launch weight of the satellite of 3551 lb. Doubling the weight allocation would essentially double the transient damping capability.

Configuration E represents a more optimum set of design conditions for the stabilization system, providing both good transient performance and low steady-state errors. This configuration is for 6000 n.mi. altitude operation. The tumbling problem, which limits the realizable booms inertias, is not nearly as severe in this case as in Configuration C, which operates at 2000 n.mi.

Configuration B provides good transient damping capability. This design explores the stabilization capability of an extremely lightweight synchronous orbit satellite. This configuration, which has very small gravity-gradient restoring torques, is therefore highly sensitive to upsetting torques caused by solar pressure on the relatively large areas of the fixed and damper booms, and steady-state errors approaching 25 degrees. Two methods are open to reducing the steady-state errors. Additional weight could be placed in the canister, thereby increasing the gravity-gradient restoring torques which must offset the solar pressure induced torques on the boom. Alternatively, the center of mass of the satellite could be shifted up by redesign of the tetrapod boom heights, so that lenticule solar pressure forces would offset a certain fraction of the solar pressure forces falling on the fixed and damper booms. It is estimated that such a counterbalancing of solar pressure torques would reduce these steady-state errors to as low as 5 degrees. This counterbalancing compensation scheme cannot, of course, provide 100 percent error compensation, because the shape of the booms is not matched by the shape of the lens. Moreover, the requirements for the booms to be fixed relative to the orbital velocity vector, and for the lens and sail to be oriented relative to the sun for orbital position keeping purposes, are somewhat incompatible with the balancing out of upsetting torques between the lens and the stabilization booms.

Configuration A shows that both good transient damping capability and acceptably low steady-state errors are achievable at synchronous altitude. This configuration is much heavier than Configuration B, having relatively much stronger gravity-gradient restoring torques.

As a result of this study, it is possible to summarize the significant performance limitations and design considerations of the stabilization system as follows:

- (1) Transient damping capability of the satellite is better at high altitudes than at low altitudes, assuming the same weight allocation of the stabilization system. This is a result of the smaller values of F and D at the lower altitudes, caused by the higher bending moments applied to the booms at the lower altitudes.
- (2) Steady-state errors are very low at low altitudes, but become the performance-limiting criterion at synchronous altitude. Large values of F and D at synchronous altitude provide very little help in attenuating steady-state attitude errors.
- (3) Increasing the weight allocation of the stabilization system gives some relief to the poorer transient damping capability of the low altitude configuration. The relief is not as great as desired.
- (4) For high-altitude satellites, a distinct trade-off between transient damping capability and steady-state errors is possible. The lower steady-state errors afforded by smaller damper booms come at the penalty of reduced transient damping capability. Such a trade-off is not required at low altitudes, however, because of greater gravity-gradient stiffness at the lower altitudes.
- (5) An effect noted indirectly in the optimization program data and in the analog simulation study involves system stability for the cases where F is smaller than D . In these cases the spring coefficient becomes low with respect to the coefficient required to maintain the damper boom in its unstable equilibrium position. In this situation, system non-linearities and large angular deflections could cause the boom to alter the inertia distribution of the satellite - damper system drastically and change the preferred orientation of the system. These effects could be reduced through the use of boom deflection limits or stops. A more thorough and expanded analysis of the satellite - damper system would be desirable for configurations where F is smaller than D .
- (6) The assumption that the effects of limits or stops on the damper boom angular deflection can be neglected appears acceptable with respect to the results shown. The damper boom mode is usually highly damped. However, it should be noted that if the damper boom is tuned to $1\omega_0$ and is not heavily damped, large excursions could result from eccentricity and solar torque disturbances.
- (7) A definite area of useful additional study involves the criteria used in this analysis concerning the inertia distribution parameter

$$J = \frac{I_{Z-Z} + I_F}{I_{X-X}} = \frac{1}{5.75}.$$

The performance of other ratios should be investigated to develop more complete parameter data. A second approach would be to maintain the satellite - damper system, including the contribution of both booms, I_F and I_D , fixed at the desired ratio of 5.75. In this case the steady-state error analysis could

be greatly simplified, while transient response optimization would become more complicated, to ensure that the constraint of inertia ratios was maintained during the optimization calculations.

INITIAL CAPTURE ANALYSIS

Introduction

The deployment and inflation sequence for the lenticular satellite cannot be expected to ensure an initial upright capture of the satellite by the gravity-gradient field. During deployment the satellite changes from a densely packaged canister into a large inflated passive communication satellite. The order of unfolding of the various layers of the wire mesh film composing the satellite and the continuously changing non-rigid body geometry during this metamorphosis cannot be accurately controlled nor analyzed. Initial attitude and attitude rate errors and various perturbing torques further reduce the likelihood of upright capture. The satellite requires an initial angular rate about its pitch axis equal to orbital rate. No simple passive means are available to impart this required initial rate of rotation. Initial rate error is nearly sufficient to cause tumbling of the satellite about its pitch axis. Perturbing torques are caused by escape of inflation gas through holes in the lens and torus. The holes are necessary to avoid entrapping air during the folding of the satellite for packaging.

It is therefore concluded that the structural integrity of the satellite must be sufficient to endure the stresses caused by initial tumbling rates conservatively estimated to be as high as five times orbital rates. In addition, either the gravity-gradient stabilization system must be augmented by some form of attitude-inversion system to ensure against inverted capture, or a satellite configuration must be required with symmetric radar frequency reflectivity characteristics.

Recommended Capture System

The recommended solution to the initial capture problem is called, for want of a better name, the "Repeated Flip System." This system requires a minimum of additional equipment and has a minimum of dependence on active elements. The additional equipment consists of a pair of beacons and a pair of attitude tumbling jets. A beacon with a high front-to-back ratio antenna is mounted on both the upper and lower canisters of the satellite. Ground station interrogation of the beacons determines whether inverted or upright capture has been achieved. If inverted capture has occurred, then the attitude tumbling jets are fired to right the satellite. Since precise attitude control will probably not exist at the time of firing the attitude jets, it is likely that the satellite will go into a tumbling phase with the tumbling rate gradually attenuated by the Ames gravity-gradient damping system. The tumbling period will then terminate in gravity-gradient capture of the satellite which, of course, may be either upright or inverted. The interrogation of the beacons and firing of the jets are repeated until an upright capture is achieved. The inversion cycle may have to be repeated as many as four times to ensure a 97 percent probability of upright capture. In this approach it is important that the gas-jet impulses are sufficient to invert the satellite, but not so large as to create a high tumbling rate that would take a long period for the Ames damper to attenuate. A good estimate of the gas

requirements may be made assuming that the required impulse from the jets is approximately 1.6 times $I\omega_0$, where I is the roll axis moment of inertia of the satellite and ω_0 is its orbital rate.

Alternate Solutions

Roll-Vee Damping System (Ref. 6). - This solution depends upon achieving a completely symmetric satellite with rf reflectivity characteristics such that an "upright" attitude is indistinguishable from an "inverted" attitude.

A two-gyro roll-vee damping system is used, replacing the Ames system. The two gyros are used as gyrostabilizers rather than merely as attitude error sensors. In this approach, the angular momentum of the gyros should be commensurate with the angular momentum of the satellite itself when rotating in inertial space about its pitch axis at an angular rate of one ω_0 , or once per orbit. Because of the large inertia of the satellite, the satellite angular momentum will be high, even though ω_0 is a very low rate.

The gyros would be mounted in the canisters with a suitable power supply. For a 1000-lb satellite at a 2000-mile altitude, it is estimated that each of the gyros would have a 50-lb wheel with a radius of gyration in the order of 10 inches and a wheel speed of 5000 rpm. The gyros must be mounted with a single degree-of-freedom gimbal with torques and pick-offs on the output axis.

Rate Gyro/Jet Capture System. - This system consists of three small rate gyros and three pairs of gas jets mounted on the lenticular satellite. The rate gyros fire the jets until the attitude of the satellite is "frozen" in inertial space. The Ames damper then may be deployed and the rate gyro/jet system turned off. The rate gyro/jet system may be turned off when a beacon with high front-to-back ratio antenna gives a coarse indication that the satellite is at that point in the orbit where its axis is reasonably close to vertical.

The advantage of this system is that the Ames dampers do not have to survive and operate through the initial tumbling period. A limitation of the system is that the initial attitude errors are not reduced to zero, and no method for supplying the initial angular rate about the pitch of one ω_0 is provided. Thus, there will be an initial libration of the satellite which, though less than tumbling, may be of significant amplitude.

All-Attitude Capture System. - This system consists of an all-attitude gyro-controlled reference stable platform and three sets of attitude-control jets. The gyro platform keeps track of launch point vertical on the basis of pure memory. After deployment and inflation of the lenticular satellite has been completed, the all-attitude reference platform sends commands to the jets, which erect the lenticular satellite to the launch vertical. On each successive orbit, there is a point at which the satellite is upright corresponding to the passage over the launch point in inertial space. At this point, the all-attitude capture system may be switched off and attitude control transferred to the Ames gravity-gradient stabilization system. A calibrated impulse from the pitch axis jet could establish the required initial pitch axis rotation rate of one ω_0 . Thus, all initial attitude and attitude rate errors would be reduced to zero and minimum attitude perturbations would be present at the time of transition to gravity-gradient stabilization.

The disadvantages of this system are the complexity of the all-attitude reference platform and certain coordinate transforms that convert gimbal axis error signals into jet-thrust commands.

CONCLUSIONS AND RECOMMENDATIONS

Design and performance data on the gravity-gradient stabilized lenticular satellite can be obtained for use in system studies from the parametric data and analyses presented herein. Previous design, fabrication, and test experience indicate that the assumptions used in the analyses are realistic. Lens radius of curvature, lens included angle, and orbital altitude are shown to be the key parameters with which to define a satellite configuration. Representative configurations defined for low and synchronous orbits verified the validity of the design and performance assumptions.

Acceptable lenticular satellite stabilization performance can be achieved with the Ames X system at orbital altitudes of 1000 n. mi. to synchronous with the stabilization system being allocated up to 10 percent of the satellite launch weight. Further, the speed of transient response and sensitivity to effects of orbital eccentricity and solar pressure torques are acceptable. Transient responses, measured in terms of numbers of orbits to achieve 95 percent decay of a step function torque input, range from 30 to 3 for low to synchronous altitudes respectively, using practical damper boom designs capable of withstanding tumbling constraints.

Stabilization error analyses made of four representative lenticular satellite configurations at 2000 n.mi., 6000 n.mi., and synchronous altitudes showed the following results:

- (1) Transient damping capability of the satellite is better at high altitudes than at low altitudes for the same stabilization system weight allowance.
- (2) Steady-state errors are not significant at low altitudes, but become the performance limiting criterion at synchronous altitude.
- (3) Some trade-off between transient damping capability and steady-state errors is possible, particularly at the higher altitudes.

The stresses likely to be encountered during the initial tumbling of the satellite are primary design criteria for some of the satellite components and the stabilization system. Estimates indicate that an initial tumbling rate as high as five times orbital rate (ω_0) may be realistic.

No single passive means of countering the initial tumbling problem is evident. A "repeated flip system" seems the simplest approach. This system utilizes a pair of beacons and a pair of attitude tumbling jets located at the canister positions to invert the satellite through ground control.

Further design and trade-off studies are recommended for high or synchronous altitude satellites to improve transient damping capability and minimize steady-state errors. A thorough design study directed specifically at synchronous altitude will allow a better definition of the trade-off parameters and lead to an earlier passive communication satellite system.

TABLE 1. - LENTICULAR LENS INCLUDED ANGLE
FOR HORIZON-TO-HORIZON COVERAGE

Orbital altitude, H n. mi.	Lenticular angle θ θ' ($\alpha = 0$)	Lenticular angle θ 2θ ($\alpha = 5^\circ$)
1 000	101.57 ⁰	101.03 ⁰
2 000	78.45 ⁰	78.10 ⁰
6 000	42.73 ⁰	42.57 ⁰
10 000	29.67 ⁰	29.53 ⁰
15 000	21.50 ⁰	21.43
19 300 sync	17.33 ⁰	17.27 ⁰

Page 35: In table 1, the column heading "Lenticular angle θ' ($\alpha = 0$)" should read "Lenticular angle $2\theta'$ ($\alpha = 0$)," and the heading "Lenticular angle θ ($\alpha = 5^\circ$)" should read "Lenticular angle 2θ ($\alpha = 5^\circ$).". In addition, the formulas below the table should be corrected as follows:

$$\theta' = \sin^{-1} \frac{R}{R + H}$$

$$\theta = \sin^{-1} \frac{R}{R + H} \sin 95^\circ$$

Also, in the left-hand sketch the angle $\theta'/2$ should be θ' and the symbol R on the tangent line should be deleted; in the right-hand sketch the angle $\theta/2$ should be θ .

α = Ground antenna elevation angle

TABLE 2. - WEIGHTS AND MASS MOMENTS OF INERTIA OF VARIOUS LENTICULAR SATELLITE COMPONENTS FOR FOUR TYPES OF LENS MATERIAL

Components			Material I	Material II	Material III $\rho = (6.884s, e^{0.22575, s}) \times 10^6$ $d = (s \pi), e^{0.1505, s}$ $0.04129 < s < 0.118$	Material IV $\rho = (6.884s, e^{2.2575, s}) \times 10^6$ $d = (s \pi), e^{1.505, s}$ $0.30268 < s < 0.6300$
Lens weight, $W_L, \text{ lb}$			$0.02488 \times 10^{-6} (1 - \cos \theta) \rho^3$	$12.566 \times 10^{-6} \left[1.086 \left(\frac{\rho}{1000} \right)^{4/3} + 19 \right] \rho^2 \times (1 - \cos \theta)$	$12.566 \rho^2 (1 - \cos \theta) \left\{ 0.1571 \left(\frac{d^2}{s} \right) + 19 \times 10^{-6} \right\}$	$12.566 \rho^2 (1 - \cos \theta) \left\{ 0.1571 \left(\frac{d^2}{s} \right) + 19 \times 10^{-6} \right\}$
Torus weight, $W_T, \text{ lb}$			$0.008320 \times 10^{-6} \rho^3 \sin^2 \theta \cos \theta$	$6.081 \times 10^{-10} \times \rho^{10/3} \sin^2 \theta \cos \theta$	$0.49548 \left(\frac{d^2 \rho^2}{s} \right) \sin^2 \theta \cos \theta$	$0.49548 \left(\frac{d^2 \rho^2}{s} \right) \sin^2 \theta \cos \theta$
Inflation system, weight, $W_I, \text{ lb}$			$0.003670 \times 10^{-6} \rho^3 f(\theta)^a$	$2.6823 \times 10^{-10} \rho^{10/3} f(\theta)^a$	$0.21856 \left(\frac{d^2 \rho^2}{s} \right) f(\theta)^a$	$0.21856 \left(\frac{d^2 \rho^2}{s} \right) f(\theta)^a$
Canister weight, $W_C, \text{ lb}$			$0.13432 (10^{-8}) \rho^3 \left\{ 1.7423 \sin^2 \theta \cos \theta + 2.6385 (1 - \cos \theta) \right\}$	$0.13432 (10^{-8}) \rho^2 \left\{ 0.12735 \rho^{4/3} \sin^2 \theta \cos \theta + 50000 (1 - \cos \theta) + 0.033538 \rho^{4/3} (1 - \cos \theta) \right\}$	$0.13432 \rho^2 \left\{ 1.0376 \left(\frac{d^2}{s} \right) \sin^2 \theta \cos \theta + 0.0005 (1 - \cos \theta) + 0.1591 (1 - \cos \theta) \left(\frac{s}{e^{0.301/s}} \right) \right\}$	$0.13432 \rho^2 \left\{ 1.0376 \left(\frac{d^2}{s} \right) \sin^2 \theta \cos \theta + 0.0005 (1 - \cos \theta) + 0.1591 (1 - \cos \theta) \left(\frac{s}{e^{3.01/s}} \right) \right\}$
Moments of inertia, lb-ft ²	Lens	Film on I_{x-x}	$0.28797 \times 10^{-10} \rho^5 (1 - \cos \theta)^2$ $(4 - \cos \theta)$	$145.44 \times 10^{-10} \rho^4 \left\{ 1.086 \left(\frac{\rho}{1000} \right)^{4/3} + 19 \right\} (1 - \cos \theta)^2 (4 - \cos \theta)$	$0.014544 \rho^4 \left\{ 0.1571 \left(\frac{d^2}{s} \right) + 19 \times 10^{-6} \right\} (1 - \cos \theta)^2 (4 - \cos \theta)$	$0.014544 \rho^4 \left\{ 0.1571 \left(\frac{d^2}{s} \right) + 19 \times 10^{-6} \right\} \times (1 - \cos \theta)^2 (4 - \cos \theta)$
		Film off I_{z-z}	$0.57596 \times 10^{-10} \rho^5 (1 - \cos \theta)^2$ $(2 + \cos \theta)$	$290.89 \times 10^{-10} \rho^4 \left\{ 1.086 \left(\frac{\rho}{1000} \right)^{4/3} + 19 \right\} (1 - \cos \theta)^2 (2 + \cos \theta)$	$0.029089 \rho^4 \left\{ 0.1571 \left(\frac{d^2}{s} \right) + 19 \times 10^{-6} \right\} (1 - \cos \theta)^2 (2 + \cos \theta)$	$0.029089 \rho^4 \left\{ 0.1571 \left(\frac{d^2}{s} \right) + 19 \times 10^{-6} \right\} \times (1 - \cos \theta)^2 (2 + \cos \theta)$
		Film on I_{x-x}	$0.28797 \times 10^{-10} \rho^5 (1 - \cos \theta)^2$ $(4 - \cos \theta)$	$157.95 \times 10^{-14} \rho^{16/3} (1 - \cos \theta)^2$ $(4 - \cos \theta)$	$0.0022849 \rho^4 (d^2/s) (1 - \cos \theta)^2 \times$ $(4 - \cos \theta)$	$0.0022849 \rho^4 (d^2/s) (1 - \cos \theta)^2 \times$ $(4 - \cos \theta)$
		Film off I_{z-z}	$0.57596 \times 10^{-10} \rho^5 (1 - \cos \theta)^2$ $(2 + \cos \theta)$	$315.91 \times 10^{-14} \rho^{16/3} (1 - \cos \theta)^2$ $(2 + \cos \theta)$	$0.004570 \rho^4 (d^2/s) (1 - \cos \theta)^2 \times$ $(2 + \cos \theta)$	$0.004570 \rho^4 (d^2/s) (1 - \cos \theta)^2 \times$ $(2 + \cos \theta)$
	Torus	I_{x-x}	$0.30670 \times 10^{-10} \rho^5 \cos \theta \sin^4 \theta$	$0.02240 \times 10^{-10} \rho^{16/3} \cos \theta \sin^4 \theta$	$18.264 \times 10^{-4} \rho^4 (d^2/s) \cos \theta \sin^4 \theta$	$18.264 \times 10^{-4} \rho^4 (d^2/s) \cos \theta \sin^4 \theta$
		I_{z-z}	$0.61292 \times 10^{-10} \rho^5 \cos \theta \sin^4 \theta$	$0.044769 \times 10^{-10} \rho^{16/3} \cos \theta \sin^4 \theta$	$36.50 \times 10^{-4} \rho^4 (d^2/s) \cos \theta \sin^4 \theta$	$36.50 \times 10^{-4} \rho^4 (d^2/s) \cos \theta \sin^4 \theta$

^a $f(\theta) = (1 - \cos \theta) (\cos^2 \theta + \cos \theta + 0.69923)$

**TABLE 3. - LENTICULAR SATELLITE CONFIGURATIONS
USING LENS MATERIAL III**

Item	Satellite configuration				
	A	B	C	D	E
Altitude, n.mi.	19,300 (syn)	19,300 (syn)	2000	2000	6000
Angle θ , (for full coverage)	$10^{\circ} 39'$	$10^{\circ} 39'$	42°	42°	$23^{\circ} 36'$
Lens radius of curvature, ρ , ft	1280	438	438	747	600
Lens wire spacing, s, in.	0.0665	0.0532	0.0532	0.05915	0.0566
Lens wire diameter, d, mils	2.2	1.0	1.0	1.5	1.25
Lens weight (film on), W_L , lb	1554.4	131.3	1957.2	6477.7	1271.5
Lens weight (film off), W'_L , lb	583.9	17.65	263.0	1550.0	236.3
Lens I_X (no film) $I_{X,L}$, lb-ft ²	8.2913×10^6	29367	7.0432×10^6	120.6×10^6	3.6567×10^6
Lens I_Z (no film) $I_{Z,L}$, lb-ft ²	16.3942×10^6	58063	11.8649×10^6	203.1×10^6	6.9167×10^6
Torus weight, W_T , lb	285.6	8.64	85.6	503.9	104.1
Inflation system weight, W_I , lb	171.2	5.18	77.2	342.3	64.2
Canister weight, W_C , lb	978.3	36.29	528.8	1688.7	346.1
Tetrapod apex weight (two places), each, lb	709.3	25.14	368	1271.1	254.6
Stabilization system weight, W_S , lb	269.1	8.81	130.1	511.2	98.9
Rim radius, R, lb	236.56	80.95	298.1	500.0	240.21
Orbit angular velocity, ω , sec ⁻¹	7.2722×10^{-5}	7.2722×10^{-5}	6.245×10^{-4}	6.245×10^{-4}	2.7304×10^{-4}
Tetrapod height, h, ft	257.16	79.17	657.6	2088.3	346.6
Rim height, h_R , in.	3.1	0.571	13.0	36	5.1
Rim foil thickness, t_R , mil	1.0	1.0	3.25	9.0	1.3
Rim weight, W_R , lb	34.4	2.17	579.3	7581.6	74.5
Rim, $I_{X,R}$, lb-ft ²	0.9625×10^6	7209	24.88×10^6	956.086×10^6	2.1494×10^6
Rim, $I_{Z,R}$, lb-ft ²	1.9250×10^6	14417	49.76×10^6	1912.17×10^6	4.2987×10^6
Tetrapod boom radius, r_B , in.	35.6	3.72	12.1	289.0	31.7
Tetrapod boom weight (total 8 booms) lb	275.9	9.34	193.5	13768.0	243.7
Booms $I_{X,B}$ (both tetra) lb-ft ²	4.3269×10^6	14852	15.3×10^6	10293.8×10^6	4.7833×10^6
Booms $I_{Z,B}$ (both tetra) lb-ft ²	2.5729×10^6	10192	2.77×10^6	573.7×10^6	2.3436×10^6
Total launch weight, W_{TF} , lb	3606.8	205.7	3551.7	31535.4	2256.5
W_{TP} (lens, torus, inflation system, canister) lb	2989.5	181.4	2648.8	9012.6	1785.9
W_{TF}/W_{TP}	1.206	1.134	1.340	3.50	1.264
Satellite orbital weight, W_O , lb	2350.7	83.5	1771.9	26101.8	1116.6
W_S/W_O	0.114	0.106	0.0735	0.02	0.089
Weight of sail (est) ^a lb	37.9	4.0	124.0	660.0	52.6

^aThe sail weight, W_{sail} , was found from equation $W_{sail}/Rh = \text{constant}$, where the value of the constant was taken from the configuration described in reference 2 (p. 67), in which $W_{sail} = 22$ lb, $R = 133.8$ ft, and $h = 260.3$ ft.

TABLE 4. - RESULTS OF DAMPING SYSTEM OPTIMIZATION STUDY

[J = 0.1739 for all data points]

Data point	F	D	K''	B''	-δ ⁰	+γ ⁰	-ψD ⁰	σ ₁	σ ₂	σ ₃	σ ₄	ω ₁	ω ₂	ω ₃	ω ₄
								(a)				(b)			
1	0.16	0.04	5.084	1.24	48.38	7.19	55.57	0.0900	0.3741	0.08981	0.0892	0.7178	1.321	1.463	2.007
2	.16	.08	4.665	1.448	43.0	14.96	57.96	.152	.303	.1674	.157	.5633	1.142	1.54	1.985
3	.16	.12	4.45	1.666	37.5	23.2	60.7	.2214	.278	.220	.210	.477	.974	1.63	1.91
4	.16	.14	4.398	1.80	36.28	28.3	64.58	.2465	.2956	.2416	.237	.4238	.9051	1.705	1.802
5	.16	.15	4.222	1.846	35.36	31.13	66.49	.340	.2532	.2305	.2345	.346	.809	1.72	1.79
6	.16	.16	4.00	1.95	35.3	35.3	70.6	.215	.948	.224	.212	.709	(c)	1.72	1.76
									.0042						
7	.12	.04	4.811	1.154	48.26	9.67	57.93	.0753	.3746	.0746	.0747	.5846	1.210	1.511	1.972
8	.12	.06	4.655	1.464	45.62	15.0	60.62	.1051	.4605	.1045	.1047	.5155	1.156	1.516	1.946
9	.12	.08	4.422	1.485	42.16	20.78	62.94	.1332	.4027	.1329	.1316	.4397	1.039	1.559	1.933
10	.12	.09	4.345	1.495	40.08	23.82	63.90	.144	.3781	.1461	.1448	.4139	.9875	1.585	1.922
11	.12	.10	4.297	1.545	38.1	27.01	65.11	.1563	.3743	.1617	.156	.3976	.9395	1.61	1.902
12	.12	.11	4.252	1.566	35.9	30.27	66.17	.1685	.3563	.1744	.1681	.3853	.8868	1.646	1.88
13	.12	.12	4.185	1.642	34.97	34.97	69.94	.1820	.3784	.180	.178	.3416	.8222	1.676	1.840
14	.12	.13	4.05	1.68	32.86	40.48	73.34	.2538	.3341	.1793	.1807	.2976	.678	1.739	1.776
15	.08	.02	4.925	1.154	50.40	7.11	57.51	.03272	.490	.03272	.0328	.5509	1.216	1.522	1.928
16	.08	.04	4.566	1.294	47.2	14.95	62.15	.0609	.4904	.0605	.0603	.445	1.106	1.538	1.924
17	.08	.05	4.435	1.372	45.43	19.34	64.77	.0730	.5091	.0739	.0720	.3992	1.0536	1.547	1.915
18	.08	.06	4.245	1.32	43.26	24.25	67.51	.0838	.4488	.0835	.0832	.3412	.9704	1.570	1.914
19	.08	.07	4.099	1.225	39.06	29.45	68.51	.0914	.3778	.0945	.0913	.3121	.8902	1.604	1.913
20	.08	.08	3.978	1.201	35.73	35.73	71.46	.0995	.3485	.1000	.0999	.2732	.8083	1.635	1.902
21	.08	.09	3.853	1.219	31.37	44.81	76.18	.1094	.3425	.1075	.1047	.2350	.6929	1.674	1.876
22	.08	.10	3.934	1.158	26.56	44.79	71.35	.1188	.2767	.121	.120	.3314	.6938	1.726	1.863
23	.08	.11	3.861	1.125	23.33	44.77	68.10	.2047	.1708	.1247	.1253	.3548	.6210	1.762	1.847
24	.08	.12	3.804	1.095	20.9	44.77	65.67	.2523	.1033	.1021	.1548	.317	.623	1.797	1.833
25	.08	.16	3.976	1.098	15.0	44.75	55.75	.261	.0401	.0403	.2944	.3465	.677	1.811	1.919
26	.04	.01	4.750	1.189	51.94	7.02	58.96	.01291	.5617	.01300	.01301	.4098	1.104	1.547	1.894
27	.04	.02	4.429	1.262	50.14	14.74	64.88	.0249	.5695	.0246	.0245	.342	1.024	1.554	1.893
28	.04	.025	4.346	1.242	49.26	19.1	68.36	.0301	.547	.02963	.02955	.3012	.9705	1.559	1.893
29	.04	.03	4.216	1.278	48.28	24.08	72.36	.0341	.5554	.0343	.0342	.2556	.9184	1.565	1.89
30	.04	.035	4.116	1.307	41.88	30.22	72.1	.0343	.5579	.0495	.0344	.2592	.8902	1.576	1.883
31	.04	.04	3.885	1.349	40.14	40.14	80.28	.0350	.5788	.0524	.0351	.1711	.7636	1.589	1.874
32	.04	.05	3.934	1.124	26.57	44.79	71.36	.03075	.4328	.0955	.03094	.3083	.7985	1.634	1.869
33	.04	.06	3.93	.8924	20.9	44.77	65.67	.0321	.3018	.1066	.0324	.3803	.7666	1.685	1.870
34	.04	.07	3.908	.6943	17.42	44.76	62.18	.0362	.2046	.0945	.0359	.4235	.7206	1.728	1.875
35	.04	.08	3.955	.691	15.0	44.75	59.75	.0399	.1863	.1053	.0413	.4664	.7053	1.764	1.867
36	.04	.09	3.921	.5480	13.19	44.75	57.94	.0543	.1169	.0744	.0528	.4831	.6627	1.791	1.876
37	.04	.10	3.921	.5807	11.79	44.75	56.54	.0896	.0862	.069	.0742	.507	.6279	1.841	1.843
38	.04	.12	3.921	.5760	9.74	44.75	54.49	.134	.0297	.0290	.1294	.4689	.6408	1.831	1.894
39	.04	.16	4.15	.8206	7.24	44.75	51.99	.1879	.01095	.0108	.2654	.4706	.6833	1.838	1.970
40	.02	.005	4.572	1.385	52.3	7.0	59.3	.005467	.6795	.00548	.0055	.30	.9957	1.56	1.878
41	.02	.01	4.389	1.316	51.76	14.5	66.26	.0106	.633	.0106	.0106	.2565	.9275	1.56	1.878
42	.02	.0125	4.30	1.372	51.23	18.8	70.03	.01286	.6658	.01291	.01291	.230	.893	1.565	1.877
43	.02	.015	4.205	1.476	50.73	23.66	74.39	.015	.704	.01497	.015	.198	.851	1.566	1.875
44	.02	.0175	4.04	1.503	50.29	29.67	79.96	.0169	.715	.01654	.0165	.148	.7627	1.569	1.872
45	.02	.02	3.828	1.51	41.51	41.51	83.02	.0141	.8996	.0251	.01425	.1221	(c)	1.577	1.867
									.524						
46	.02	.025	3.897	1.246	26.56	44.78	71.34	.01052	.5654	.0519	.01056	.2483	.8182	1.593	1.866
47	.02	.03	3.907	1.08	20.9	44.77	65.67	.00963	.468	.0692	.00946	.306	.8293	1.611	1.865
48	.02	.04	3.915	.849	15.0	44.75	59.75	.00884	.3345	.0894	.00874	.3785	.8066	1.634	1.864
49	.02	.06	3.922	.5769	9.735	44.75	54.49	.0097	.1926	.0974	.00974	.4673	.7327	1.733	1.863
50	.02	.08	3.908	.3406	7.238	44.75	51.99	.0159	.0921	.0609	.0149	.5217	.654	1.796	1.864
51	.02	.09	3.93	.2936	6.42	44.74	51.16	.0234	.0655	.0477	.0233	.542	.632	1.824	1.863
52	.02	.095	3.929	.2727	6.076	44.74	50.816	.03367	.04741	.0356	.0325	.547	.6194	1.835	1.864
53	.02	.10	3.903	.2896	5.768	44.74	50.51	.0598	.0257	.0258	.0478	.536	.6097	1.844	1.861
54	.02	.11	3.931	.2923	5.238	44.74	49.978	.0696	.0133	.0135	.0657	.522	.6226	1.841	1.888
55	.02	.12	3.99	.35	4.76	41.5	46.26	.086	.00856	.00847	.0926	.5217	.641	1.85	1.91
56	.01	.0025	4.357	1.412	52.71	6.973	59.68	.00243	.7006	.00243	.00243	.2156	.865	1.567	1.871
57	.01	.005	4.263	1.513	52.13	14.49	66.62	.004773	.7458	.00473	.00474	.1895	.828	1.568	1.871
58	.01	.00625	4.20	1.528	51.93	18.68	70.61	.00579	.7515	.00582	.00582	.1716	.799	1.569	1.87
59	.01	.0075	4.12	1.561	51.71	23.42	75.13	.00676	.8932	.00698	.00681	.1481	(c)	1.57	1.87
									.637						
60	.01	.00875	3.99	1.543	51.52	29.24	80.76	.00756	1.095(d)	.00762	.00762	.112	(c)	1.57	1.87
61	.01	.01	3.63	1.723	44.15	44.15	88.3	.00653	1.564	.0104	.00643	.0391	(c)	1.575	1.865
									.130						
62	.01	.0125	3.804	1.429	26.57	44.79	71.36	.00429	.690	.02492	.00420	.1876	.7734	1.579	1.865
63	.01	.015	3.834	1.295	20.904	44.77	65.67	.003514	.6155	.0346	.00354	.2308	.8195	1.584	1.864
64	.01	.02	3.882	1.243	15.0	44.75	59.75	.002926	.5762	.0521	.00286	.287	.8573	1.591	1.863
65	.01	.025	3.92	1.051	11.65	40.72	52.37	.00252	.465	.06834	.00253	.3378	.866	1.608	1.863
66	.01	.03	3.92	.930	9.686	42.16	51.846	.00237	.395	.0795	.00237	.366	.8464	1.628	1.86
67	.01	.035	3.93	.8587	8.264	42.33	50.59	.00227	.350	.0895	.00229	.393	.8328	1.646	1.862
68	.01	.04	3.907	.7361	7.239	44.75	51.99	.00228	.288	.0902	.00225	.4125	.798	1.67	1.86

σ₁, σ₂, σ₃, and σ₄ are negative real parts of roots of system characteristic equations.ω₁, ω₂, ω₃, and ω₄ are the damped frequencies associated with the respective σ's.

In cases where there are three, rather than four, complex conjugate pairs of roots, two negative roots (σ's) replace the fourth conjugate pair.

One of two real roots (see footnote c).

TABLE 5. - OPAQUENESS VERSUS RADIUS OF CURVATURE FOR
VARIOUS LENS MATERIALS

Lens material	Lens radius of curvature, ρ , in.	Wire diameter, in.	Wire spacing, in.	<u>Solid area</u> <u>total area,</u> μ
Material II	1 200			0.0151206010
	3 000			.0278523940
	5 000			.0391527050
	10 000			.0621510570
	20 000			.0986586700
	40 000			.1566108400
	80 000			.2486042500
	120 000			.3257639700
Material III	1 185	0.00034	0.04121	.0165129360
	3 767	.00078	.05000	.0313799840
	9 593	.00155	.06000	.0518231460
	19 158	.00260	.07000	.0741559480
	32 765	.00388	.08000	.0970203100
	50 435	.00538	.09000	.1195755100
	72 015	.00707	.10000	.1413402800
	119 911	.01049	.11800	.1778155200
Material IV	1 201	.00067	.30268	.0044102101
	3 808	.00151	.35000	.0086379920
	9 747	.00296	.40000	.0147858450
	20 528	.00505	.45000	.0224597730
	37 668	.00784	.50000	.0313799840
	62 463	.01135	.55000	.0412564140
	95 931	.01555	.60000	.0518231460
	120 492	.01840	.63000	.0583979930

TABLE 6. - WORKSHEET FOR CONFIGURATION A, 0° TO SUN LINE

Steady-State Errors							
Configuration A - Synchronous (0° to sun line)							
Conditions							
$I_{x-x} = \frac{7.82 \times 10^6}{\text{slug-ft}^2}$		$F = \frac{0.1}{0.08}$	$F'_{x0} = \frac{0}{\text{lb}}$				
$\omega_0^2 = \frac{52.82 \times 10^{-10}}{\text{rad/sec}^2}$		$D/F = \frac{0.8}{410 \text{ ft}}$	$F'_{x1} = \frac{-4.6 \times 10^{-6}}{\text{lb}}$				
$C_1 = \frac{-6.06 \times 10^{-4}}{\text{ft-lb}}$		$L = \frac{675 \text{ ft}}{0.512 \text{ in.}}$	$F'_{y0} = \frac{0}{\text{lb}}$				
		$r = \frac{0.512 \text{ in.}}{0.512 \text{ in.}}$	$F'_{y1} = \frac{3.9 \times 10^{-6}}{\text{lb}}$				
Type of Disturbance			Reference Figure	Normalizing Factor	Error, deg		
					θ	ϕ	ψ
1% Eccentricity			37 38		1.06°	0.02°	1.4°
Sinusoidal Torques	Pitch	$T''_{yB} = \frac{h \left(\frac{Lr}{300} \right) F'_{y1} \sin \omega_0 t}{I_{x-x} \omega_0^2}$	48 49	4.46×10^{-2}	(0.46) 2.05°	(0.05) 0.223°	(0.615) 2.74°
		$T''_{yS} = \frac{C_1 \sin 2\omega_0 t}{I_{x-x} \omega_0^2}$	42 43	1.47×10^{-2}	(0.26) 0.38°	(0.29) 0.42°	0
	Roll	$T''_{xB} = \frac{h \left(\frac{Lr}{300} \right) F'_{x1} \sin \omega_0 t}{I_{x-x} \omega_0^2}$	44 45 46	-5.26×10^{-2}	(0.055) 0.29°	(0.215) 1.13°	(0.27) 1.42°
		$T''_{xS} = 0$	44 45 46		0	0	0
	Constant Torques	$T''_{yB} = \frac{h \left(\frac{Lr}{300} \right) F'_{y0}}{I_{x-x} \omega_0^2}$	50		0	0	0
		$T''_{xB} = \frac{h \left(\frac{Lr}{300} \right) F'_{x0}}{I_{x-x} \omega_0^2}$	50		0	0	0
Summation of Errors					3.78°	1.79°	5.56°
RMS of Errors					2.1°	1.2°	3.1°

TABLE 7. - WORKSHEET FOR CONFIGURATION A, 45° TO SUN LINE

Steady-State Errors

Configuration A - Synchronous (45° to sun line)

Conditions

$$I_{x-x} = 7.82 \times 10^6 \text{ slug-ft}^2$$

$$\omega_0^2 = 52.82 \times 10^{-10} \text{ rad/sec}^2$$

$$C_1 = -6.06 \times 10^{-4} \text{ ft-lb}$$

$$F = 0.1$$

$$D = 0.08$$

$$D/F = 0.8$$

$$h = 410 \text{ ft}$$

$$L = 675 \text{ ft}$$

$$r = 0.512 \text{ in.}$$

$$F'_{x0} = 9.4 \times 10^{-6} \text{ lb}$$

$$F'_{x1} = -3.3 \times 10^{-6}$$

$$F'_{y0} = 4.2 \times 10^{-6}$$

$$F'_{y1} = 2.8 \times 10^{-6}$$

Type of Disturbance			Reference Figure	Normalizing Factor	Error, deg		
					θ	ϕ	ψ
1% Eccentricity			37 38		1.06°	0.02°	1.4°
Sinusoidal Torques	Pitch	$T''_{yB} = \frac{h \left(\frac{Lr}{300} \right) F'_{y1} \sin \omega_0 t}{I_{x-x} \omega_0^2}$	48 49	3.2×10^{-2}	(0.46) 1.47°	(0.05) 0.16°	(0.615) 1.97°
		$T''_{yS} = \frac{(C_1/2) \sin 2\omega_0 t}{I_{x-x} \omega_0^2}$	42 43	0.733×10^{-2}	(0.26) 0.19°	(0.29) 0.21°	0
	Roll	$T''_{xB} = \frac{h \left(\frac{Lr}{300} \right) F'_{x1} \sin \omega_0 t}{I_{x-x} \omega_0^2}$	44 45 46	-3.76×10^{-2}	(0.055) 0.21°	(0.215) 0.81°	(0.27) 1.01°
		$T''_{xS} = \frac{C_1 \cos \omega_0 t}{I_{x-x} \omega_0^2}$	44 45 46	1.47×10^{-2}	0.08°	0.32°	0.40°
Constant Torques		$T''_{yB} = \frac{h \left(\frac{Lr}{300} \right) F'_{y0}}{I_{x-x} \omega_0^2}$	50	4.81×10^{-2}	(0.33) 1.59°	(-0.065) -0.31°	0
		$T''_{xB} = \frac{h \left(\frac{Lr}{300} \right) F'_{x0}}{I_{x-x} \omega_0^2}$	50	10.75×10^{-2}	(0.015) -0.70°	(0.2) 2.15°	0
Summation of Errors					3.90°	3.36°	4.78°
RMS of Errors					(2.3°)	(2.36)	(2.25)

TABLE 8. - WORKSHEET FOR CONFIGURATION B, 0° TO SUN LINE

Steady-State Errors								
Configuration B - Synchronous (0° to sun line)								
Conditions								
$I_{x-x} = \frac{40.305 \times 10^3}{\text{slug-ft}^2}$		$F = \frac{0.12}{\text{}}$	$F'_{x0} = 0 \text{ lb}$					
$\omega_0^2 = \frac{52.88 \times 10^{-10}}{\text{rad/sec}^2}$		$D = \frac{0.10}{\text{}}$	$F'_{x1} = -4.6 \times 10^{-6}$					
$C_1 = \frac{22.4 \times 10^{-6}}{\text{ft-lb}}$		$D/F = \frac{0.833}{\text{}}$	$F'_{y0} = 0$					
		$h = \frac{160.5 \text{ ft}}{\text{}}$	$F'_{y1} = 3.9 \times 10^{-6}$					
		$L = \frac{300 \text{ ft}}{\text{}}$						
		$r = \frac{0.145 \text{ in.}}{\text{}}$						
Type of Disturbance			Reference Figure	Normalizing Factor	Error, deg			
					θ	ϕ	ψ	
1% Eccentricity			37 38		1.19°	0.14°	1.7°	
Sinusoidal Torques	Pitch	$T''_{yB} = \frac{h \left(\frac{Lr}{300} \right) F'_{y1} \sin \omega_0 t}{I_{x-x} \omega_0^2}$	48 49	42.6 x 10 ⁻²	(0.51) 21.7°	(0.08) 3.4°	(0.73) 31.1°	
		$T''_{yS} = \frac{C_1 \sin 2\omega_0 t}{I_{x-x} \omega_0^2}$	42 43	10.51 x 10 ⁻²	(0.225) 2.37°	(0.275) 2.9°	0	
	Roll	$T''_{xB} = \frac{h \left(\frac{Lr}{300} \right) F'_{x1} \sin \omega_0 t}{I_{x-x} \omega_0^2}$	44 45 46	-50.3 x 10 ⁻²	(0.065) 3.27°	(0.215) 10.8°	(0.275) 13.8°	
		$T''_{xS} = 0$	44 45 46		0	0	0	
	Constant Torques	$T''_{yB} = \frac{h \left(\frac{Lr}{300} \right) F'_{y0}}{I_{x-x} \omega_0^2}$	50		0	0	0	
		$T''_{xB} = \frac{h \left(\frac{Lr}{300} \right) F'_{x0}}{I_{x-x} \omega_0^2}$	50		0	0	0	
	Summation of Errors					28.5°	17.2°	46.6°
	RMS of Errors					22.1°	11.7°	34.0°

TABLE 9. - WORKSHEET FOR CONFIGURATION B, 45° TO SUN LINE

Steady-State Errors

Configuration B - Synchronous (45° to sun line)

Conditions

$$I_{x-x} = 40.305 \times 10^3 \text{ slug-ft}^2$$

$$\omega_0^2 = 52.88 \times 10^{-10} \text{ rad/sec}^2$$

$$C_1 = 22.4 \times 10^{-6} \text{ ft-lb}$$

$$F = 0.12$$

$$D = 0.10$$

$$D/F = 0.833$$

$$h = 160.5 \text{ ft}$$

$$L = 300 \text{ ft}$$

$$r = 0.145 \text{ in.}$$

$$F'_{x0} = 9.4 \times 10^{-6} \text{ lb}$$

$$F'_{x1} = -3.3 \times 10^{-6}$$

$$F'_{y0} = 4.2 \times 10^{-6}$$

$$F'_{y1} = 2.8 \times 10^{-6}$$

Type of Disturbance			Reference Figure	Normalizing Factor	Error, deg		
					θ	ϕ	ψ
1% Eccentricity			37 38		1.19°	0.14°	1.7°
Sinusoidal Torques	Pitch	$T''_{yB} = \frac{h \left(\frac{Lr}{300} \right) F'_{y1} \sin \omega_0 t}{I_{x-x} \omega_0^2}$	48 49	30.6×10^{-2}	(0.51) 15.6°	(0.08) 2.45°	(0.73) 22.4°
		$T''_{yS} = \frac{(C_1/2) \sin 2\omega_0 t}{I_{x-x} \omega_0^2}$	42 43	5.25×10^{-2}	(0.225) 1.18°	(0.275) 1.44°	0
	Roll	$T''_{xB} = \frac{h \left(\frac{Lr}{300} \right) F'_{x1} \sin \omega_0 t}{I_{x-x} \omega_0^2}$	44 45 46	-36.1×10^{-2}	(0.065) 2.34°	(0.215) 7.75°	(0.275) 9.9°
		$T''_{xS} = \frac{C_1 \cos \omega_0 t}{I_{x-x} \omega_0^2}$	44 45 46	10.5×10^{-2}	0.68°	2.26°	2.89°
Constant Torques	$T''_{yB} = \frac{h \left(\frac{Lr}{300} \right) F'_{y0}}{I_{x-x} \omega_0^2}$	50	46×10^{-2}	(0.365) 16.8°	(-0.083) -3.8°	0	
	$T''_{xB} = \frac{h \left(\frac{Lr}{300} \right) F'_{x0}}{I_{x-x} \omega_0^2}$	50	103×10^{-2}	(-0.083) -8.5°	(0.215) 22.1°	0	
Summation of Errors					29.3°	32.34°	36.89°
RMS of Errors					(24.6)	(24.0)	(24.6)

TABLE 10. - WORKSHEET FOR CONFIGURATION C, 0° TO SUN LINE

Steady-State Errors							
Configuration <u>C - 2000 N.Mi. (0° to sun line)</u>							
Conditions							
$I_{x-x} = \underline{12.036 \times 10^6}$ slug-ft ²		$F = \underline{0.008}$	$F'_{x0} = \underline{0}$ lb				
$\omega_0^2 = \underline{38.94 \times 10^{-8}}$ rad/sec ²		$D = \underline{0.006}$	$F'_{x1} = \underline{-4.6 \times 10^{-6}}$				
$C_1 = \underline{-15.9 \times 10^{-4}}$ ft-lb		$D/F = \underline{0.75}$	$F'_{y0} = \underline{0}$				
		$h = \underline{680}$ ft	$F'_{y1} = \underline{3.9 \times 10^{-6}}$				
		$L = \underline{330}$ ft					
		$r = \underline{0.531}$ in.					
Type of Disturbance			Reference Figure	Normalizing Factor	Error, deg		
					θ	ϕ	ψ
1% Eccentricity			37 38		0.8	0	0.06°
Sinusoidal Torques	Pitch	$T''_{yB} = \frac{h \left(\frac{Lr}{300} \right) F'_{y1} \sin \omega_0 t}{I_{x-x} \omega_0^2}$	48 49	0.033 x 10 ⁻²	(0.39) 0.013°	0	(0.01) 0
		$T''_{yS} = \frac{C_1 \sin 2\omega_0 t}{I_{x-x} \omega_0^2}$	42 43	0.0339 x 10 ⁻²	(0.37) 0.0125°	(0.015) 0	0
	Roll	$T''_{xB} = \frac{h \left(\frac{Lr}{300} \right) F'_{x1} \sin \omega_0 t}{I_{x-x} \omega_0^2}$	44 45 46	0.0388 x 10 ⁻²	(0.005) 0	(0.228) 0.0077	(0.225) 0.0076
		$T''_{xS} = 0$	44 45 46		0	0	0
	Constant Torques	$T''_{yB} = \frac{h \left(\frac{Lr}{300} \right) F'_{y0}}{I_{x-x} \omega_0^2}$	50		0	0	0
		$T''_{xB} = \frac{h \left(\frac{Lr}{300} \right) F'_{x0}}{I_{x-x} \omega_0^2}$	50		0	0	0
Summation of Errors					0.83°	0.008°	0.068°
RMS of Errors					0.018°	0.008°	0.008°

TABLE 11. - WORKSHEET FOR CONFIGURATION C, 45° TO SUN LINE

Steady-State Errors							
Configuration C - 2000 N.Mi. (45° to sun line)							
Conditions							
$I_{x-x} = 12.036 \times 10^6$ slug-ft ²		$F = 0.008$	$F'_{x0} = 9.4 \times 10^{-6}$ lb				
$\omega_0^2 = 38.94 \times 10^{-8}$ rad/sec ²		$D = 0.006$	$F'_{x1} = -3.3 \times 10^{-6}$				
$C_1 = -15.9 \times 10^{-4}$ ft-lb		$D/F = 0.75$	$F'_{y0} = 4.2 \times 10^{-6}$				
		$h = 680$ ft	$F'_{y1} = 2.8 \times 10^{-6}$				
		$L = 330$ ft					
		$r = 0.531$ in.					
Type of Disturbance			Reference Figure	Normalizing Factor	Error, deg		
					θ	ϕ	ψ
1% Eccentricity			37 38		0.8°	0	0.06°
Sinusoidal Torques	Pitch	$T''_{yB} = \frac{h \left(\frac{Lr}{300} \right) F'_{y1} \sin \omega_0 t}{I_{x-x} \omega_0^2}$	48 49	0.0242 x 10 ⁻²	(0.39) 0.009°	0	(0.01) 0
		$T''_{yS} = \frac{(C_1/2) \sin 2\omega_0 t}{I_{x-x} \omega_0^2}$	42 43	0.017 x 10 ⁻²	(0.37) 0.006°	(0.015) 0	0
	Roll	$T''_{xB} = \frac{h \left(\frac{Lr}{300} \right) F'_{x1} \sin \omega_0 t}{I_{x-x} \omega_0^2}$	44 45 46	0.0285 x 10 ⁻²	(0.005) 0	(0.228) 0.0065	(0.225) 0.0064
		$T''_{xS} = \frac{C_1 \cos \omega_0 t}{I_{x-x} \omega_0^2}$	44 45 46	0.034 x 10 ⁻²	0	0.008°	0.008°
Constant Torques		$T''_{yB} = \frac{h \left(\frac{Lr}{300} \right) F'_{y0}}{I_{x-x} \omega_0^2}$	50	0.036 x 10 ⁻²	(0.240) 0.009°	(0.01) 0	0
		$T''_{xB} = \frac{h \left(\frac{Lr}{300} \right) F'_{x0}}{I_{x-x} \omega_0^2}$	50	0.081 x 10 ⁻²	(-0.01) 0	(0.18) 0.014°	0
Summation of Errors					0.82°	0.03°	0.07°
RMS of Errors					0.014°	0.017°	0.012°

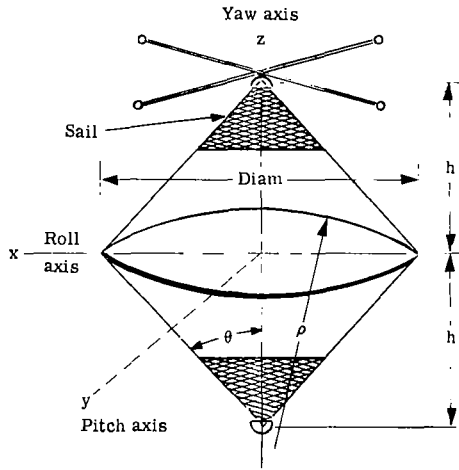
TABLE 12. - WORKSHEET FOR CONFIGURATION E, 0° TO SUN LINE

Steady-State Errors							
Configuration <u>E - 6000 N. Mi. (0° to sun line)</u>							
Conditions							
$I_{x-x} = 2.866 \times 10^6$ slug-ft ²		$F = 0.02$	$F'_{x0} = 0$ lb				
$\omega_0^2 = 7.399 \times 10^{-8}$ rad/sec ²		$D = 0.015$	$F'_{x1} = -4.6 \times 10^{-6}$				
$C_1 = -10.35 \times 10^{-4}$ ft-lb		$D/F = 0.75$	$F'_{y0} = 0$				
		$h = 400$ ft	$F'_{y1} = 3.9 \times 10^{-6}$				
		$L = 330$ ft					
		$r = 0.45$ in.					
Type of Disturbance			Reference Figure	Normalizing Factor	Error, deg		
					θ	ϕ	ψ
1% Eccentricity			37 38		0.8°	0.02°	0.20°
Sinusoidal Torques	Pitch	$T''_{yB} = \frac{h \left(\frac{Lr}{300} \right) F'_{y1} \sin \omega_0 t}{I_{x-x} \omega_0^2}$	48 49	0.364 x 10 ⁻²	(0.39) 0.142°	(0.01) 0.004°	(0.09) 0.033°
		$T''_{yS} = \frac{C_1 \sin 2\omega_0 t}{I_{x-x} \omega_0^2}$	42 43	-0.488 x 10 ⁻²	(0.368) 0.18°	(0.053) 0.026°	0
	Roll	$T''_{xB} = \frac{h \left(\frac{Lr}{300} \right) F'_{x1} \sin \omega_0 t}{I_{x-x} \omega_0^2}$	44 45 46	-0.43 x 10 ⁻²	(0.01) 0.004°	(0.23) 0.099°	(0.225) 0.096°
		$T''_{xS} = 0$	44 45 46		0	0	0
	Constant Torques	$T''_{yB} = \frac{h \left(\frac{Lr}{300} \right) F'_{y0}}{I_{x-x} \omega_0^2}$	50		0	0	0
		$T''_{xB} = \frac{h \left(\frac{Lr}{300} \right) F'_{x0}}{I_{x-x} \omega_0^2}$	50		0	0	0
Summation of Errors					1.13°	0.15°	0.33°
RMS of Errors					0.23°	0.10°	0.10°

TABLE 13. - WORKSHEET FOR CONFIGURATION E, 45° TO SUN LINE

Steady-State Errors							
Configuration E - 6000 N.Mi. (45° to sun line)							
Conditions							
$I_{x-x} = \underline{2.866 \times 10^6}$ slug-ft ²		$F = \underline{0.02}$	$F'_{x0} = \underline{9.4 \times 10^{-6}}$ lb				
$\omega_0^2 = \underline{7.399 \times 10^{-8}}$ rad/sec ²		$D = \underline{0.015}$	$F'_{x1} = \underline{-3.3 \times 10^{-6}}$				
$C_1 = \underline{-10.35 \times 10^{-4}}$ ft-lb		$D/F = \underline{0.75}$	$F'_{y0} = \underline{4.2 \times 10^{-6}}$				
		$h = \underline{400}$ ft	$F'_{y1} = \underline{2.8 \times 10^{-6}}$				
		$L = \underline{330}$ ft					
		$r = \underline{0.45}$ in.					
Type of Disturbance		Reference Figure	Normalizing Factor	Error, deg			
				θ	ϕ	ψ	
1% Eccentricity		37 38		0.8°	0.02°	0.20°	
Sinusoidal Torques	Pitch	$T''_{yB} = \frac{h \left(\frac{Lr}{300} \right) F'_{y1} \sin \omega_0 t}{I_{x-x} \omega_0^2}$	48 49	0.26 x 10 ⁻²	(0.39) 0.1°	(0.005) 0	(0.09) 0.02°
		$T''_{yS} = \frac{(C_1/2) \sin 2\omega_0 t}{I_{x-x} \omega_0^2}$	42 43	-0.24 x 10 ⁻²	(0.368) 0.09°	(0.053) 0.01°	0
	Roll	$T''_{xB} = \frac{h \left(\frac{Lr}{300} \right) F'_{x1} \sin \omega_0 t}{I_{x-x} \omega_0^2}$	44 45 46	-0.307 x 10 ⁻²	(0.01) 0	(0.23) 0.07°	(0.225) 0.07°
		$T''_{xS} = \frac{C_1 \cos \omega_0 t}{I_{x-x} \omega_0^2}$	44 45 46	-0.49 x 10 ⁻²	0	0.11°	0.11°
	Constant Torques	$T''_{yB} = \frac{h \left(\frac{Lr}{300} \right) F'_{y0}}{I_{x-x} \omega_0^2}$	50	0.391 x 10 ⁻²	(0.24) 0.09°	(-0.01) 0	0
		$T''_{xB} = \frac{h \left(\frac{Lr}{300} \right) F'_{x0}}{I_{x-x} \omega_0^2}$	50	0.875 x 10 ⁻²	(-0.01) -0.01°	(0.18) 0.16°	0
Summation of Errors				1.07°	0.37°	0.39°	
RMS of Errors			(125)	0.16°	0.21°	0.13°	

TABLE 14. - SUMMARY OF STABILIZATION ERROR ANALYSIS AND TRANSIENT DAMPING CAPABILITY

			Parameters	Configuration A, synchronous altitude. large size	Configuration B, synchronous altitude. small size	Configuration C, 2000 n.mi. altitude.	Configuration E, 6000 n.mi. altitude.	
			Lens half angle, θ , degrees	10.67	10.67	42	23.6	
			Lens radius of curvature, ρ , ft	1280	438	438	600	
			Lens diameter, ft	473	161.9	586	480	
			Tetrapod boom height, h, ft	410	160.5	680	400	
			Roll and pitch axis inertia, $I_{x-x} = I_{y-y}$, slug-ft ²	78.2×10^5	40.4×10^3	12.04×10^6	28.66×10^5	
			Yaw axis inertia, I_{z-z} , slug-ft ²	6.336×10^5	2.18×10^3	2×10^6	4.359×10^5	
			Package launch weight, lb	3636.7	211.5	3551.7	2256.5	
			Lensat orbital weight, lb	2380.6	89.3	1771.9	1116.6	
			Stabilization system weight, lb	269.1	8.3	130.1	98.9	
			Damper boom inertia, I_F , slug-ft ²	7.82×10^5	4.84×10^3	9.5×10^4	5.73×10^4	
			Damper boom half-length, ft	675	300	330	330	
			Damper boom diameter, in.	1.024	0.29	1.06	0.9	
STABILIZATION SYSTEM PERFORMANCE	Decay Time of Transient Attitude Errors of Least-Damped Mode		Number of orbits to achieve 95% transient decay	4.2	3.1	120	31	
			Time required to achieve 95% transient decay Days	4.2	3.1	14	8.3	
	STEADY-STATE ERRORS	Sensitivity to orbital eccentricity stabilization error caused by 1% eccentricity of orbit, degrees	Pitch	1.06	1.19	0.8	0.8	
			Roll	0.02	0.14	---	0.02	
			Yaw	1.4	1.7	0.06	0.2	
		Stabilization Errors Caused by Solar Pressure Torques	Sun located in the orbital plane	Pitch	2.1	22.1	0.018	0.23
				Roll	1.2	11.7	0.008	0.10
				Yaw	3.1	34.0	0.008	0.10
			Sun inclined 45° to the orbital plane	Pitch	2.3	24.6	0.014	0.16
				Roll	2.36	24.0	0.017	0.21
	Yaw			2.25	24.6	0.012	13.0	

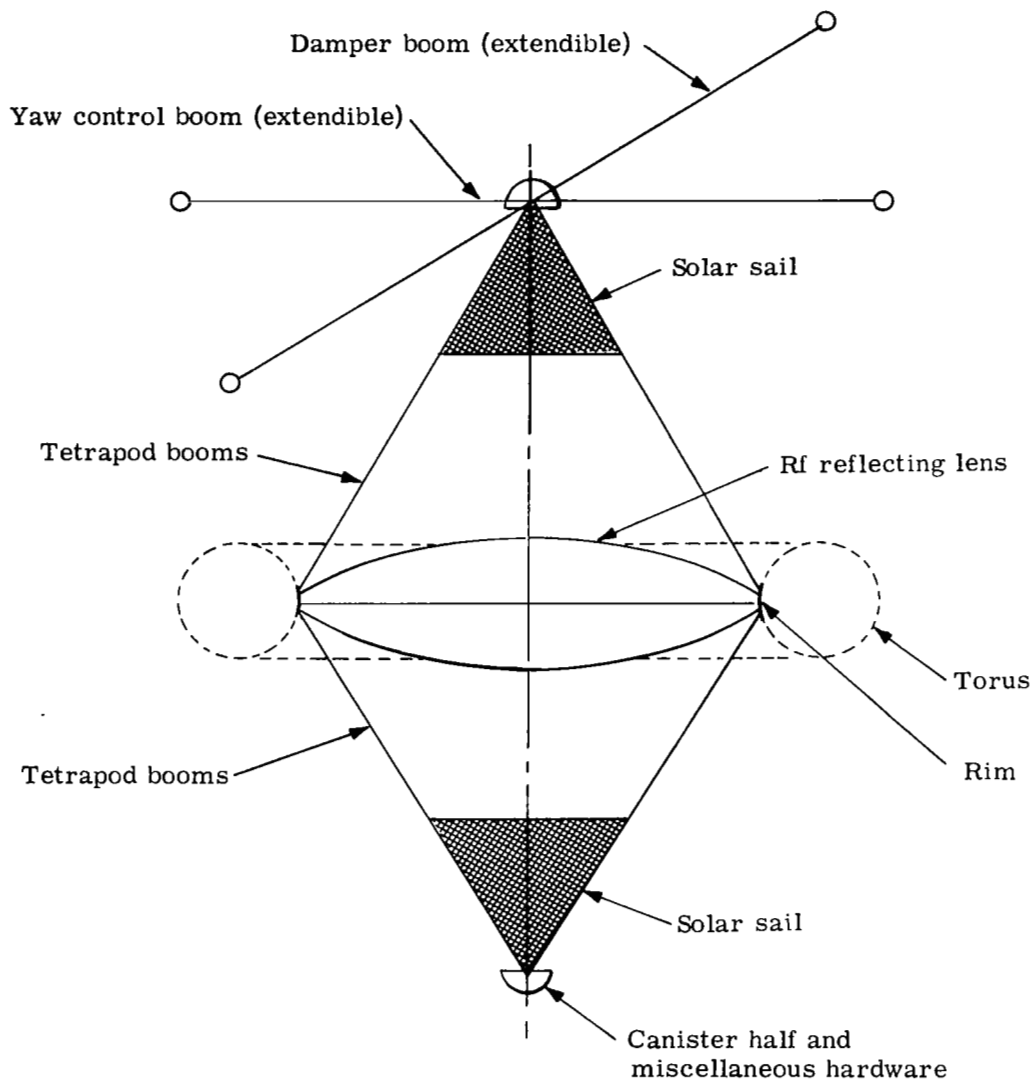
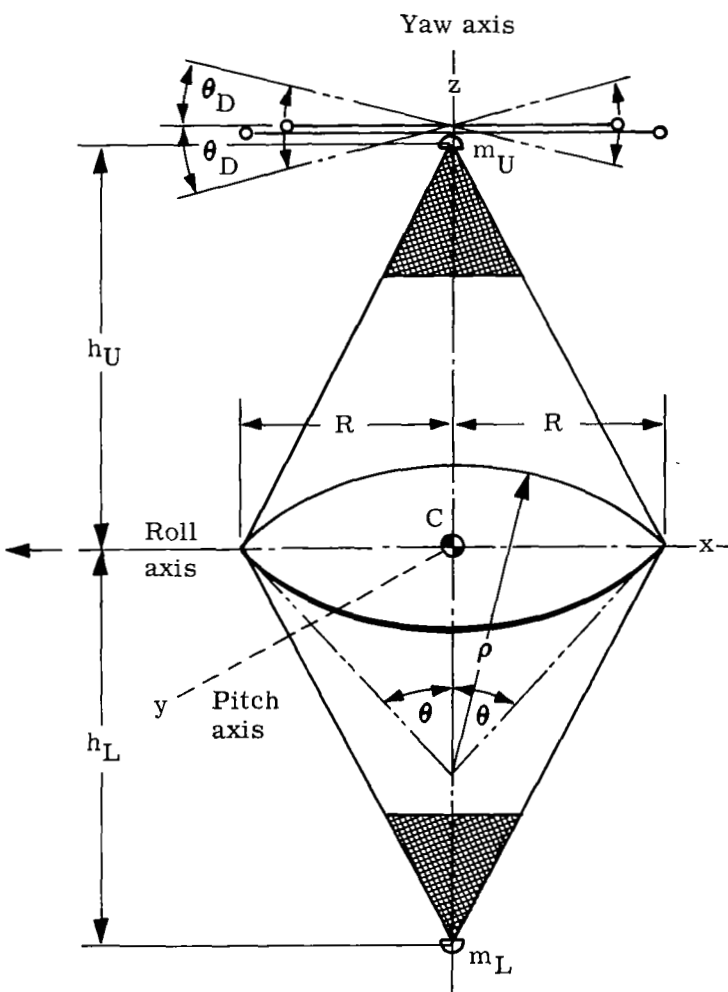


Figure 1. - Schematic of lenticular satellite with gravity-gradient stabilization.


$$\begin{aligned}\phi &= \text{Roll angle} \\ \theta &= \text{Pitch angle} \\ \psi &= \text{Yaw angle}\end{aligned}$$
$$\left. \begin{array}{l} I_{x-x} \\ I_{y-y} \\ I_{z-z} \end{array} \right\} \begin{array}{l} \text{Moment of inertia} \\ \text{of the satellite} \\ \text{about c.g.} \end{array}$$

M = Satellite mass
 M_D = Damper mass
 I_D = Moment of inertia of
the damper about
its center
 M_F = Mass of fixed boom
 I_F = Moment of inertia of
fixed boom about its
center

50

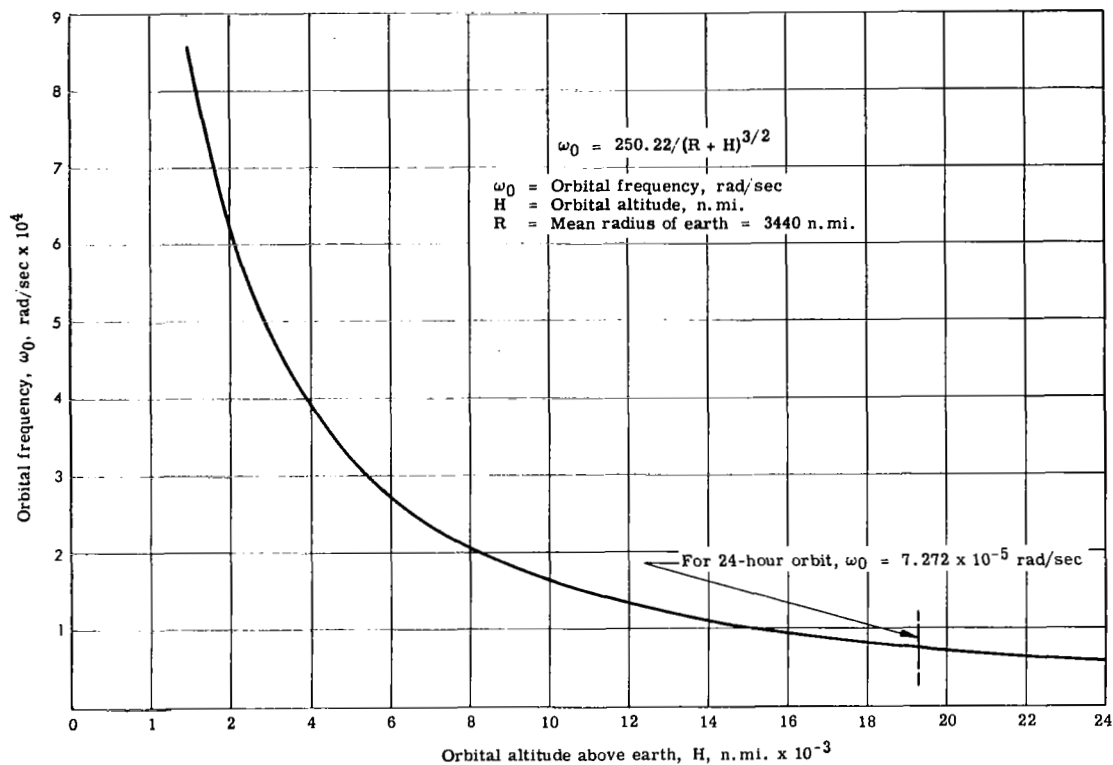


Figure 3. - Satellite orbital frequency as a function of orbital altitude.

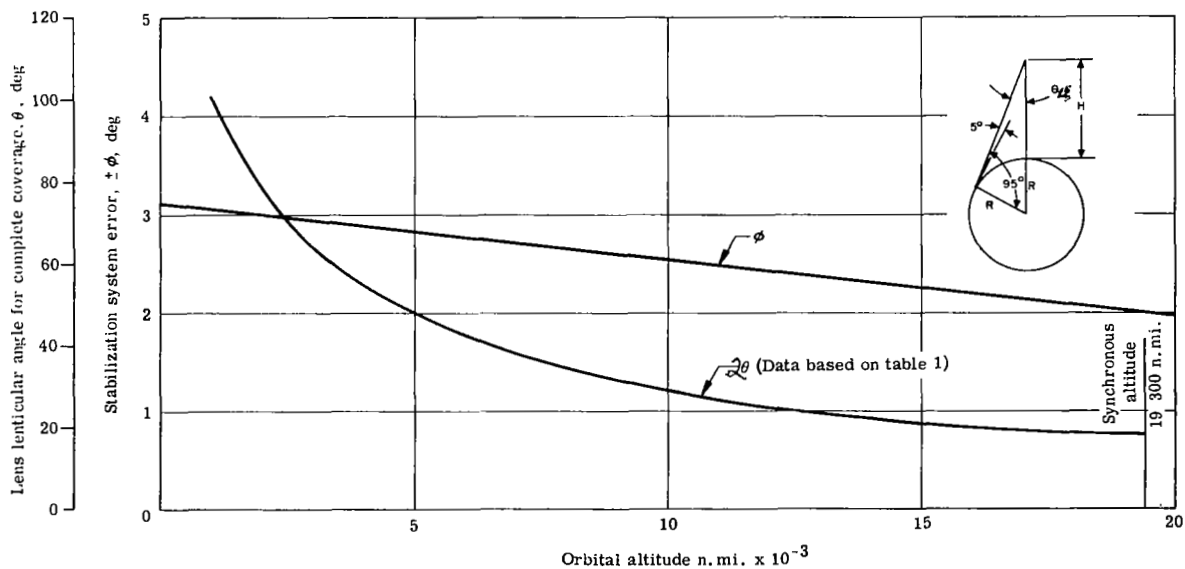


Figure 4. - Lens lenticular angle for horizon-to-horizon coverage and stabilization system error as a function of orbital altitude.

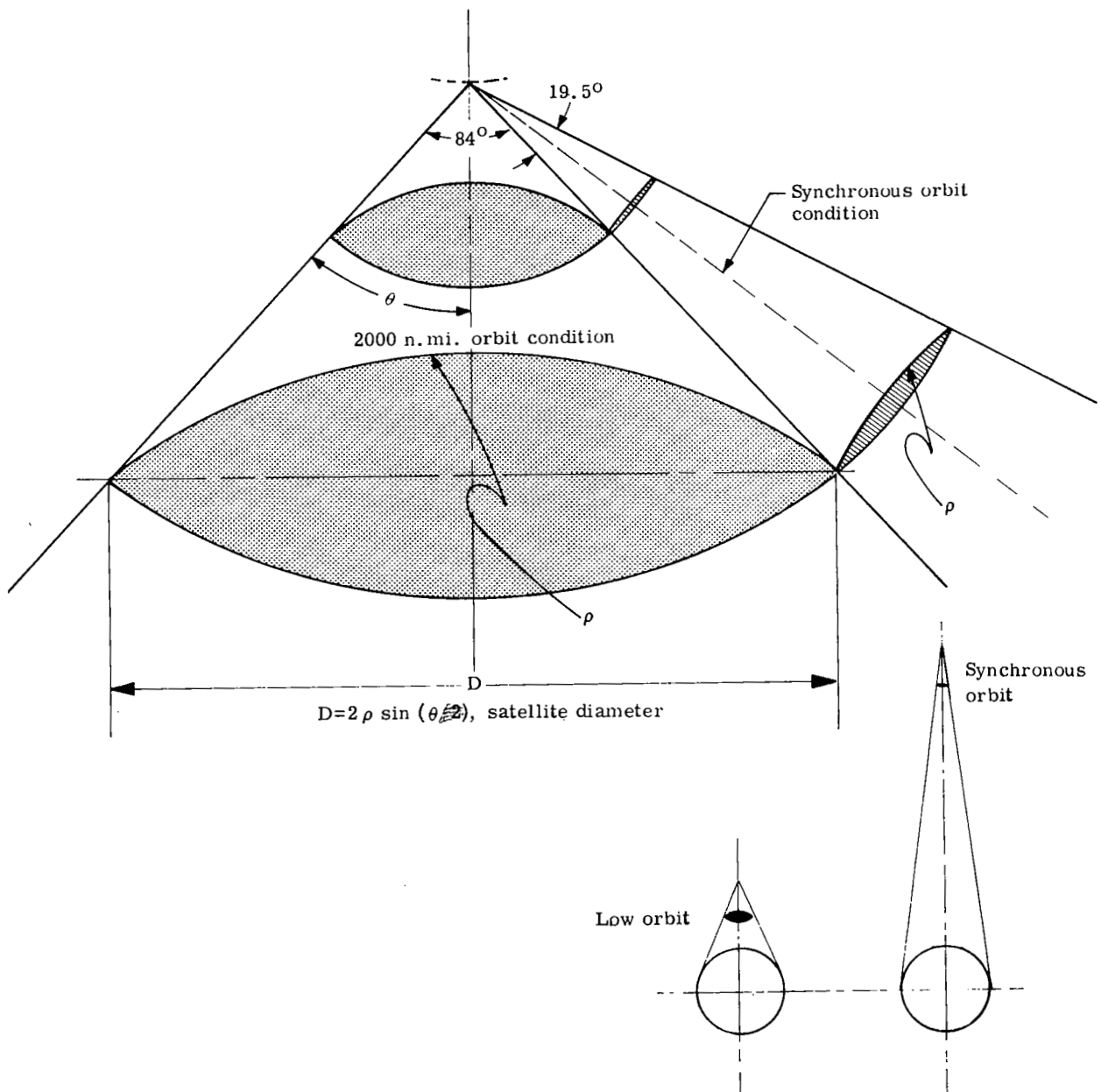


Figure 5. - Effect of lens radius of curvature and lenticular angle on satellite size.

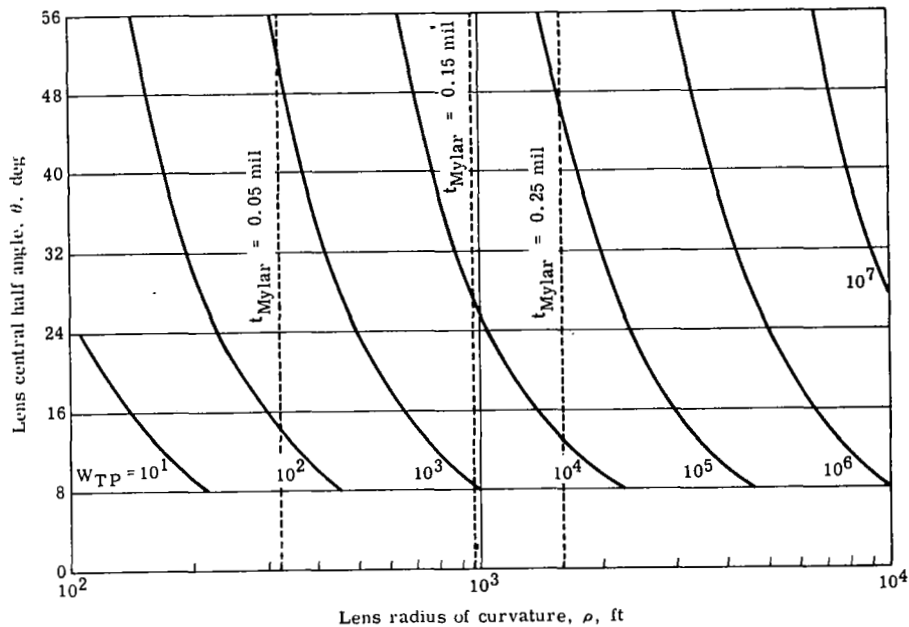


Figure 6. - Lens central half angle versus radius of curvature for various satellite weights - lens material I. (The weight W_{TP} , includes the lens, torus, canister, and inflation system.)

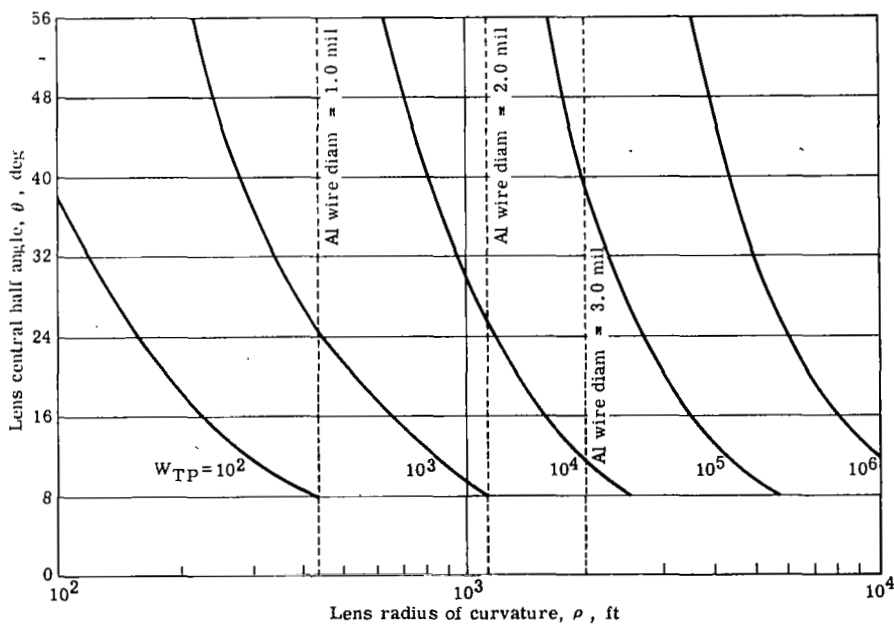


Figure 7. - Lens central half angle versus radius of curvature for various satellite weights - lens material III. (The weight, W_{TP} , includes the lens, torus, canister, and inflation system.)

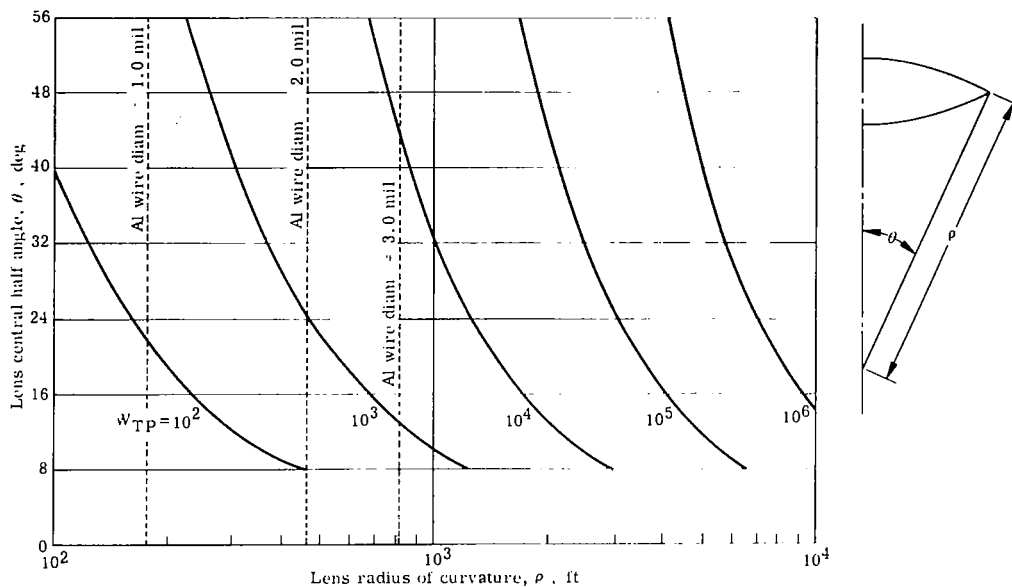


Figure 8. - Lens central half angle versus radius of curvature for various satellite weights - lens material IV. (The weight, W_{TP} includes the lens, torus, canister, and inflation system.)

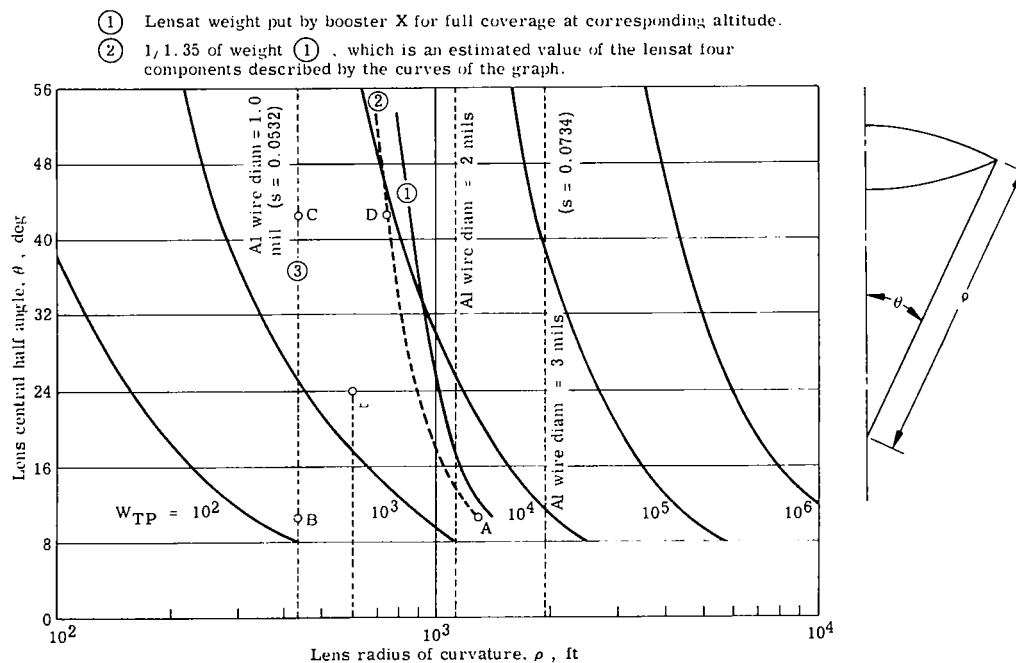


Figure 9. - Definition of lens half angle and radius of curvature for representative satellite configurations based on material III characteristics and contemplated launch boosters.

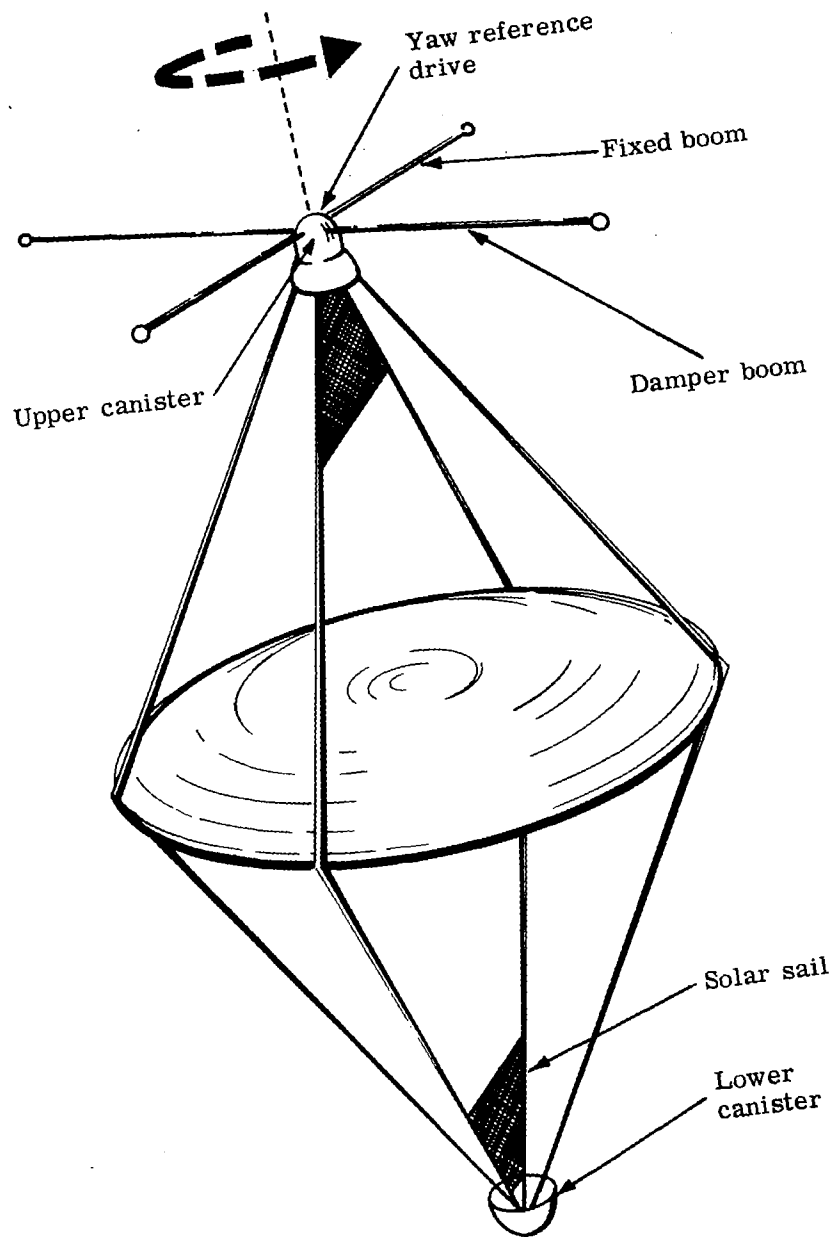


Figure 10. - Gravity-gradient stabilization system with solar sails and yaw controller.

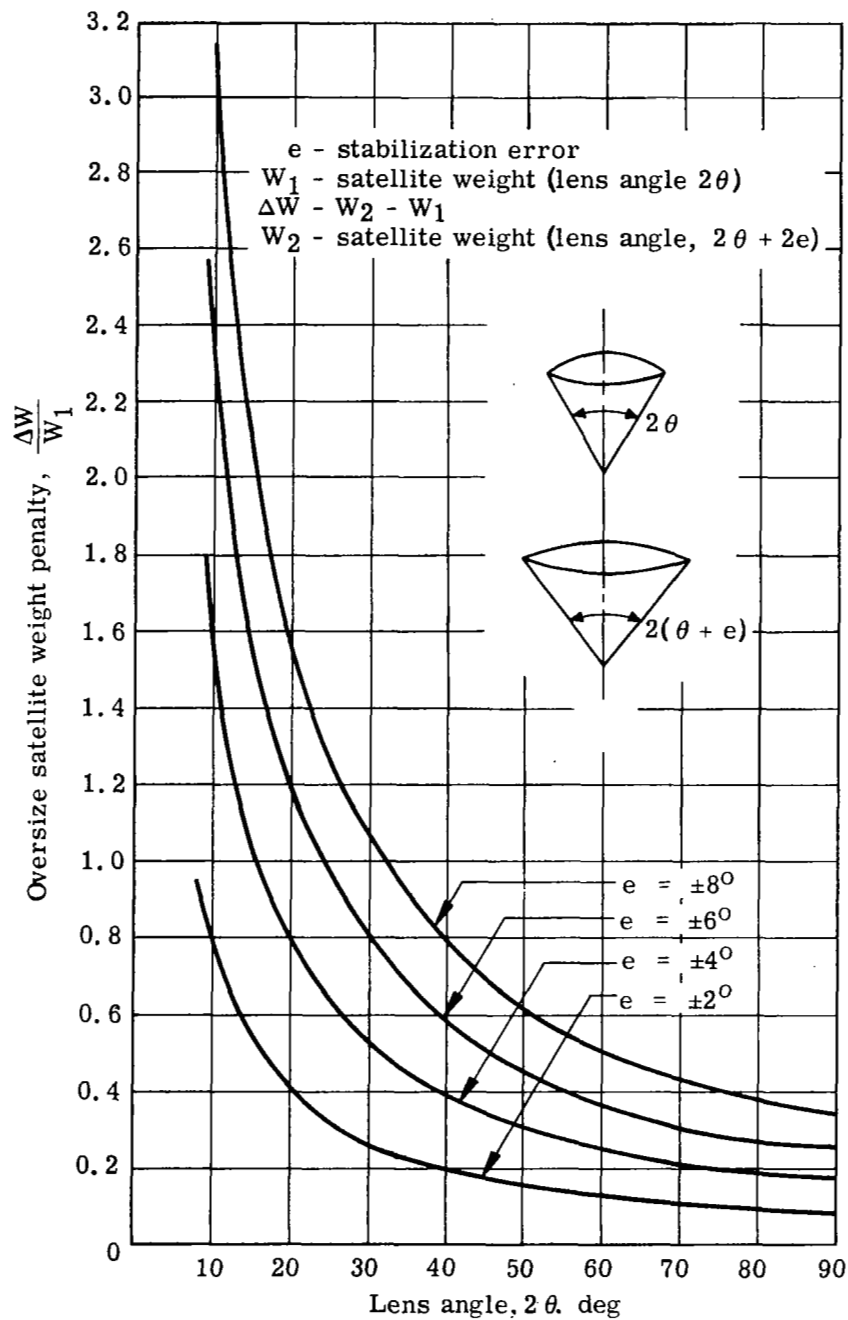


Figure 11. - Weight penalty of oversize lens angle to offset stabilization error.

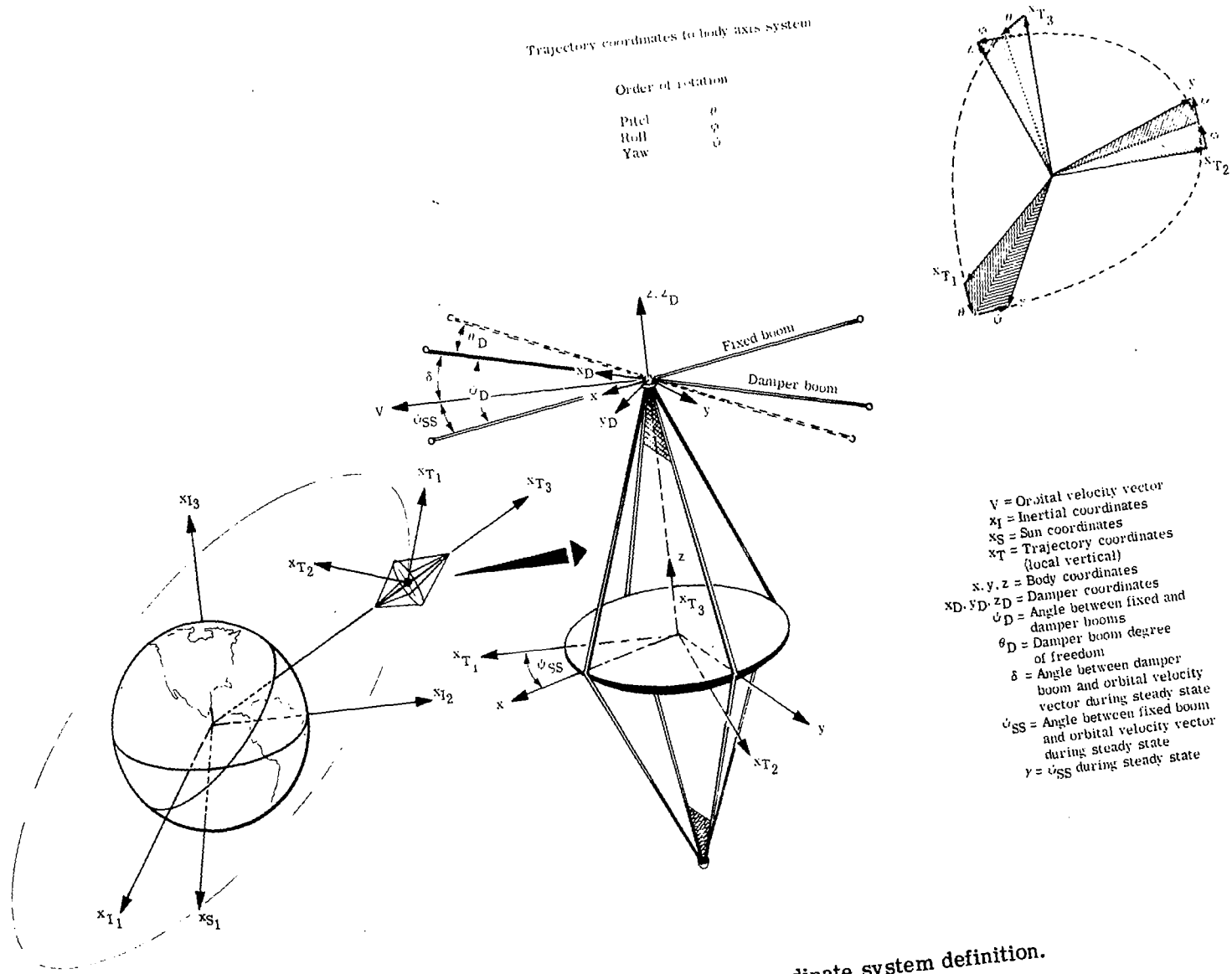


Figure 12. - Stabilization system axes and coordinate system definition.

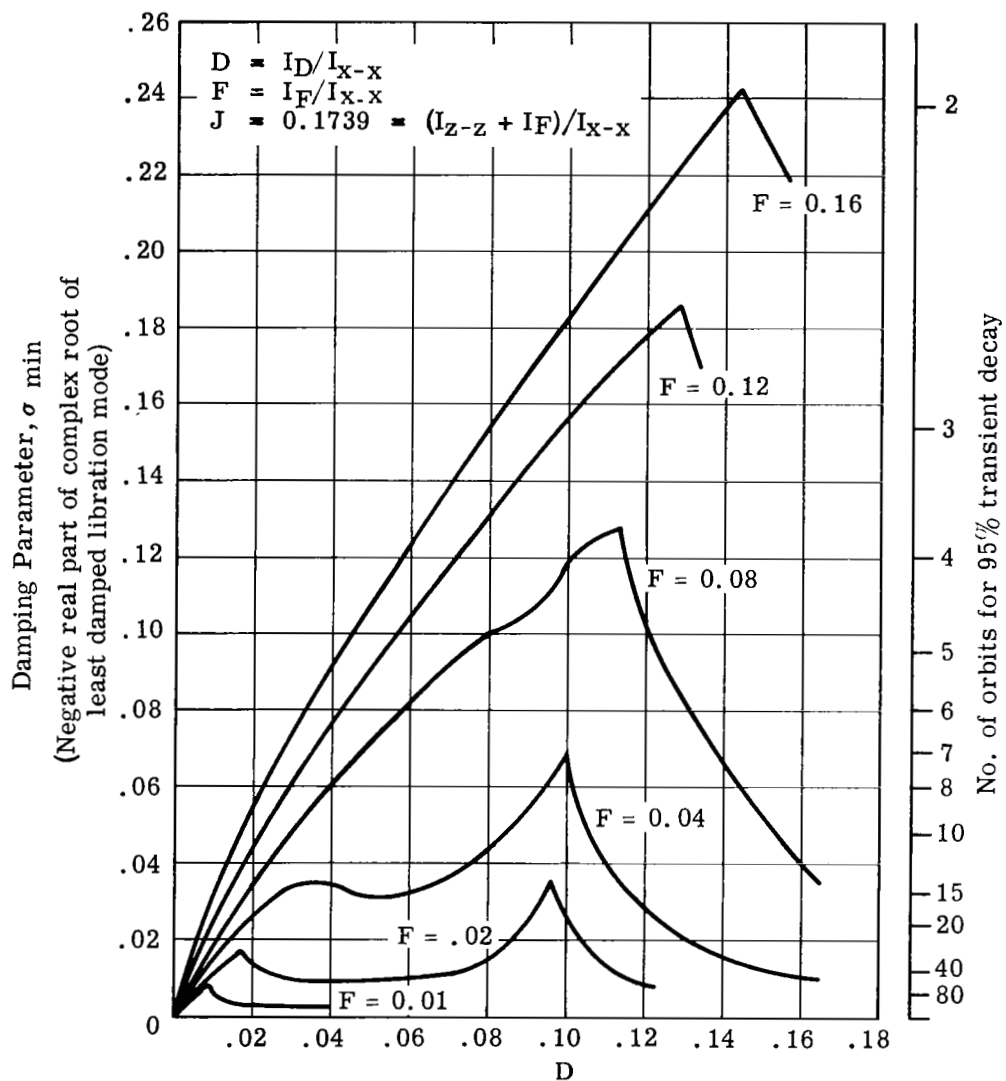


Figure 13. - Optimum transient response as function of boom inertias.

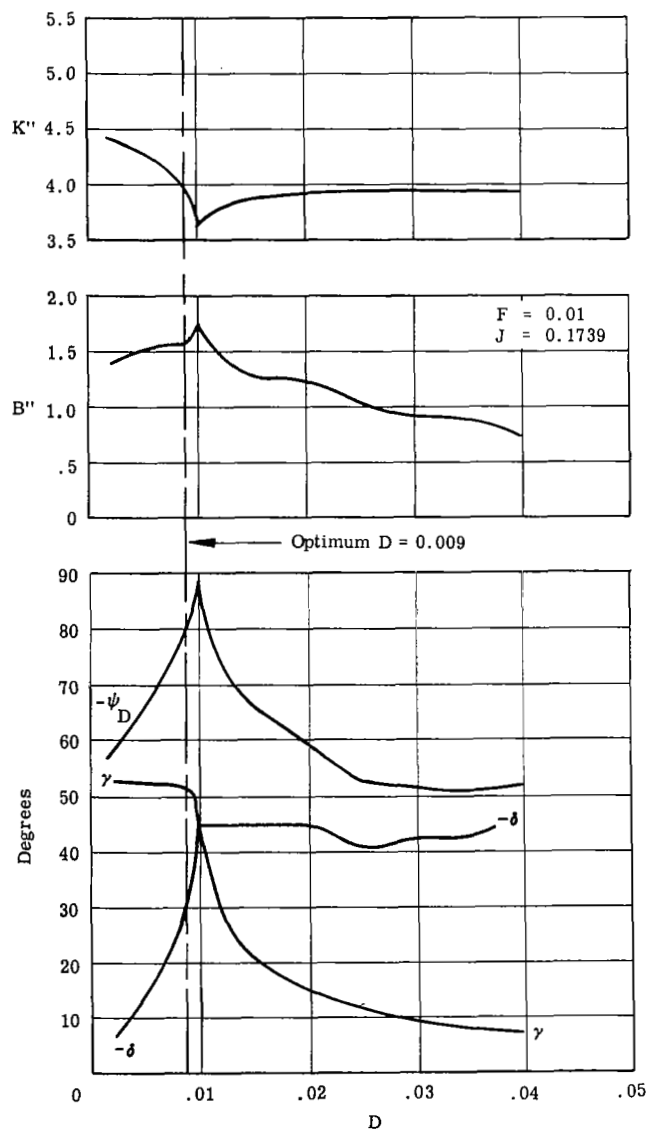


Figure 14. - Damper system parameters associated with $F = 0.01$.

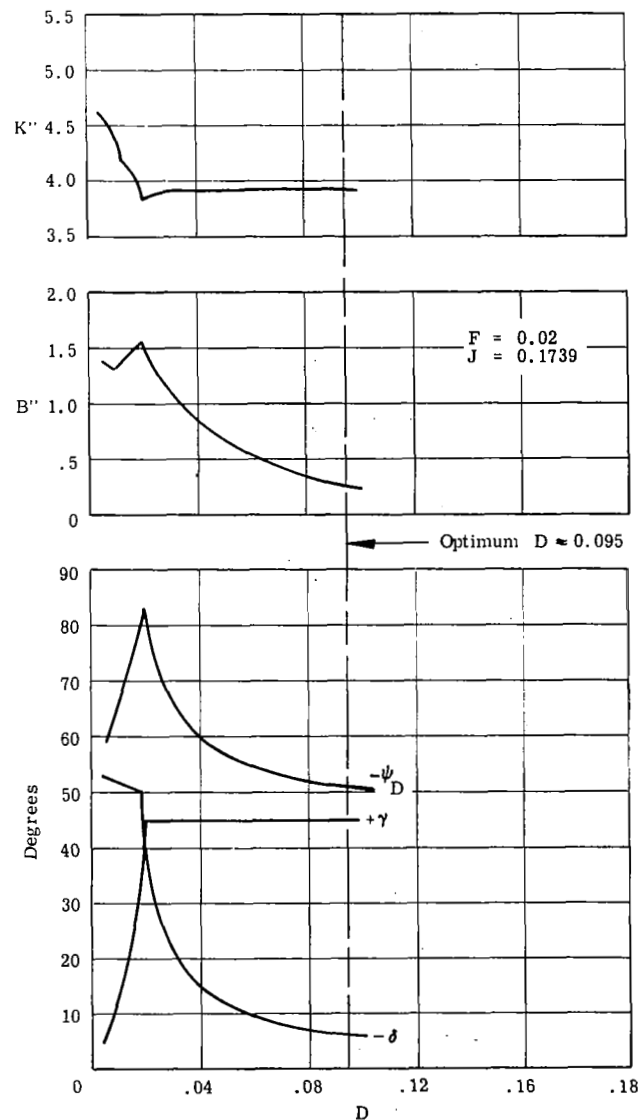


Figure 15. - Damper system parameters associated with $F = 0.02$.

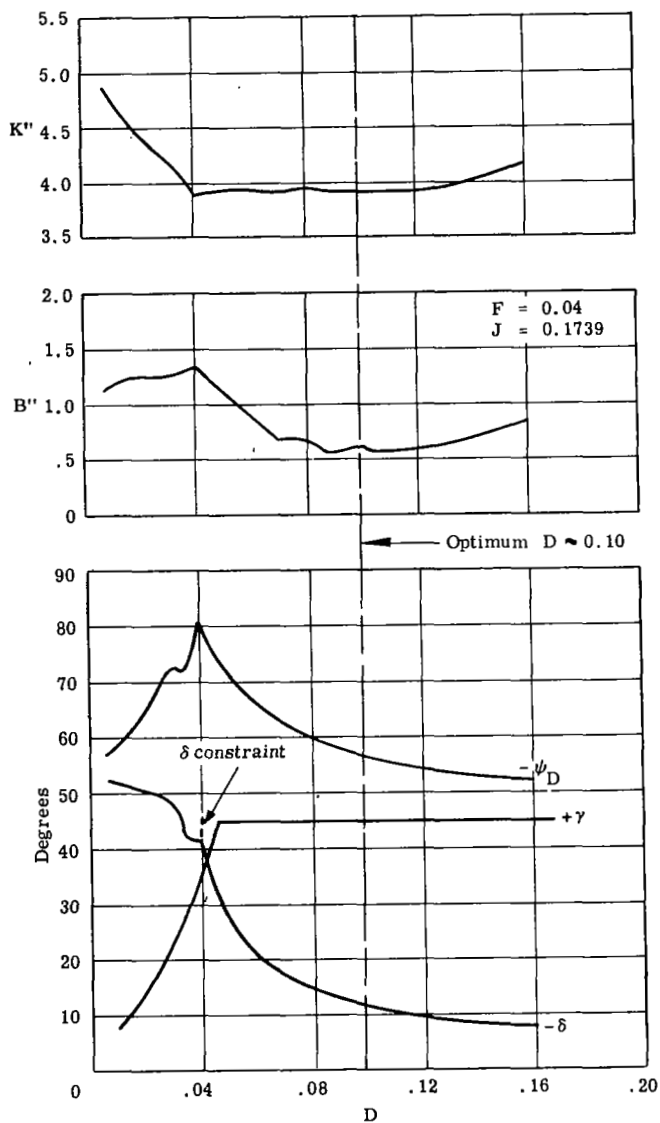


Figure 16. - Damper system parameters associated with $F = 0.04$.

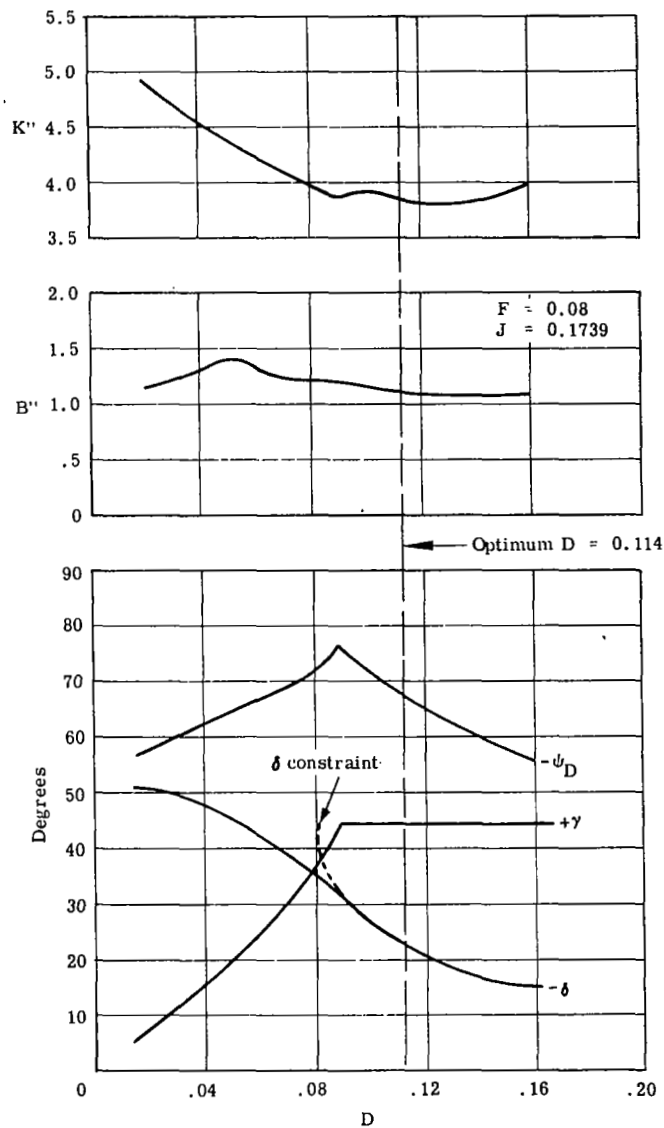


Figure 17. - Damper system parameters associated with $F = 0.08$.

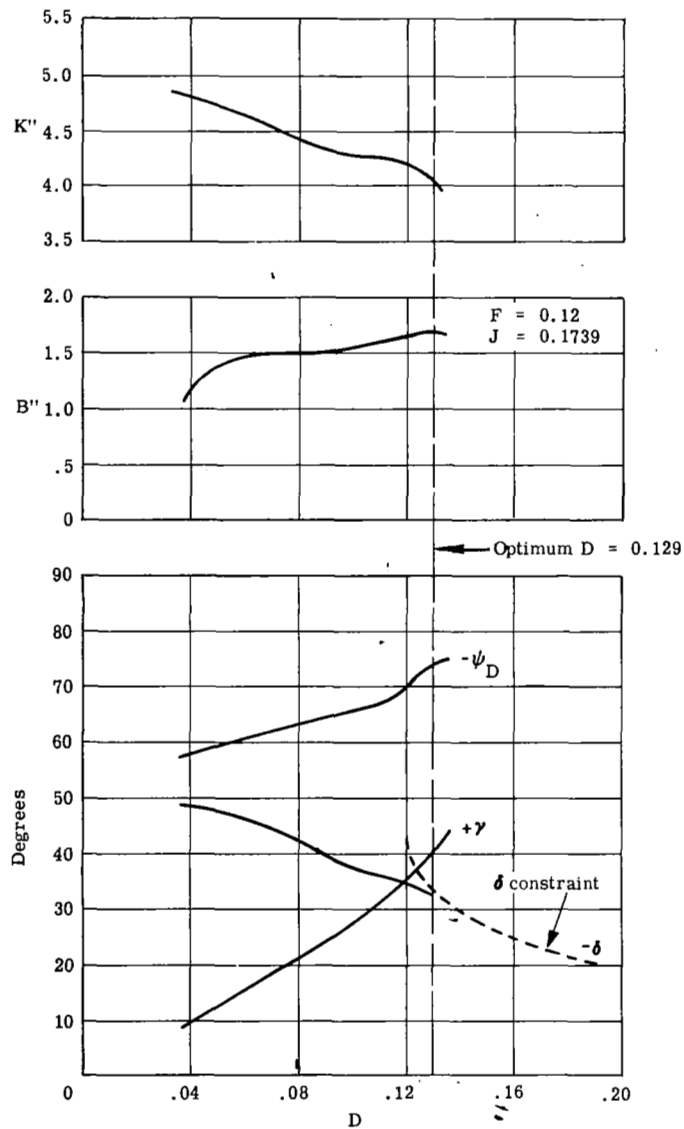


Figure 18. - Damper system parameters associated with $F = 0.12$.

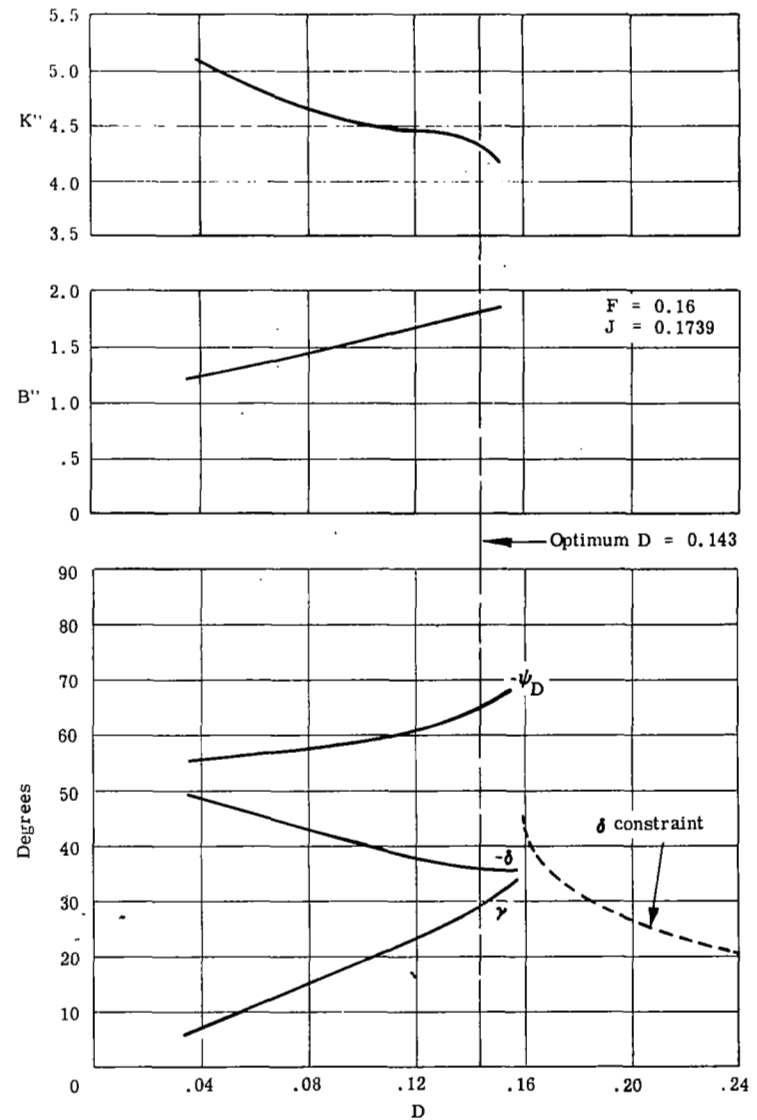
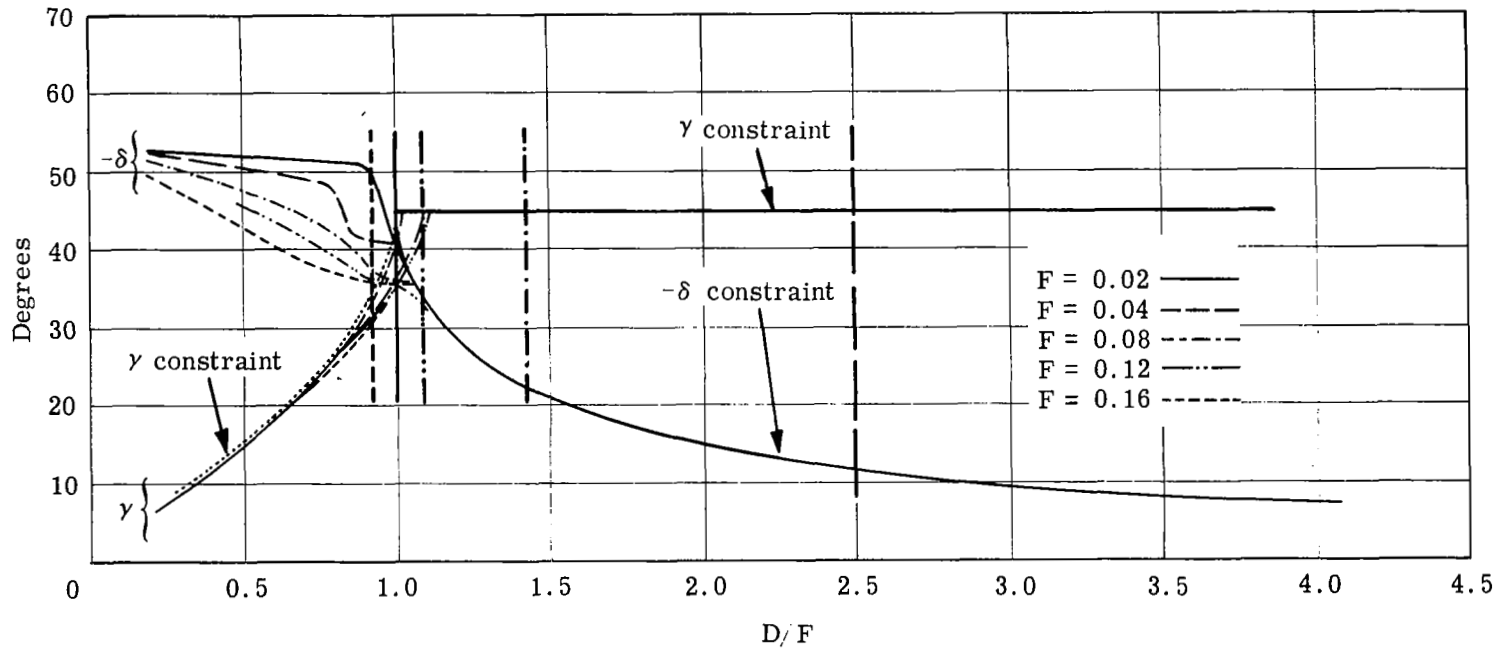


Figure 19. - Damper system parameters associated with $F = 0.16$.



[The vertical lines show optimum D/F ratios for the indicated values of F .]

Figure 20. - Damper system angular parameters and constraints versus optimum configuration values.

RUN NO. 1

$F = 0.16$	$K'' = 4.33$	Initial Condition
$D = 0.143$	$B'' = 1.81$	
$J = 0.1739$	$\psi_D = -65^\circ$	
	$\gamma = 29^\circ$	
		$\theta = 5^\circ$
		$\phi = 0$
		$\psi = 0 + \gamma$

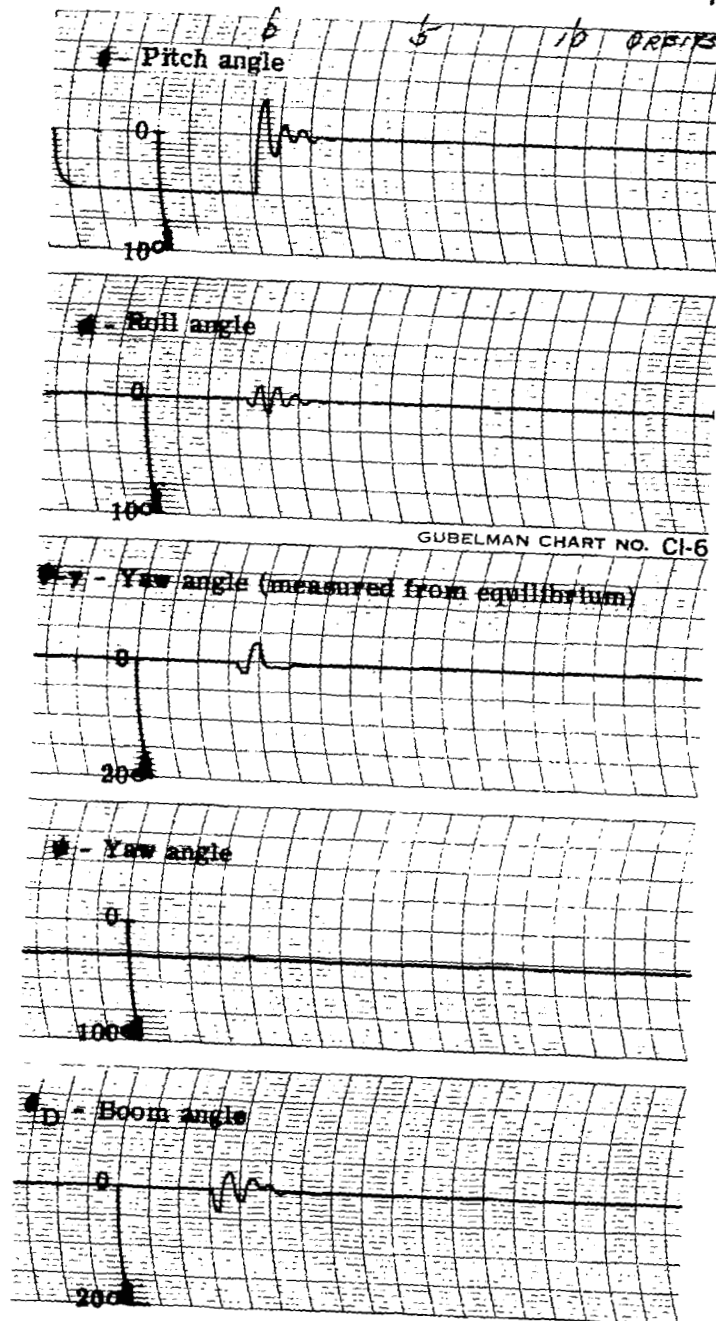


Figure 21. - Transient response when optimum boom inertias are $F = 0.16$ and $D = 0.143$.

RUN NO. 2

$F = 0.16$
 $D = 0.143$
 $J = 0.1739$

$K'' = 4.33$
 $B'' = 1.81$
 $\psi_D = -65^\circ$
 $\gamma = 29^\circ$

Initial Condition

$\theta = 0$
 $\phi = 5^\circ$
 $\psi = 0 + \gamma$

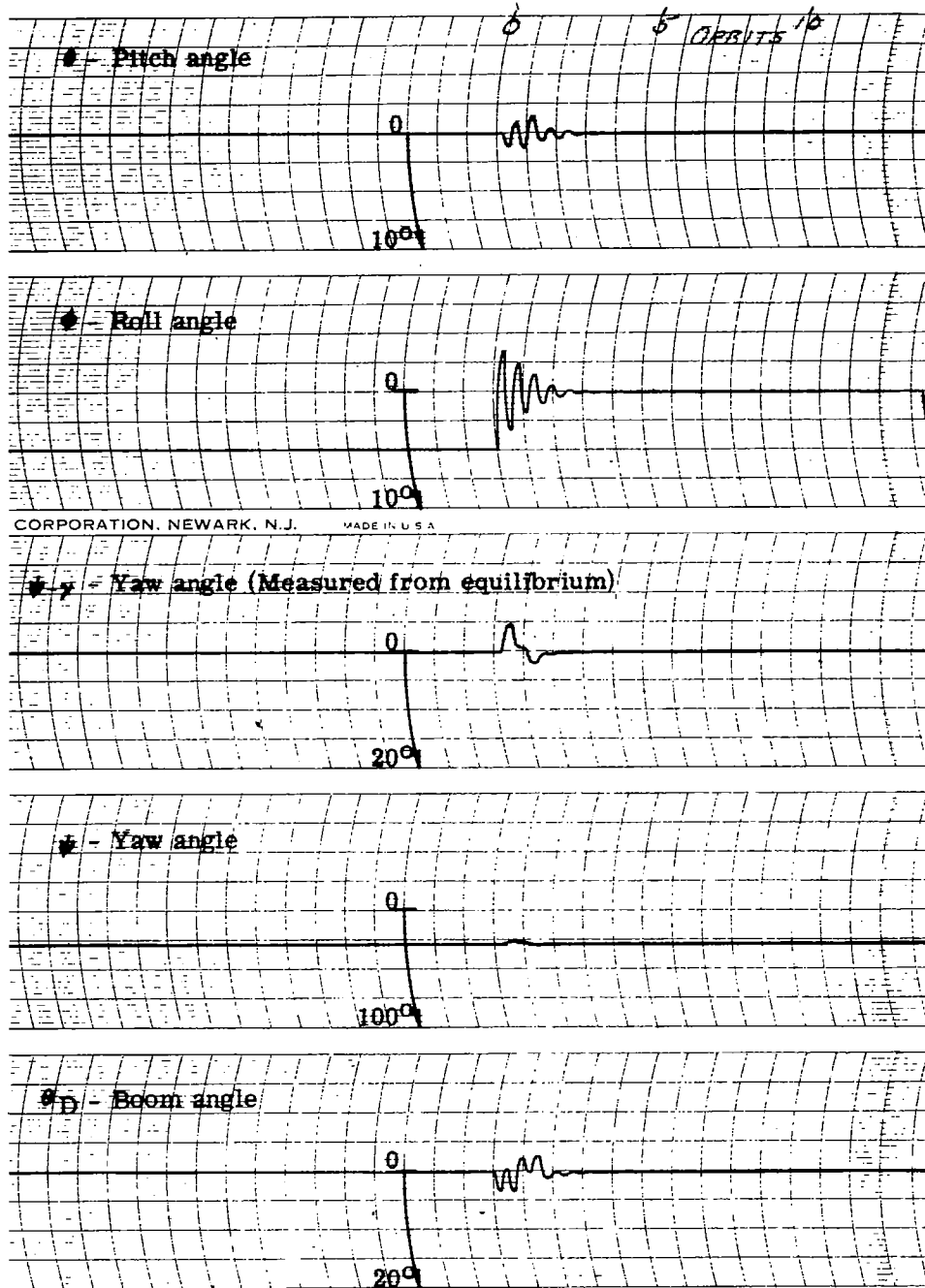


Figure 21. - Continued

RUN NO. 3

F = 0.16
D = 0.143
J = 0.1739

K'' = 4.33
B'' = 1.81
 $\psi_D = -65^\circ$
 $\gamma = 29^\circ$

Initial Condition
 $\theta = 0$
 $\phi = 0$
 $\psi = -5^\circ + \gamma$

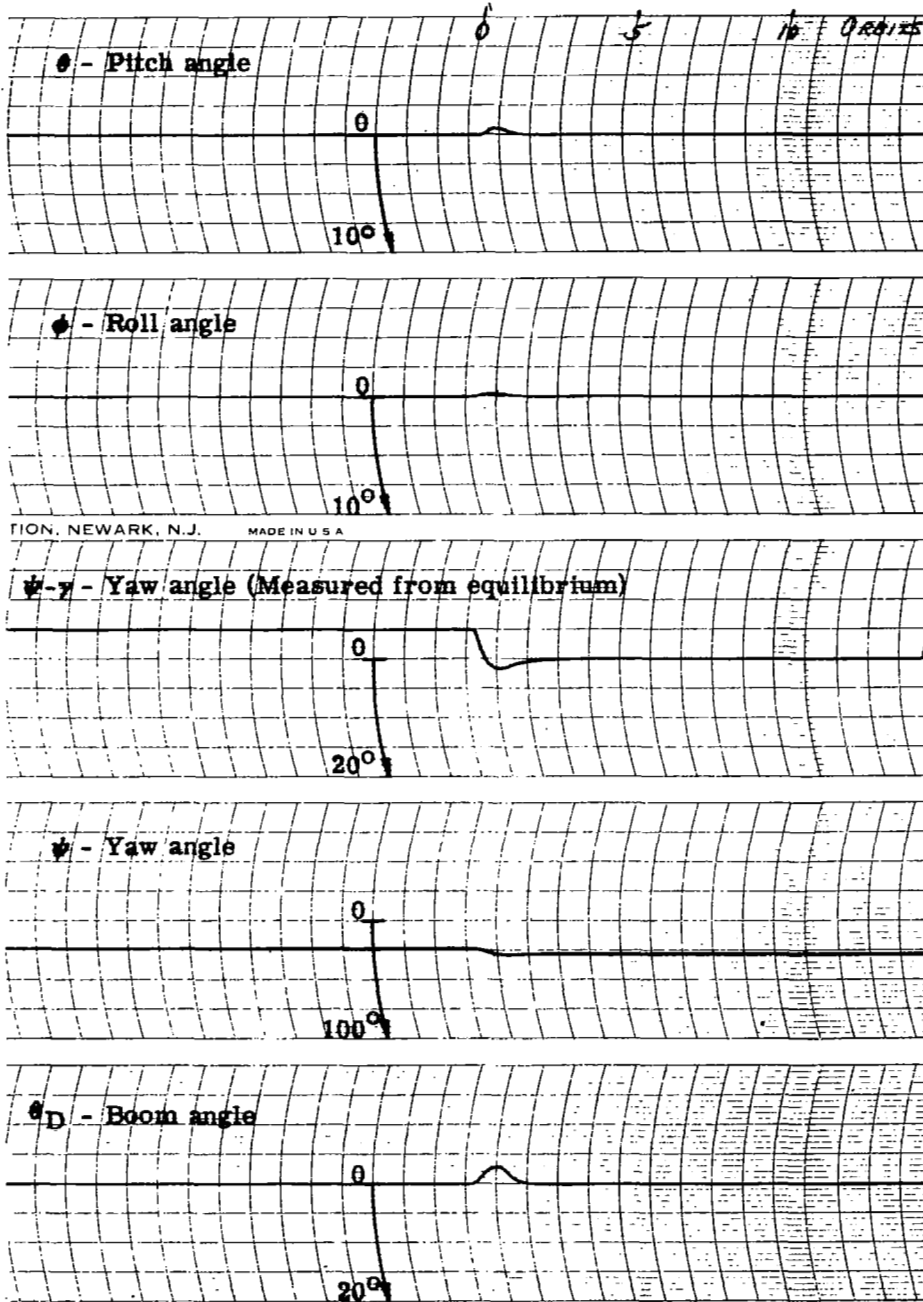


Figure 21. - Continued.

RUN NO. 4

F = 0.16
D = 0.143
J = 0.1739

K'' = 4.33
B'' = 1.81
 $\psi_D = -65^\circ$
 $\gamma = 29^\circ$

Initial Condition

$\theta = 5^\circ$
 $\phi = 5^\circ$
 $\psi = -5^\circ + \gamma$

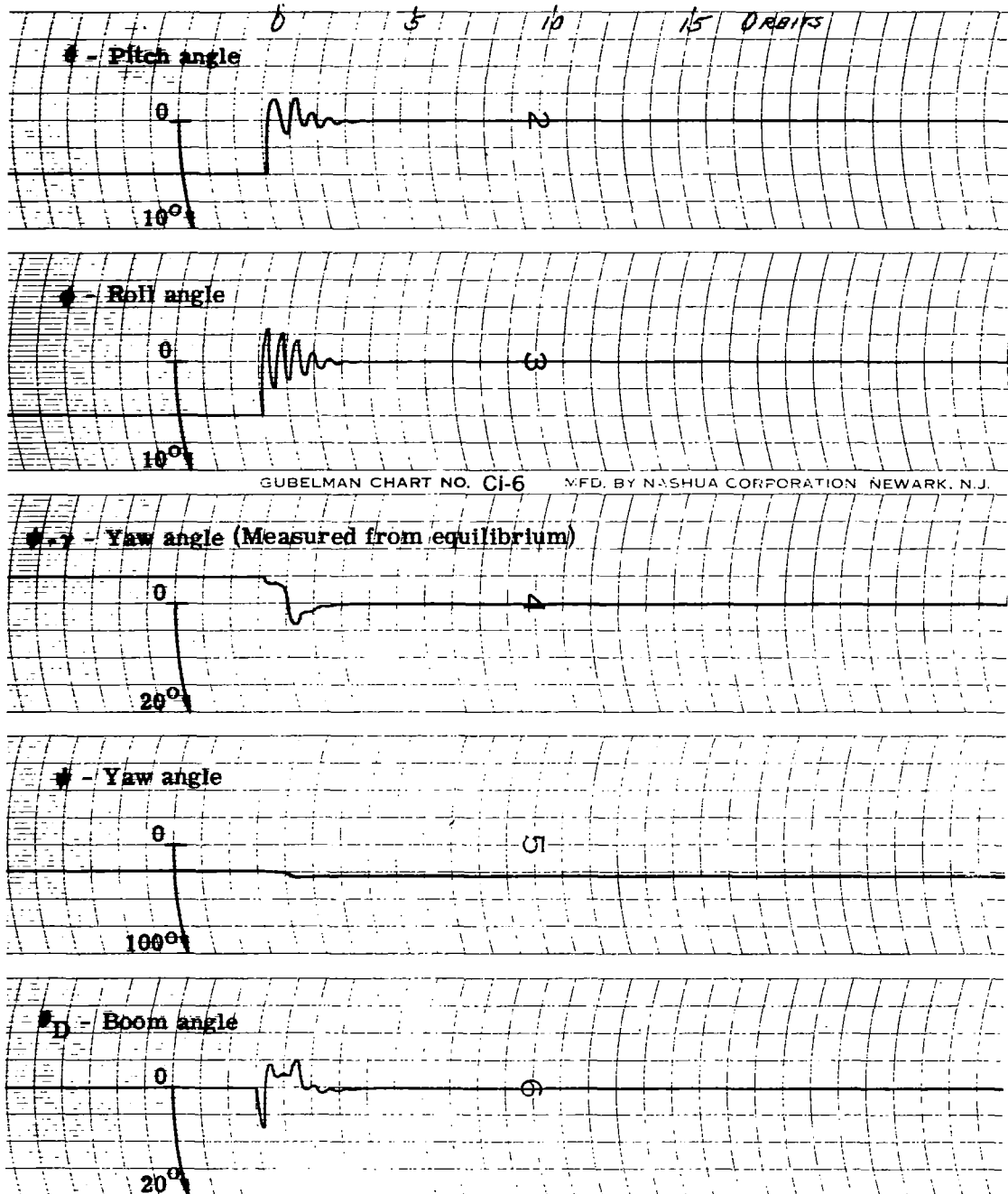


Figure 21. - Concluded.

RUN NO. 5

F = 0.12
D = 0.129
J = 0.1739

K'' = 4.07
B'' = 1.70
 $\psi_D = -73.5^\circ$
 $\gamma = 40^\circ$

Initial Condition

$\theta = 5^\circ$

$\phi = 0^\circ$

$\psi = 0^\circ + \gamma$

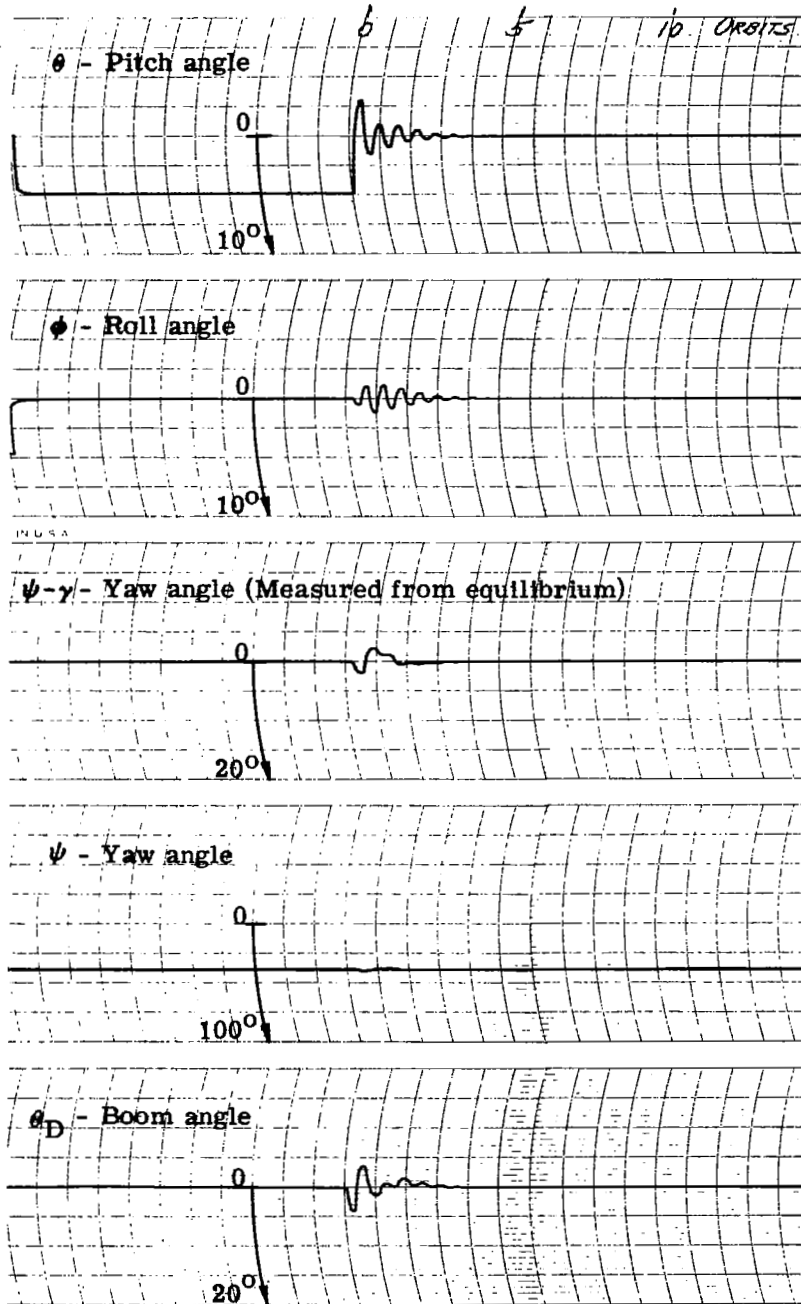


Figure 22. - Transient response when optimum boom inertias are F = 0.12 and D = 0.129.

RUN NO. 6

$F = 0.12$
 $D = 0.129$
 $J = 0.1739$

$K'' = 4.07$
 $B'' = 1.70$
 $\psi_D = -73.5^\circ$
 $\gamma = 40^\circ$

Initial Condition
 $\theta = 0$
 $\phi = 5^\circ$
 $\psi = 0 + \gamma$

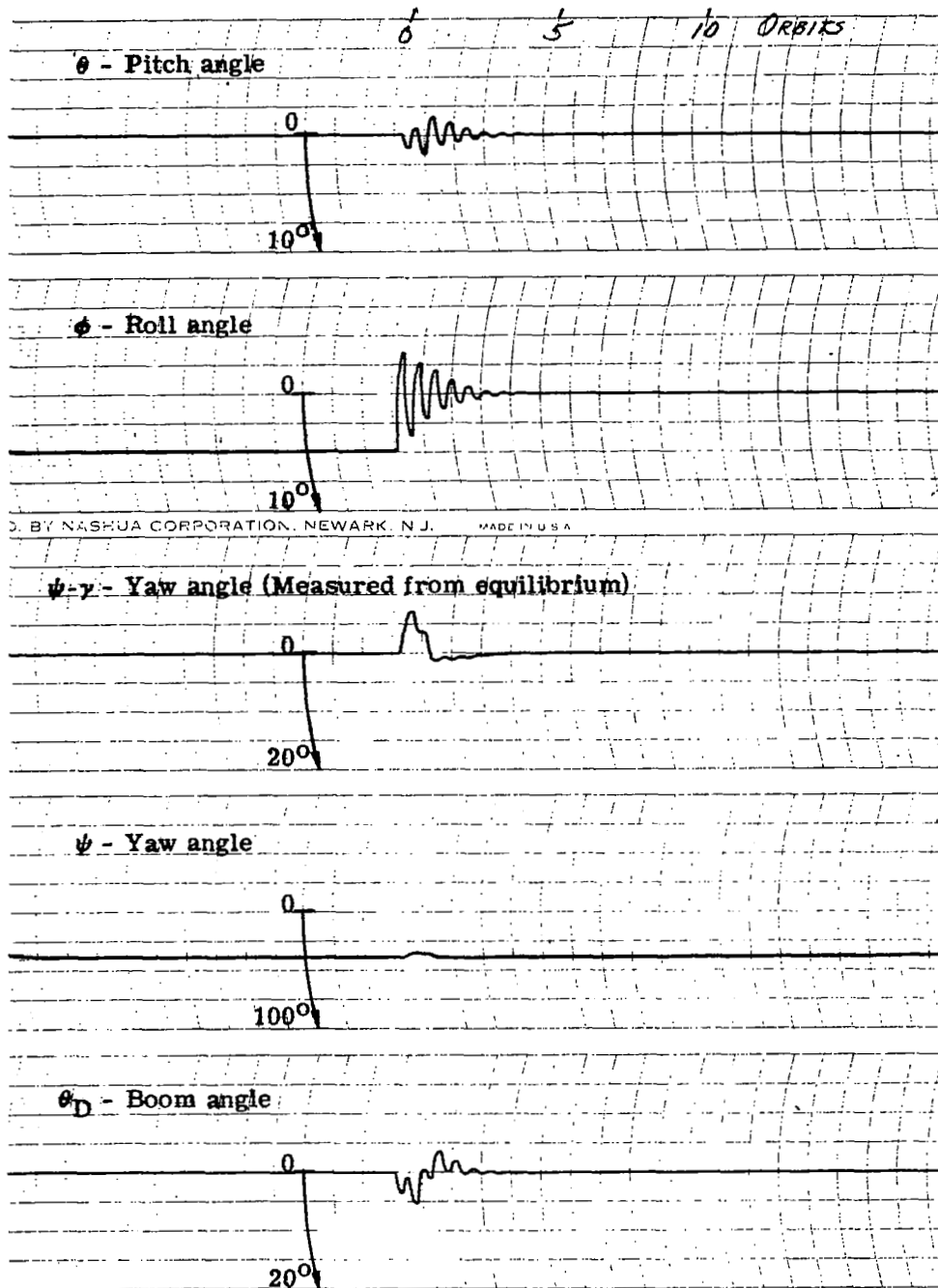


Figure 22. - Continued.

RUN NO. 7

F = 0.12
D = 0.129
J = 0.1739

K'' = 4.07
B'' = 1.70
 $\psi_D = -73.5^\circ$
 $\gamma = 40^\circ$

Initial Condition
 $\theta = 0$
 $\phi = 0$
 $\psi = -5^\circ + \gamma$

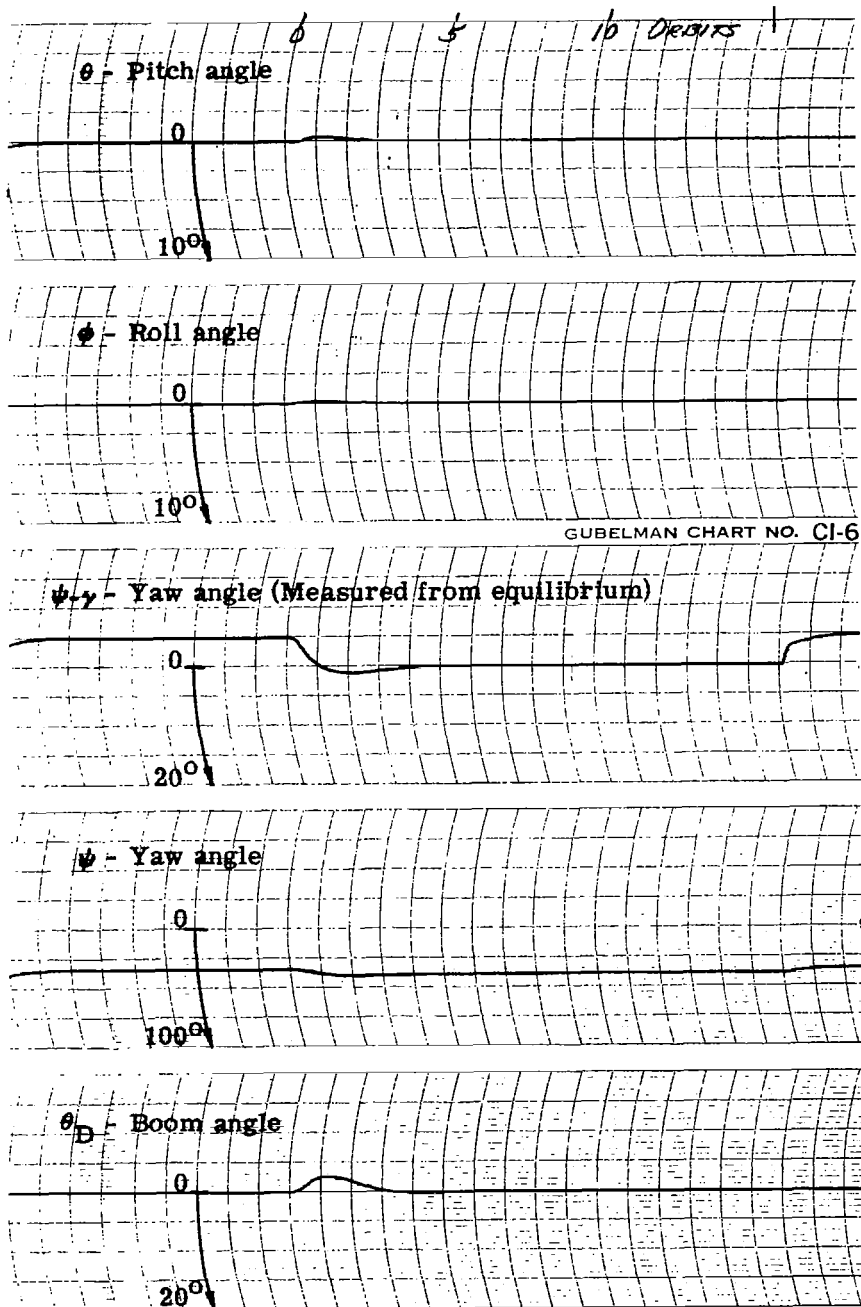


Figure 22. - Continued.

RUN NO. 8

F = 0.12
D = 0.129
J = 0.1739

K'' = 4.07
B'' = 1.70
 $\psi_D = -73.5^\circ$
 $\gamma = 40^\circ$

Initial Condition
 $\theta = 5^\circ$
 $\phi = 5^\circ$
 $\psi = -5^\circ + \gamma$

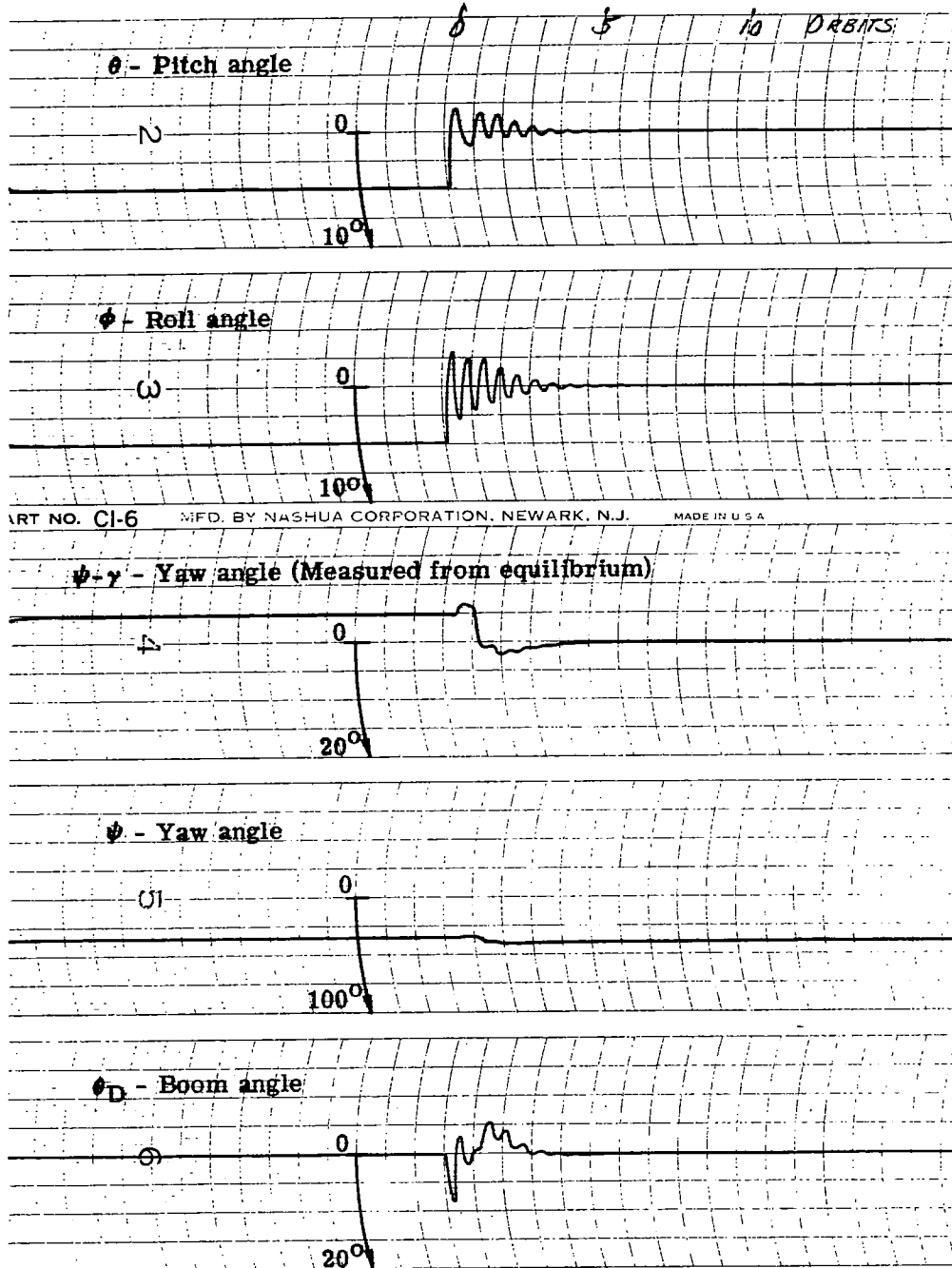


Figure 22. - Concluded.

RUN NO. 9

$F = 0.08$
 $D = 0.114$
 $J = 0.1739$

$K'' = 3.84$
 $B'' = 1.10$
 $\psi_D = -67^\circ$
 $\gamma = 44.8^\circ$

Initial Condition
 $\theta = 5^\circ$
 $\phi = 0$
 $\psi = 0 + \gamma$

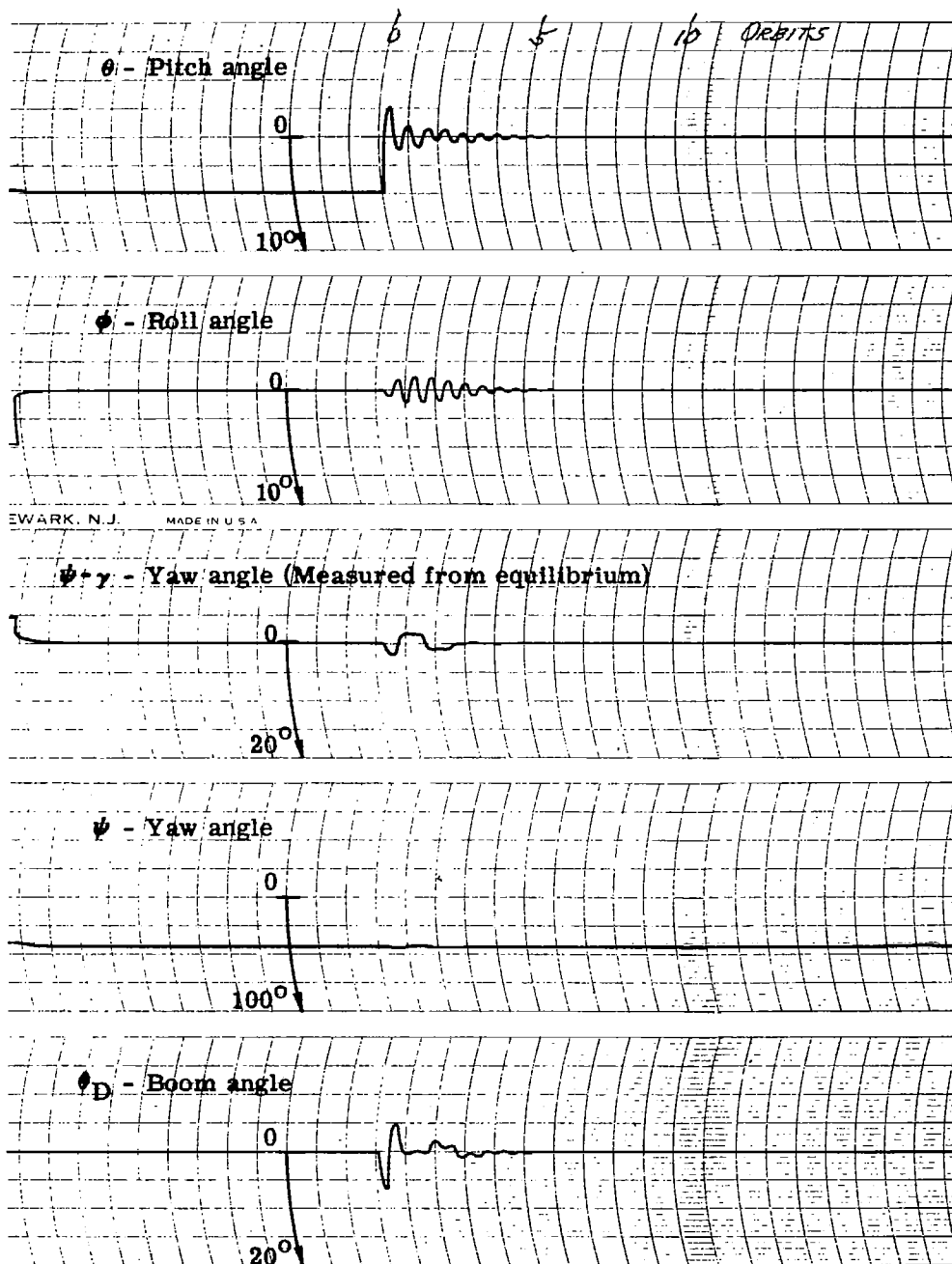


Figure 23. - Transient response when optimum boom inertias are $F = 0.08$ and $D = 0.114$.

RUN NO. 10

$F = 0.08$
 $D = 0.114$
 $J = 0.1739$

$K'' = 3.84$
 $B'' = 1.10$
 $\psi_D = -67^\circ$
 $\gamma = 44.8^\circ$

Initial Condition
 $\theta = 0$
 $\phi = 5^\circ$
 $\psi = 0 + \gamma$

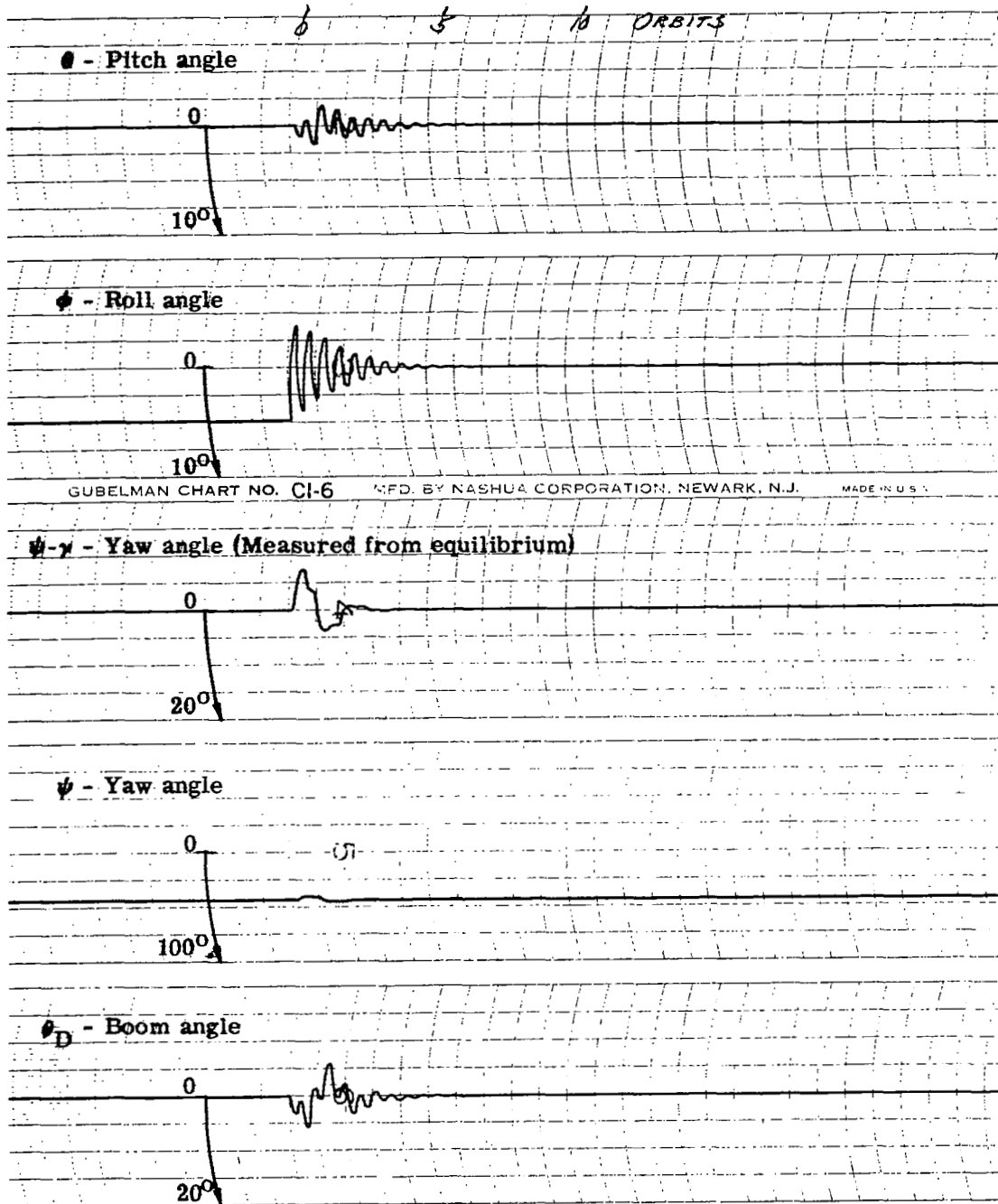


Figure 23. - Continued.

RUN NO. 11

F = 0.08
D = 0.114
J = 0.1739

K'' = 3.84
B'' = 1.10
 $\psi_D = -67^\circ$
 $\gamma = 44.8^\circ$

Initial Condition

$\theta = 0$
 $\phi = 0$
 $\psi = -5^\circ + \gamma$

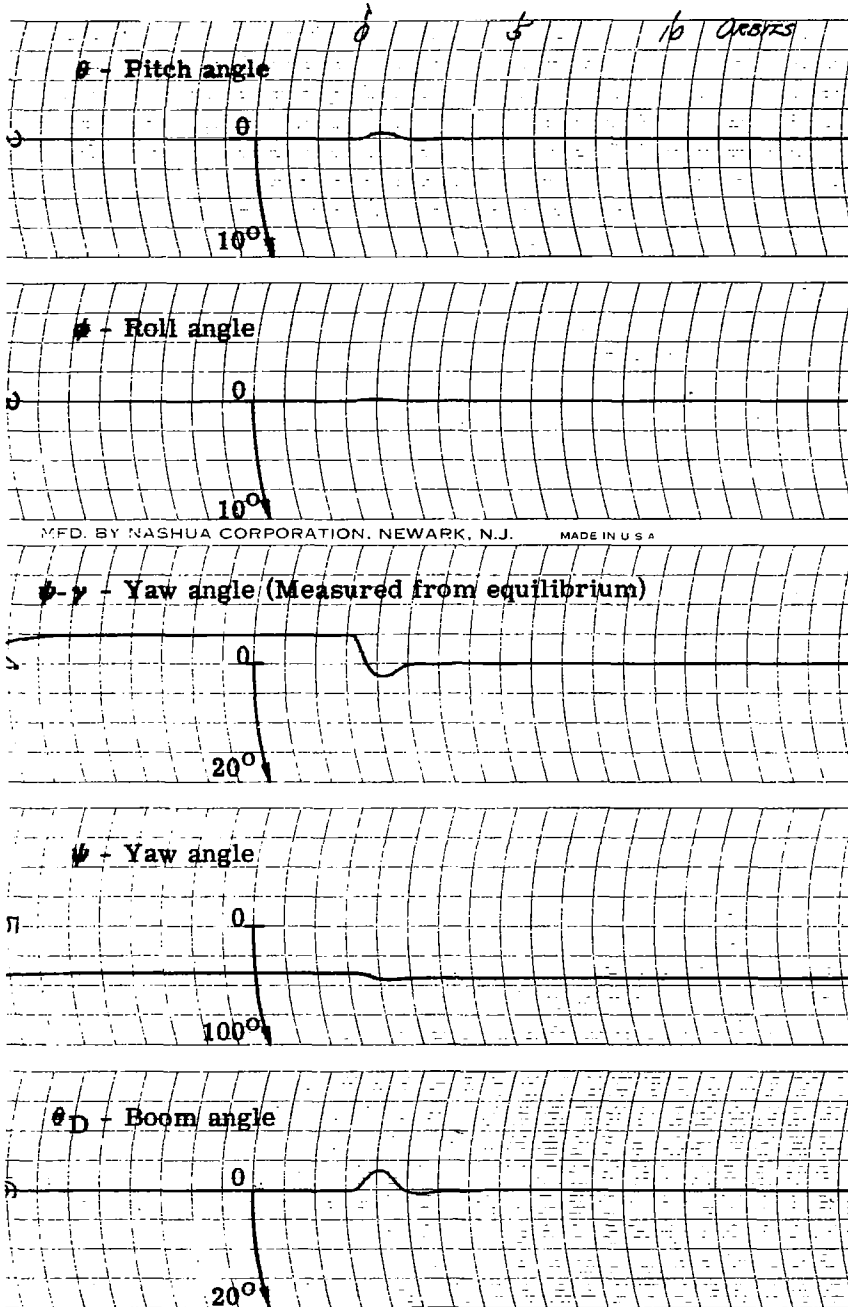


Figure 23. - Continued.

RUN NO. 12

F = 0.08
D = 0.114
J = 0.1739

K'' = 3.84
B'' = 1.10
 $\psi_D = -67^\circ$
 $\gamma = 44.8^\circ$

Initial Condition

$\theta = 5^\circ$
 $\phi = 5^\circ$
 $\psi = -5^\circ + \gamma$

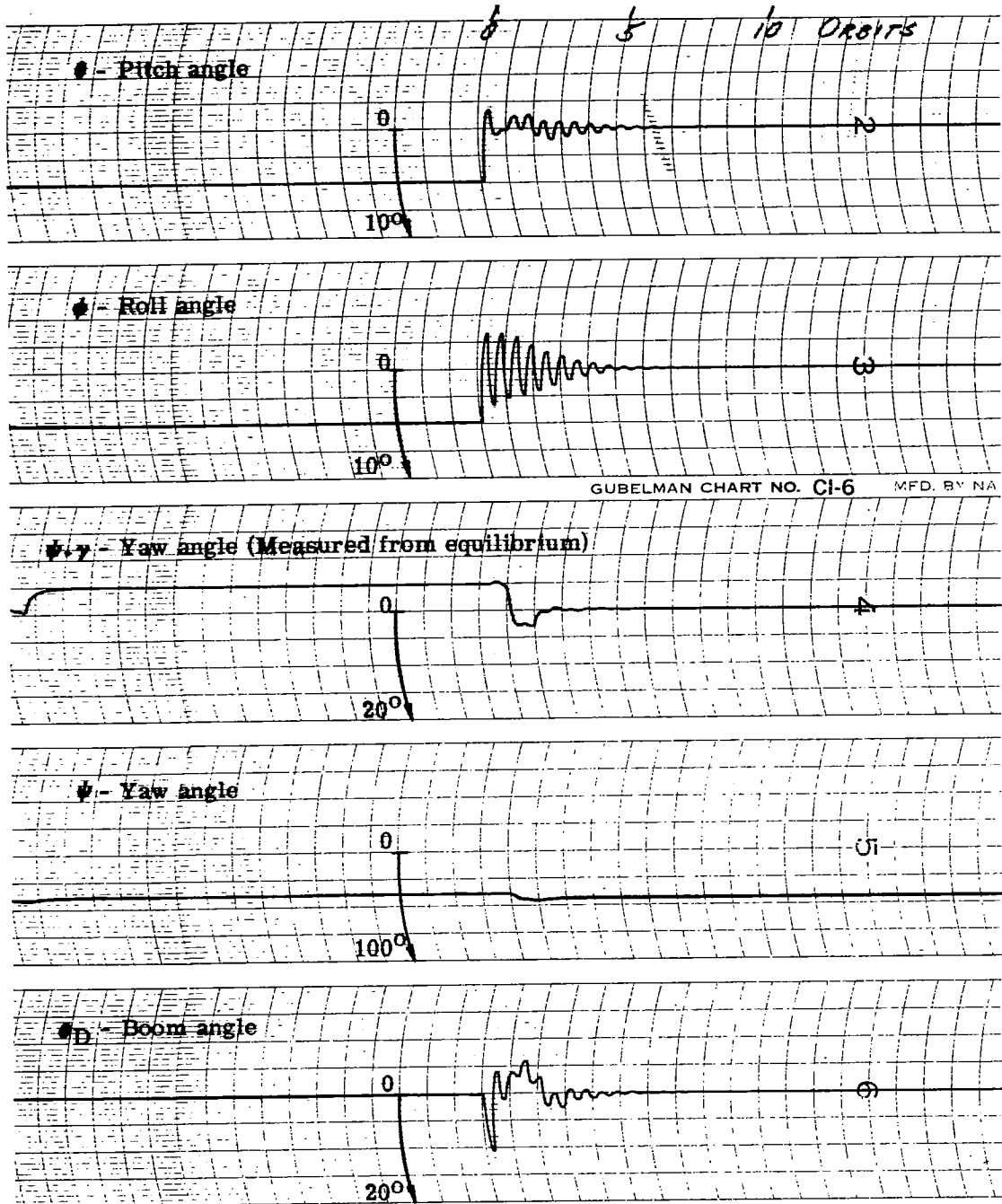


Figure 23. - Concluded.

RUN NO. 13

$F = 0.04$
 $D = 0.10$
 $J = 0.1739$

$K'' = 3.92$
 $B'' = 0.58$
 $\psi_D = -56.5^\circ$
 $\gamma = 44.8^\circ$

Initial Condition

$\theta = 5^\circ$

$\phi = 0$

$\psi = 0 + \gamma$

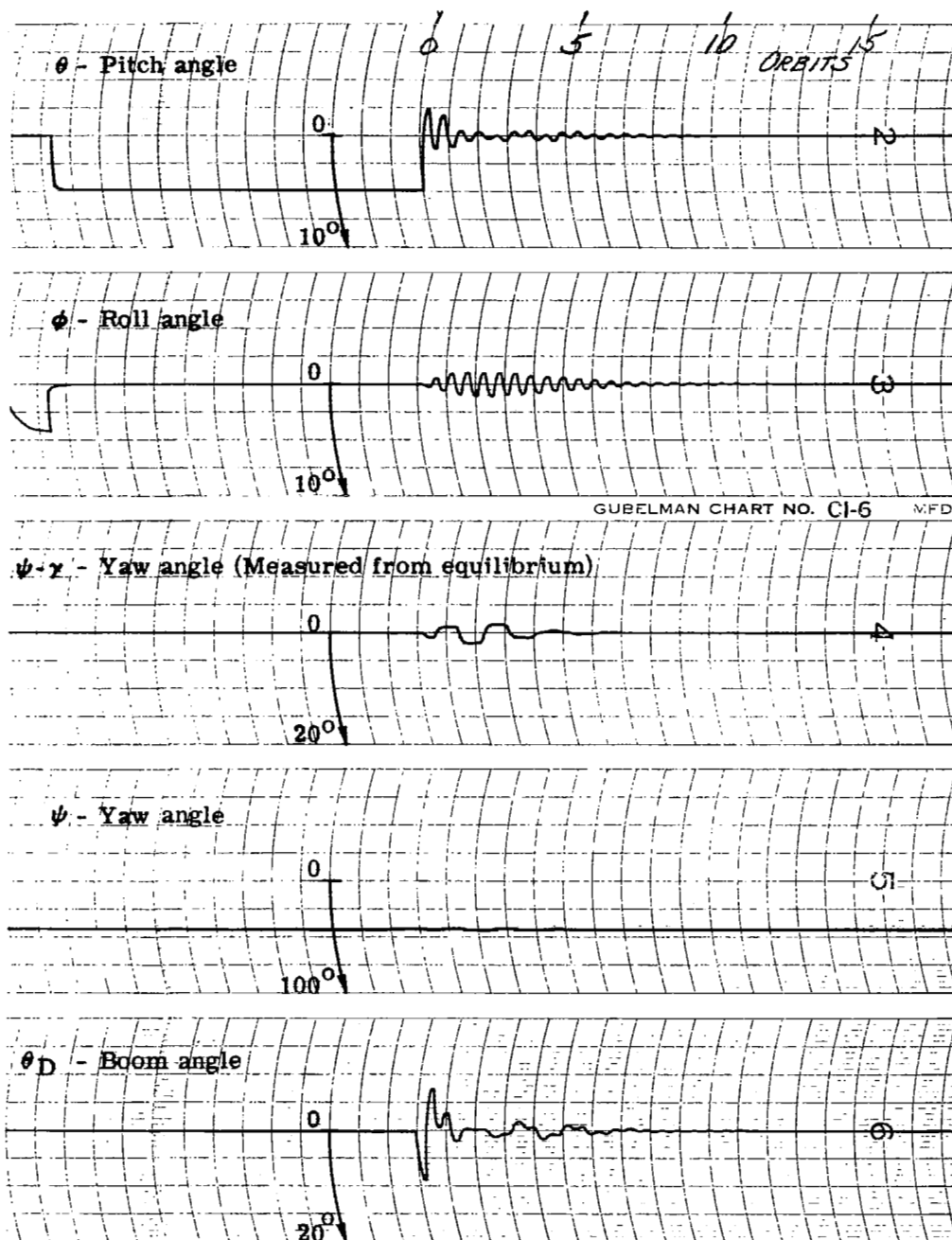


Figure 24. - Transient response when optimum boom inertias are $F = 0.04$ and $D = 0.10$.

RUN NO. 14

$F = 0.04$
 $D = 0.10$
 $J = 0.1739$

$K'' = 3.92$
 $B'' = 0.58$
 $\psi_D = -56.5^\circ$
 $\gamma = 44.8$

Initial Condition

$\theta = 0$
 $\phi = 5^\circ$
 $\psi = 0 + \gamma$

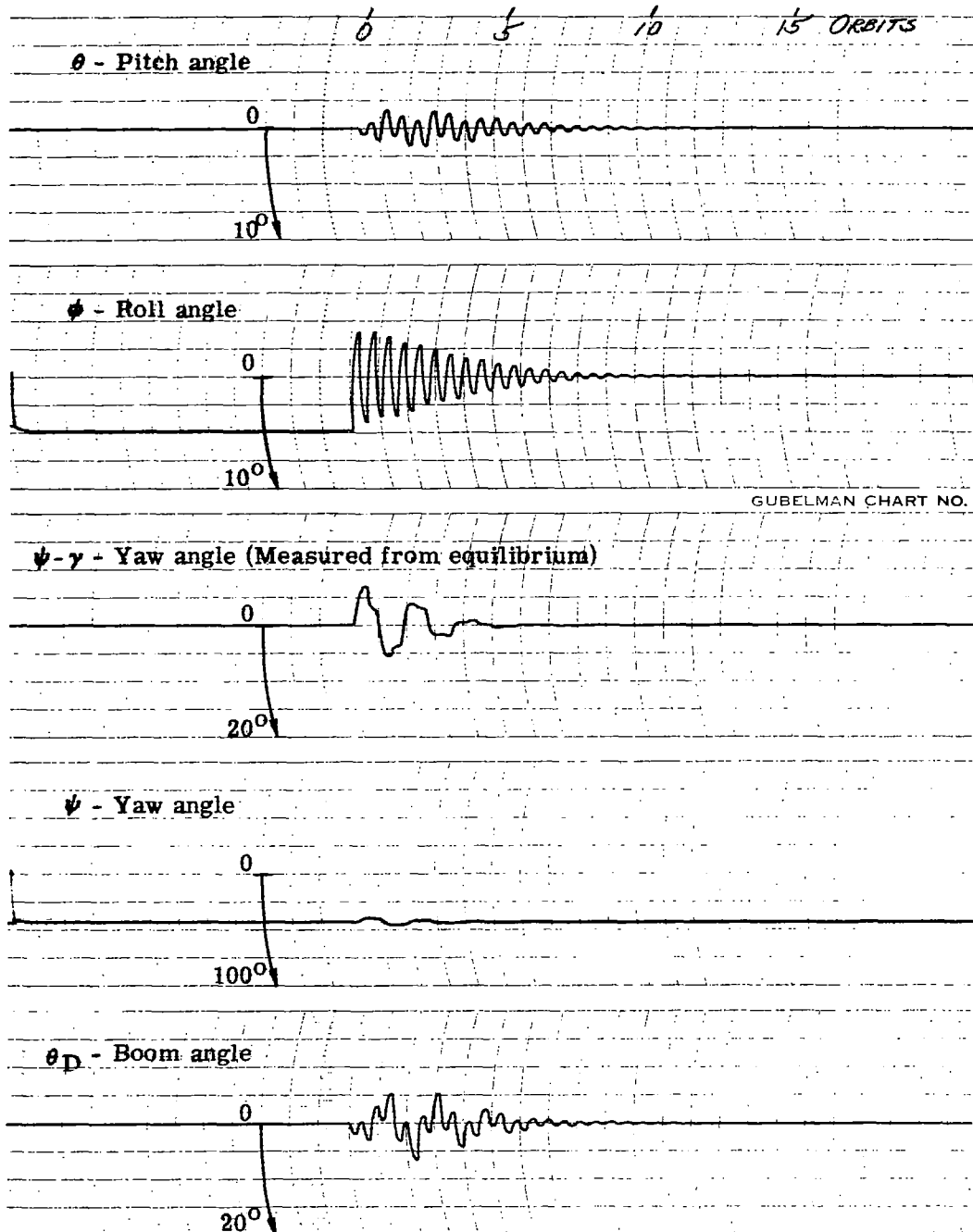


Figure 24. - Continued.

RUN NO. 15

$F = 0.04$
 $D = 0.10$
 $J = 0.1739$

$K'' = 3.92$
 $B'' = 0.58$
 $\psi_D = -56.5^\circ$
 $\gamma = 44.8^\circ$

Initial Condition
 $\theta = 0$
 $\phi = 0$
 $\psi = -5^\circ + \gamma$

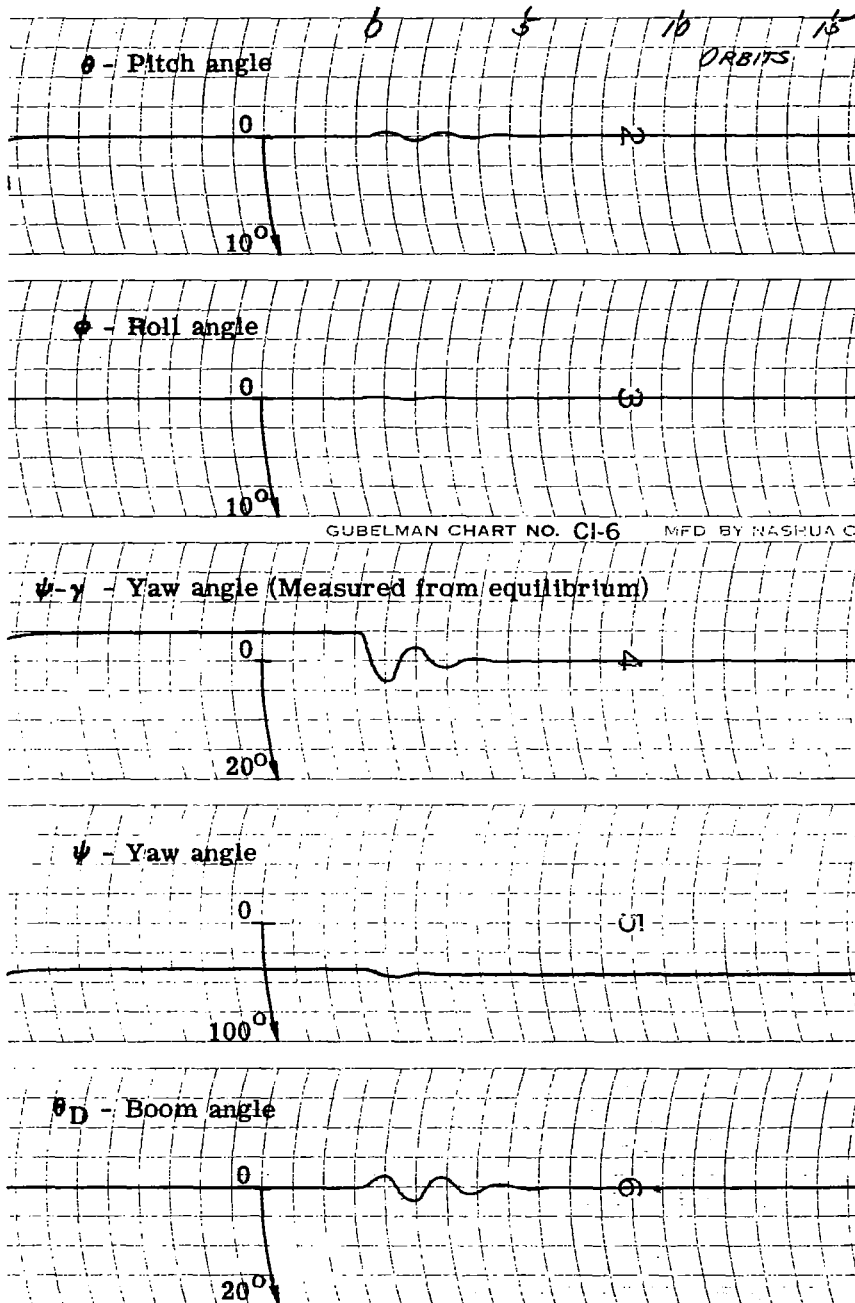


Figure 24. - Continued.

RUN NO. 16

$F = 0.04$
 $D = 0.10$
 $J = 0.1739$

$K'' = 3.92$
 $B'' = 0.58$
 $\psi_D = -56.5^\circ$
 $\gamma = 44.8^\circ$

Initial Condition
 $\theta = 5^\circ$
 $\phi = 5^\circ$
 $\psi = -5^\circ + \gamma$

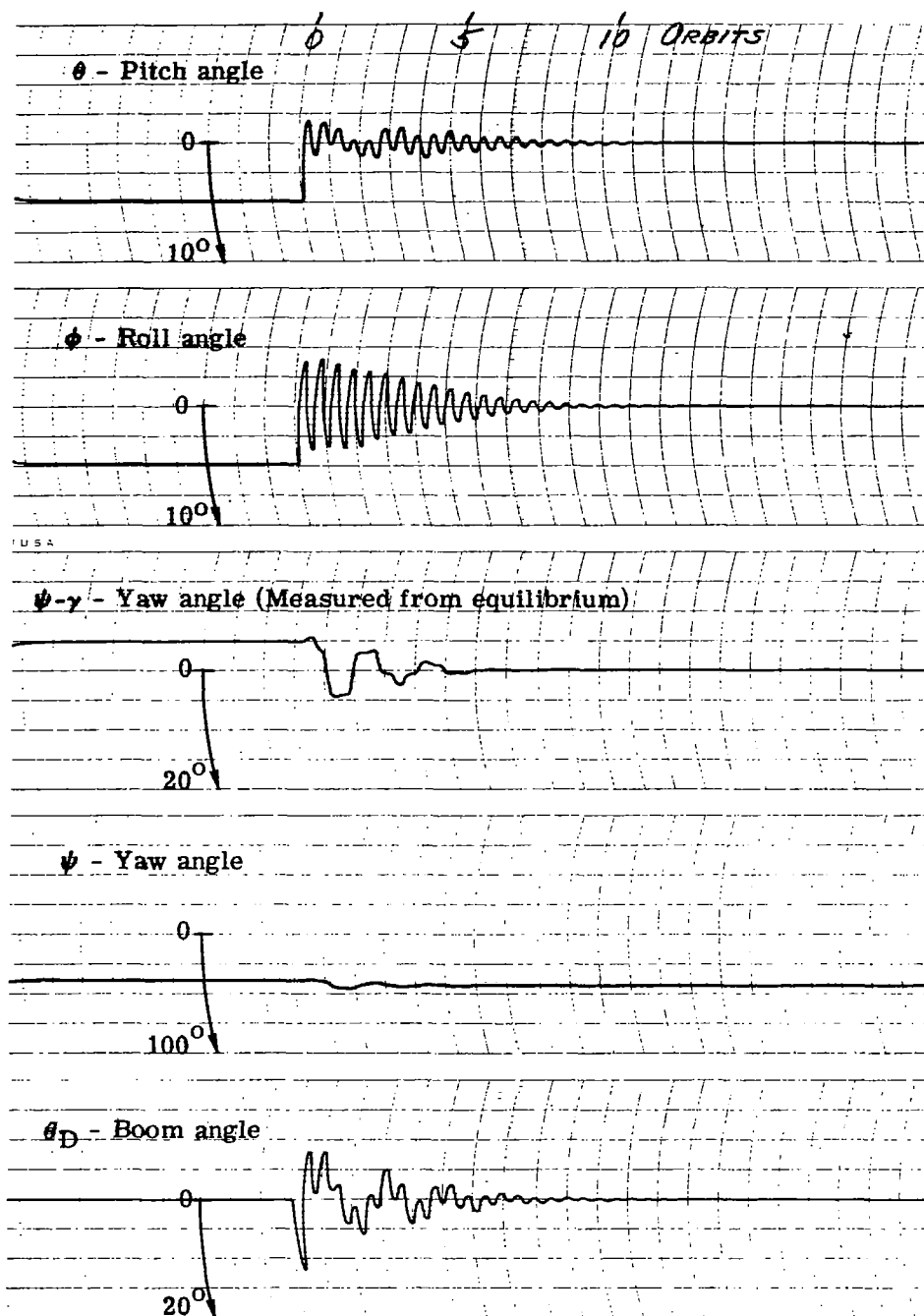


Figure 24. - Concluded.

RUN NO. 17

F = 0.04
D = 0.03
J = 0.1739

K'' = 4.216
B'' = 1.278
 $\psi_D = -72.4^\circ$
 $\gamma = 24.1^\circ$

Initial Condition

$\theta = 5^\circ$
 $\phi = 0$
 $\psi = 0^\circ + \gamma$

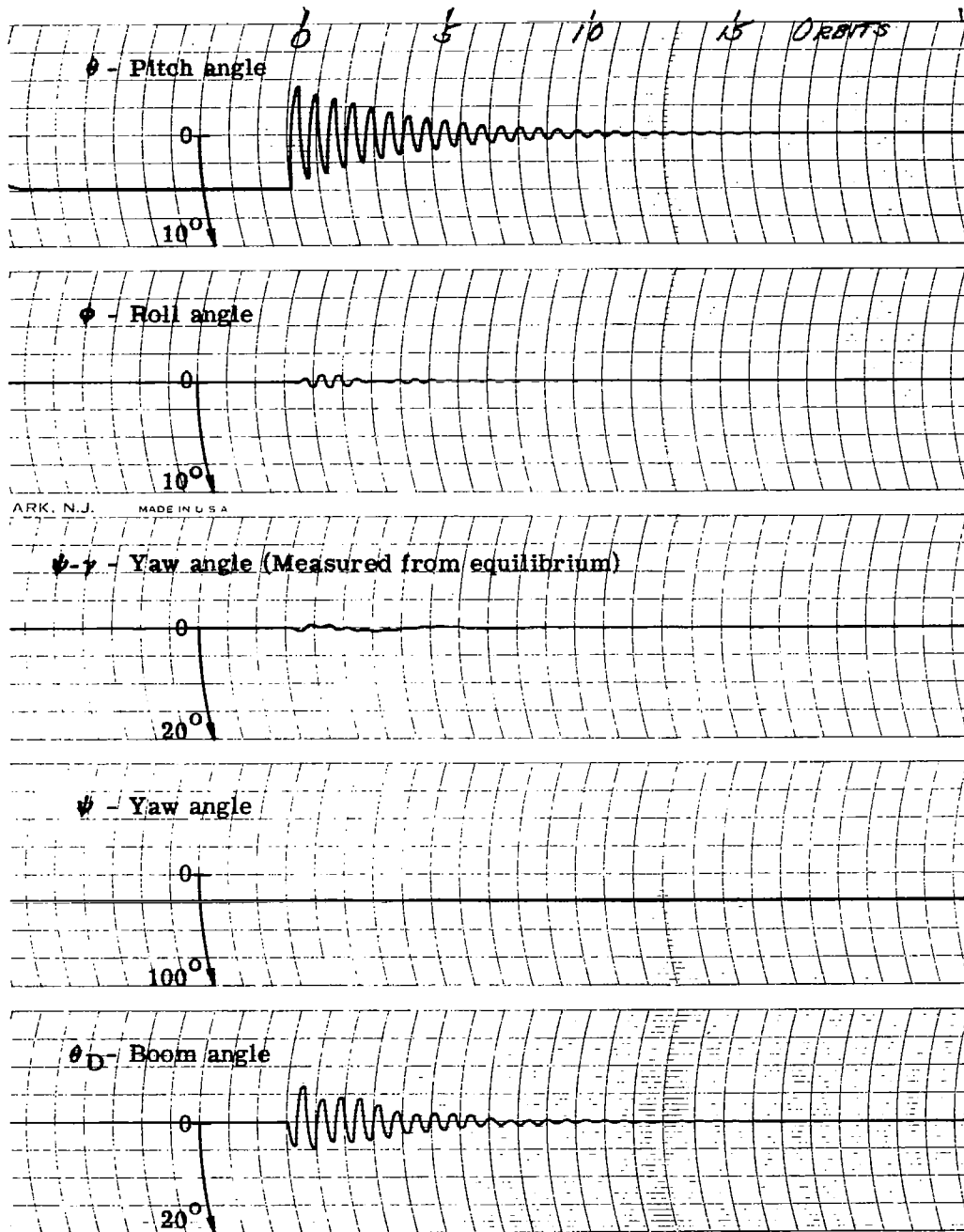


Figure 25. - Transient response when optimum boom inertias are F = 0.04 and D = 0.03.

RUN NO. 18

F = 0.04
D = 0.03
J = 0.1739

K'' = 4.216
B'' = 1.278
 $\psi_D = -72.4^\circ$
 $\gamma = 24.1^\circ$

Initial Condition
 $\theta = 0$
 $\phi = 5^\circ$
 $\psi = 0 + \gamma$

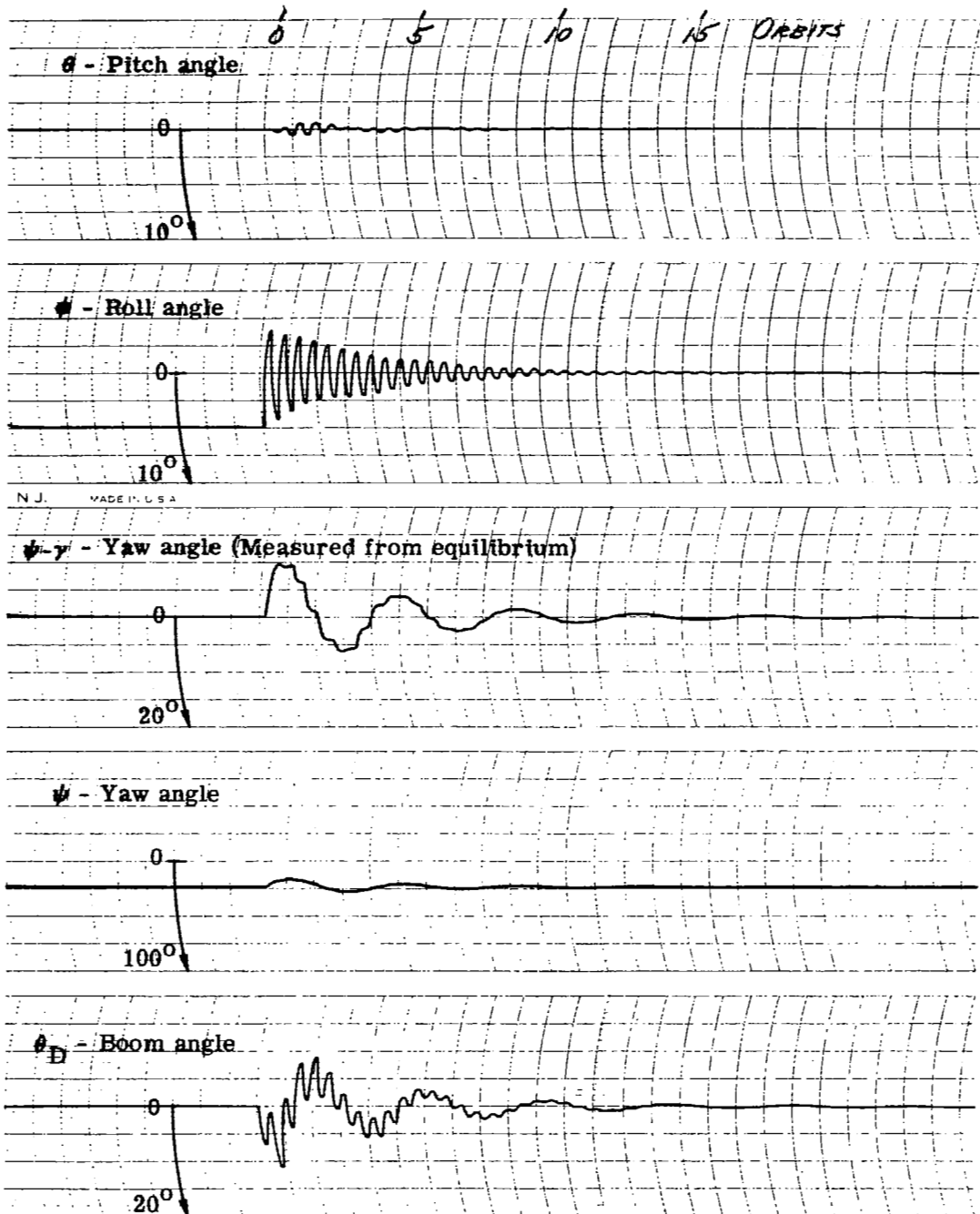


Figure 25. - Continued.

RUN NO. 19

F = 0.04
D = 0.03
J = 0.1739

K'' = 4.216
B'' = 1.278
 $\psi_D = -72.4^\circ$
 $\gamma = 24.1^\circ$

Initial Condition
 $\theta = 0$
 $\phi = 0$
 $\psi = -5^\circ + \gamma$

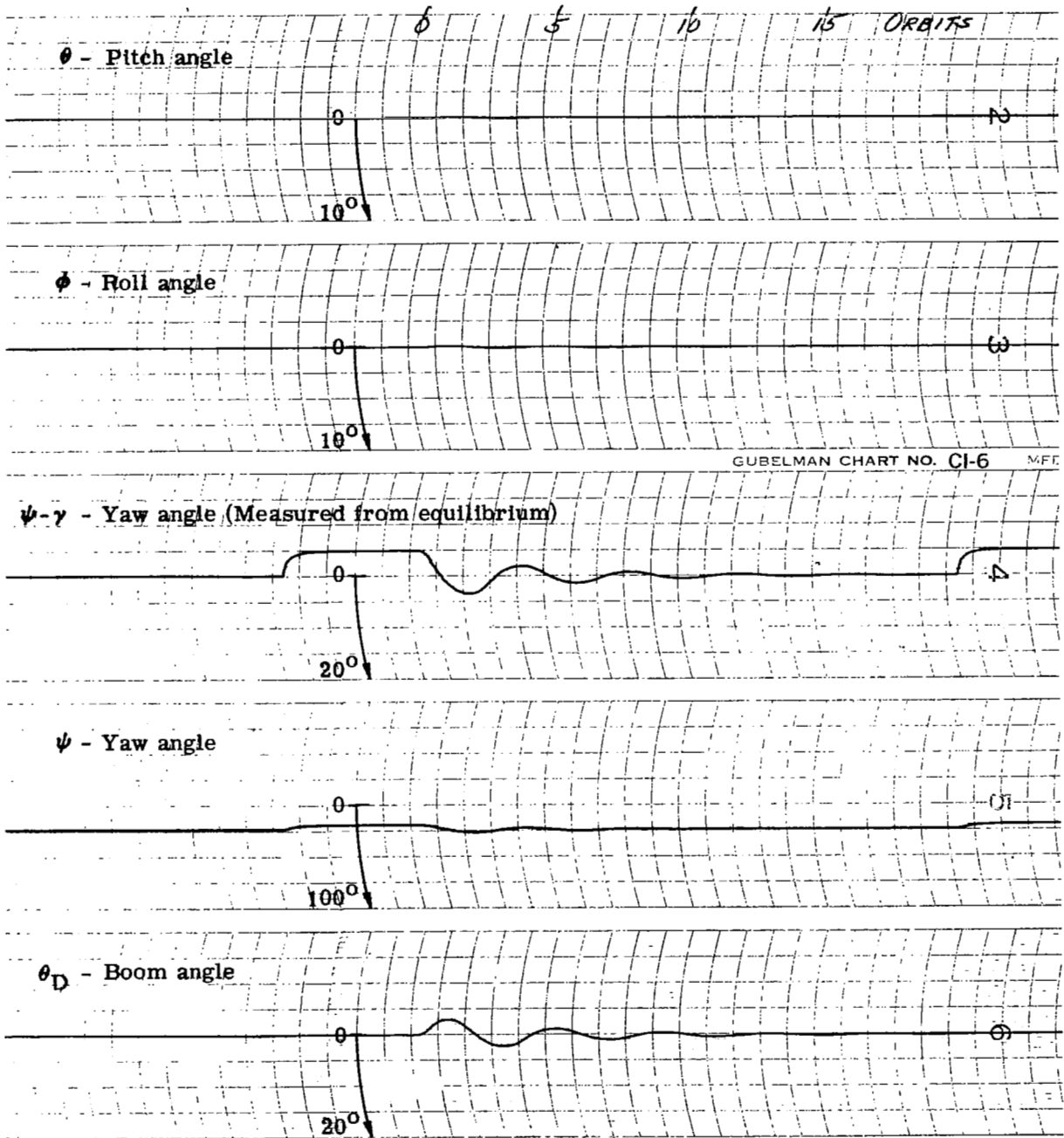


Figure 25. - Continued.

RUN NO. 20

F = 0.04
D = 0.03
J = 0.1739

K'' = 4.216
B'' = 1.278
 $\psi_D = -72.4^\circ$
 $\gamma = 24.1$

Initial Condition

$\theta = 5^\circ$
 $\phi = 5^\circ$
 $\psi = -5^\circ + \gamma$

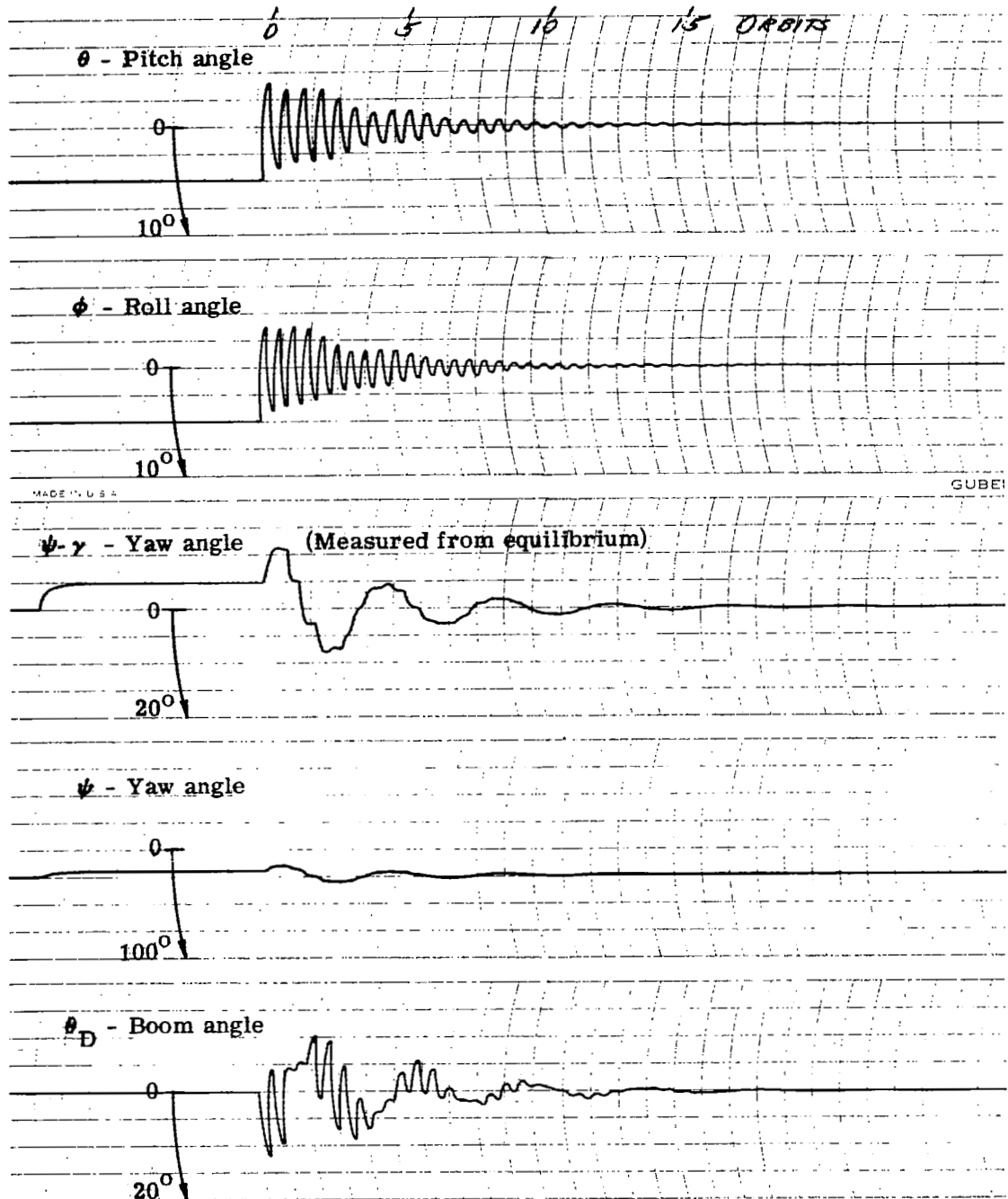


Figure 25. - Concluded.

RUN NO. 21

F = 0.02
D = 0.095
J = 0.1739

K'' = 3.929
B'' = 0.2727
 $\psi_D = -50.8^\circ$
 $\gamma = 44.8$

Initial Condition
 $\theta = 5^\circ$
 $\phi = 0$
 $\psi = 0 + \gamma$

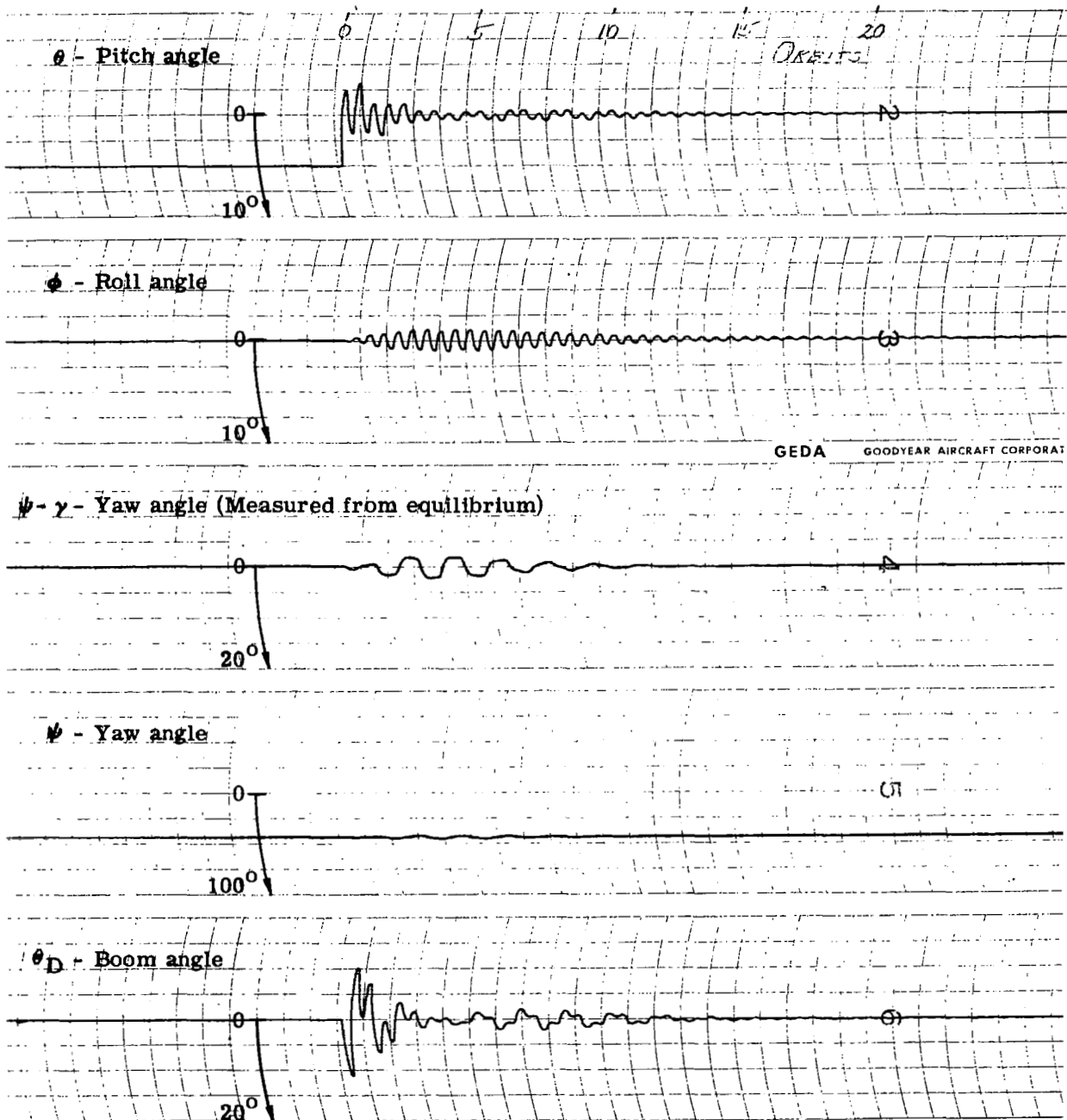


Figure 26. - Transient response when optimum boom inertias are $F = 0.02$ and $D = 0.095$.

RUN NO. 22

$F = 0.02$
 $D = 0.095$
 $J = 0.1739$

$K'' = 3.929$
 $B'' = 0.2727$
 $\psi_D = -50.8^\circ$
 $\gamma = 44.8^\circ$

Initial Condition

$\theta = 0$
 $\phi = 5^\circ$
 $\psi = 0 + \gamma$

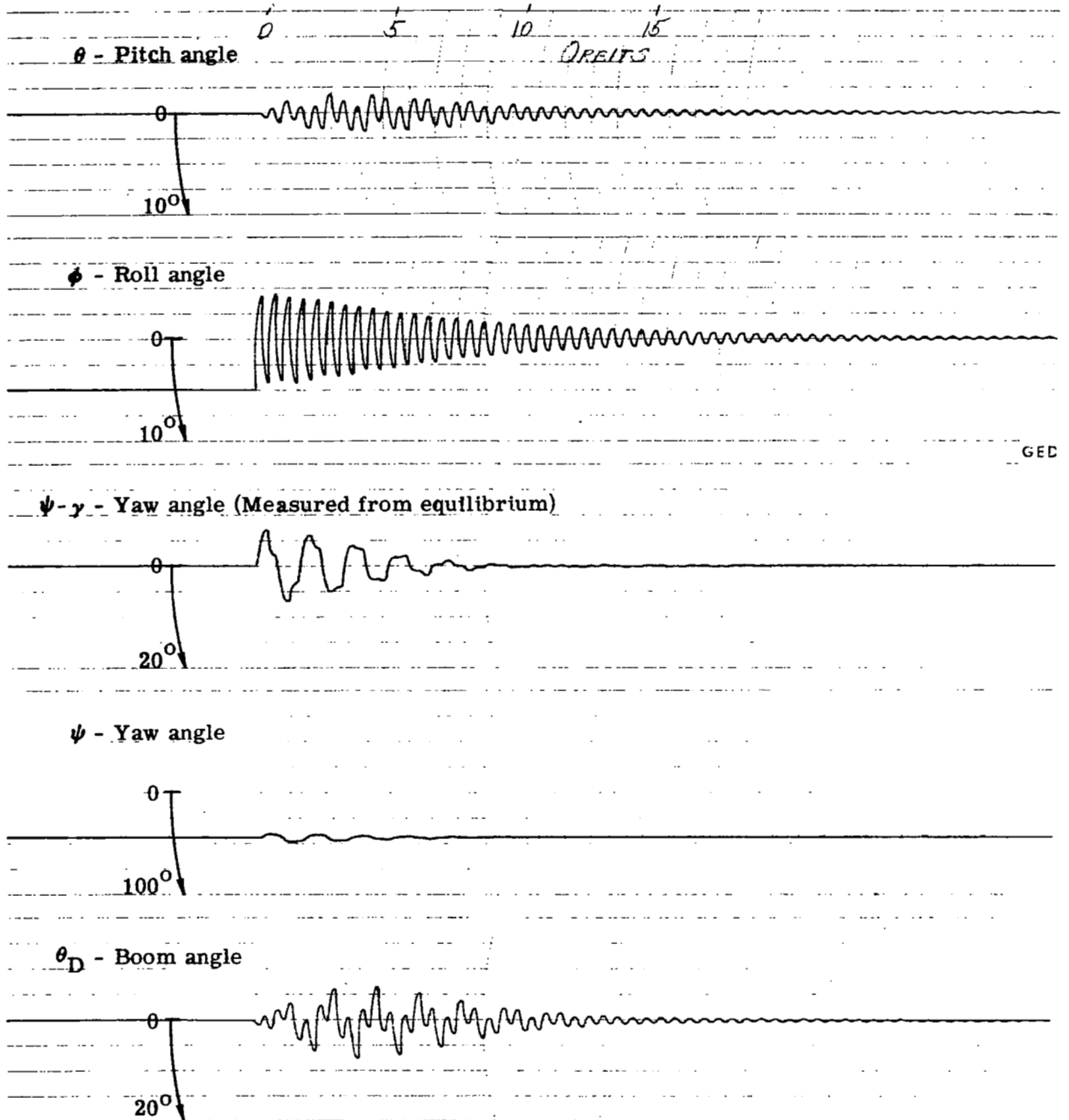


Figure 26. - Continued.

RUN NO. 23

$F = 0.02$
 $D = 0.095$
 $J = 0.1739$

$K'' = 3.929$
 $B'' = 0.2727$
 $\psi_D = -50.8^\circ$
 $\gamma = 44.8^\circ$

Initial Condition

$\theta = 0$

$\phi = 0$

$\psi = -50^\circ + \gamma$

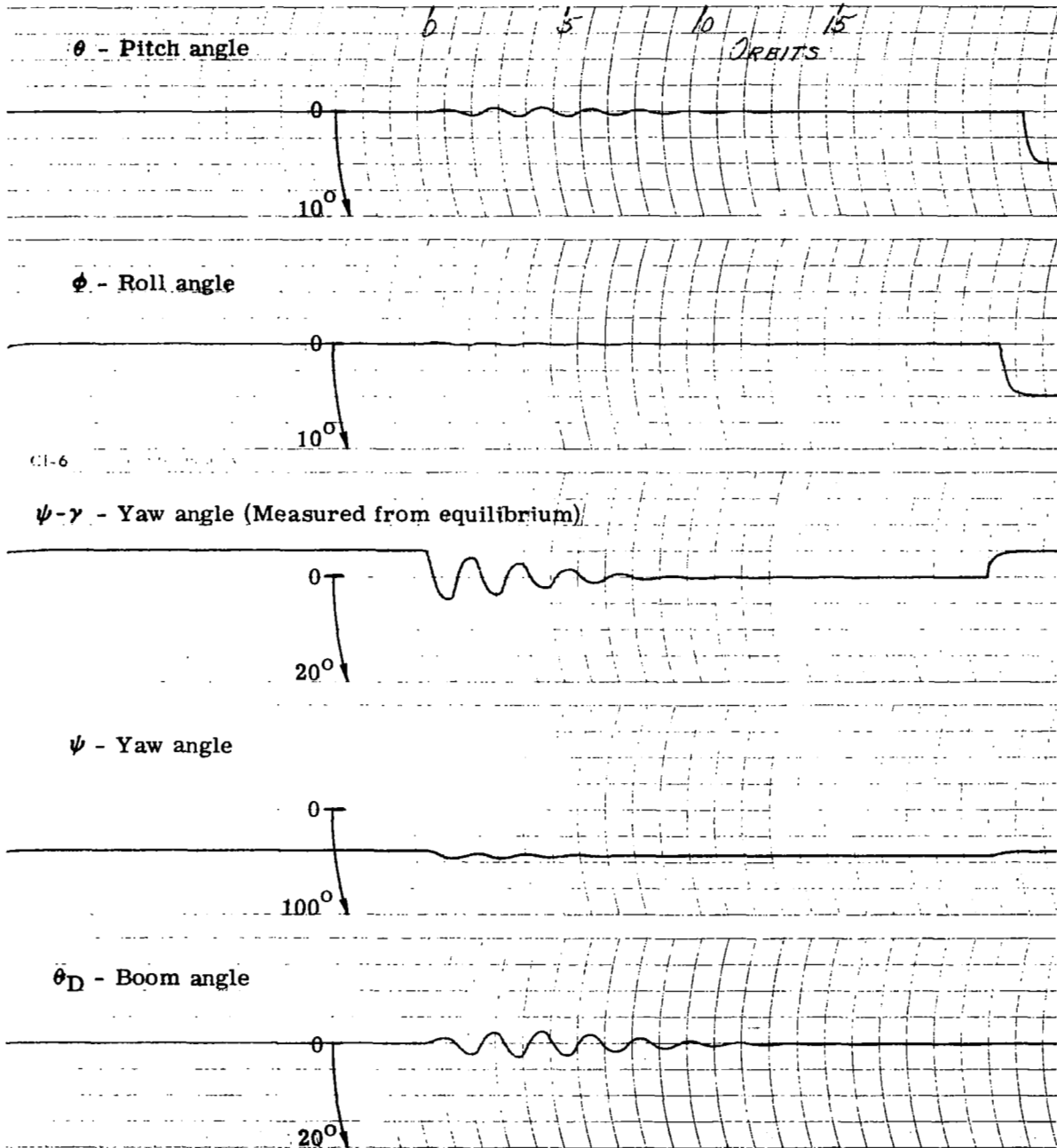


Figure 26. - Continued.

RUN NO. 24

F = 0.02
D = 0.095
J = 0.1739

K'' = 3.929
B'' = 0.2727
 $\psi_D = -50.8^\circ$
 $\gamma = 44.8$

Initial Condition
 $\theta = 5^\circ$
 $\phi = 5^\circ$
 $\psi = -5^\circ + \gamma$

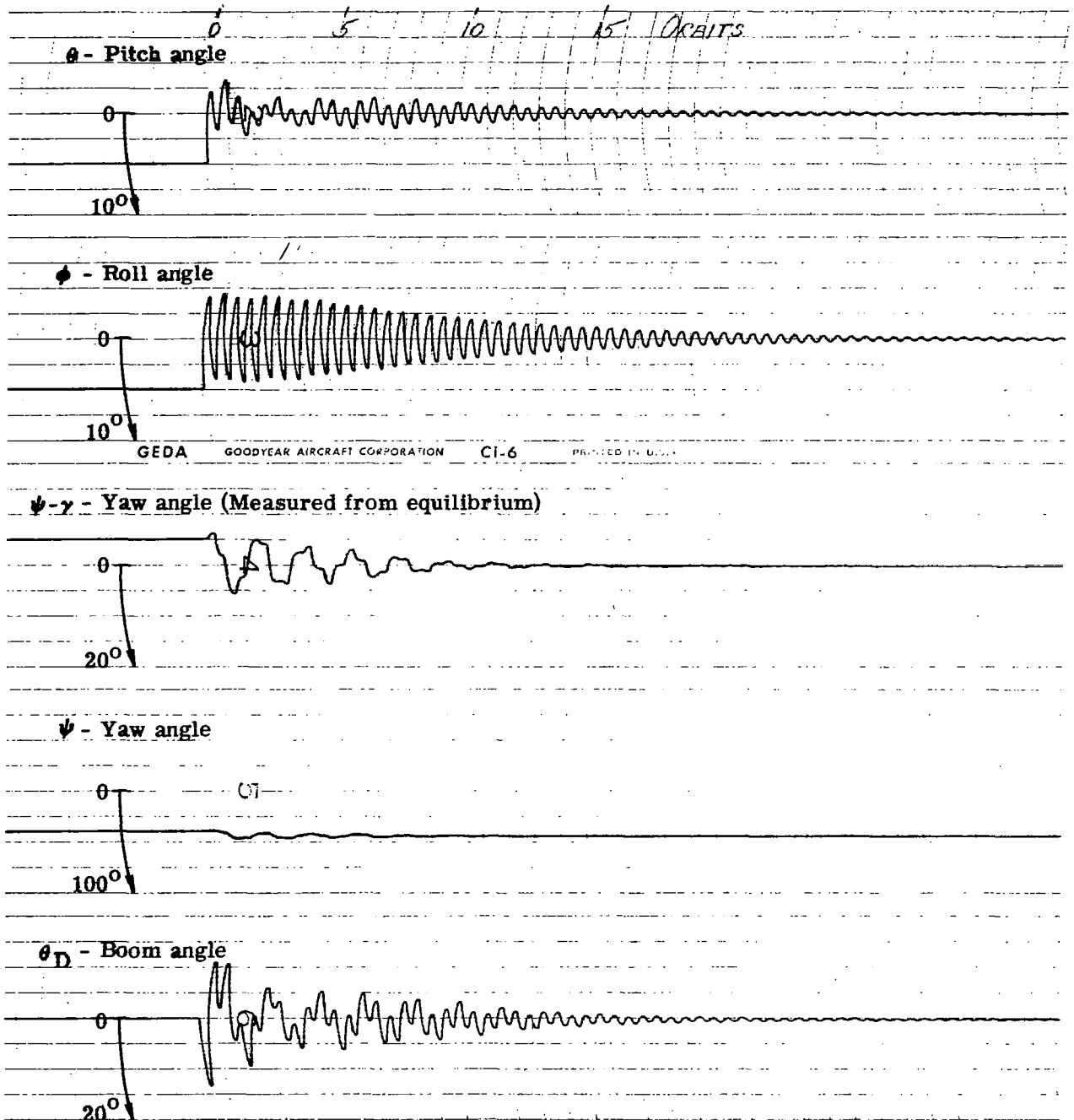


Figure 26. - Concluded.

RUN NO. 25

$F = 0.02$
 $D = 0.0175$
 $J = 0.1739$

$K'' = 4.04$
 $B'' = 1.503$
 $\psi_D = -80^\circ$
 $\gamma = 29.7^\circ$

Initial Condition
 $\theta = 5^\circ$
 $\phi = 0$
 $\psi = 0 + \gamma$

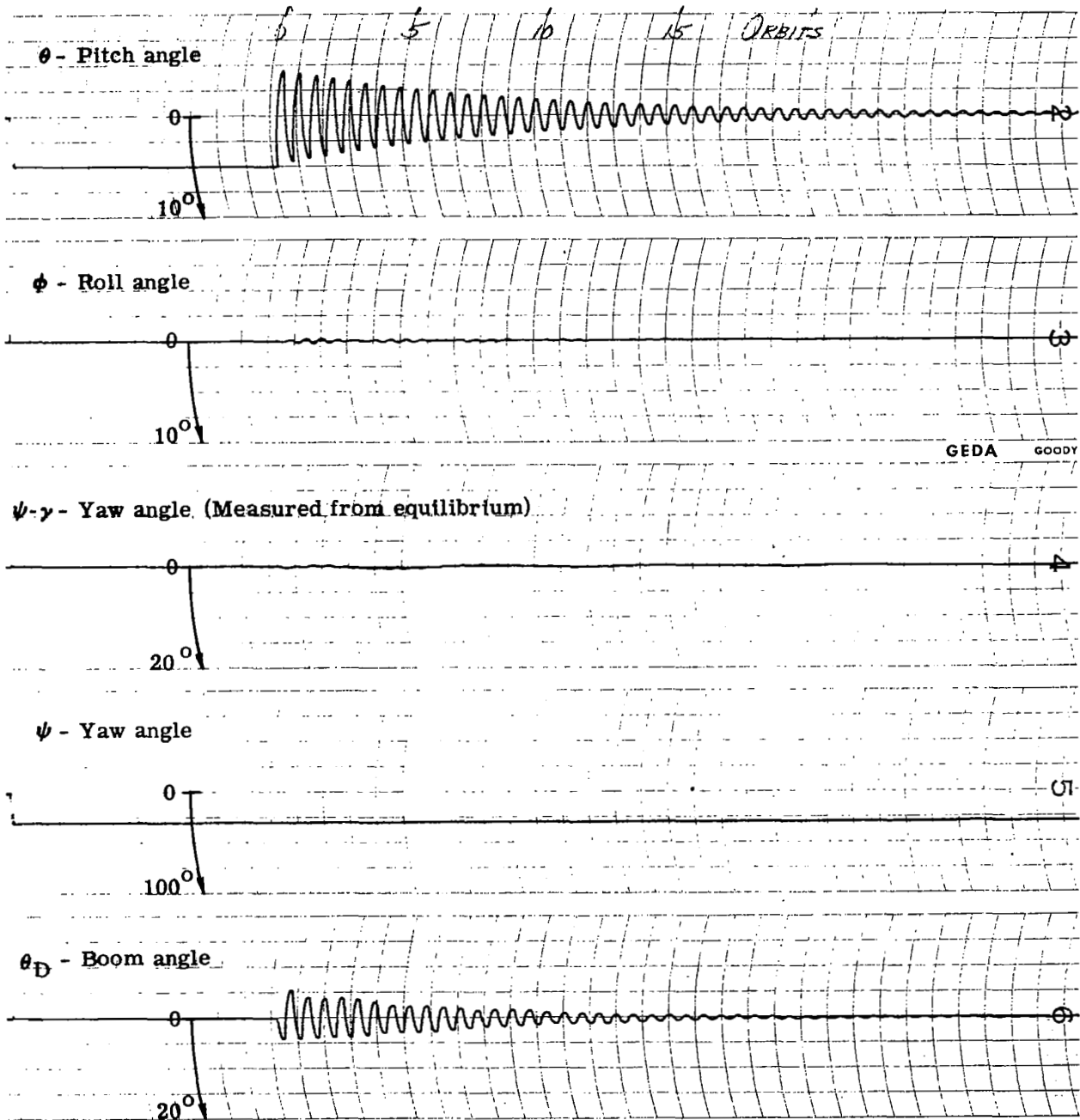


Figure 27. - Transient response when optimum boom inertias are $F = 0.02$ and $D = 0.0175$.

RUN NO. 26

F = 0.02
D = 0.0175
J = 0.1739

K'' = 4.04
B'' = 1.503
 $\psi_D = -29.7^\circ$
 $\gamma = 29.7^\circ$

Initial Condition
 $\theta = 0$
 $\phi = 5^\circ$
 $\psi = 0 + \gamma$

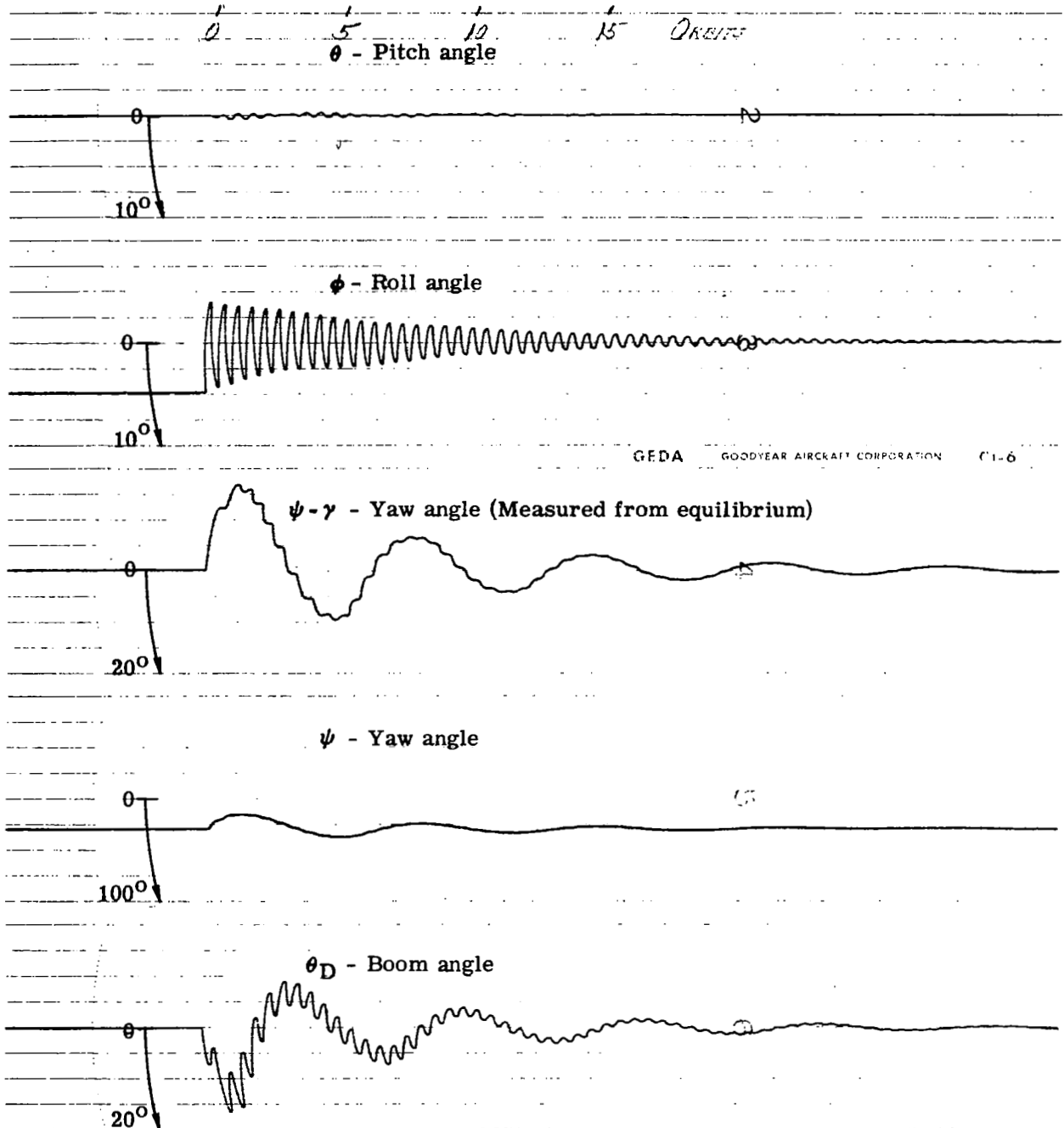


Figure 27. - Continued.

RUN NO. 27

$F = 0.02$
 $D = 0.0175$
 $J = 0.1739$

$K'' = 4.04$
 $B'' = 1.503$
 $\psi_D = -80^\circ$
 $\gamma = 29.7^\circ$

Initial Condition

$\theta = 0$
 $\phi = 0$
 $\psi = -5^\circ + \gamma$

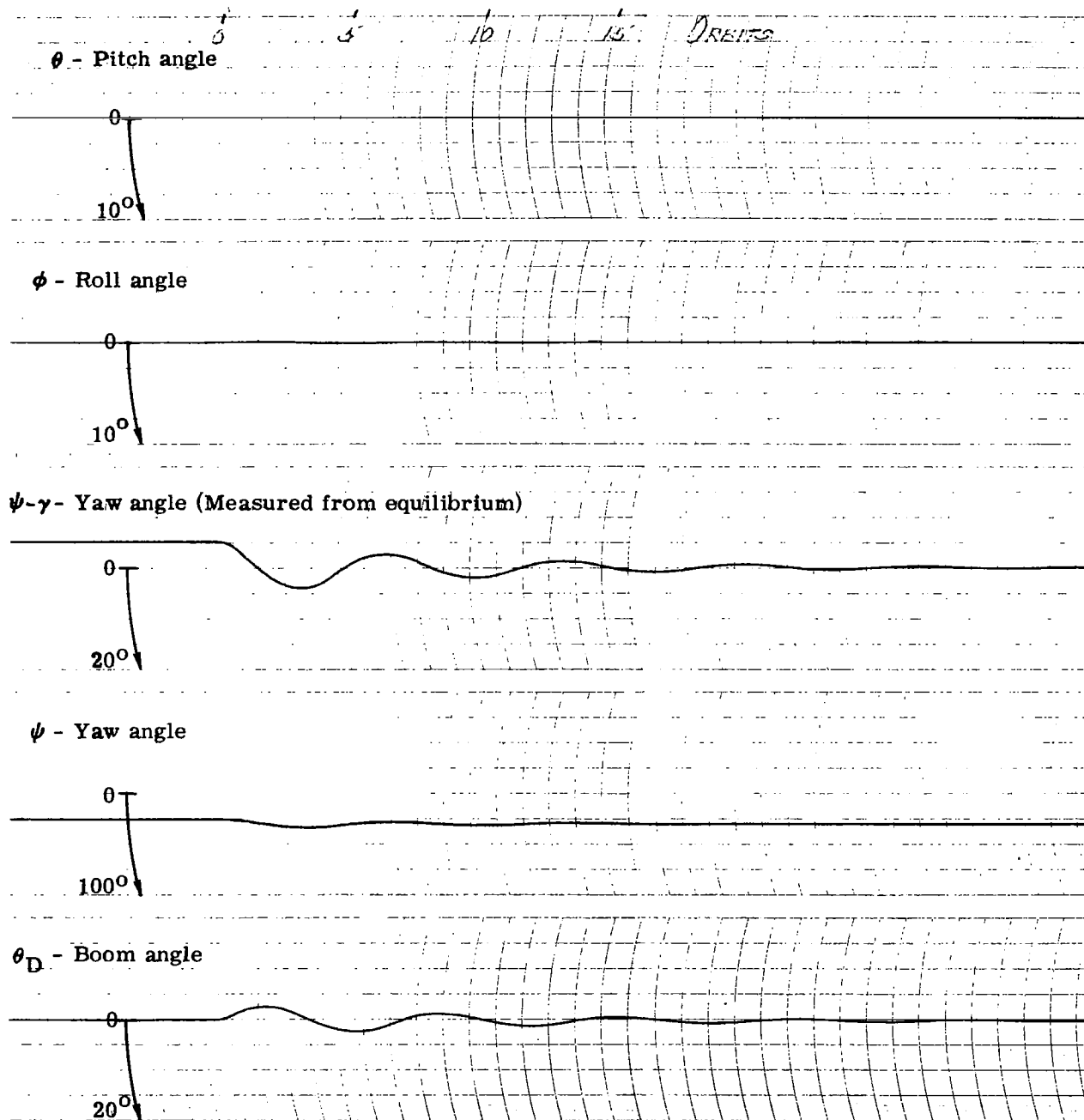


Figure 27. - Continued.

RUN NO. 28

F = 0.02
D = 0.0175
J = 0.1739

K'' = 4.04
B'' = 1.503
 $\psi_D = -80^\circ$
 $\gamma = 29.7^\circ$

Initial Condition
 $\theta = 5^\circ$
 $\phi = 5^\circ$
 $\psi = -5^\circ + \gamma$

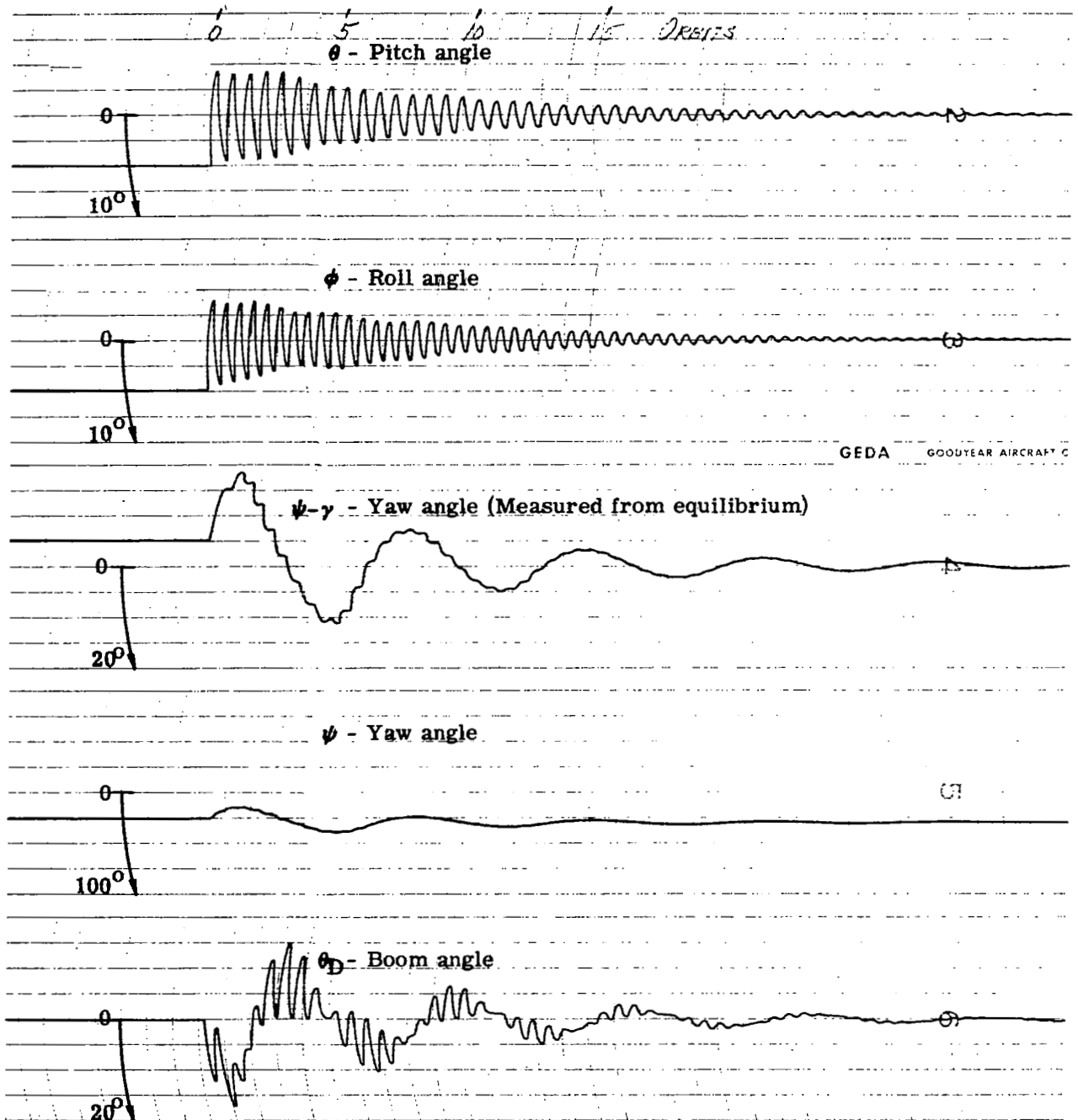


Figure 27. - Concluded.

RUN NO. 29

$F = 0.01$
 $D = 0.00875$
 $J = 0.1739$

$K'' = 3.99$
 $B'' = 1.543$
 $\psi_D = -80.8^\circ$
 $\gamma = 29.2$

Initial Condition
 $\theta = 5^\circ$
 $\phi = 0$
 $\psi = 0 + \gamma$

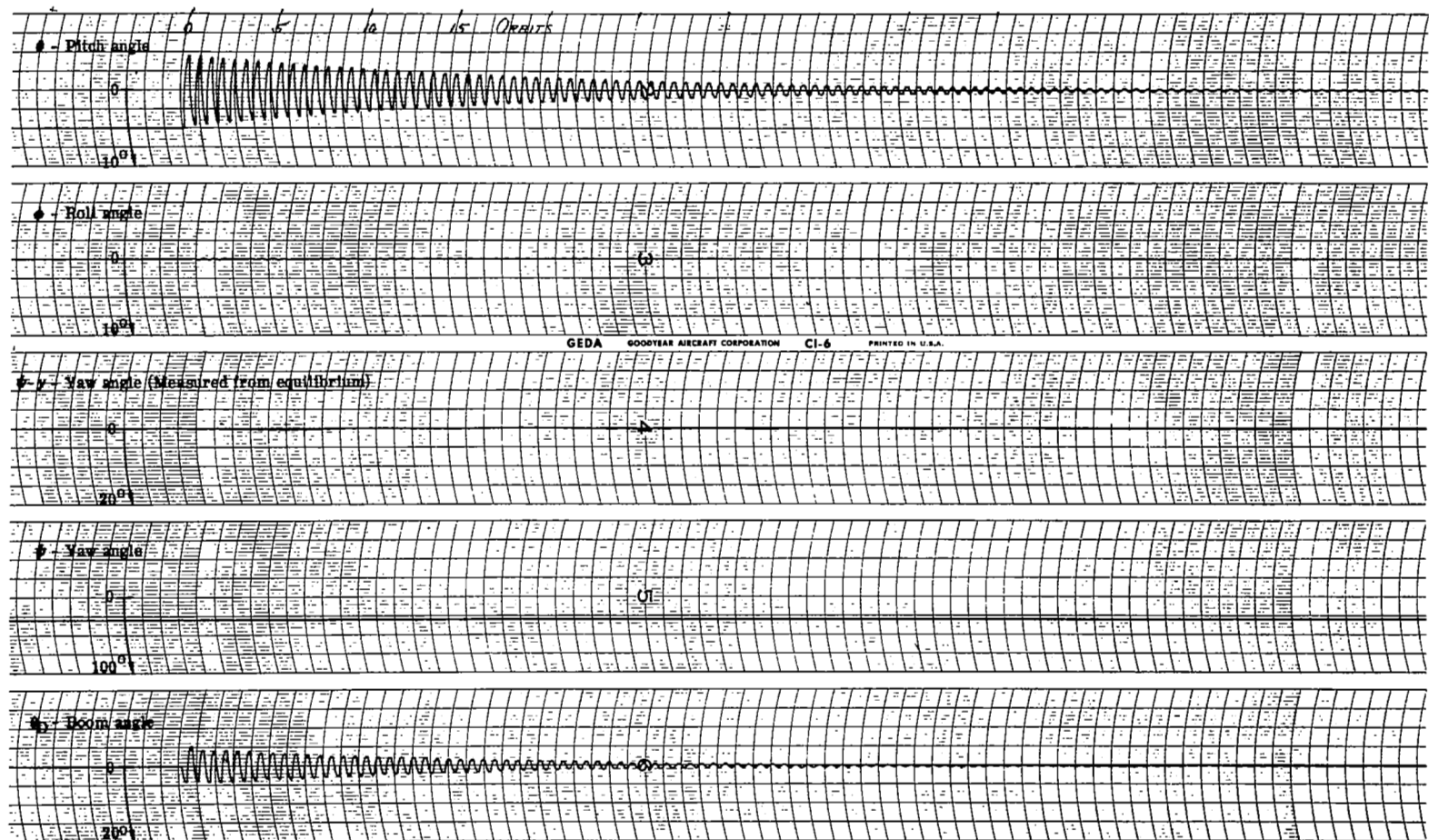


Figure 28. Transient response when optimum boom inertias are $F = 0.01$ and $D = 0.00875$.

RUN NO. 30

$F = 0.01$
 $D = 0.00875$
 $J = 0.1739$

$K'' = 3.99$
 $B'' = 1.543$
 $\psi_D = -80.8^\circ$
 $\gamma = 29.2^\circ$

Initial Condition

$\theta = 0$
 $\phi = 5^\circ$
 $\psi = 0 + \gamma$

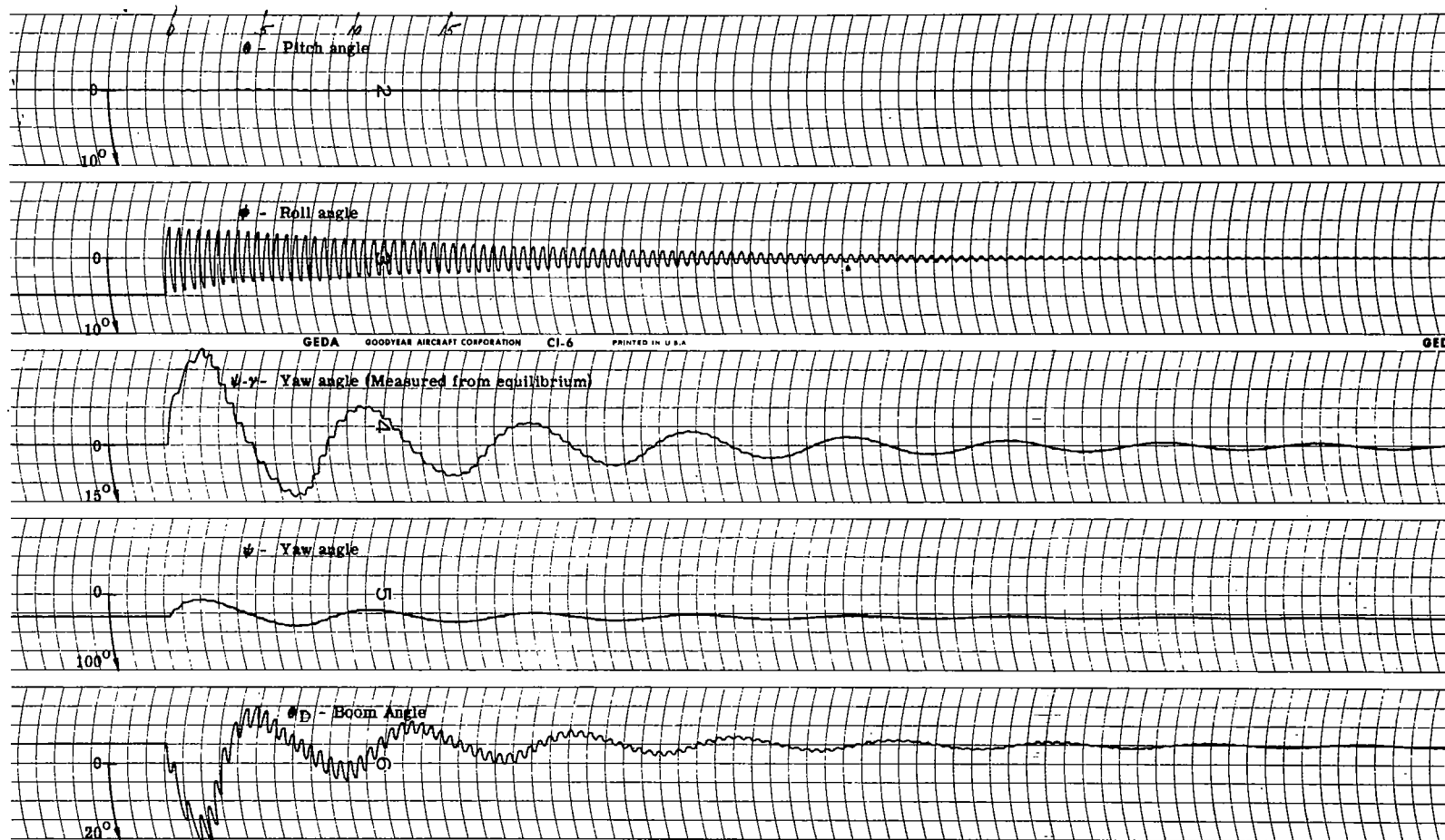


Figure 28. - Continued.

RUN NO. 31

$F = 0.01$
 $D = 0.00875$
 $J = 0.1739$

$K'' = 3.99$
 $B'' = 1.543$
 $\psi_D = -80.8^\circ$
 $\gamma = 29.2^\circ$

Initial Condition

$\theta = 0$
 $\phi = 0$
 $\psi = -5^\circ + \gamma$

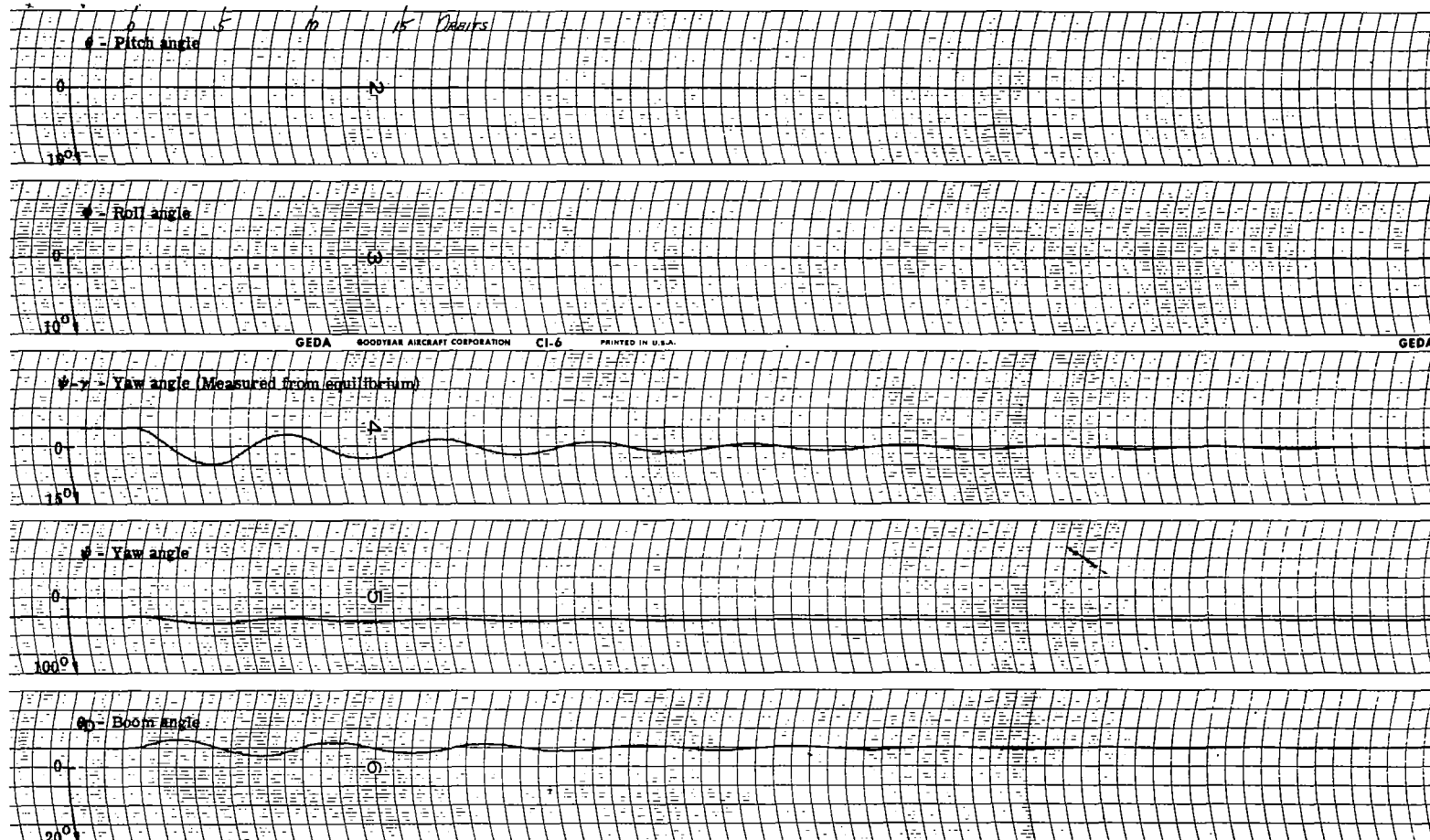


Figure 28. - Continued.

RUN NO. 32

$F = 0.01$
 $D = 0.00875$
 $J = 0.1739$

$K'' = 3.99$
 $B'' = 1.54$
 $\psi_D = -80.8^\circ$
 $\gamma = 29.2^\circ$

Initial Condition
 $\theta = 5^\circ$
 $\phi = 5^\circ$
 $\psi = -5^\circ + \gamma$

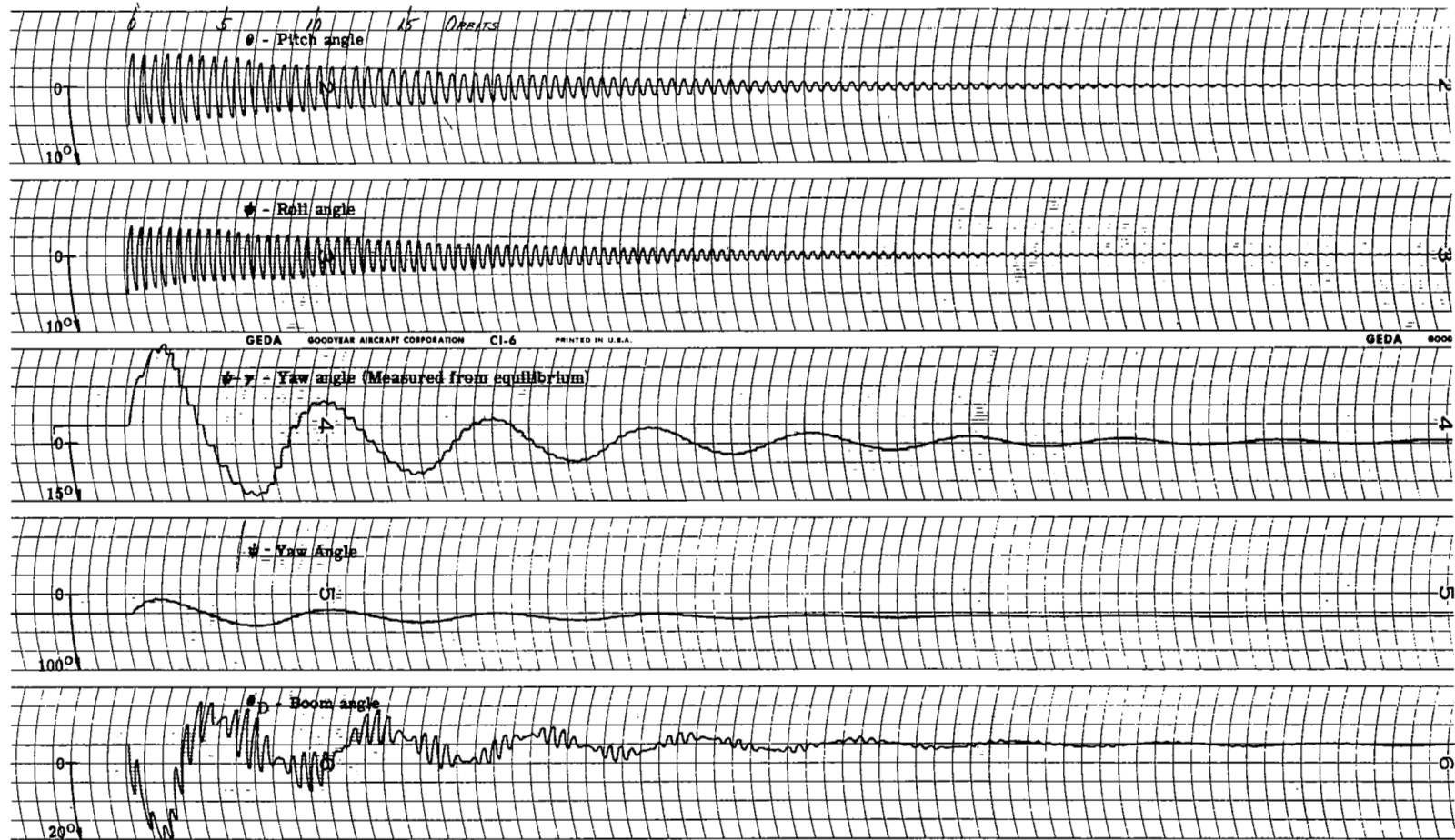


Figure 28. - Concluded.

RUN NO. 33

F = 0.10
D = 0.08
J = 0.1739

K'' = 4.20
B'' = 1.393
 $\psi_D = -67.2^\circ$
 $\gamma = 26^\circ$

Initial Condition
 $\theta = 5^\circ$
 $\phi = 0$
 $\psi = 0 + \gamma$

One orbit/day

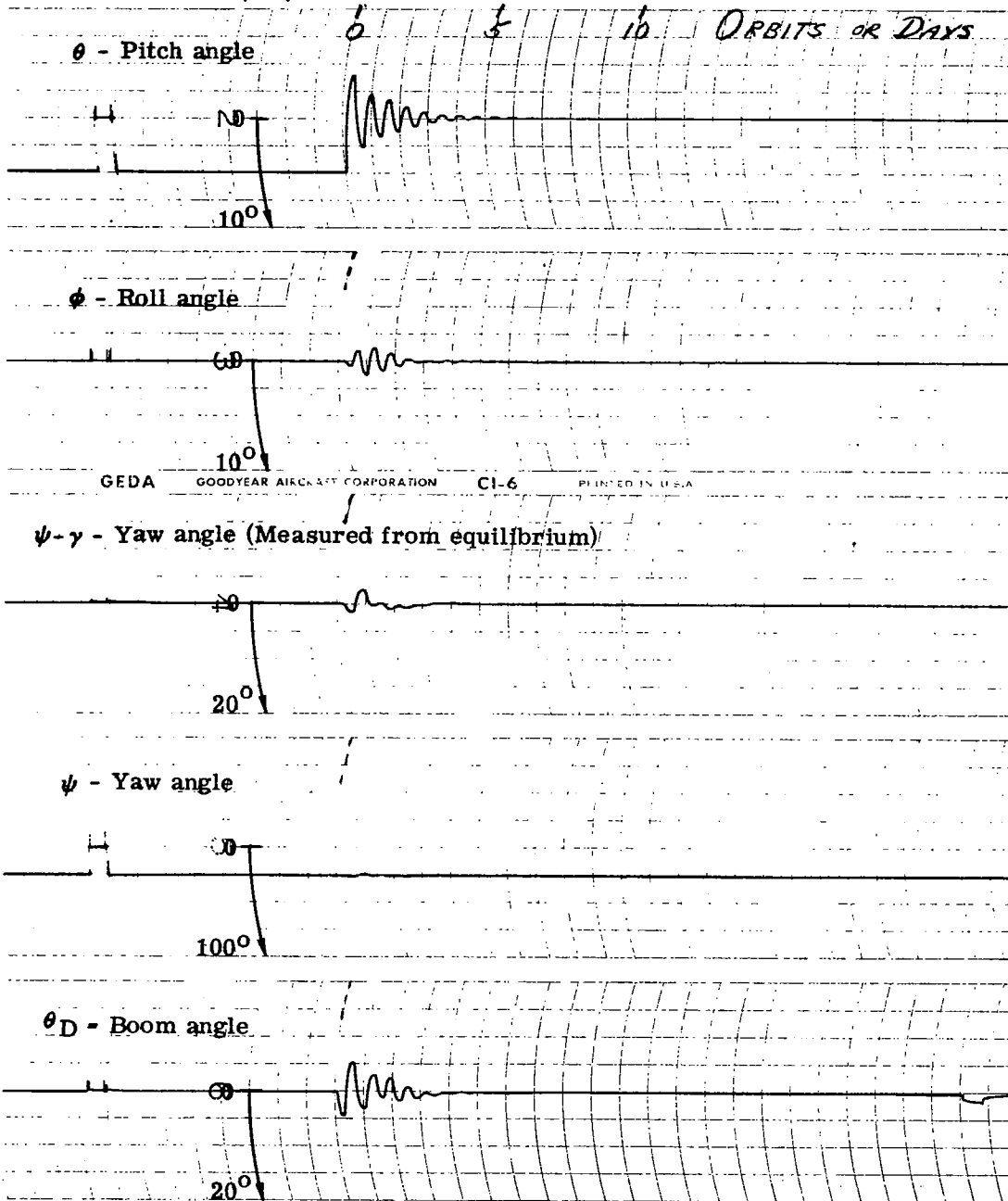


Figure 29. - Transient response for configuration A at synchronous orbit.

RUN NO. 34

$F = 0.10$
 $D = 0.08$
 $J = 0.1739$

$K'' = 4.20$
 $B'' = 1.393$
 $\psi_D = -67.2^\circ$
 $\gamma = 26^\circ$

Initial Condition

$\theta = 0$

$\phi = 5^\circ$

$\psi = 0 + \gamma$

One orbit/day

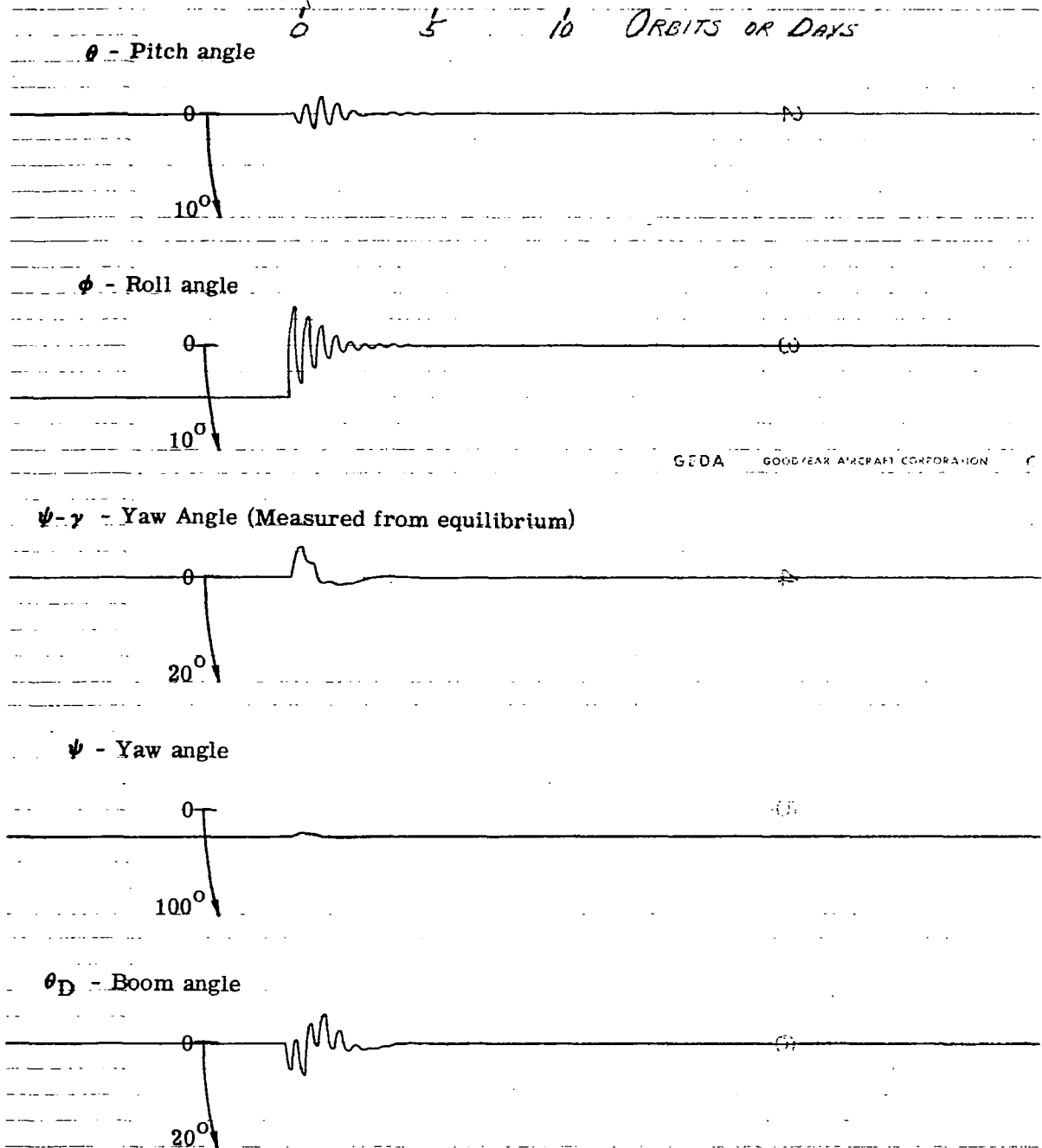


Figure 29. - Continued.

RUN NO. 35

$F = 0.10$

$D = 0.08$

$J = 0.1739$

$K'' = 4.20$

$B'' = 1.393$

$\psi_D = -67.2^\circ$

$\gamma = 26^\circ$

Initial Condition

$\theta = 0$

$\phi = 0$

$\psi = -5^\circ + \gamma$

One orbit/day

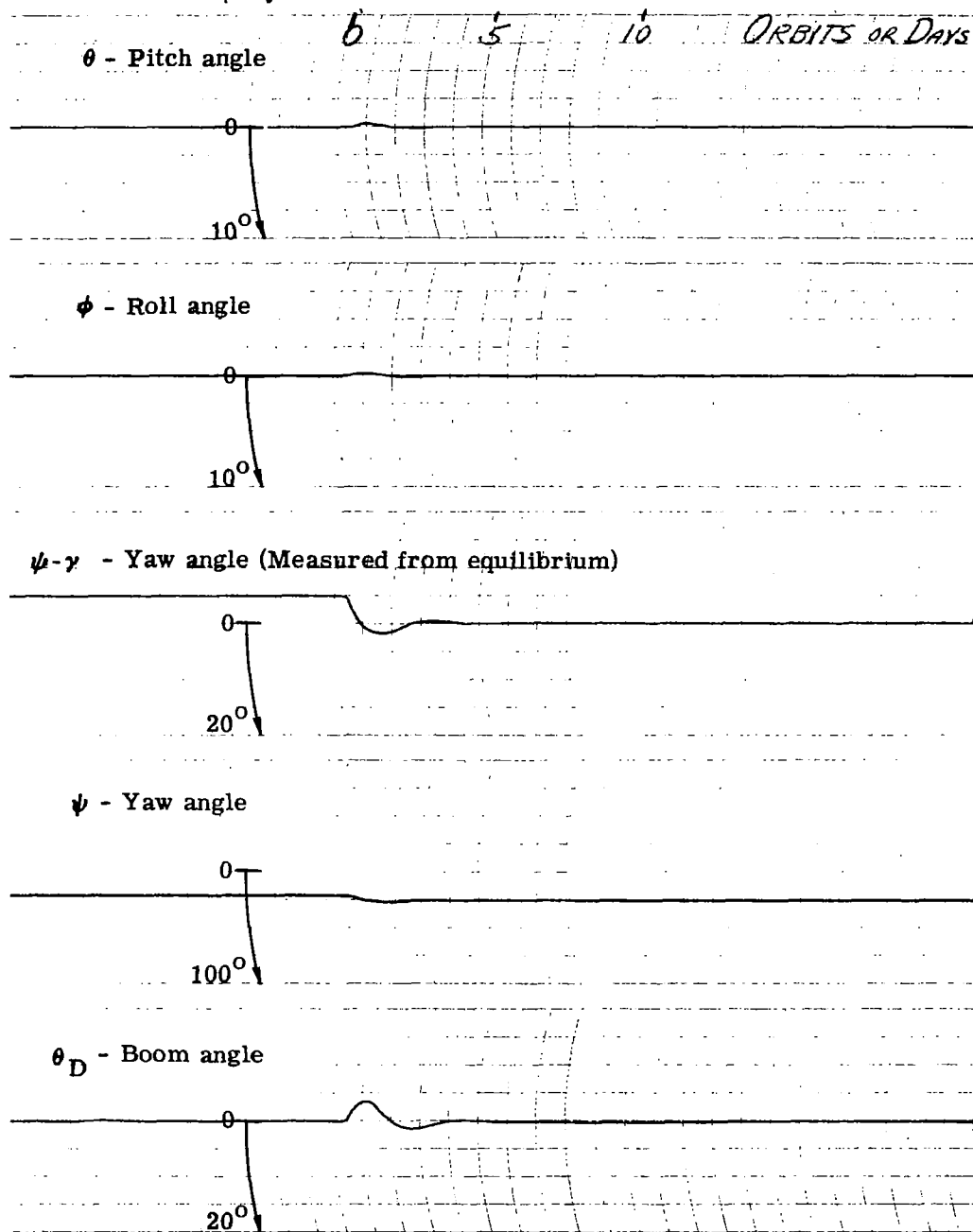


Figure 29. - Continued.

RUN NO. 36

$F = 0.10$
 $D = 0.08$
 $J = 0.1739$

$K'' = 4.20$
 $B'' = 1.393$
 $\psi_D = -67.2^\circ$
 $\gamma = 26^\circ$

Initial Condition
 $\theta = 5^\circ$
 $\phi = 5^\circ$
 $\psi = -5^\circ + \gamma$

One orbit/day

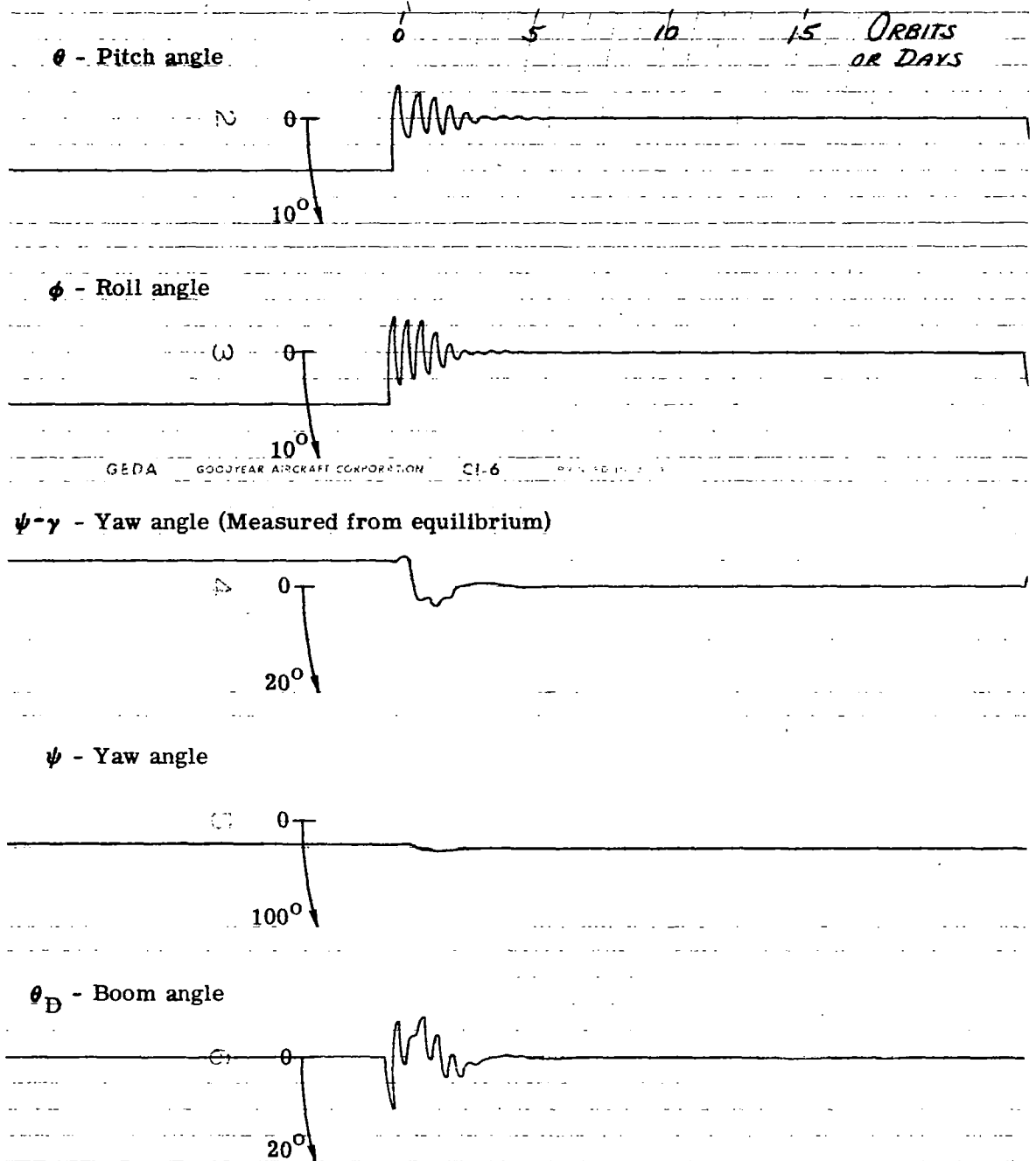


Figure 29. - Concluded.

RUN NO. 37

F = 0.12
D = 0.1
J = 0.1739

K'' = 4.297
B'' = 1.545
 $\psi_D = -65.1^\circ$
 $\gamma = +27^\circ$

Initial Condition
 $\theta = 5^\circ$
 $\phi = 0^\circ$
 $\psi = 0^\circ + \gamma$

One orbit/day

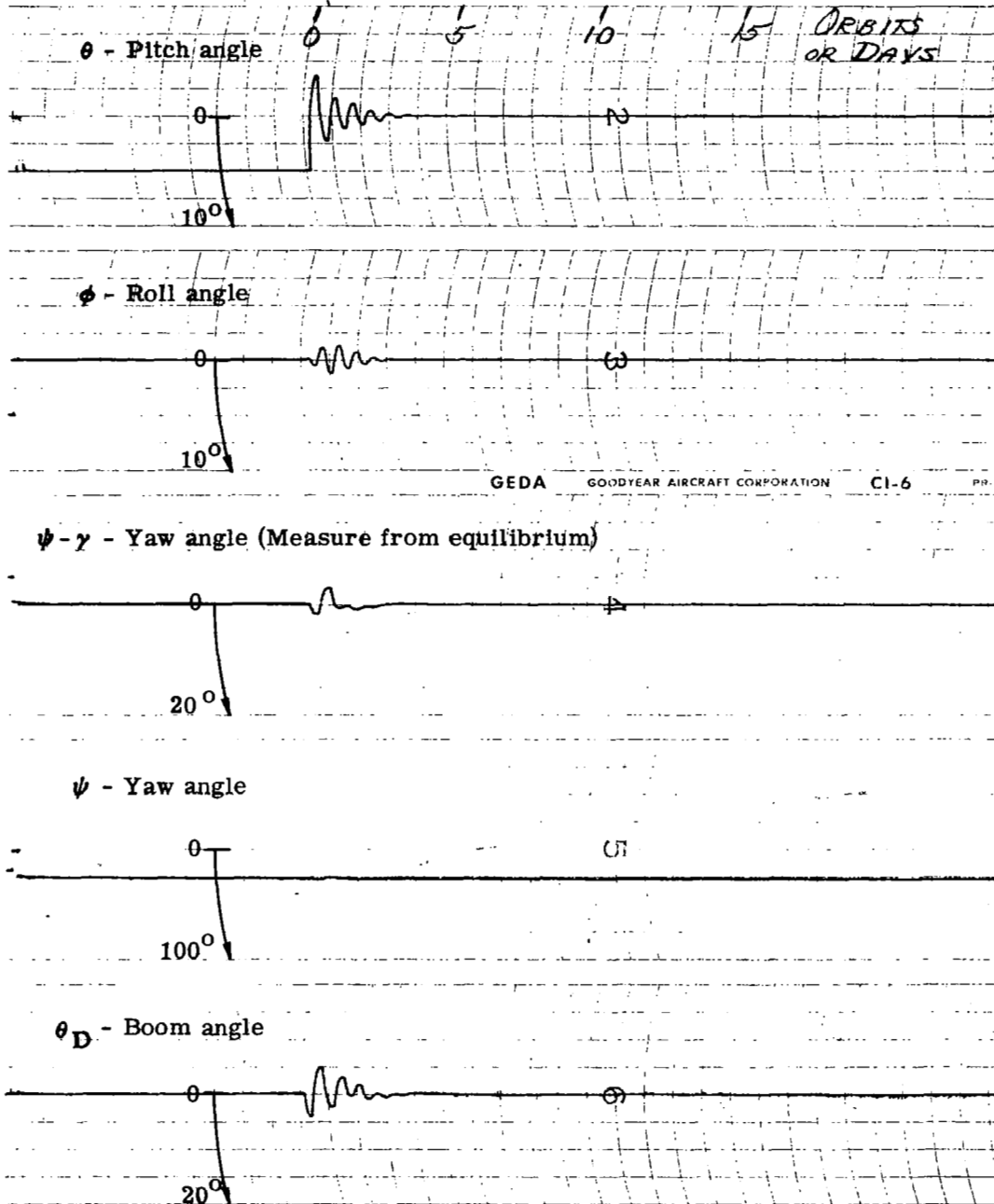


Figure 30. - Transient response for configuration B at synchronous orbit.

RUN NO. 38

$F = 0.12$
 $D = 0.1$
 $J = 0.1739$

$K'' = 4.297$
 $B'' = 1.545$
 $\psi_D = -65.1^\circ$
 $\gamma = +27^\circ$

Initial Condition
 $\theta = 0$
 $\phi = 5^\circ$
 $\psi = 0 + \gamma$

One orbit/day

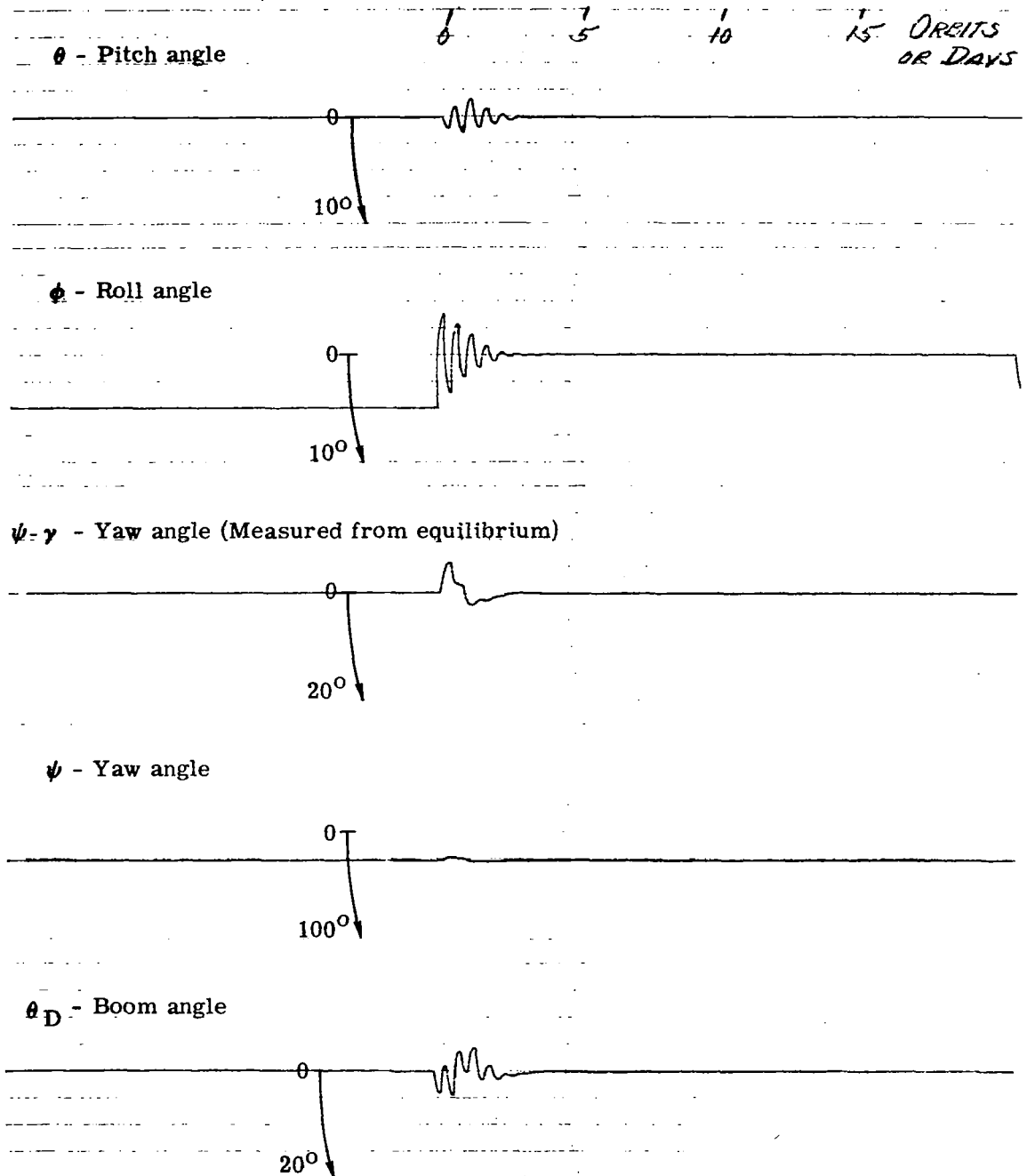


Figure 30. - Continued.

RUN NO. 39

$F = 0.12$

$D = 0.1$

$J = 0.1739$

$K'' = 4.297$

$B'' = 0.1545$

$\psi_D = -65.1^\circ$

$\gamma = +27^\circ$

Initial Condition

$\theta = 0$

$\phi = 0$

$\psi = -5^\circ + \gamma$

One orbit/day

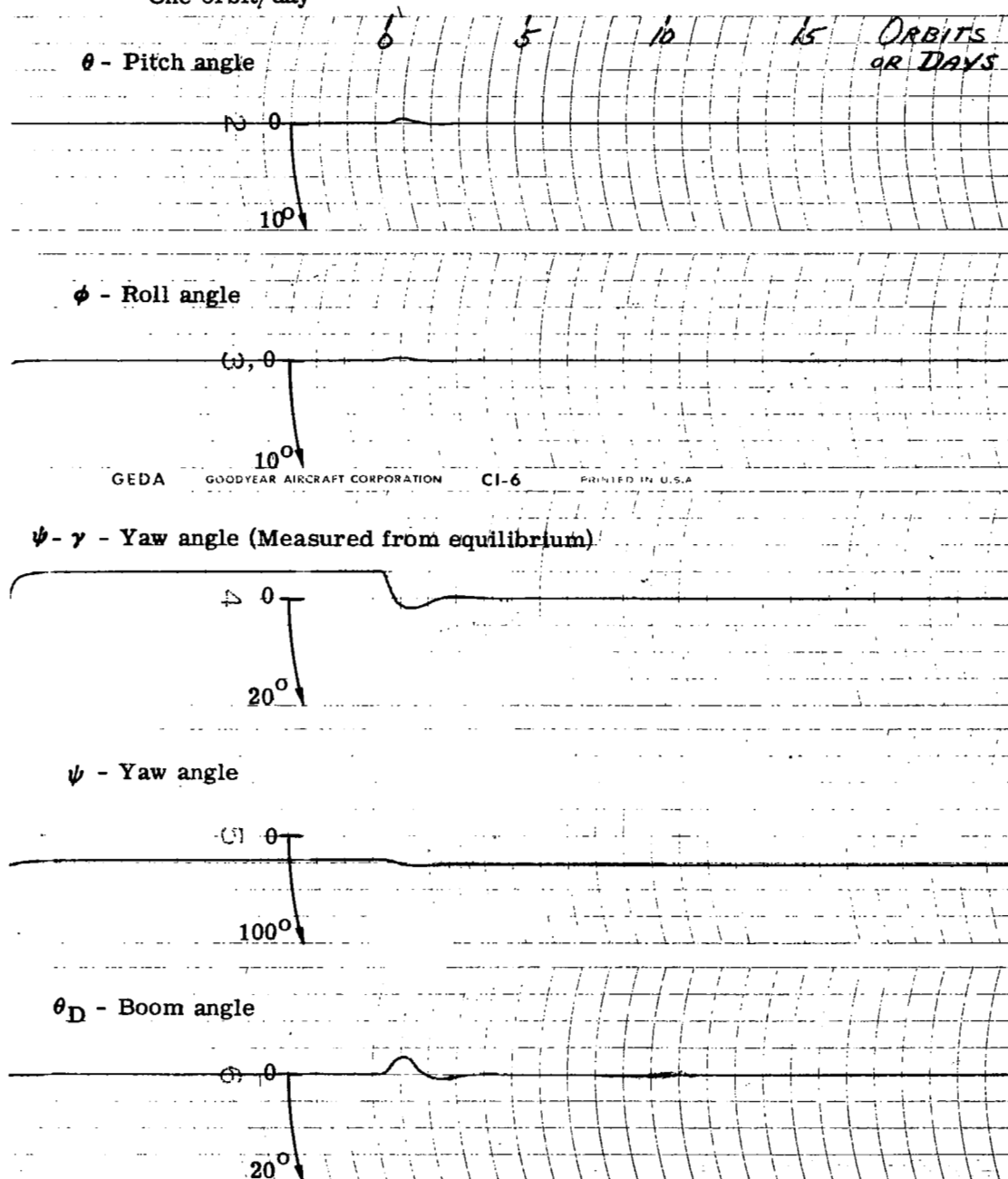


Figure 30. - Continued.

RUN NO. 40

$F = 0.12$
 $D = 0.1$
 $J = 0.1739$

$K'' = 4.297$
 $B'' = 1.545$
 $\psi_D = -65.1^\circ$
 $\gamma = +27^\circ$

Initial Condition
 $\theta = 5^\circ$
 $\phi = 5^\circ$
 $\psi = -5^\circ + \gamma$

One orbit/day

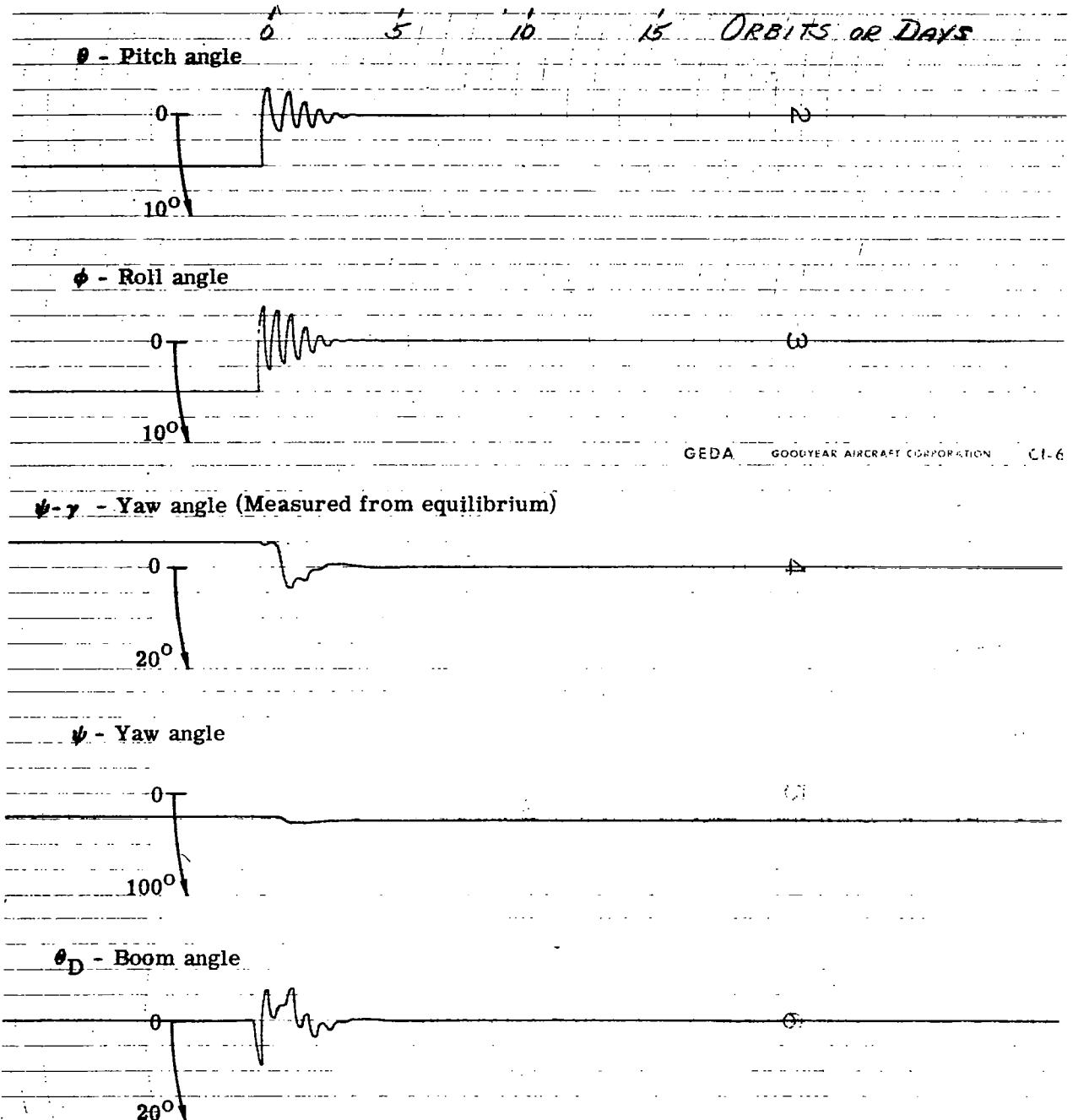


Figure 30. - Concluded.

RUN NO. 41

$F = 0.008$
 $D = 0.006$
 $J = 0.1739$

$K'' = 4.125$
 $B'' = 1.56$
 $\psi_D = -78^\circ$
 $\gamma = 23.3^\circ$

Initial Condition
 $\theta = 5^\circ$
 $\phi = 0^\circ$
 $\psi = 0 + \gamma$

8.58 orbits/day

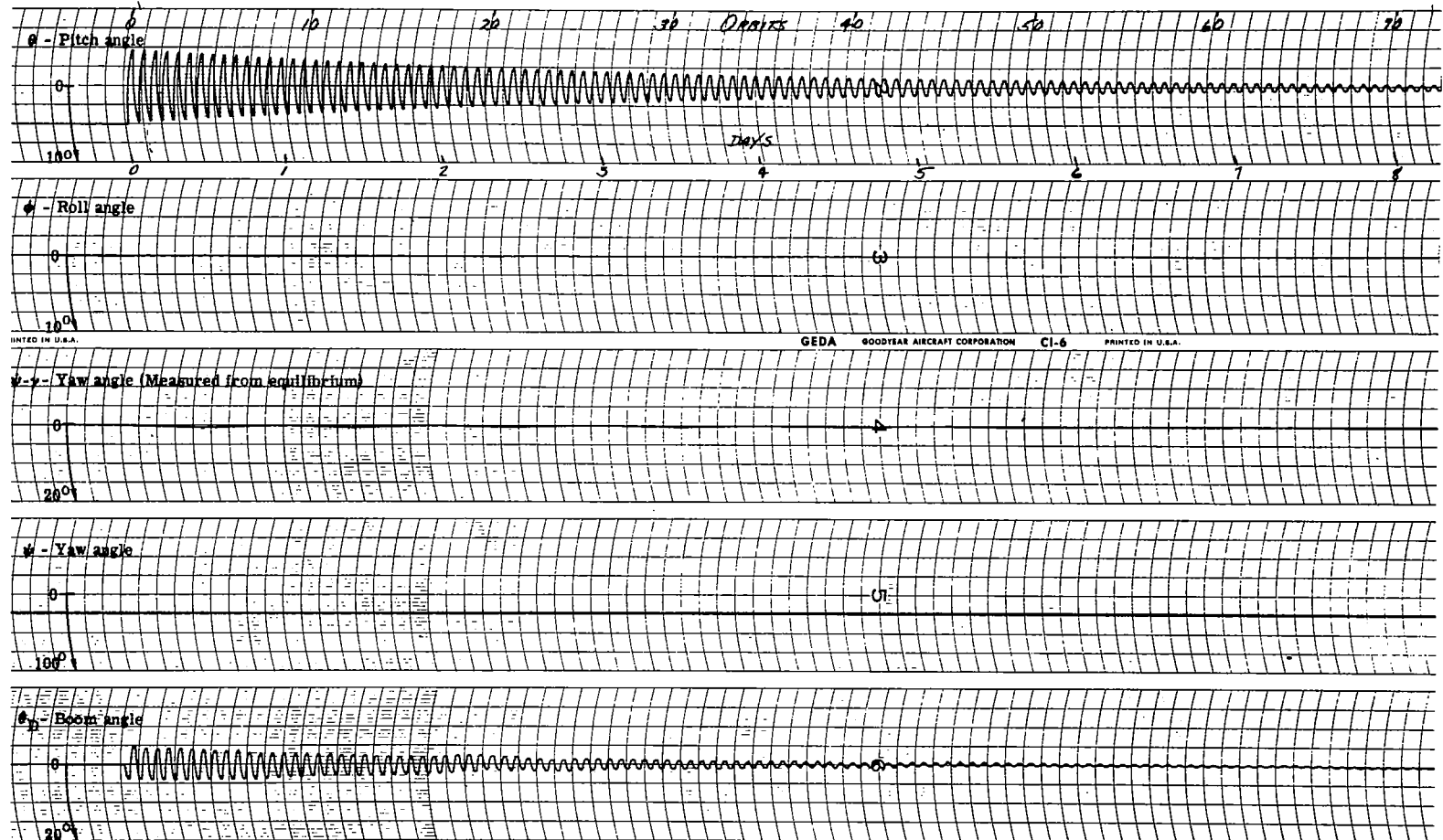


Figure 31. - Transient response for configuration C at 2000 n. mi. altitude with booms designed for non-tumbling orbital condition.

RUN NO. 42

$F = 0.008$
 $D = 0.006$
 $J = 0.1739$

$K'' = 4.125$
 $B'' = 1.56$
 $\psi_D = -78^\circ$
 $\gamma = +23.3^\circ$

Initial Condition
 $\theta = 0$
 $\phi = 5^\circ$
 $\psi = 0 + \gamma$

8.58 orbits/day

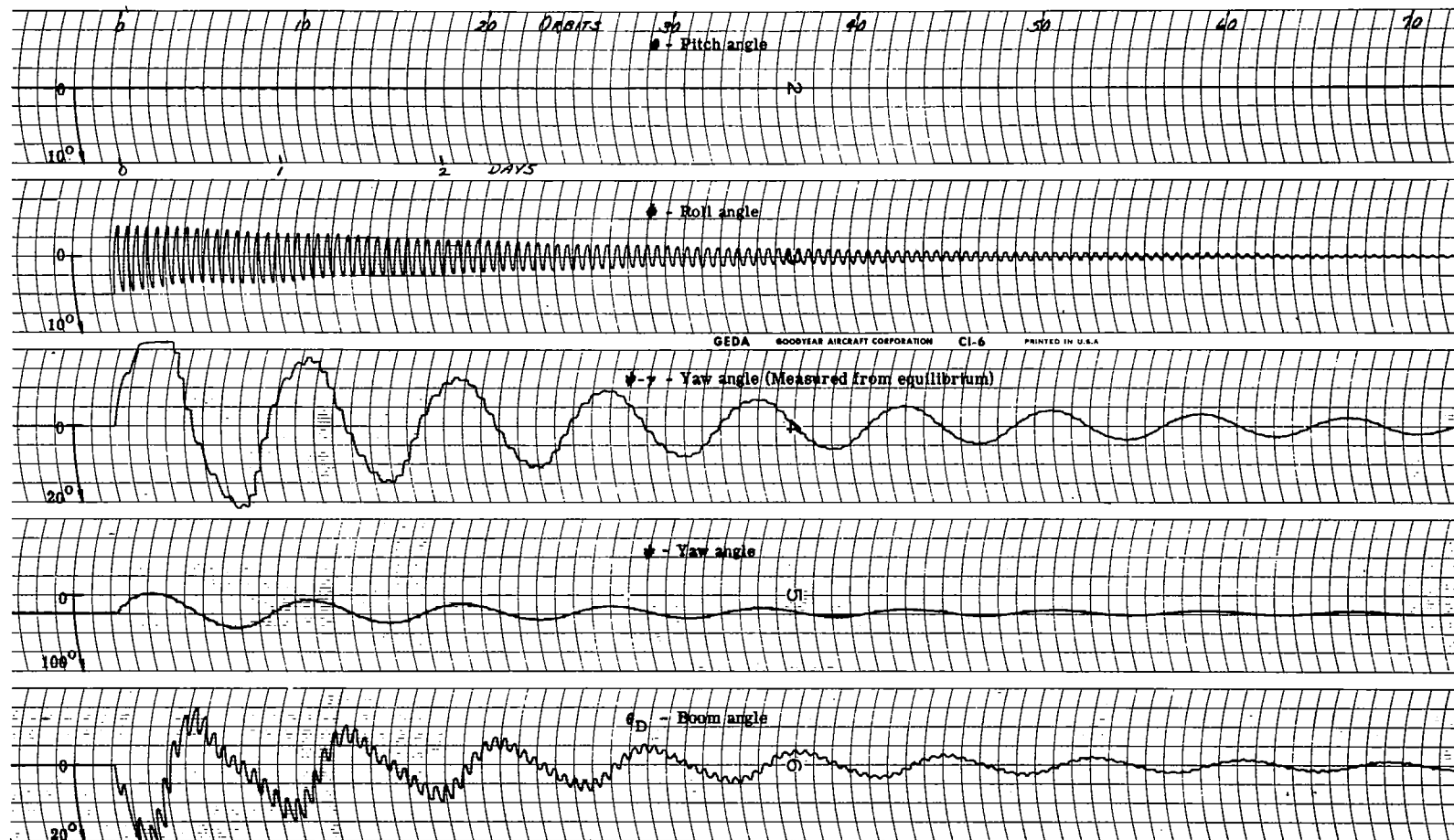


Figure 31. - Continued.

RUN NO. 43

$F = 0.008$
 $D = 0.006$
 $J = 0.1739$

$K'' = 4.125$
 $B'' = 1.56$
 $\psi_D = -78^\circ$
 $\gamma = 23.3$

Initial Condition
 $\theta = 0$
 $\phi = 0$
 $\psi = -5^\circ + \gamma$

8.58 orbits/day

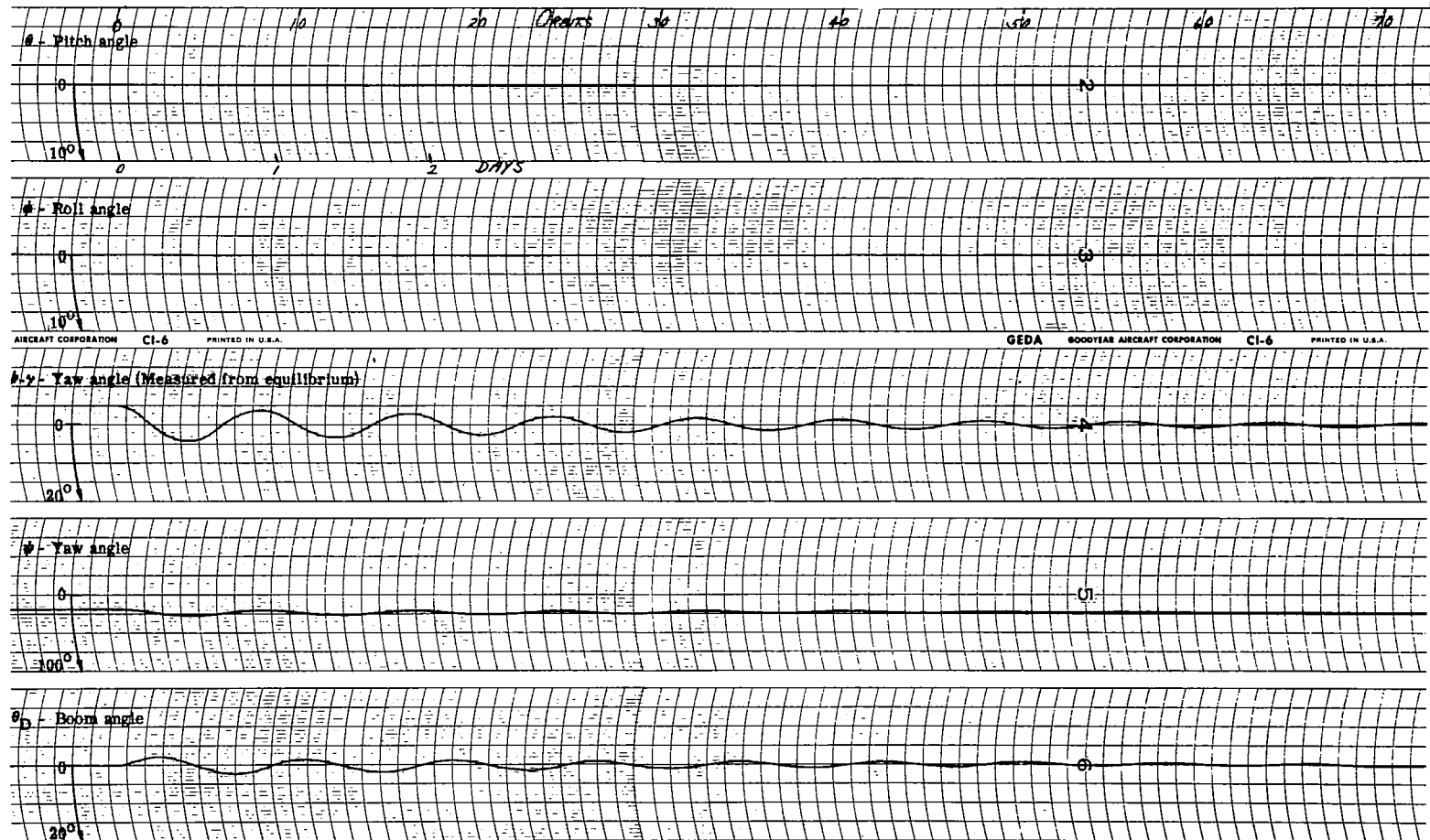


Figure 31. - Continued.

RUN NO. 44

$F = 0.008$
 $D = 0.006$
 $J = 0.1739$

$K'' = 4.125$
 $B'' = 1.56$
 $\psi_D = -78^\circ$
 $\gamma = +23.3^\circ$

Initial Condition

 $\theta = 5^\circ$ $\phi = 5^\circ$ $\psi = -5^\circ + \gamma$

8.58 orbits/day

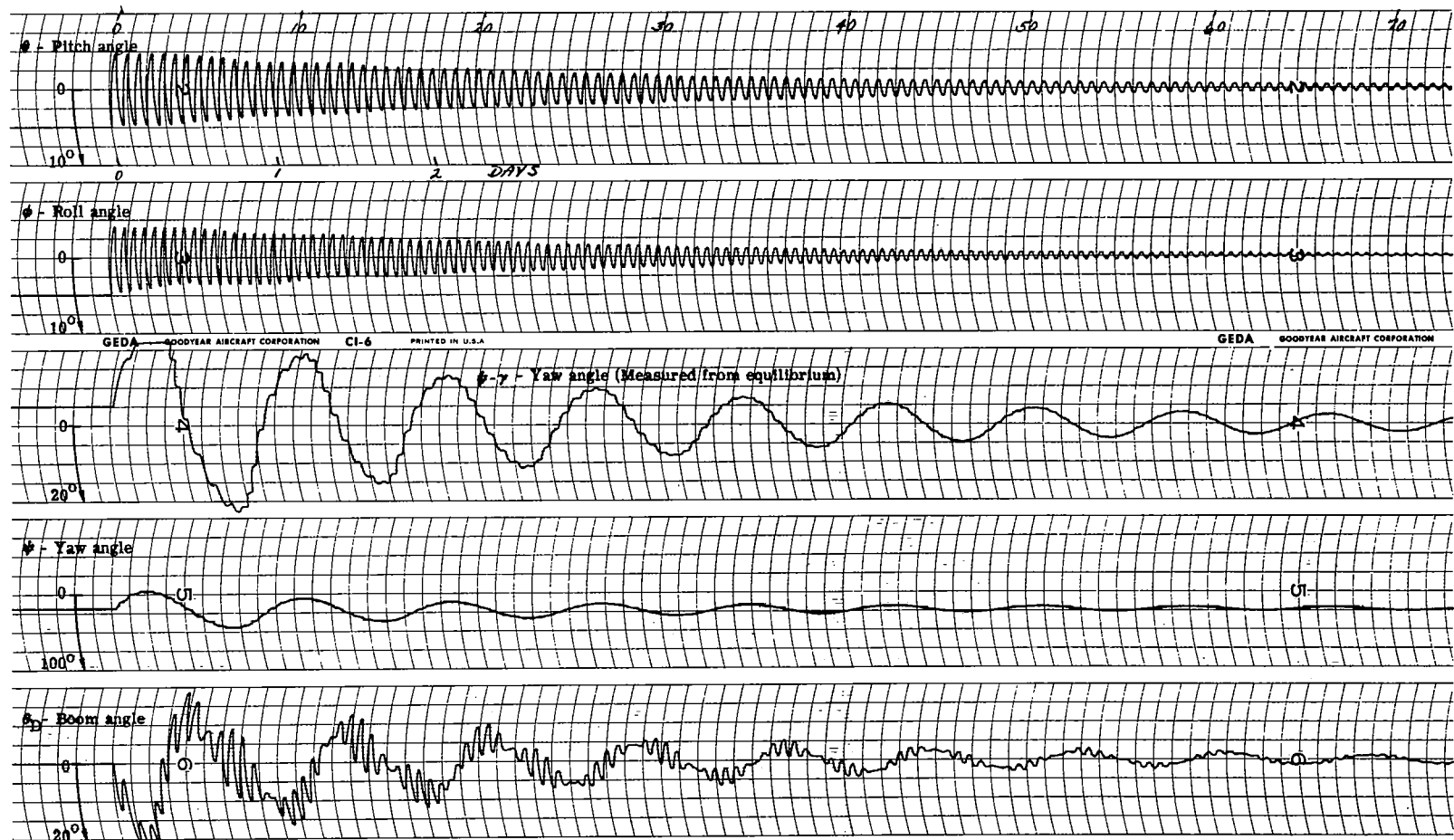


Figure 31. - Concluded.

RUN NO. 45

$F = 0.02$
 $D = 0.015$
 $J = 0.1739$

$K'' = 4.205$
 $B'' = 1.476$
 $\psi_D = -74.4^\circ$
 $\gamma = 23.7^\circ$

Initial Condition
 $\theta = 5^\circ$
 $\phi = 0$
 $\psi = 0 + \gamma$

3.74 orbits/day

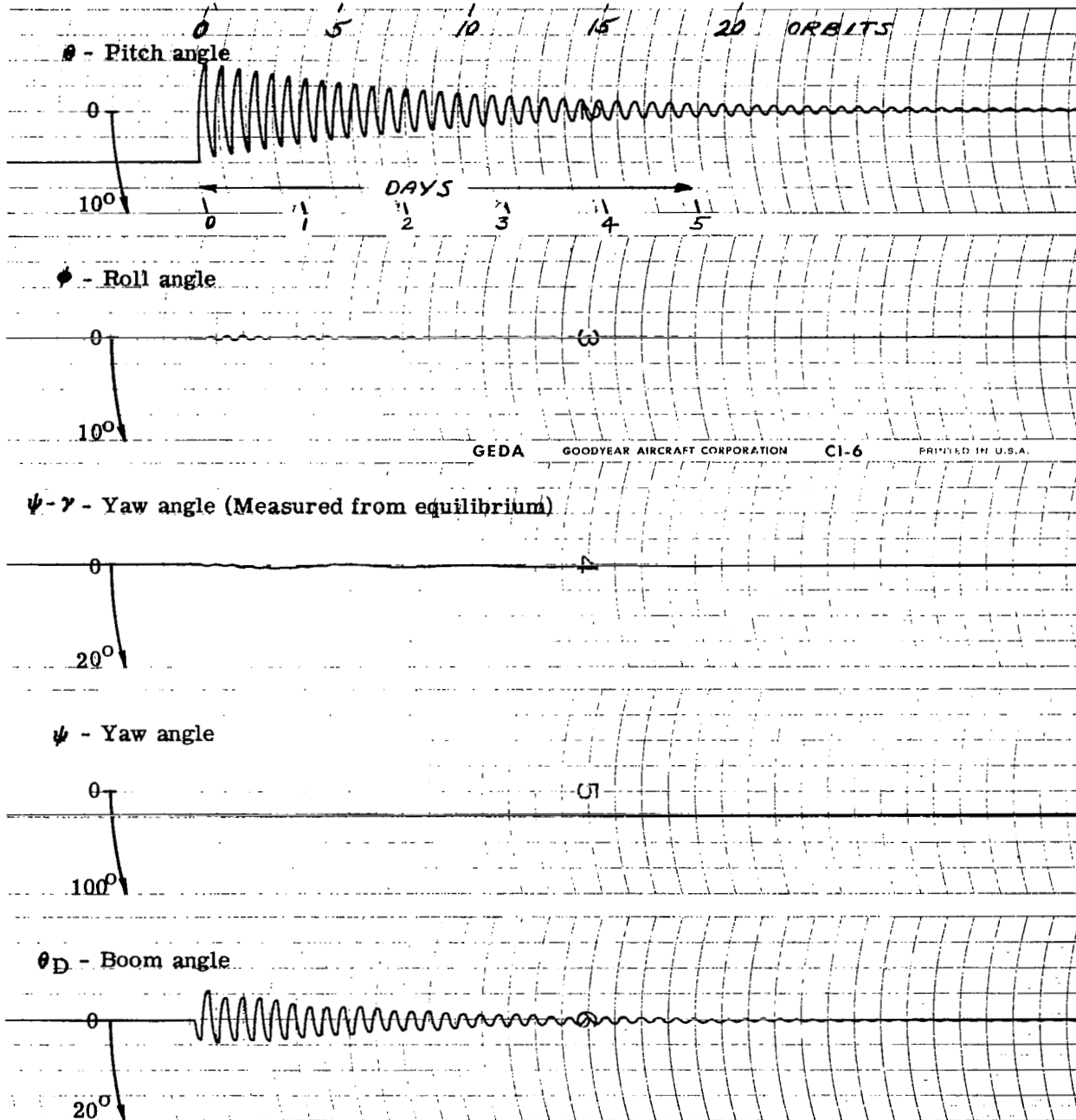


Figure 32. - Transient response for configuration E at 6000 n. mi. altitude.

RUN NO. 46

$F = 0.02$
 $D = 0.015$
 $J = 0.1739$

$K'' = 4.205$
 $B'' = 1.476$
 $\psi_D = -74.4^\circ$
 $\gamma = 23.7^\circ$

Initial Condition
 $\theta = 0$
 $\phi = 5^\circ$
 $\psi = 0 + \gamma$

3.74 orbits/day

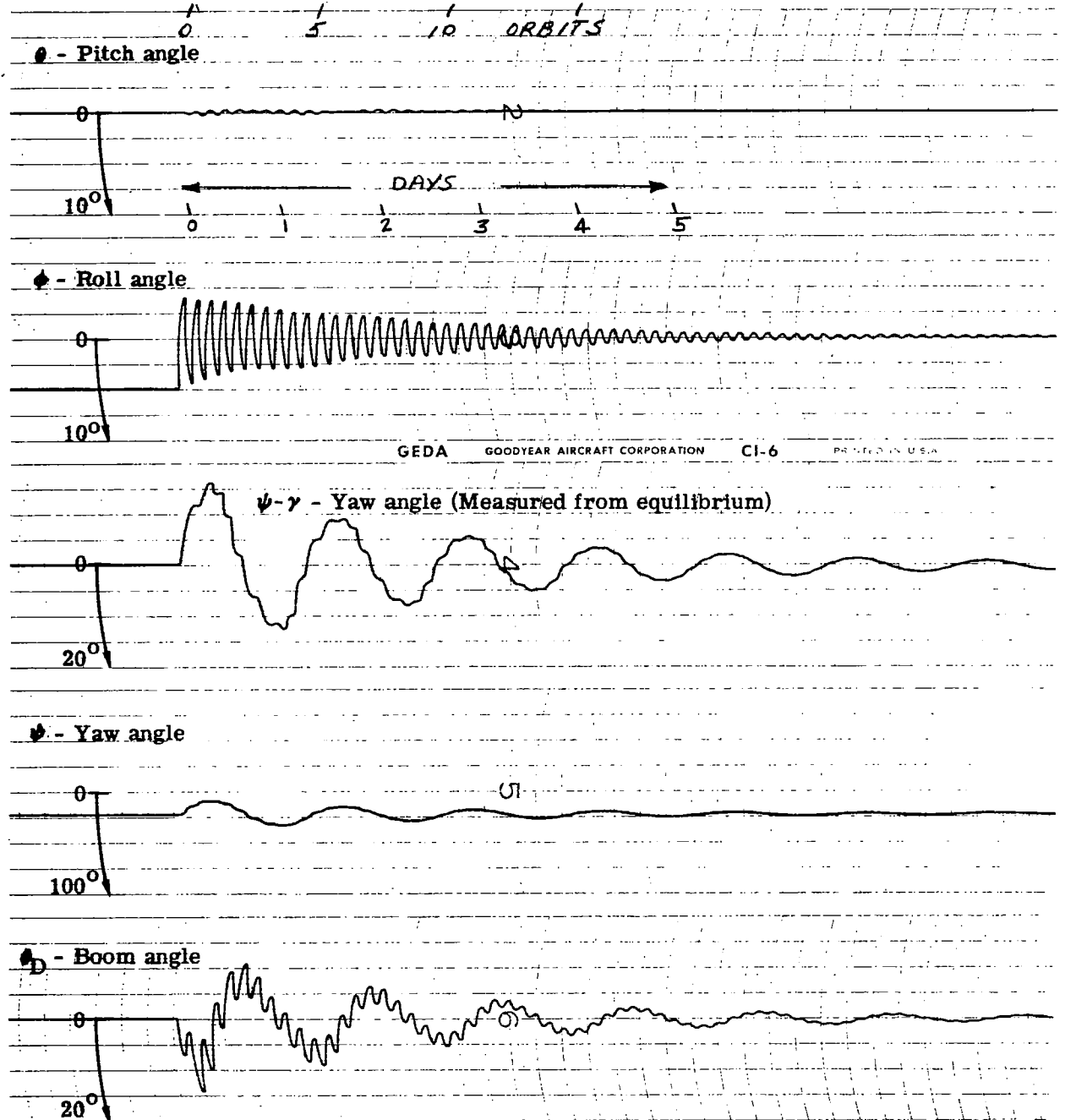


Figure 32. - Continued.

RUN NO. 47

$F = 0.02$
 $D = 0.015$
 $J = 0.1739$

$K'' = 4.205$
 $B'' = 1.476$
 $\psi_D = -74.5^\circ$
 $\gamma = 23.7^\circ$

Initial Condition
 $\theta = 0$
 $\phi = 0$
 $\psi = -5^\circ + \gamma$

3.74 orbits/day

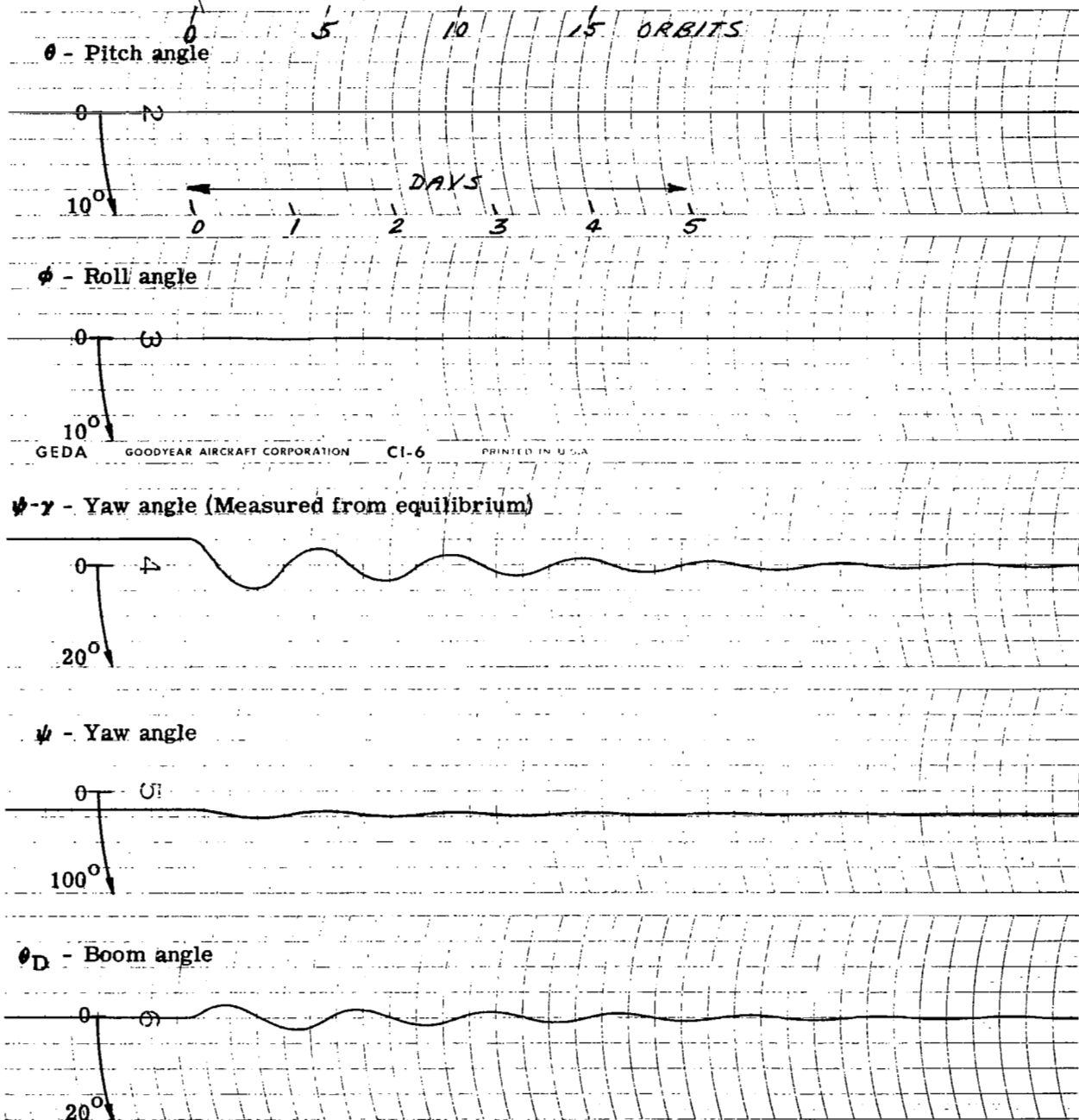


Figure 32. - Continued.

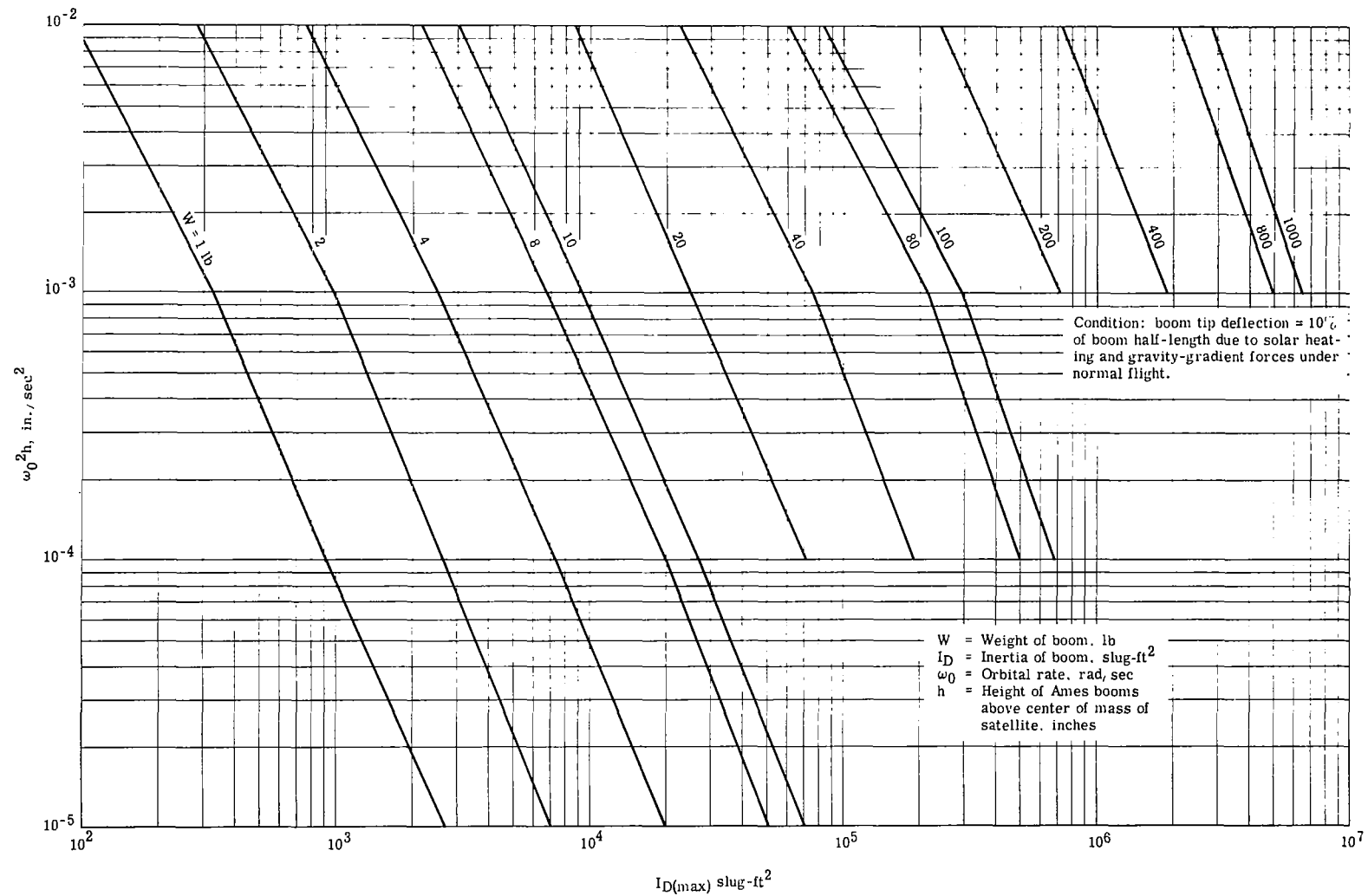


Figure 33. - Maximum moment of inertia of damper boom about its mid-point for case 1.

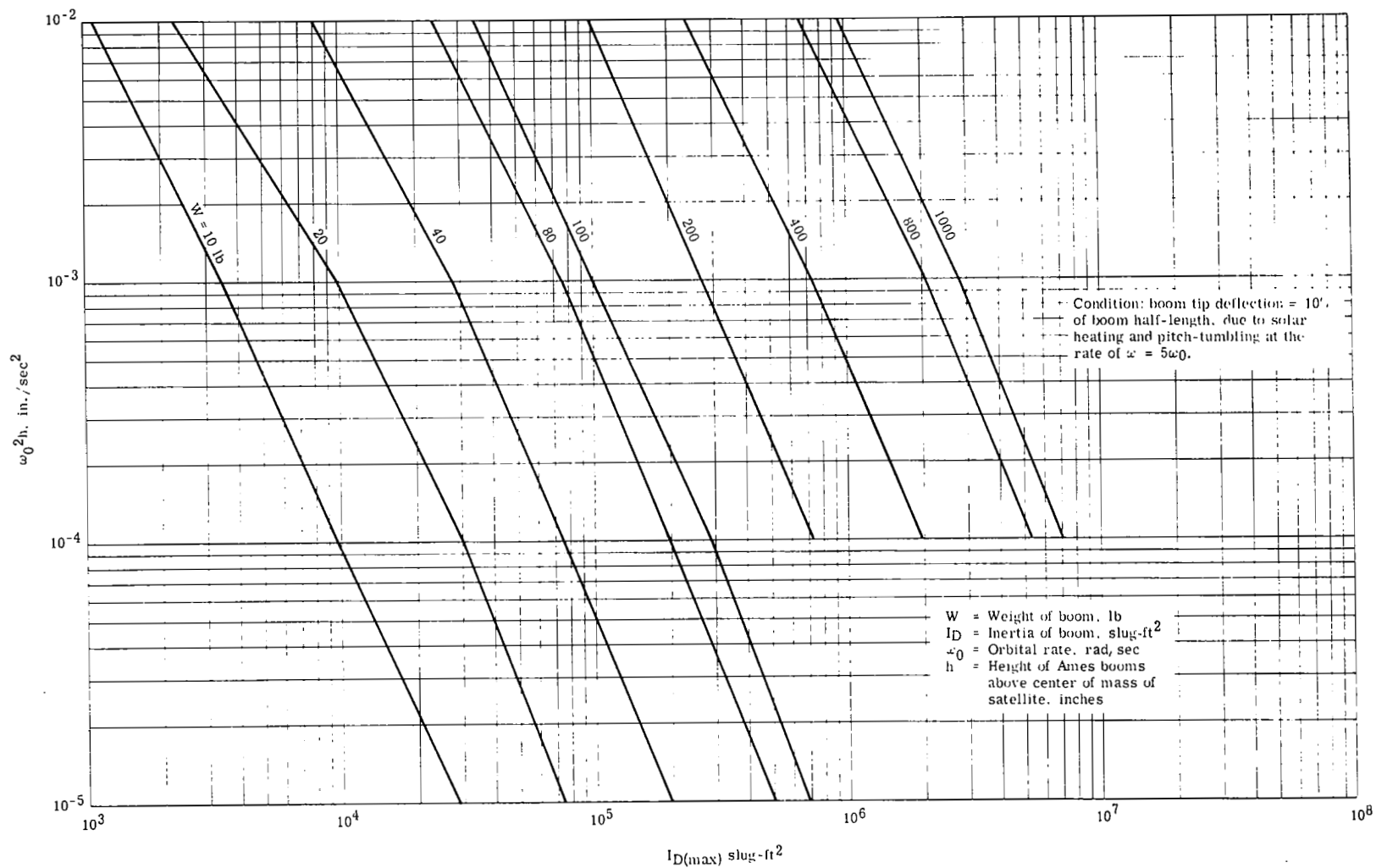


Figure 34. - Maximum moment of inertia of damper boom about its mid-point for case 2.

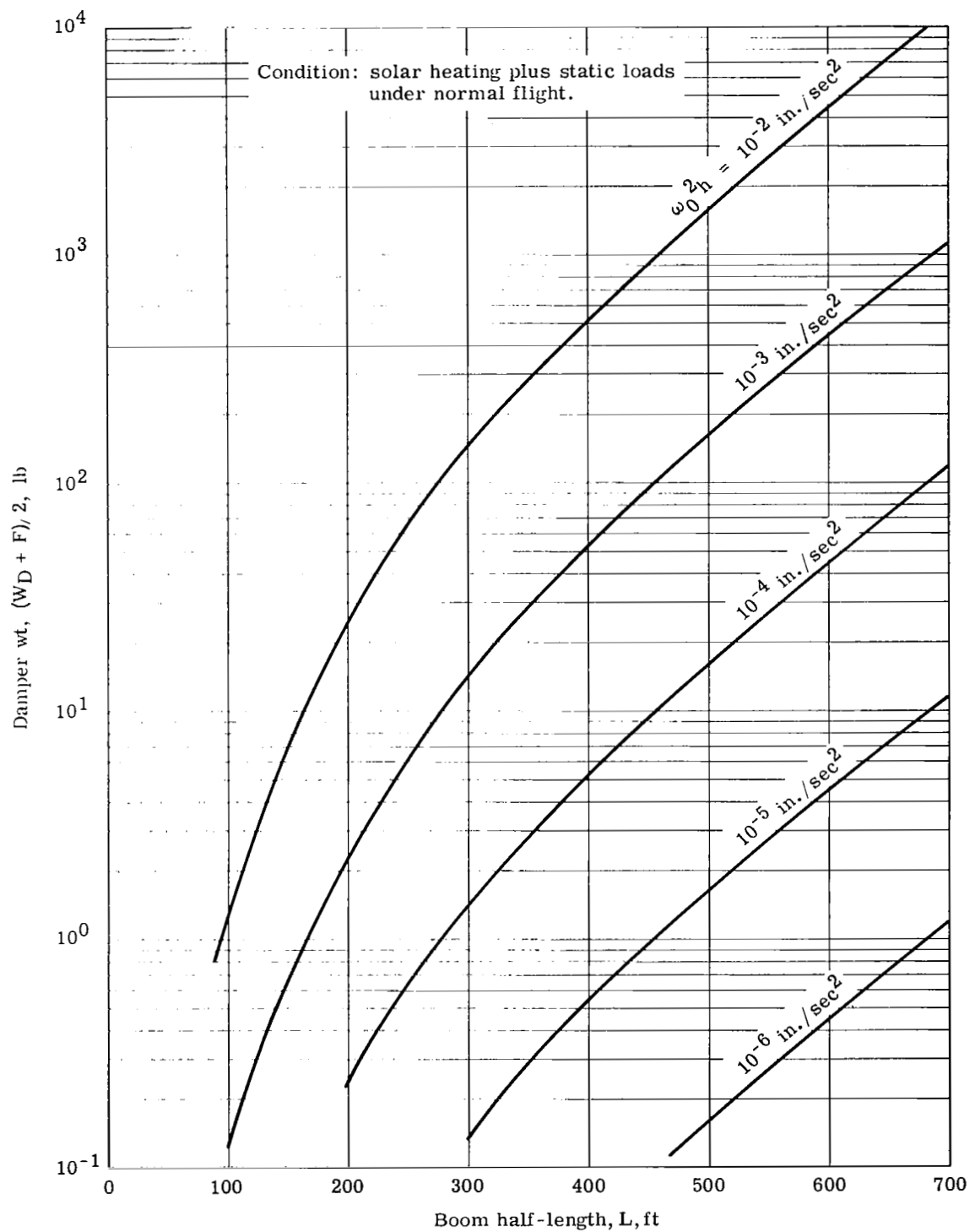


Figure 35. - Damper boom weight versus boom half-length for maximum mid-point moment of inertia for case 1.

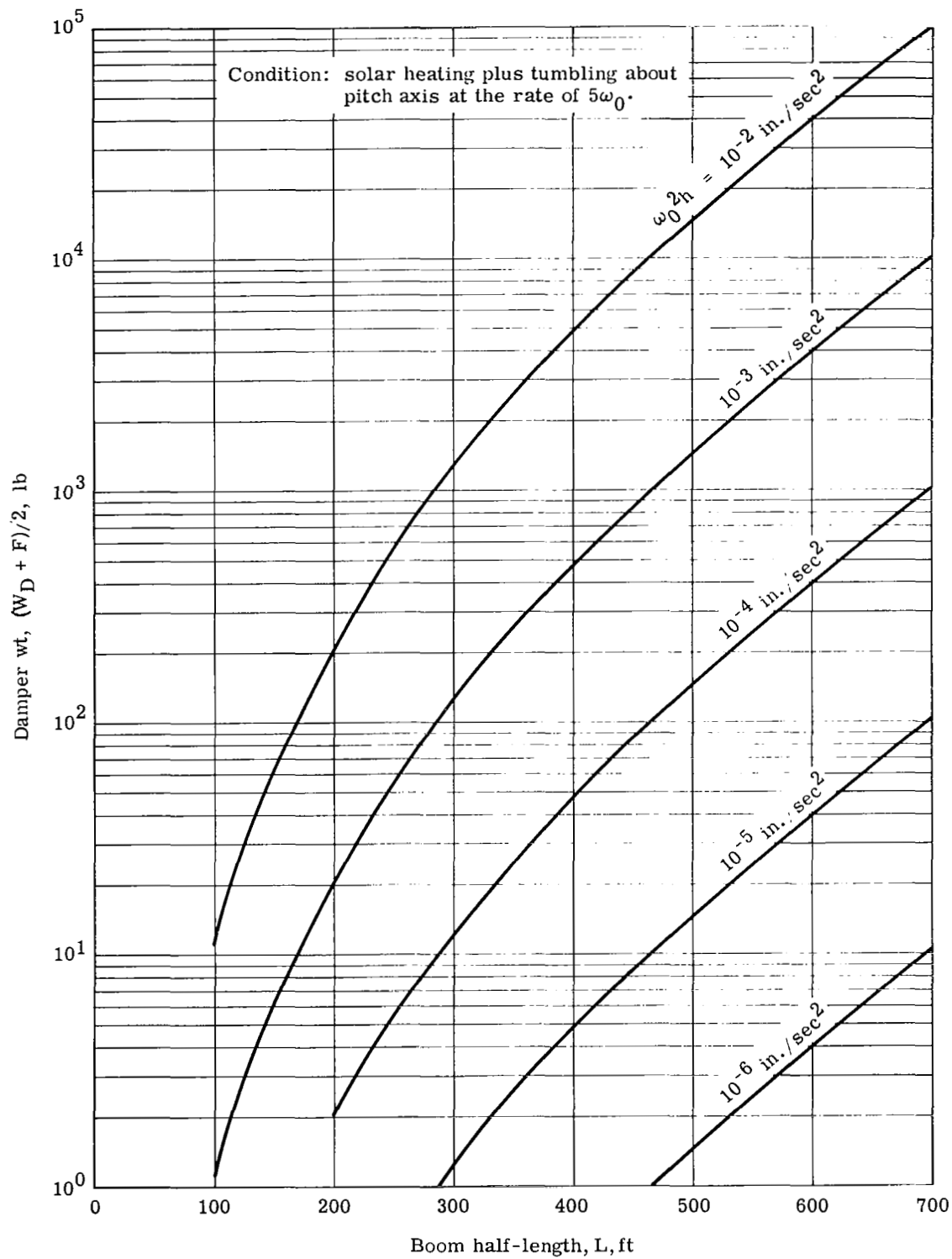


Figure 36. - Damper boom weight versus boom half-length for maximum mid-point moment of inertia for case 2.

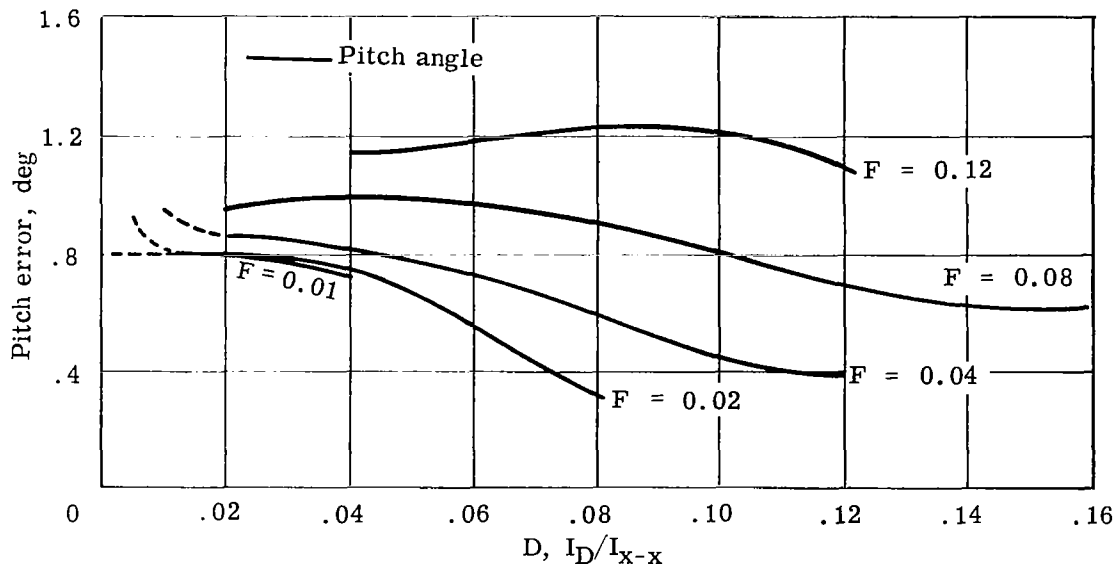


Figure 37. - Pitch error for one percent eccentricity.

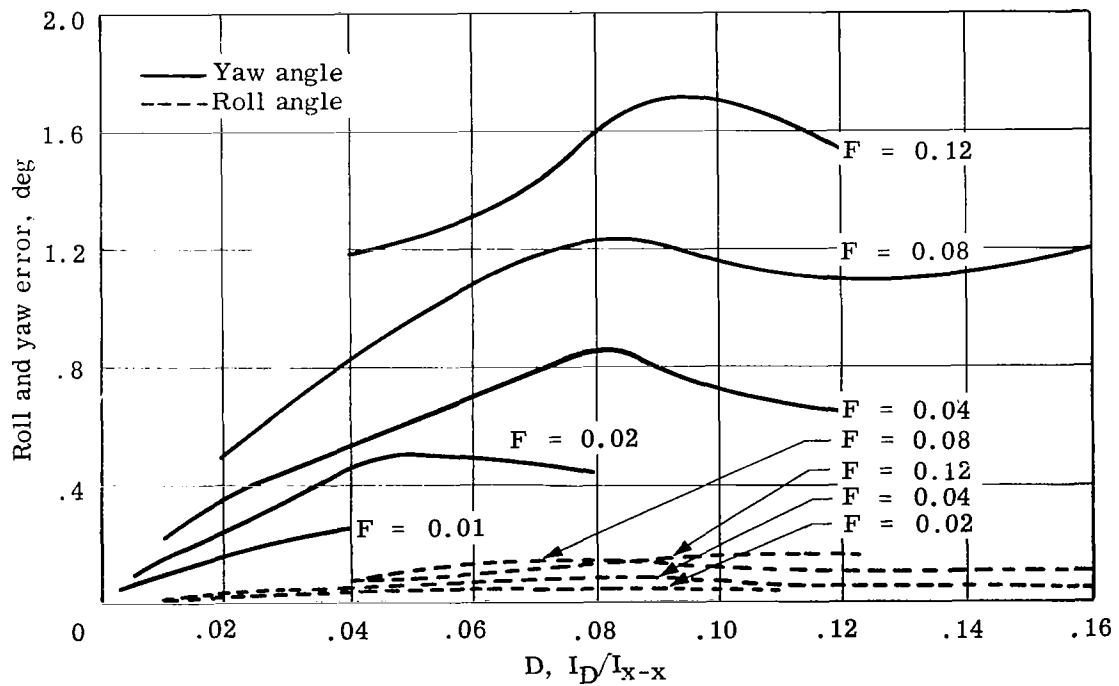


Figure 38. - Roll and yaw error for one percent eccentricity.

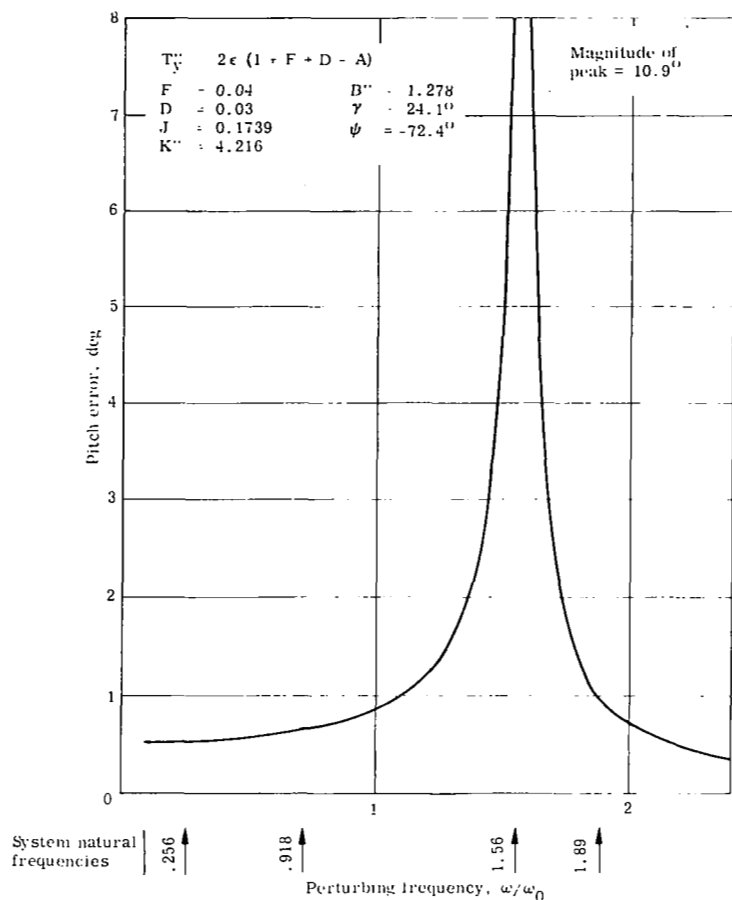


Figure 39. - Frequency response for pitch axis torque corresponding to 0.01 eccentricity - pitch error.

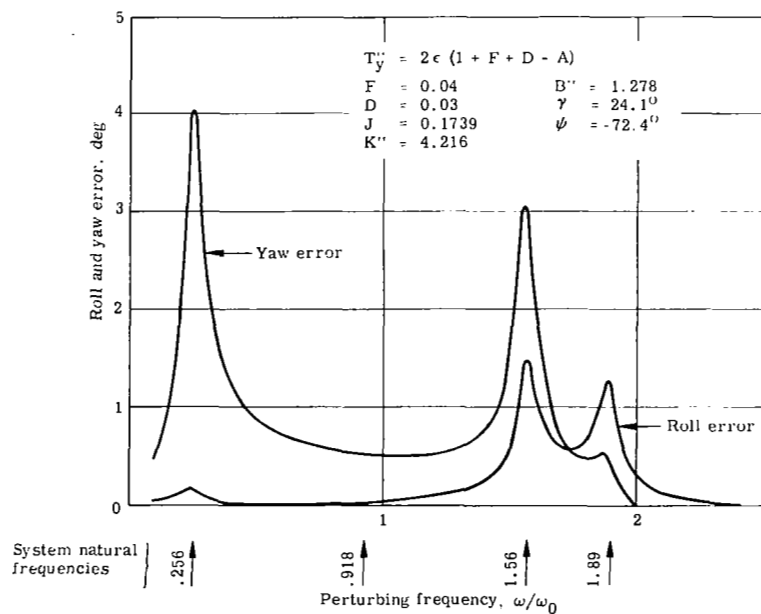


Figure 40. - Frequency response for pitch axis torque corresponding to 0.01 eccentricity - roll and yaw error.

Figure 41. - Frequency response for pitch axis torque corresponding to 0.01 eccentricity - boom error.

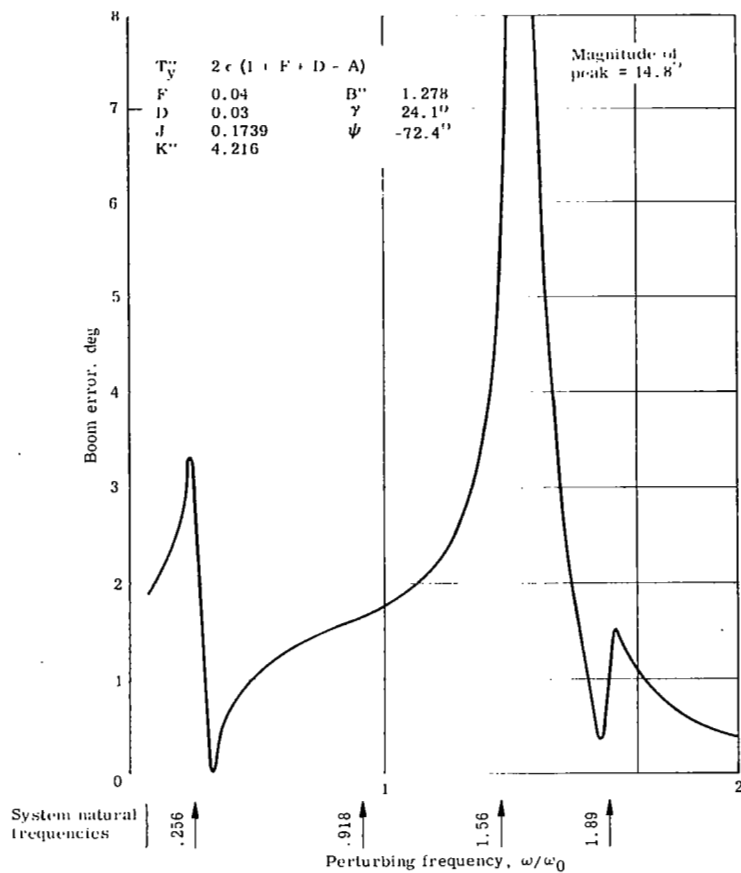
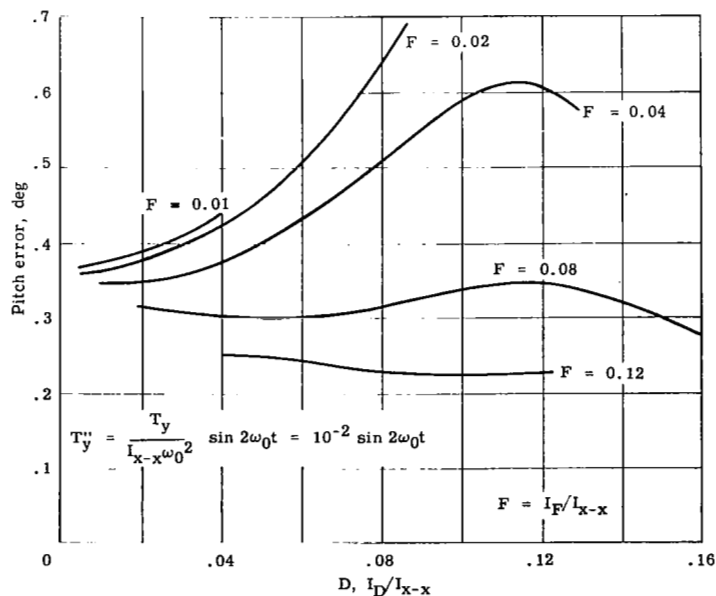


Figure 42. - Pitch error for disturbance torque T_y'' about the pitch axis.



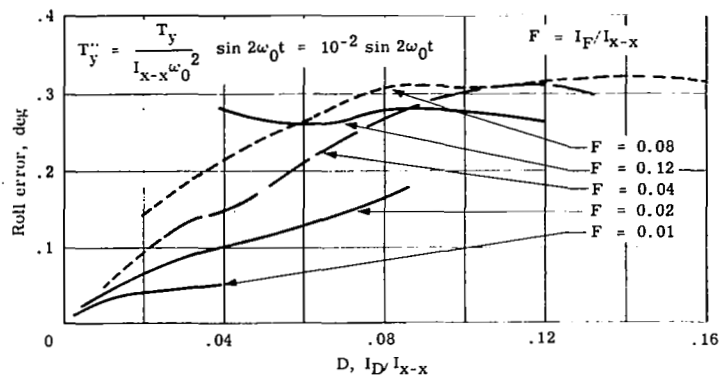


Figure 43. - Roll error for disturbance torque T_y'' about the pitch axis.

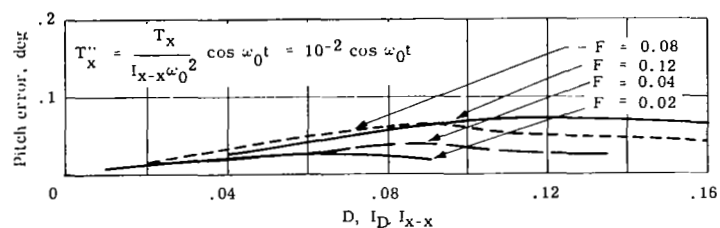


Figure 44. - Pitch error for disturbance torque T_x'' about the roll axis.

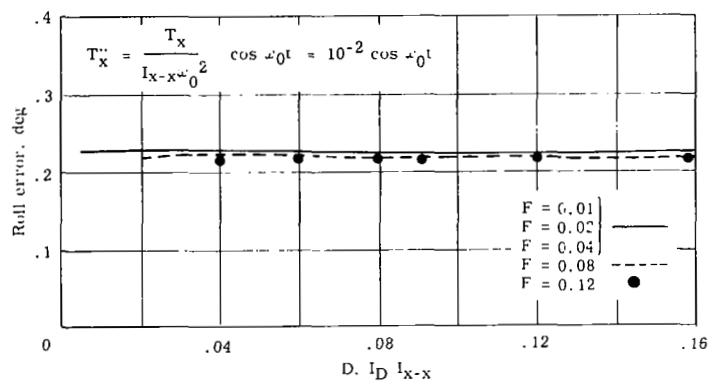


Figure 45. - Roll error for disturbance torque T_x'' about the roll axis.

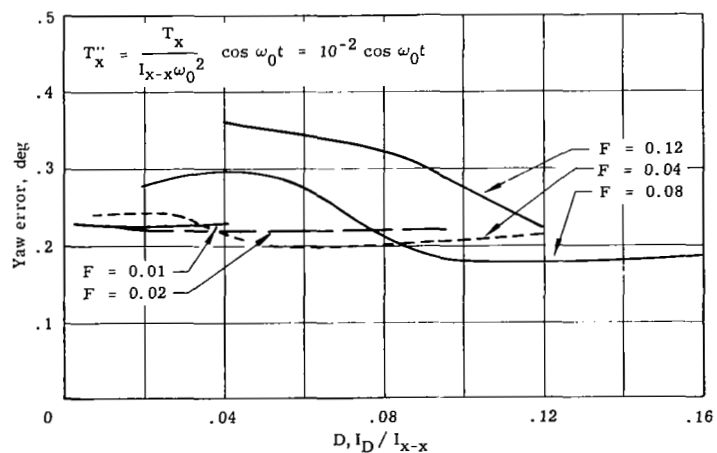


Figure 46. - Yaw error for disturbance torque T_x'' about the roll axis.

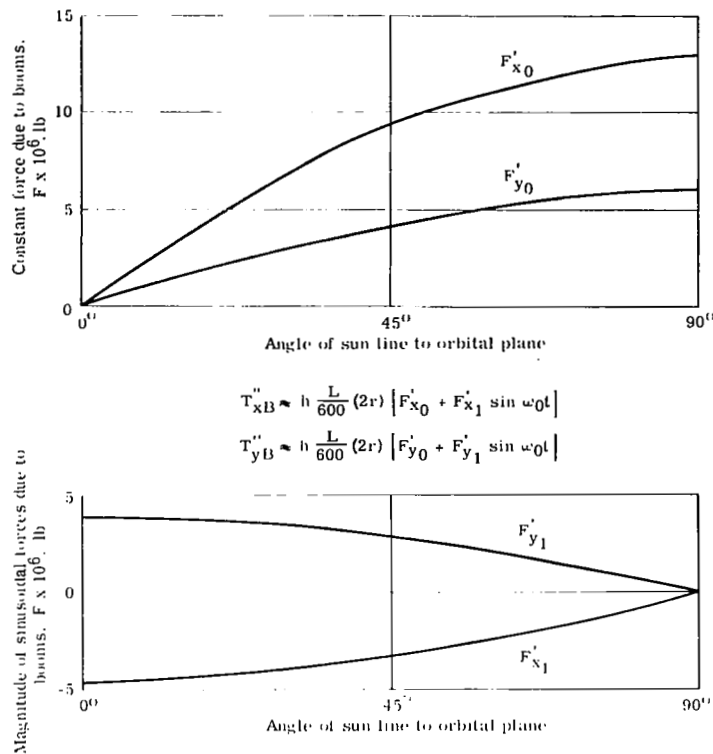


Figure 47. - Magnitude of constant and sinusoidal forces due to booms.

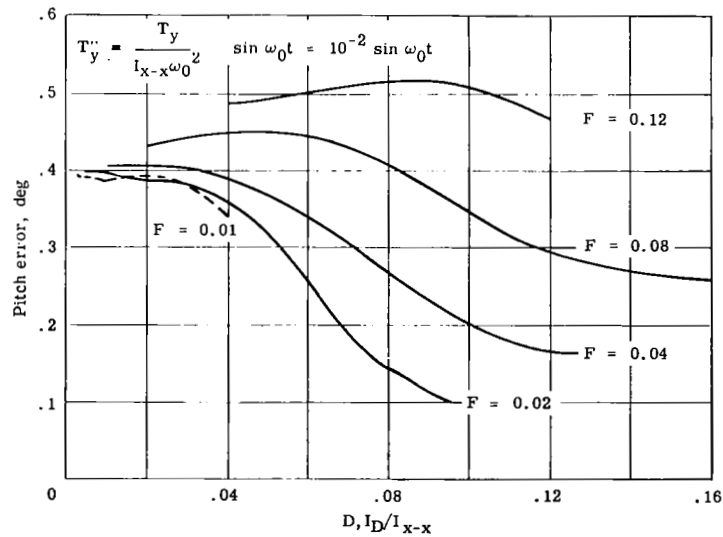


Figure 48. - Pitch error for disturbance torque T''_y about the pitch axis.

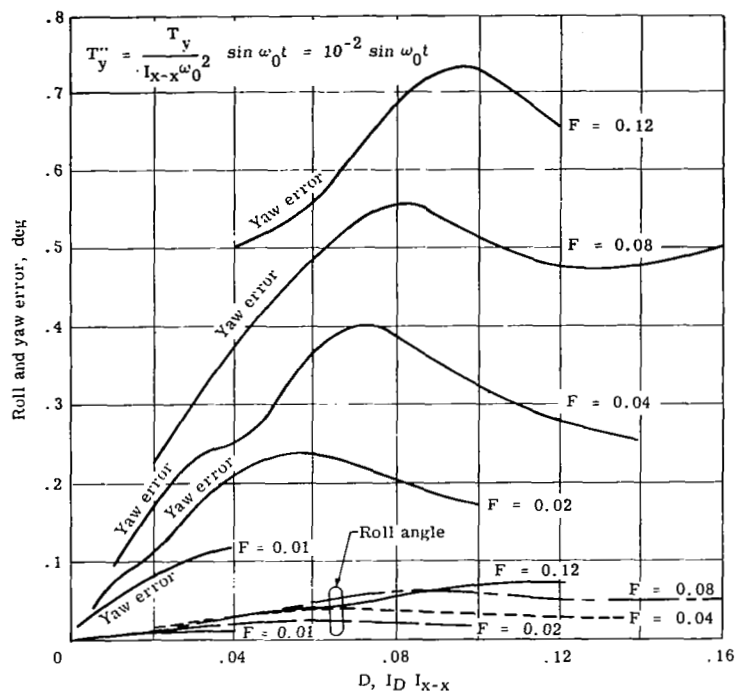


Figure 49. Roll and yaw error for disturbance torque T_y'' about the pitch axis.

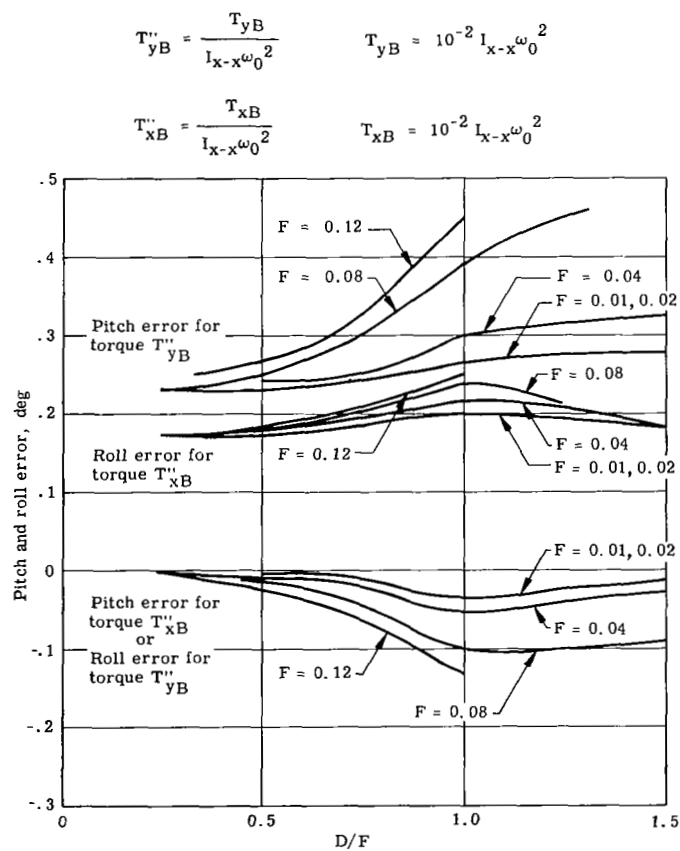


Figure 50. Hang-off error for constant torques $T_y''B$ and $T_x''B$ about the pitch and roll axes.

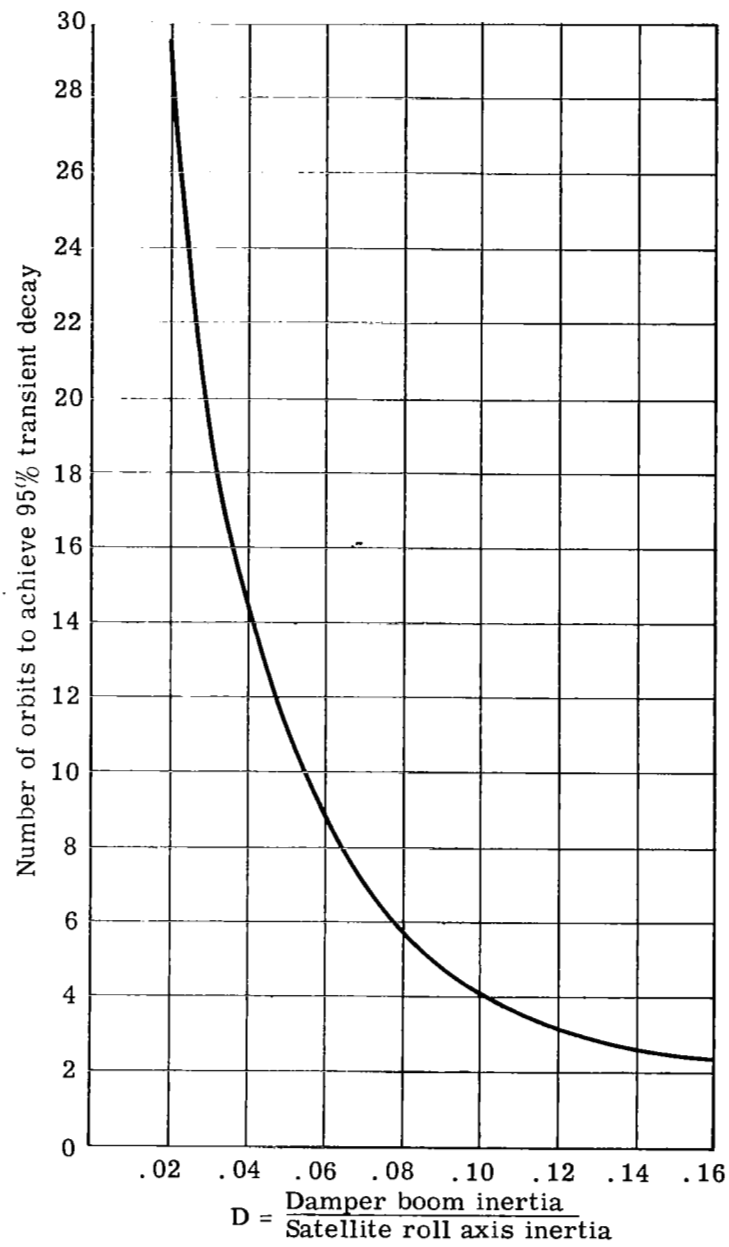


Figure 51. Transient damping capability of gravity-gradient stabilization system.

APPENDIX A

MATERIALS DEFINITIONS

Material I

Definition. - Material I is aluminum-Mylar sandwich material, in which the face-to-core thickness ratio, t_F/t_C , is optimized against buckling (refer to page 124). The optimum value t_F/t_C is 0.569, rounded off to 0.5 (as it occurs in the Echo II material) with no substantial weight penalty against buckling caused by solar pressure.

Minimum gages and material properties. - Properties and present state of the art minimum gages for aluminum and Mylar are given in Table A1.

TABLE A1. - MINIMUM GAGES AND PROPERTIES OF
CONSTITUENTS OF MATERIAL I

Material	Density, lb/in. ³	Modulus of elasticity, psi	Yield strength, psi	Minimum gage ^a
Aluminum	0.1	10×10^6	4000	0.075 mil
Mylar	0.05	---	---	0.15 mil

(a) The present state of the art is $t_{F(\min)} = 0.05$ mil and $t_{C(\min)} = 0.15$ mil. In order to have $t_F/t_C = 1/2$, the minimum t_F should be taken as 0.075 mil.

Buckling equation. - The critical buckling pressure for a sphere is given by equation

$$p_{cr} = (2/\rho)^2 \sqrt{DK} \quad (\text{ref. 7}). \quad (A1)$$

Using a factor 0.233 (ref. 7, p. 16), equation (A1) becomes

$$p_{cr} = 0.933 \frac{1}{\rho^2} \sqrt{DK} \quad (A2)$$

In equation (A2) the meaning of D and K is as follows:

$$D = \frac{EI}{1 - \mu^2} = \frac{Et_F}{6(1 - \mu^2)} \left[\frac{2}{t_F} + 3(t_F + t_C)^2 \right] \quad (A3)$$

and

$$K = 2t_F E \quad (A4)$$

APPENDIX A

Substituting equations (A3) and (A4) into Equation (A2), with $p_{cr} = 1.3 \times 10^{-9}$ psi, results in

$$1.3 \times 10^{-9} = \frac{0.933 E t_F^2}{\rho^2 \sqrt{3(1 - \mu^2)}} \sqrt{4 + 6(t_C/t_F) + 3(t_C/t_F)^2} \quad (A5)$$

Unit Weight. - The weight per unit area of laminate material can be found from equation

$$w_L = 2w_F t_F + w_C t_C \quad (A6)$$

Noting that $t_C = 2t_F$ for this material, and using $\mu = 0.3$, equation (A5) becomes

$$\frac{t_C}{2} = t_F = \frac{\rho}{1.516} \times 10^{-8} \quad (A7)$$

Substituting equation (A7) and the numerical values $w_F = 0.1$ and $w_C = 0.05$ in Equation (A6) results in

$$\left. \begin{aligned} w_L &= 0.198 \times 10^{-8} \rho \text{ lb/in.}^2 \text{ for } \rho > 11370 \text{ in.} \\ w_L &= 22.5 \times 10^{-6} \text{ lb/in.}^2 \text{ (constant) for } \rho \leq 11370 \text{ in.} \end{aligned} \right\} \quad (A8)$$

where the limiting value $\rho = 11370$ in. was found from equation (A7) for $t_F = t_{F(\min)} = 0.075$ mil.

Rigidization pressure. - Preliminary investigation (see also ref. 8, p. 547) indicated that due to the low stiffness of Mylar relative to the stiffness of aluminum, the Mylar takes only 4.6 percent of the total tensile load applied on the laminate. Hence in calculating the rigidization pressure, the Mylar strength can be neglected. For a 4000 psi yield strength for aluminum, the required rigidization pressure for the laminate can be found from equation

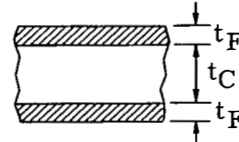
$$\frac{p_L \rho}{2(2t_F)} = 4000.$$

Substituting equation (A7) in the last equation and solving the resulting equation for p_L yields $p = 105.5 \times 10^{-6}$ psi (constant). However, for values of $\rho < 11370$, in the thickness t_F is constant ($t_F = 0.000075$ in.) and the last equation becomes $p_L = 1.2/\rho$ psi. Hence

$$\left. \begin{aligned} p_L &= \frac{1.2}{\rho} \text{ psi for } \rho \leq 11370 \text{ in.} \\ p_L &= 105.5 \times 10^{-6} \text{ psi for } \rho > 11370 \text{ in.} \end{aligned} \right\} \quad (A9)$$

Optimum face-to-core thickness ratio in a laminate against buckling. - The problem here is to minimize the laminate unit weight,

$$w = 2t_F w_F + t_C w_C$$



(A10)

for a given value of the product DK (ref. 7, page 564), where D is the flexural stiffness, $(EI)/(1 - \mu^2)$, and K the extensional stiffness of the sandwich material. Noting that

$$D = k E t_F \left[t_F^2 + 3(t_F + t_C)^2 \right] \text{ and } K = 2 E t_F,$$

APPENDIX A

the following equation is obtained

$$F_1(t_F, t_C) = t_F^2 [t_F^2 + 3(t_F + t_C)^2] - \lambda = 0 \quad (A11)$$

where $\lambda = DK/2E^2k$ (const) and k is a numerical coefficient.

$$\text{For minimum weight } dw = 2w_F dt_F + w_C dt_C = 0$$

$$\text{or } 2w_F + w_C \frac{dt_C}{dt_F} = 0 \quad (A12)$$

But from equation (A11)

$$\frac{dt_C}{dt_F} = - \frac{\partial F_1 / \partial t_F}{\partial F_1 / \partial t_C} = - \frac{4t_F^3 + 6t_F(t_F + t_C)^2 + 6t_F^2(t_F + t_C)}{6t_F^2(t_F + t_C)}$$

Then equation (A12) becomes

$$2w_F - w_C \left[1 + \frac{(t_F + t_C)^2 + \frac{2}{3} t_F^2}{t_F(t_F + t_C)} \right] = 0 \quad (A13)$$

For aluminum-Mylar-aluminum sandwich, $w_F = 0.1$ and $w_C = 0.05$ lb/in.³ Then equation (A13) solved for t_F/t_C gives $t_F/t_C = 0.569$.

The unit weight of a sphere with a radius ρ , capable of withstanding the solar pressure of 1.3×10^{-9} psi, may be found from equation

$$1.3 \times 10^{-9} = \frac{0.933}{\rho^2} \sqrt{DK}.$$

- (1) For $t_F/t_C = 1/2$ (Echo II proportion), the above equation gives $t_F = (1/1.516) \times 10^{-8} \rho$, from which

$$w = 2t_F w_F + t_C w_C = 2 \times (0.1) t_F + 0.05 t_C = 0.198 \times 10^{-8} \rho \text{ lb/in.}^2$$

- (2) For optimum material, i.e., for $t_F/t_C = 0.569$, the unit weight is $w = 0.1978 \times 10^{-8} \text{ lb/in.}^2$, which for all practical purposes is identical with Echo II material proportions.

Material II

Definition. - This is wire-film material with copper wires forming a woven square grid of 21 wires per inch in both directions and 1/2-mil photolyzable film.

Minimum gages and material properties. - Refer to table A2.

APPENDIX A

TABLE A2. - MINIMUM GAGES AND PROPERTIES OF
CONSTITUENTS OF MATERIAL II

Material	Density, lb/in. ³	Modulus of elasticity, psi	Yield strength, psi	Minimum gage	Wire spacing
Copper	0.324	10 x 10 ⁶	23 000	d = 1.0 mil	s = 1/21 in., both direc- tions
Photolyzable film	0.038	---	---	t = 0.5 mil (constant)	---

Buckling equation. - Using the factor 0.233 the buckling equation (refer to eq. A1) for the present case of a wire grid material becomes

$$p_{cr} = 0.191 E \frac{d^3}{s\rho^2} \quad (\text{ref. 1, p. 104}). \quad (\text{A14})$$

Substituting $p_{cr} = 1.3 \times 10^{-9}$ and $E = 10^7$ into equation (A14) results in

$$d^3 = 0.3241 \rho^2 \times 10^{-16} \quad (\text{A15})$$

Unit weight. - The weight of wire-film material per square inch is

$$w_L = \frac{2}{s} \frac{\pi d^2}{4} (0.324) + 0.0005 \times 0.038 = 10.688d^2 + 19 \times 10^{-6} \quad (\text{A16})$$

Eliminating d between equations (A15) and (A16) yields

$$\left. \begin{aligned} w_L &= \left[1.086 \left(\frac{\rho}{1000} \right)^{4/3} + 19 \right] \times 10^{-6} \text{ lb/in.}^2 \text{ for } \rho > 5555 \text{ in.} \\ &= 29.7 \times 10^{-6} \text{ lb/in.}^2 \text{ (constant) for } \rho \leq 5555 \text{ in.} \end{aligned} \right\} \quad (\text{A17})$$

The limiting value of $\rho = 5555 \text{ in.}$ was found from equation (A15) for $d = d_{\min} = 0.001 \text{ inch.}$

Rigidization pressure. - The required rigidization pressure can be found from equation

$$\frac{p_L \rho}{2(\pi d^2/4s)} = 23 \text{ 000} \quad (\text{A18})$$

Eliminating d between equations (A15) and (A18), and solving the resulting equation for p_L , yields

$$\left. \begin{aligned} p_L &= 7.711 \times \rho^{1/3} \times 10^{-6} \text{ psi} && \text{for } \rho > 5555 \text{ in.} \\ p_L &= 0.75873/\rho \text{ psi} && \text{for } \rho \leq 5555 \text{ in.} \end{aligned} \right\} \quad (\text{A19})$$

where the second portion of equation (A19) was found from equation (A18) for $d = d_{\min} = 0.001 \text{ inch.}$

APPENDIX A

Material III

Definition. - This is a wire-film material consisting of aluminum wires wound on 1/2-mil photolyzable film in the form of a square grid. Spacing and diameter of wires in the grid are adjusted to an 8000 Mc microwave frequency, and 96 percent reflected power coefficient.

Minimum gages and material properties. - Refer to table A3.

TABLE A3. - MINIMUM GAGES AND PROPERTIES OF
CONSTITUENTS OF MATERIAL III

Material	Density, lb/in. ³	Modulus of elasticity, psi	Yield strength, psi	Minimum gage	Microwave frequency, Mc
Aluminum	0.1	10 x 10 ⁶	4000	2.0 mil	8000
Photolyzable film	0.038	---	---	1/2 mil (constant)	---

Buckling equation. - For $p_{cr} = 1.3 \times 10^{-9}$, the buckling equation (refer to eq. A14) becomes

$$d^3 = 6.806 \epsilon \rho^2 \times 10^{-16} \quad (A19)$$

Microwave frequency equation. -

$$r_p = \frac{1}{1 + \left[0.1695 \text{ sf} \times 10^{-9} \ln \left(\frac{s}{\pi d} \right) \right]^2} \quad (\text{ref. 4, p. C-6}). \quad (A20)$$

For $r_p = 0.96$ and $f = 8000$ Mc, equation (A20) becomes

$$s \ln \left(\frac{s}{\pi d} \right) = 0.1505 \quad (A21)$$

Unit weight. - The weight of the wire-film per square inch is

$$\left. \begin{aligned} w_L &= \frac{2}{s} \left(\frac{\pi d^2}{4} \right) (0.1) + 0.0005 \times 0.038 \\ &= 0.1571 \frac{d^2}{s} + 19.0 \times 10^{-6} \text{ lb/in.}^2 \end{aligned} \right\} \quad (A22)$$

The unit weight w_L as a function of ρ can be found as follows. Equation (A21) solved for d gives

$$d = \frac{s/\pi}{e^{0.1505/s}}$$

From this equation values of d are determined against s and from equation (A22) w is calculated. Finally, the corresponding values of ρ are determined from equation (A19), which can be written in the form

APPENDIX A

$$\rho = \frac{6.884s}{e^{0.22575/s}} \times 10^6.$$

Corresponding numerical values are given in table A4 of this report. To find the minimum weight, first the wire spacing, s , is determined for $d = 0.002$ inch. This is $s = 0.0646$ inch. Then from equation (A22), $w_{\min} = 28.7 \times 10^{-6}$ lb/in.². The limiting value of ρ is 13 496 inches or 1125 feet.

Rigidization pressure. - The rigidization pressure can be found from equation

$$\frac{p_L \rho}{2 \left(\frac{\pi d^2}{4s} \right)} = 4000, \quad (A23)$$

from which

$$p_L = \frac{6283d^2}{\rho s} \text{ psi for } \rho > 13\,496 \text{ in.}$$

also

$$p_L = \frac{0.384}{\rho} \text{ psi for } \rho \leq 13\,496 \text{ in.}$$

where the second portion of equation (A24) was found from the first with the substitution $d = 0.002$ inch and $s = 0.0646$ inch. Values of the pressure p_L are also given in table A4.

TABLE A4. - CORRESPONDING VALUES OF s , d , ρ , w_L , and p_L FOR MATERIAL III

(1) s	(2) $\frac{0.1505}{e^s}$	(3) $\frac{0.22575}{e^s}$	(4) $\frac{s}{\pi}$	(5) $d = \frac{(4) + (2)}{\text{in.}}$	(6) $\rho [\text{in.}] = \frac{[6.884 \times (1)]}{\div (3)] \times 10^6}$	(7) ρ feet	(8) d^2/s $\times 10^6$	(9) $w_L [\text{lb/in.}^2] = \frac{[0.1571 \times (8)]}{\div (6)] \times 10^{-6}}$	(10) $p_L [\text{psi}] = \frac{[6283 \times (8)]}{\div (6)] \times 10^{-6}}$	ρ feet	ρ in.	$p_L [\text{psi}] = 0.389 \cdot \rho$
0.0646	10.278	32.950	0.02056	0.00200	13496	1125	61.92	0.0000287	0.0000288	100	1200	0.000324
0.07	8.5849	25.154	0.02228	0.002595	19157	1596	96.20	0.0000341	0.0000316	200	2400	0.000162
0.08	6.5535	16.811	0.02546	0.003885	32760	2713	188.67	0.0000486	0.0000362	300	3600	0.000108
0.09	5.3227	12.272	0.02865	0.005383	50486	4207	321.96	0.0000696	0.0000400	400	4800	0.000081
0.10	4.5042	9.4949	0.03183	0.007067	72502	6042	499.42	0.0000975	0.0000433	500	6000	0.000065
0.118	3.5787		0.03756	0.01005	120000	10000	934.3	0.0001658	0.0000489	600	7200	0.000054
										700	8400	0.000046
										800	9600	0.000041
										900	10800	0.000036
										1000	12000	0.000033
										1100	13200	0.000029
										1125	13500	0.000029

APPENDIX A

Material IV

Definition. - This material is the same as Material III, adjusted to a microwave frequency of 800 Mc and a reflective power coefficient $r_p = 0.96$ (same as in Material III).

Minimum gages and material properties. - Same as Material III (see table A3).

Buckling equation. - Buckling equation (A19) holds for this material. The microwave frequency equation (A20) for $f = 800$ megacycles leads to

$$s \ln \left(\frac{s}{\pi d} \right) = 1.505 \quad (A25)$$

Then

$$d = \frac{s/\pi}{e^{1.505/s}}, \text{ and } \rho = 6.884 \frac{s}{e^{2.2575/s}} \times 10^6 \quad (A26)$$

For $d = 0.002$ inch the spacing $s = 0.3694$ inch and the limiting value of the radius of curvature $\rho = 5638$ inch = 470 feet. As a consequence, the inflation pressure for $\rho \leq 470$ feet, (as determined from the first portion of eq. (A24)), is

$$p_L = \frac{0.068}{\rho} \text{ lb/in.}^2 \quad (A27)$$

Unit weight. - Equation (A22) for the unit weight, and the first portion of equation (A24) for the inflation pressure (for $\rho > 470$ ft) hold for this material. Corresponding values of s , d , ρ , w_L and p_L are given in table A5.

Summary. - Table A6 summarizes the results of this study for the four lens materials considered, and figures A1 and A2 graphically show these results. In both figures the dashed lines represent the weight or pressure variation versus lens radius of curvature when minimum material gages are considered as defined above.

TABLE A5.- CORRESPONDING VALUES OF s , d , ρ , w_L , and p_L FOR MATERIAL IV

(1) s	(2) $\frac{1.505}{e^{s}}$	(3) $\frac{2.2575}{e^{s}}$	(4) $\frac{s}{\pi}$	(5) $d = \frac{(4) \div (2)}{\text{in.}}$	(6) $\rho \left[\frac{\text{in.}}{(3)} \right] = \frac{6.884 \times (1)}{(3)} \times 10^6$	(7) ρ feet	(8) d^2/s $\times 10^6$	(9) $w_L \left[\frac{\text{lb/in.}^2}{(0.1571 \times (8) \div (6)) \times 10^{-6}} \right] =$	(10) $p_L \left[\frac{\text{psi}}{(6283 \times (8) \div (6)) \times 10^{-6}} \right] =$	ρ feet	ρ in.	$p_L \left[\frac{\text{psi}}{\rho} \right]$
0.3694	58.810	451.02	0.1176	0.00200	5638	470	10.83	0.0000207	0.0000121	100	1200	0.0000567
0.40	43.393	282.63	0.1273	0.00293	9743	812	21.46	0.0000224	0.0000138	200	2400	0.0000283
0.45	28.333	151.00	0.1432	0.00505	20515	1710	56.67	0.0000279	0.0000174	300	3600	0.0000189
0.50	20.287	91.402	0.1592	0.00785	37658	3138	123.2	0.0000384	0.0000206	400	4800	0.0000141
0.55	15.425	60.649	0.1751	0.01135	62428	5202	234.2	0.0000558	0.0000236	470	5638	0.0000121
0.60	12.280	42.578	0.1910	0.01555	97008	8084	403.0	0.0000823	0.0000261			
0.63	10.902	35.991	0.2005	0.01839	120500	10042	536.9	0.0001033	0.0000280			

APPENDIX A

**TABLE A6. - WEIGHTS AND RIGIDIZATION PRESSURES FOR
FOUR TYPES OF LENS MATERIALS**

Item	Material I (a)			Material II (b)			Material III (c)			Material IV (d)		
Minimum gages	Aluminum $t_F = 0.075$ mil Mylar $t_C = 0.15$ mil			Copper wire diam $d_{min} = 1.0$ mil			Aluminum wire diam $d_{min} = 2.0$ mil			Aluminum wire diam $d_{min} = 2.0$ mil		
Minimum weight lb/in. ²	22.5×10^{-6}			29.7×10^{-6}			28.7×10^{-6}			20.7×10^{-6}		
Maximum radius of curvature corresponding to minimum weight	947.5 ft			463 ft			1125 ft			470 ft		
Rigidization pressure corresponding to minimum weight	105.5×10^{-6} psi			136.6×10^{-6} psi			28.8×10^{-6} psi			12.1×10^{-6} psi		
	(1)	(2)	(3)	(1)	(2)	(3)	(1)	(2)	(3)	(1)	(2)	(3)
(1) ρ , radius of curvature	100	22.5	1000	100	29.7	632.3	100	28.7	324	100	20.7	57
	300		333	300	29.7	210.8	200	28.7	162	200	20.7	28
(2) w_L , weight of lens material, lb/in. ² x 10^6	500		200	463	29.7	136.6	300	28.7	108	300	20.7	19
	700		142.9	700	37.5	156.7	400	28.7	81	400	20.7	14
(3) p_L , rigidization pressure, psi x 10^6	947.5	22.5	105.5	850	43.0	167.2	500	28.7	65	470	20.7	12
	1000	23.8	105.5	1000	48.8	176.5	600	28.7	54	812	22.4	14
	2000	47.5	105.5	2000	94.2	222.4	700	28.7	46	1710	27.9	17
	3000	71.3	105.5	3000	148.1	254.6	800	28.7	41	3138	38.4	21
	4000	95.0	105.5	4000	208.4	280.2	900	28.7	36	5202	55.8	24
	5000	118.8	105.5	5000	272.7	300.2	1125	28.7	29	8084	82.3	26
	6000	142.6	105.5	6000	344.3	320.8	1596	34.1	32	10042	103.3	28
	7000	166.3	105.5	7000	418.5	337.7	2713	48.6	36			
	8000	190.1	105.5	8000	496.4	353.1	4207	69.6	40			
	9000	213.8	105.5	9000	577.5	367.2	6042	97.5	43			
	10000	237.6	105.5	10000	661.8	380.3	10000	165.8	49			

^aAluminum-Mylar-sandwich in the proportion of Echo II material.

^bWire-film material with 21 copper wires per inch in both directions and 0.5-mil photolyzable film.

^cAluminum wire-1/2 mil photolyzable film for an operating frequency of 8000 Mc and a reflected power coefficient of 0.96

^dAluminum wire-1/2 mil photolyzable film for an operating frequency of 800 Mc and a reflected power coefficient of 0.96

APPENDIX A

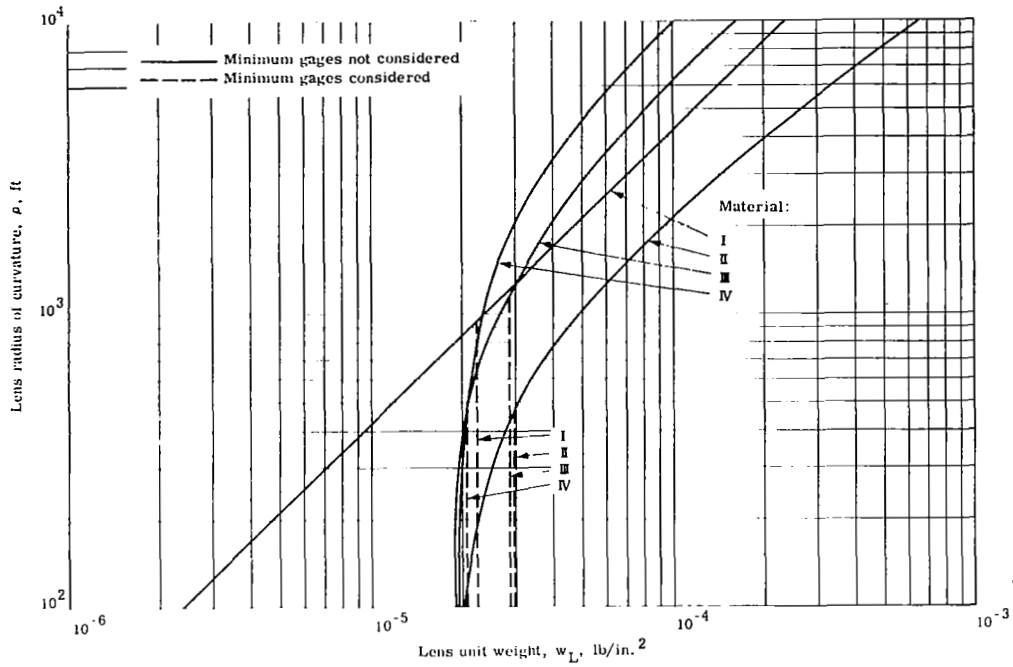


Figure A1. - Lens unit weight versus lens radius of curvature for materials I, II, III, and IV.

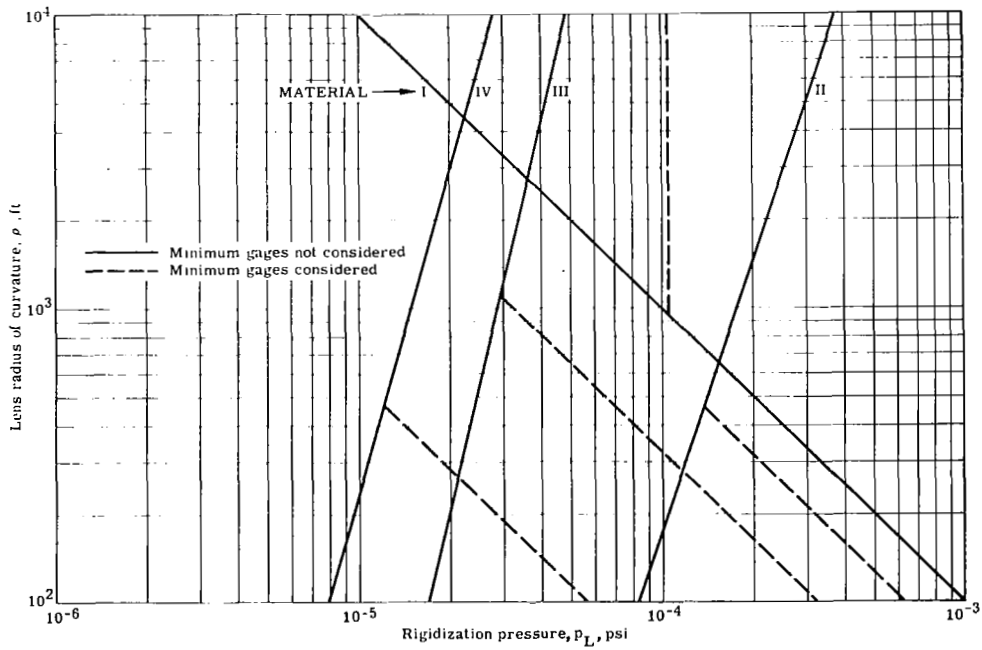
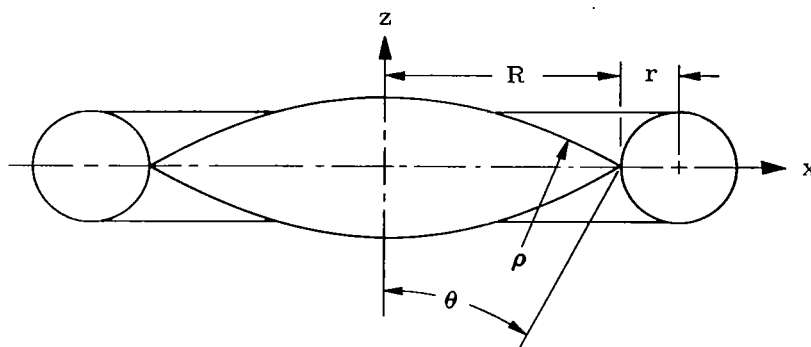


Figure A2. - Lens rigidization pressure versus lens radius of curvature for materials I, II, III, and IV.

APPENDIX B

SURFACE AREA, VOLUME, AND MASS MOMENTS OF INERTIA OF LENS, TORUS, AND RIM, AND SECTION PROPERTIES OF RIM



Properties	Lens (two caps) (a)	Torus (b)	Rim (beryllium; density = 0.297 lb/in. ³ (c)
Surface area	$4\pi\rho^2 (1 - \cos \theta)$	$4\pi^2 r (R + r)$	Actual developed area $13.160 R h_R$
Volume	$2/3\pi\rho^3 (1 - \cos \theta)^2 (2 + \cos \theta)$	$2\pi^2 r^2 (R + r)$	Actual material volume $13.16 R h_R t_R$
Moment of inertia about z-axis	$4/3\pi\rho^4 m_L (1 - \cos \theta)^2 (2 + \cos \theta)$	$4\pi^2 r^3 m_T (R + r) \times$ $\left[\left(\frac{R}{r} + 1 \right)^2 + 3/2 \right]$	$13.16 R^3 h_R m_R$
Moment of inertia about x-axis	$2/3\pi\rho^4 m_L (-\cos \theta)^2 (4 - \cos \theta)$	$2\pi^2 r^3 m_T (R + r) \times$ $\left[\left(\frac{R}{r} + 1 \right)^2 + 5/2 \right]$	$6.58 R^3 h_R m_R$

^a m_L = lens mass per unit surface area

^b m_T = mass of torus unit surface area

^c m_R = 0.297 t_R (mass per square inch of rim material)

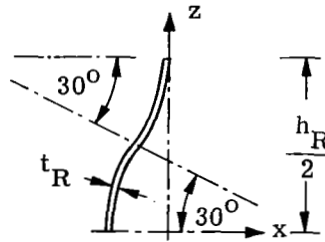
APPENDIX B

Cross section area $A = 2.0944 h_R t_R$

Moments of inertia $\begin{cases} I_x = 0.17314 h_R^3 t_R \\ I_z = 0.01437 h_R^3 t_R \end{cases}$

Torsional stiffness $J = 0.03429 h_R^3 t_R$

RIM CROSS SECTION



(QUARTER CROSS SECTION)

APPENDIX C

UNIT WEIGHTS OF LENS AND TORUS MATERIAL, MATERIAL VOLUME
PER SQUARE INCH OF LENS MATERIAL, AND RIGIDIZATION
PRESSURES FOR FOUR TYPES OF LENS MATERIAL

UNIT WEIGHTS OF LENS AND TORUS MATERIAL, MATERIAL VOLUME PER SQUARE INCH OF LENS MATERIAL,
AND RIGIDIZATION PRESSURES FOR FOUR TYPES OF LENS MATERIAL^a

Material	Description	Minimum gages establishing the limiting value of ρ	Unit weight, lb in. ²			Lens rigidization pressure p_L (psi)	Material volume per sq in. of lens material (in. ³)
			Lens. w _L		Torus		
			Film on	Film off	w _T		
I	Al - Mylar- Al sandwich in the proportion of Echo II material	Al t _p = 0.075 mil Mylar t _C = 0.15 mil	$0.198 \rho \times 10^{-8}$ ($\rho > 11\ 370$ in.)	$0.198 \rho \times 10^{-8}$ ($\rho > 11\ 370$ in.)	$0.001164 a_1 a_2 \rho \cos \theta, k_T$ ($\rho > 11\ 370$ in.)	105.5×10^{-6} ($\rho > 11\ 370$ in.)	$2.6385 \rho \times 10^{-8}$ ($\rho > 11\ 370$ in.)
			22.5×10^{-6} ($\rho \leq 11\ 370$ in.)	22.5×10^{-6} ($\rho \leq 11\ 370$ in.)	$(13.24 a_1 a_2 \cos \theta) k_T$ ($\rho \leq 11\ 370$ in.)	$1.2/\rho$ ($\rho \leq 11\ 370$ in.)	3.00×10^{-4} ($\rho \leq 11\ 370$ in.)
II	Wire film material with 21 copper wires per inch in both direc- tions and 0.5-mil photolyzable film	Copper wire diam d = 1.0 mil	$\left[1.086 \left(\frac{\rho}{1000}\right)^{4/3} + 19\right] \times 10^{-6}$ ($\rho > 5555$ in.)	$1.086 \left(\frac{\rho}{1000}\right)^{4/3} \times 10^{-6}$ ($\rho > 5555$ in.)	$0.00008508 a_1 a_2 \rho^4 \cos \theta, k_T$ ($\rho > 5555$ in.)	$7.711 \rho^{1/3} \times 10^{-6}$ ($\rho > 5555$ in.)	$0.0005 - 3.3538 \rho^{4/3} \times 10^{-10}$ ($\rho > 5555$ in.)
			29.7×10^{-6} ($\rho \leq 5555$ in.)	10.7×10^{-6} ($\rho \leq 5555$ in.)	$8.371 a_1 a_2 \cos \theta, k_T$ ($\rho \leq 5555$ in.)	$0.75873/\rho$ ($\rho \leq 5555$ in.)	0.000533 ($\rho \leq 5555$ in.)
III	Al wire - 1/2-mil photolyzable film for an operating frequency of 8000 Mc and a re- flected power coef- ficient of 0.96	Al wire diam d = 2.0 mil	$0.1571 \frac{d^2}{s} + 19 \times 10^{-6}$ ($\rho > 13\ 496$ in.)	$0.1571 \frac{d^2}{s}$ ($\rho > 13\ 496$ in.)	$69\ 320 a_1 a_2 d^2 \cos \theta, (k_T s)$ ($\rho > 13\ 496$ in.)	$6283 d^2, \rho s$ ($\rho > 13\ 496$ in.)	$0.0005 - 0.1591 \frac{s}{e^{0.301 s}}$ ($\rho > 13\ 496$ in.)
			28.7×10^{-6} ($\rho \leq 13\ 496$ in.)	9.7×10^{-6} ($\rho \leq 13\ 496$ in.)	$(4.237 a_1 a_2 \cos \theta), k_T$ ($\rho \leq 13\ 496$ in.)	$0.384/\rho$ ($\rho \leq 13\ 496$ in.)	0.0005973 ($\rho \leq 13\ 496$ in.)
IV	Same as material III with f = 800 Mc	Al wire diam d = 2.0 mil	$0.1571 \frac{d^2}{s} + 19 \times 10^{-6}$ ($\rho > 5640$ in.)	$0.1571 \frac{d^2}{s}$ ($\rho > 5640$ in.)	$69320 a_1 a_2 d^2 \cos \theta, (k_T s)$ ($\rho > 5640$ in.)	$6283 d^2, \rho s$ ($\rho > 5640$ in.)	$0.0005 - 0.1591 s e^{\frac{3.01}{s}}$ ($\rho > 5640$ in.)
			20.7×10^{-6} ($\rho \leq 5640$ in.)	1.7×10^{-6} ($\rho \leq 5640$ in.)	$(0.75 a_1 a_2 \cos \theta), k_T$ ($\rho \leq 5640$ in.)	$0.068/\rho$ ($\rho \leq 5640$ in.)	0.0005159 ($\rho \leq 5640$ in.)

^a In this table the minimum material gages presented in the main text were considered. The quantities associated with the smaller values of ρ in all four lens materials correspond to the minimum lens material gages.

APPENDIX D

WEIGHT AND MASS MOMENTS OF INERTIA OF LENS, TORUS, INFLATION SYSTEM, AND CANISTER VERSUS LENS RADIUS OF CURVATURE AND CENTRAL HALF ANGLE FOR VARIOUS LENS MATERIALS

This appendix contains the digital computer output for four types of lens materials and for various values of the parameters of the lens radius of curvature, ρ , and the central half angle, θ . The data consists of the weights of the lens, torus, inflation system, canister, and the combined weights of these four components; canister volumes; mass moments of inertia of photolyzed lens about the x (roll) and z (yaw) axes; and combined mass moments of inertia of unphotolyzed lens and torus about x and z axes. The data is presented in table D1.

The numerical values for these parameters were chosen from considerations of altitude, coverage, and information capacity of the satellite. Thus ρ was taken from 100 to 10 000 feet and θ (lens central half angle) from 8 to 56 degrees. It should be noted that for lens materials III and IV it was more convenient to assign values to the wire spacing, s , rather than arbitrary values to the lens radius, ρ . This was due to the transcendental form of equations relating the quantities d , s , and ρ . This explains why the values of ρ for materials III and IV in the computer output appear to be odd numbers. The symbols used as column heads are explained below.

M	Lens material type (1 stands for material I, i. e., for the Echo II proportion laminate; 2 stands for II, etc)
RADIUS	Lens radius of curvature, ρ , inches
TH	Lens central half-angle, θ , degrees
LENS WT	Lens weight, W_L , pounds
TORUS WT	Torus weight, W_T , pounds
INF SY WT	Inflation system weight W_I , pounds
CANIST WT	Canister weight, W_C , pounds
TOTAL WT	Combined weight of lens, torus, inflation system, and canister, pounds
X INRT ON	Combined lens (film on) and torus pitch or roll moment of inertia, lb-ft ²
Z INRT ON	Combined lens (film on) and torus yaw moment of inertia, lb-ft ²
X INRT OFF	Combined lens (film off) and torus pitch or roll moment of inertia, lb-ft ²
Z INRT OFF	Combined lens (film off) and torus yaw moment of inertia, lb-ft ²
VOL OF CNST	Canister volume, cubic feet

Following Table D1 is a series of 40 graphs, which can be thought of as four groups with ten graphs per group. The four groups represent the four lens materials, and the graphs for each group are plotted to give the dependent variable (ordinate) against ρ (abscissa), for various values of θ (family of curves). The dependent variable for each group is (1) lens weight; (2) torus weight; (3) inflation system weight; (4) canister weight; (5) sum of weight of items 1 through 4; (6) canister volume; (7) I_{x-x} of unphotolyzed lens and torus; (8) I_{z-z} of unphotolyzed lens and torus; (9) I_{x-x} of photolyzed lens and (10) I_{z-z} of photolyzed lens. The 40 graphs are presented as follows:

Material I - figures D1 to D10
Material II - figures D11 to D20

Material III - figures D21 to D30
Material IV - figures D31 to D40

APPENDIX D

TABLE D1. - DIGITAL COMPUTER DATA

M	RADIUS	TH	LENS WT	TORUS WT	INF SY WT	CANIST WT	TOTAL WT	X INRT ON	Z INRT ON	X INRT OFF	Z INRT OFF	VOL OF CNST
1	1200.	8.	4.134E-01	2.718E-01	1.648E-01	1.371E-01	9.961E-01	4.878E-01	9.724E-01	2.042E-01	4.059E-01	3.713E-02
1	1200.	16.	1.665E-00	1.070E-00	6.349E-01	5.325E-01	3.883E-00	7.507E-02	1.483E-03	3.267E-02	6.368E-02	1.442E-01
1	1200.	24.	3.717E-00	2.173E-00	1.342E-00	1.140E-00	8.372E-00	3.561E-03	6.934E-03	1.653E-03	3.121E-03	3.087E-01
1	1200.	32.	6.533E-00	3.424E-00	2.184E-00	1.893E-00	1.403E-01	1.032E-04	1.962E-04	5.215E-03	9.424E-03	5.125E-01
1	1200.	40.	1.006E-01	4.570E-00	3.045E-00	2.712E-00	2.037E-01	2.266E-04	4.164E-04	1.268E-04	2.170E-04	7.343E-01
1	1200.	48.	1.422E-01	5.313E-00	3.811E-00	3.520E-00	2.687E-01	4.170E-04	7.300E-04	2.613E-04	4.188E-04	9.530E-01
1	1200.	56.	1.895E-01	5.526E-00	4.392E-00	4.253E-00	3.312E-01	6.806E-04	1.116E-05	4.791E-04	7.126E-04	1.151E-00
1	3000.	8.	6.537E-00	4.309E-00	2.575E-00	2.143E-00	1.556E-01	4.763E-03	9.496E-03	1.995E-03	3.964E-03	5.801E-01
1	3000.	16.	2.602E-01	1.641E-01	9.921E-00	8.320E-00	6.067E-01	7.326E-04	1.448E-05	3.191E-04	6.219E-04	2.252E-00
1	3000.	24.	5.807E-01	3.395E-01	2.097E-01	1.782E-01	1.308E-02	3.477E-05	6.771E-05	1.614E-05	3.048E-05	4.824E-00
1	3000.	32.	1.071E-02	5.350E-01	3.413E-01	2.958E-01	2.193E-02	1.008E-06	1.916E-06	5.092E-05	9.203E-05	8.009E-00
1	3000.	40.	1.572E-02	7.110E-01	4.757E-01	4.238E-01	3.182E-02	2.213E-06	4.067E-06	1.239E-06	2.119E-06	1.147E-01
1	3000.	48.	2.223E-02	8.301E-01	5.954E-01	5.500E-01	4.198E-02	4.072E-06	7.127E-06	2.551E-06	4.089E-06	1.489E-01
1	3000.	56.	2.961E-02	8.634E-01	6.862E-01	6.646E-01	5.175E-02	6.647E-06	1.089E-07	4.678E-06	6.959E-06	1.799E-01
1	5000.	8.	3.027E-01	1.985E-01	1.192E-01	9.920E-00	7.205E-01	6.126E-04	1.221E-05	2.565E-04	5.097E-04	2.686E-00
1	5000.	16.	1.205E-02	7.575E-01	4.593E-01	3.652E-01	2.809E-02	9.421E-05	1.863E-06	4.103E-05	7.998E-05	1.043E-01
1	5000.	24.	2.689E-02	1.572E-02	9.706E-01	8.250E-01	6.056E-02	4.472E-06	8.708E-06	2.076E-06	3.919E-06	2.233E-01
1	5000.	32.	4.726E-02	2.477E-02	1.580E-02	1.370E-02	1.015E-03	1.296E-07	2.464E-07	6.549E-06	1.184E-07	3.708E-01
1	5000.	40.	7.276E-02	3.242E-02	2.202E-02	1.962E-02	1.473E-03	2.846E-07	5.230E-07	1.593E-07	2.725E-07	5.312E-01
1	5000.	48.	1.029E-03	3.843E-02	2.757E-02	2.546E-02	1.944E-03	5.237E-07	9.168E-07	3.281E-07	5.259E-07	6.894E-01
1	5000.	56.	1.371E-03	3.997E-02	3.177E-02	3.077E-02	2.396E-03	8.548E-07	1.401E-08	6.016E-07	8.950E-07	8.329E-01
1	10000.	8.	2.421E-02	1.596E-02	9.536E-01	7.936E-01	5.764E-02	1.960E-06	3.908E-06	8.208E-05	1.631E-06	2.149E-01
1	10000.	16.	9.638E-02	6.076E-02	3.674E-02	3.081E-02	2.247E-03	3.015E-07	5.960E-07	1.313E-07	2.559E-07	8.342E-01
1	10000.	24.	2.131E-03	1.257E-03	7.765E-02	6.600E-02	4.845E-03	1.431E-08	2.787E-08	6.643E-07	1.254E-08	1.787E-02
1	10000.	32.	3.780E-03	1.931E-03	1.264E-03	1.096E-03	8.121E-03	4.147E-08	7.886E-08	2.096E-08	3.787E-08	2.966E-02
1	10000.	40.	5.821E-03	2.633E-03	1.762E-03	1.570E-03	1.179E-04	9.108E-08	1.673E-09	5.097E-08	8.719E-08	4.249E-02
1	10000.	48.	8.232E-03	3.075E-03	2.205E-03	2.037E-03	1.555E-04	1.676E-09	2.934E-09	1.050E-09	1.683E-09	5.515E-02
1	10000.	56.	1.097E-04	3.128E-03	2.542E-03	2.461E-03	1.917E-04	2.735E-09	4.483E-09	1.925E-09	2.864E-09	6.663E-02
1	20000.	8.	1.937E-03	1.277E-03	7.629E-02	6.349E-02	4.611E-03	6.273E-07	1.251E-08	2.627E-07	5.219E-07	1.719E-02
1	20000.	16.	7.710E-03	4.861E-03	2.939E-03	2.465E-03	1.798E-04	9.647E-08	1.907E-09	4.202E-08	8.190E-08	6.674E-02
1	20000.	24.	1.721E-04	1.006E-04	6.212E-03	5.280E-03	3.876E-04	4.579E-09	8.917E-09	2.126E-09	4.013E-09	1.429E-03
1	20000.	32.	3.024E-04	1.585E-04	1.011E-04	8.765E-03	6.497E-04	1.327E-10	2.523E-10	6.706E-09	1.212E-10	2.373E-03
1	20000.	40.	4.637E-04	2.167E-04	1.410E-04	1.256E-04	9.428E-04	2.914E-10	5.355E-10	1.631E-10	2.790E-10	3.399E-03
1	20000.	48.	6.585E-04	2.460E-04	1.764E-04	1.630E-04	1.244E-05	5.363E-10	9.388E-10	3.360E-10	5.385E-10	4.412E-03
1	20000.	56.	8.774E-04	2.538E-04	2.033E-04	1.969E-04	1.533E-05	8.753E-10	1.435E-11	6.161E-10	9.165E-10	5.331E-03
1	40000.	8.	1.550E-04	1.021E-04	6.103E-03	5.079E-03	3.689E-04	2.007E-09	4.007E-09	8.405E-08	1.670E-09	1.375E-03
1	40000.	16.	6.168E-04	3.889E-04	2.552E-04	1.972E-04	1.438E-05	3.087E-10	6.103E-10	1.245E-10	2.621E-10	3.339E-03
1	40000.	24.	1.377E-05	8.047E-04	4.970E-04	4.224E-04	3.101E-05	1.465E-11	2.853E-11	6.802E-10	1.284E-11	1.143E-04
1	40000.	32.	2.419E-05	1.268E-05	8.089E-04	7.012E-04	5.198E-05	4.246E-11	8.075E-11	2.146E-11	3.878E-11	1.898E-04
1	40000.	40.	3.725E-05	1.645E-05	1.128E-05	1.005E-05	7.543E-05	9.326E-11	1.714E-12	5.219E-11	8.929E-11	2.720E-04
1	40000.	48.	5.268E-05	1.968E-05	1.411E-05	1.304E-05	9.951E-05	1.716E-12	3.004E-12	1.075E-12	1.723E-12	3.530E-04
1	40000.	56.	7.019E-05	2.047E-05	1.627E-05	1.575E-05	1.227E-06	2.801E-12	4.591E-12	1.971E-12	2.933E-12	4.265E-04
1	80000.	8.	1.240E-05	8.170E-04	4.863E-04	4.063E-04	2.951E-05	6.423E-10	1.281E-11	2.690E-10	5.345E-10	1.100E-04
1	80000.	16.	4.935E-05	3.111E-05	1.881E-05	1.578E-05	1.150E-06	9.879E-11	1.953E-12	4.303E-11	8.386E-11	4.271E-04
1	80000.	24.	1.101E-06	6.438E-05	3.976E-05	3.379E-05	2.481E-06	4.689E-12	9.131E-12	2.177E-12	4.110E-12	9.148E-04

APPENDIX D

TABLE D1. - DIGITAL COMPUTER DATA - Continued

M	RADIUS	TH	LENS WT	TORUS WT	INF SY WT	CANIST WT	TOTAL WT	X INRT ON	Z INRT ON	X INRT OFF	Z INRT OFF	VOL OF CNST
1	80000.	32.	1.936E 06	1.014E 06	6.471E 05	5.610E 05	4.15HE 06	1.359E 13	2.584E 13	6.867E 12	1.241E 13	1.519E 05
1	80000.	40.	2.980E 06	1.348E 06	9.021E 05	8.036E 05	6.034E 06	2.984E 13	5.484E 13	1.670E 13	2.857E 13	2.176E 05
1	80000.	48.	4.215E 06	1.574E 06	1.129E 06	1.043E 06	7.961E 06	5.492E 13	9.613E 13	3.441E 13	5.514E 13	2.824E 05
1	80000.	56.	5.615E 06	1.637E 06	1.301E 06	1.260E 06	9.814E 06	8.963E 13	1.469E 14	6.309E 13	9.385E 13	3.412E 05
1	120000.	8.	4.194E 05	2.758E 05	1.648E 05	1.371E 05	9.961E 05	4.878E 11	9.124E 11	2.042E 11	4.059E 11	3.713E 04
1	120000.	16.	1.665E 06	1.050E 06	6.349E 05	5.325E 05	3.883E 06	7.507E 12	1.483E 13	3.267E 12	6.368E 12	1.442E 05
1	120000.	24.	3.717E 06	2.173E 06	1.342E 06	1.140E 06	8.372E 06	3.561E 13	6.934E 13	1.653E 13	3.121E 13	3.087E 05
1	120000.	32.	6.533E 06	3.424E 06	2.184E 06	1.893E 06	1.403E 07	1.032E 14	1.962E 14	5.215E 13	9.424E 13	5.125E 05
1	120000.	40.	1.006E 07	4.550E 06	3.045E 06	2.712E 06	2.037E 07	2.266E 14	4.164E 14	1.268E 14	2.170E 14	7.343E 05
1	120000.	48.	1.422E 07	5.313E 06	3.811E 06	3.520E 06	2.687E 07	4.170E 14	7.300E 14	2.613E 14	4.188E 14	9.530E 05
1	120000.	56.	1.845E 07	5.520E 06	4.392E 06	4.253E 06	3.312E 07	6.806E 14	1.116E 15	4.791E 14	7.126E 14	1.151E 06
2	1200.	8.	3.570E 00	2.142E 01	1.280E 01	1.009E 00	4.941E 00	1.972E 02	3.922E 02	1.190E 01	2.366E 01	2.733E 01
2	1200.	16.	1.429E 01	8.155E 01	4.931E 01	4.008E 00	1.961E 01	3.132E 03	6.120E 03	1.904E 02	3.712E 02	1.085E 00
2	1200.	24.	3.189E 01	1.648E 00	1.642E 00	8.907E 00	4.353E 01	1.566E 04	2.973E 04	9.634E 02	1.819E 03	2.411E 00
2	1200.	32.	5.605E 01	2.659E 00	1.696E 00	1.557E 01	7.597E 01	4.870E 04	8.877E 04	3.039E 03	5.493E 03	4.215E 00
2	1200.	40.	8.630E 01	3.534E 00	2.365E 00	2.381E 01	1.160E 02	1.166E 05	2.016E 05	7.392E 03	1.265E 04	6.447E 00
2	1200.	48.	1.220E 02	4.126E 00	2.960E 00	3.343E 01	1.626E 02	2.362E 05	3.834E 05	1.523E 04	2.441E 04	9.051E 00
2	1200.	56.	1.626E 02	4.292E 00	3.411E 00	4.420E 01	2.145E 02	4.266E 05	6.427E 05	2.772E 04	4.154E 04	1.197E 01
2	3000.	8.	2.608E 01	4.542E 00	2.714E 00	7.330E 00	4.067E 01	1.087E 04	2.164E 04	1.578E 03	3.135E 03	1.985E 00
2	3000.	16.	1.038E 02	1.729E 01	1.646E 01	2.896E 01	1.605E 02	1.709E 05	3.352E 05	2.524E 04	4.920E 04	7.840E 00
2	3000.	24.	2.317E 02	3.579E 01	2.210E 01	6.384E 01	3.534E 02	8.403E 05	1.608E 06	1.277E 05	2.411E 05	1.728E 01
2	3000.	32.	4.072E 02	5.639E 01	3.597E 01	1.104E 02	6.100E 02	2.557E 06	4.721E 06	4.028E 05	7.280E 05	2.988E 01
2	3000.	40.	6.270E 02	7.495E 01	5.015E 01	1.666E 02	9.187E 02	5.968E 06	1.051E 07	9.798E 05	1.676E 06	4.510E 01
2	3000.	48.	8.868E 02	8.750E 01	6.276E 01	2.304E 02	1.267E 03	1.178E 07	1.952E 07	2.018E 06	3.235E 06	6.237E 01
2	3000.	56.	1.181E 03	2.101E 01	7.234E 01	2.998E 02	1.645E 03	2.074E 07	3.191E 07	3.701E 06	5.505E 06	8.115E 01
2	5000.	8.	8.647E 01	2.473E 01	1.490E 01	2.429E 01	1.506E 02	1.178E 05	2.345E 05	2.406E 04	4.780E 04	6.576E 00
2	5000.	16.	3.442E 02	4.422E 01	5.740E 01	9.547E 01	5.920E 02	1.837E 06	3.612E 06	3.849E 05	7.501E 05	2.585E 01
2	5000.	24.	7.642E 02	1.964E 02	1.213E 02	2.087E 02	1.295E 03	8.924E 06	1.719E 07	1.947E 06	3.676E 06	5.651E 01
2	5000.	32.	1.350E 03	3.095E 02	1.974E 02	3.568E 02	2.214E 03	2.671E 07	4.981E 07	6.142E 06	1.110E 07	9.660E 01
2	5000.	40.	2.079E 03	4.114E 02	2.753E 02	5.310E 02	3.297E 03	6.116E 07	1.091E 08	1.494E 07	2.556E 07	1.438E 02
2	5000.	48.	2.940E 03	4.803E 02	3.445E 02	7.225E 02	4.487E 03	1.182E 08	1.991E 08	3.078E 07	4.932E 07	1.956E 02
2	5000.	56.	3.917E 03	4.996E 02	3.971E 02	9.231E 02	5.736E 03	2.035E 08	3.189E 08	5.643E 07	8.394E 07	2.499E 02
2	10000.	8.	5.185E 02	2.513E 02	1.502E 02	1.455E 02	1.065E 03	3.550E 06	7.076E 06	9.700E 05	1.927E 06	3.939E 01
2	10000.	16.	2.064E 03	9.568E 02	5.786E 02	5.669E 02	4.166E 03	5.489E 07	1.083E 08	1.552E 07	3.024E 07	1.535E 02
2	10000.	24.	4.606E 03	1.980E 03	1.223E 03	1.221E 03	9.030E 03	2.629E 08	5.097E 08	7.850E 07	1.482E 08	3.307E 02
2	10000.	32.	8.095E 03	3.120E 03	1.490E 03	2.046E 03	1.525E 04	7.714E 08	1.456E 09	2.476E 08	4.475E 08	5.538E 02
2	10000.	40.	1.246E 04	4.147E 03	2.774E 03	2.965E 03	2.235E 04	1.723E 09	3.128E 09	6.023E 08	1.030E 09	8.026E 02
2	10000.	48.	1.763E 04	4.841E 03	3.472E 03	3.305E 03	2.985E 04	3.233E 09	5.572E 09	1.241E 09	1.989E 09	1.057E 03
2	10000.	56.	2.358E 04	5.035E 03	4.002E 03	4.805E 03	3.733E 04	5.397E 09	8.680E 09	2.275E 09	3.384E 09	1.301E 03
2	20000.	8.	3.813E 03	2.533E 03	1.514E 03	1.069E 03	8.929E 03	1.240E 08	2.472E 08	3.911E 07	7.771E 07	2.894E 02
2	20000.	16.	1.518E 04	3.644E 03	5.831E 03	4.132E 03	3.479E 04	1.907E 09	3.770E 09	6.256E 08	1.219E 09	1.119E 03
2	20000.	24.	3.398E 04	1.996E 04	1.232E 04	8.782E 03	7.494E 04	9.049E 09	1.762E 10	3.165E 09	5.975E 09	2.377E 03
2	20000.	32.	5.924E 04	3.145E 04	2.906E 04	1.441E 04	1.255E 05	2.621E 10	4.986E 10	9.984E 09	1.804E 10	3.902E 03
2	20000.	40.	9.167E 04	4.179E 04	2.796E 04	2.033E 04	1.818E 05	5.755E 10	1.058E 11	2.428E 10	4.154E 10	5.504E 03
2	20000.	48.	1.296E 05	4.810E 04	3.500E 04	2.585E 04	2.393E 05	1.059E 11	1.854E 11	5.003E 10	8.017E 10	6.998E 03

APPENDIX D

TABLE D1. - DIGITAL COMPUTER DATA - Continued

M	RADIUS	TH	LENS WT	TORUS WT	INF SY WT	CANIST WT	TOTAL WT	X INRT ON	Z INRT ON	X INRT OFF	Z INRT OFF	VOL OF CNST
2	20000.	8.	1.727E 05	2.075E 04	4.034E 04	3.043E 04	2.942E 05	1.727E 11	2.831E 11	9.172E 10	1.364E 11	8.238E 03
2	40000.	8.	3.279E 04	2.533E 04	1.520E 04	9.186E 03	8.276E 04	4.692E 09	9.358E 09	1.577E 09	3.133E 09	2.487E 03
2	60000.	16.	1.305E 05	2.720E 04	5.878E 04	3.532E 04	3.218E 05	7.197E 10	1.424E 11	2.522E 10	4.916E 10	9.563E 03
2	80000.	24.	2.913E 05	2.011E 05	1.242E 05	7.440E 04	6.910E 05	3.400E 11	6.637E 11	1.276E 11	2.409E 11	2.014E 04
2	100000.	32.	5.119E 05	3.170E 05	2.022E 05	1.205E 05	1.152E 06	9.786E 11	1.869E 12	4.025E 11	7.274E 11	3.261E 04
2	120000.	40.	7.882E 05	4.213E 05	2.819E 05	1.667E 05	1.658E 06	2.130E 12	3.939E 12	9.791E 11	1.675E 12	4.513E 04
2	140000.	48.	1.115E 06	4.918E 05	3.528E 05	2.065E 05	2.166E 06	3.876E 12	6.845E 12	2.017E 12	3.232E 12	5.591E 04
2	160000.	56.	1.485E 06	5.115E 05	4.060E 05	2.347E 05	2.638E 06	6.243E 12	1.035E 13	3.698E 12	5.501E 12	6.354E 04
2	180000.	64.	3.079E 05	2.573E 05	1.538E 05	8.673E 04	8.052E 05	1.843E 11	3.875E 11	6.357E 10	1.263E 11	2.335E 04
2	200000.	72.	1.225E 06	9.747E 05	5.924E 05	3.307E 05	3.128E 06	2.823E 12	5.590E 12	1.017E 12	1.982E 12	8.954E 04
2	220000.	80.	2.735E 06	2.077E 06	1.252E 06	6.934E 05	6.708E 06	1.331E 13	2.601E 13	5.144E 12	9.712E 12	1.877E 05
2	240000.	88.	4.807E 06	3.195E 06	2.038E 06	1.115E 06	1.115E 07	3.820E 13	7.309E 13	1.623E 13	2.933E 13	3.019E 05
2	260000.	96.	7.401E 06	4.246E 06	2.841E 06	1.527E 06	1.602E 07	8.283E 13	1.536E 14	3.947E 13	6.752E 13	4.135E 05
2	280000.	104.	1.047E 07	4.957E 06	3.556E 06	1.866E 06	2.085E 07	1.500E 14	2.659E 14	8.132E 13	1.303E 14	5.050E 05
2	300000.	112.	1.394E 07	5.156E 06	4.098E 06	2.078E 06	2.528E 07	2.402E 14	4.000E 14	1.491E 14	2.218E 14	5.625E 05
2	320000.	120.	1.165E 06	9.941E 05	5.941E 05	3.264E 05	3.080E 06	1.590E 12	3.172E 12	5.576E 11	1.098E 12	8.837E 04
2	340000.	128.	4.639E 06	3.785E 06	2.289E 06	1.251E 06	1.196E 07	2.435E 13	4.822E 13	8.840E 12	1.723E 13	3.387E 05
2	360000.	136.	1.035E 07	7.833E 06	4.837E 06	2.619E 06	2.564E 07	1.148E 14	2.243E 14	4.472E 13	8.443E 13	7.090E 05
2	380000.	144.	1.820E 07	1.234E 07	7.873E 06	4.202E 06	4.261E 07	3.291E 14	6.299E 14	1.411E 14	2.549E 14	1.138E 06
2	400000.	152.	2.802E 07	1.640E 07	1.098E 07	5.739E 06	6.113E 07	7.128E 14	1.323E 15	3.431E 14	5.870E 14	1.554E 06
2	420000.	160.	3.962E 07	1.915E 07	1.374E 07	6.978E 06	7.949E 07	1.289E 15	2.288E 15	7.069E 14	1.133E 15	1.889E 06
2	440000.	168.	5.279E 07	1.992E 07	1.583E 07	7.722E 06	9.626E 07	2.061E 15	3.436E 15	1.296E 15	1.928E 15	2.091E 06
3	1185.	8.	3.339E-00	3.750E-02	2.241E-02	9.366E-01	4.336E-00	1.627E 02	3.234E 02	3.609E-00	7.172E-00	2.536E-01
3	1185.	16.	1.329E 01	1.428E-01	8.634E-02	3.726E-00	1.725E 01	2.599E 03	5.069E 03	5.774E 01	1.125E 02	1.009E-00
3	1185.	24.	2.966E 01	2.955E-01	1.825E-01	8.310E-00	3.845E 01	1.312E 04	2.480E 04	2.921E 02	5.515E 02	2.750E-00
3	1185.	32.	5.214E 01	4.656E-01	2.970E-01	1.459E 01	6.749E 01	4.127E 04	7.471E 04	9.214E 02	1.665E 03	3.950E-00
3	1185.	40.	8.027E 01	6.188E-01	4.140E-01	2.244E 01	1.037E 02	1.000E 05	1.715E 05	2.241E 03	3.834E 03	6.074E-00
3	1185.	48.	1.135E 02	7.224E-01	5.182E-01	3.169E 01	1.465E 02	2.054E 05	3.301E 05	4.617E 03	7.400E 03	8.578E-00
3	1185.	56.	1.512E 02	7.514E-01	5.972E-01	4.216E 01	1.948E 02	3.756E 05	5.600E 05	8.465E 03	1.259E 04	1.141E 01
3	3767.	8.	3.632E 01	1.660E-00	9.919E-01	1.010E 01	4.907E 01	1.915E 04	3.808E 04	1.614E 03	3.207E 03	2.734E-00
3	3767.	16.	1.446E 02	6.320E-00	3.822E-00	4.012E 01	1.948E 02	3.046E 05	5.949E 05	2.582E 04	5.032E 04	1.086E 01
3	3767.	24.	3.227E 02	1.308E 01	8.076E-00	8.924E 01	4.331E 02	1.527E 06	2.896E 06	1.306E 05	2.466E 05	2.416E 01
3	3767.	32.	5.671E 02	2.061E 01	1.315E 01	1.562E 02	7.571E 02	4.763E 06	8.666E 06	4.120E 05	7.446E 05	4.228E 01
3	3767.	40.	8.732E 02	2.739E 01	1.833E 01	2.393E 02	1.158E 03	1.144E 07	1.974E 07	1.002E 06	1.714E 06	6.477E 01
3	3767.	48.	1.235E 03	3.198E 01	2.294E 01	3.365E 02	1.626E 03	2.327E 07	3.766E 07	2.064E 06	3.309E 06	9.109E 01
3	3767.	56.	1.645E 03	3.326E 01	2.644E 01	4.456E 02	2.151E 03	4.217E 07	6.335E 07	3.785E 06	5.631E 06	1.206E 02
3	9593.	8.	2.850E 02	3.523E 01	2.105E 01	7.767E 01	4.190E 02	1.121E 06	2.230E 06	2.222E 05	4.415E 05	2.103E 01
3	9593.	16.	1.135E 03	1.341E 02	8.112E 01	3.074E 02	1.657E 03	1.768E 07	3.464E 07	3.555E 06	6.928E 06	8.323E 01
3	9593.	24.	2.532E 03	2.776E 02	1.714E 02	6.800E 02	3.661E 03	8.755E 07	1.670E 08	1.798E 07	3.395E 07	1.841E 02
3	9593.	32.	4.451E 03	4.374E 02	2.790E 02	1.181E 03	6.348E 03	2.687E 08	4.936E 08	5.673E 07	1.025E 08	3.197E 02
3	9593.	40.	6.852E 03	5.814E 02	3.896E 02	1.792E 03	9.615E 03	6.337E 08	1.107E 09	1.380E 08	2.360E 08	4.852E 02
3	9593.	48.	9.691E 03	6.788E 02	4.869E 02	2.495E 03	1.335E 04	1.265E 09	2.077E 09	2.842E 08	4.556E 08	6.753E 02
3	9593.	56.	1.291E 04	7.060E 02	5.612E 02	3.268E 03	1.745E 04	2.250E 09	3.432E 09	5.217E 08	7.753E 08	8.846E 02
3	19150.	8.	1.531E 03	3.336E 02	2.006E 02	4.068E 02	2.474E 03	2.785E 07	5.543E 07	8.442E 06	1.678E 07	1.101E 02
3	19150.	16.	6.095E 03	1.278E 03	7.778E 02	1.603E 03	9.749E 03	4.361E 08	8.565E 08	1.351E 08	2.632E 08	4.339E 02

APPENDIX D

TABLE D1. - DIGITAL COMPUTER DATA - Continued

M	RADIUS	TH	LENS WT	TORUS WT	INF SY WT	CANIST WT	TOTAL WT	X INRT ON	Z INRT ON	X INRT OFF	Z INRT OFF	VOL OF CNST
1	1915h	24.	1.360E 04	2.645E 03	1.633E 03	3.519E 03	2.140E 04	2.134E 09	4.094E 09	6.832E 08	1.290E 09	9.526E 02
1	1915h	32.	2.341E 04	4.167E 03	2.658E 03	6.049E 03	3.678E 04	6.447E 09	1.195E 10	2.155E 09	3.845E 09	1.638E 03
1	1915h	40.	3.641E 04	5.539E 03	3.706E 03	9.667E 03	5.512E 04	1.493E 10	2.642E 10	5.242E 09	8.968E 09	2.455E 03
1	1915h	48.	5.206E 04	6.417E 03	4.638E 03	1.244E 04	7.560E 04	2.920E 10	4.871E 10	1.080E 10	1.731E 10	3.367E 03
1	1915h	56.	6.936E 04	6.726E 03	5.346E 03	1.604E 04	9.747E 04	5.094E 10	7.897E 10	1.980E 10	2.946E 10	4.342E 03
1	32765	8.	6.377E 03	1.921E 03	1.148E 03	1.657E 03	1.110E 04	3.793E 08	7.553E 08	1.413E 08	2.808E 08	4.485E 02
1	32765	16.	2.538E 04	7.313E 03	4.422E 03	6.501E 03	4.362E 04	5.911E 09	1.163E 10	2.260E 09	4.406E 09	1.760E 03
1	32765	24.	5.665E 04	1.513E 04	9.346E 03	1.417E 04	9.530E 04	2.869E 10	5.526E 10	1.144E 10	2.159E 10	3.837E 03
1	32765	32.	9.937E 04	2.385E 04	1.521E 04	2.414E 04	1.628E 05	8.575E 10	1.600E 11	3.608E 10	6.520E 10	6.535E 03
1	32765	40.	1.533E 05	3.169E 04	2.121E 04	3.575E 04	2.420E 05	1.959E 11	3.501E 11	8.774E 10	1.501E 11	9.679E 03
1	32765	48.	2.169E 05	3.700E 04	2.654E 04	4.837E 04	3.287E 05	3.777E 11	6.374E 11	1.808E 11	2.897E 11	1.309E 04
1	32765	56.	2.888E 05	3.849E 04	3.059E 04	6.140E 04	4.193E 05	6.490E 11	1.019E 12	3.314E 11	4.930E 11	1.662E 04
1	50435	8.	2.163E 04	7.777E 03	4.647E 03	5.530E 03	3.958E 04	3.278E 09	6.529E 09	1.356E 09	2.694E 09	1.497E 03
1	50435	16.	8.610E 04	2.961E 04	1.791E 04	2.163E 04	1.553E 05	5.093E 10	1.003E 11	2.169E 10	4.227E 10	5.856E 03
1	50435	24.	1.922E 05	6.128E 04	3.784E 04	4.693E 04	3.382E 05	2.460E 11	4.749E 11	1.097E 11	2.071E 11	1.270E 04
1	50435	32.	3.377E 05	3.656E 04	6.159E 04	7.934E 04	5.752E 05	7.304E 11	1.369E 12	3.461E 11	6.255E 11	2.148E 04
1	50435	40.	5.200E 05	1.283E 05	8.586E 04	1.164E 05	8.506E 05	1.655E 12	2.975E 12	8.418E 11	1.440E 12	3.152E 04
1	50435	48.	7.354E 05	1.498E 05	1.075E 05	1.558E 05	1.148E 06	3.162E 12	5.374E 12	1.734E 12	2.779E 12	4.217E 04
1	50435	56.	9.798E 05	1.558E 05	1.239E 05	1.952E 05	1.455E 06	5.379E 12	8.515E 12	3.180E 12	4.730E 12	5.285E 04
1	72015	8.	6.181E 04	2.461E 04	1.471E 04	1.563E 04	1.168E 05	1.998E 10	3.981E 10	8.748E 09	1.738E 10	4.231E 03
1	72015	16.	2.460E 05	9.372E 04	5.667E 04	6.102E 04	4.574E 05	3.100E 11	6.108E 11	1.399E 11	2.728E 11	1.652E 04
1	72015	24.	5.491E 05	1.939E 05	1.198E 05	1.319E 05	9.947E 05	1.493E 12	2.886E 12	7.080E 11	1.337E 12	3.571E 04
1	72015	32.	9.651E 05	3.056E 05	1.950E 05	2.219E 05	1.688E 06	4.415E 12	8.292E 12	2.234E 12	4.036E 12	6.007E 04
1	72015	40.	1.496E 06	4.062E 05	2.718E 05	3.235E 05	2.487E 06	9.956E 12	1.795E 13	5.432E 12	9.293E 12	8.759E 04
1	72015	48.	2.101E 06	4.742E 05	3.402E 05	4.294E 05	3.345E 06	1.891E 13	3.228E 13	1.119E 13	1.794E 13	1.162E 05
1	72015	56.	2.800E 06	4.932E 05	3.920E 05	5.331E 05	4.218E 06	3.197E 13	5.086E 13	2.052E 13	3.052E 13	1.443E 05
1	119911	8.	2.911E 05	1.275E 05	7.617E 04	7.278E 04	5.675E 05	2.727E 11	5.434E 11	1.256E 11	2.496E 11	1.970E 04
1	119911	16.	1.159E 06	4.853E 05	2.935E 05	2.835E 05	2.221E 06	4.224E 12	8.329E 12	2.009E 12	3.916E 12	7.675E 04
1	119911	24.	2.586E 06	1.964E 06	6.202E 05	6.105E 05	4.821E 06	2.029E 13	3.927E 13	1.016E 13	1.919E 13	1.653E 05
1	119911	32.	4.545E 06	1.582E 06	1.009E 06	1.022E 06	8.158E 06	5.977E 13	1.125E 14	3.206E 13	5.795E 13	2.766E 05
1	119911	40.	6.947E 06	2.103E 06	1.407E 06	1.479E 06	1.199E 07	1.342E 14	2.427E 14	7.799E 13	1.334E 14	4.005E 05
1	119911	48.	9.896E 06	2.456E 06	1.761E 06	1.946E 06	1.606E 07	2.534E 14	4.345E 14	1.607E 14	2.575E 14	5.269E 05
1	119911	56.	1.318E 07	2.554E 06	2.030E 06	2.391E 06	2.016E 07	4.258E 14	6.809E 14	2.946E 14	4.382E 14	6.473E 05
1	1201	8.	3.395E-00	2.019E-02	1.206E-02	9.534E-01	4.380E-00	1.663E 02	3.305E 02	1.997E-00	3.968E-00	2.581E-01
1	1201	16.	1.351E 01	7.647E-02	4.648E-02	3.794E-00	1.743E 01	2.660E 03	5.185E 03	3.195E 01	6.227E 01	1.027E-00
1	1201	24.	3.016E 01	1.591E-01	9.824E-02	8.464E-00	3.888E 01	1.346E 04	2.541E 04	1.616E 02	3.051E 02	2.291E-00
1	1201	32.	5.300E 01	2.507E-01	1.599E-01	1.487E 01	6.828E 01	4.244E 04	7.671E 04	5.099E 02	9.214E 02	4.025E-00
1	1201	40.	8.160E 01	3.331E-01	2.229E-01	2.288E 01	1.050E 02	1.032E 05	1.766E 05	1.240E 03	2.121E 03	6.193E-00
1	1201	48.	1.154E 02	3.890E-01	2.790E-01	3.233E 01	1.484E 02	2.126E 05	3.408E 05	2.555E 03	4.094E 03	8.753E-00
1	1201	56.	1.538E 02	4.045E-01	3.216E-01	4.304E 01	1.975E 02	3.897E 05	5.798E 05	4.684E 03	6.968E 03	1.165E 01
1	380h	8.	3.551E 01	8.998E-01	5.377E-01	9.925E-00	4.688E 01	1.755E 04	3.488E 04	8.942E 02	1.777E 03	2.687E-00
1	380h	16.	1.414E 02	3.426E-00	2.072E-00	3.946E 01	1.863E 02	2.807E 05	5.471E 05	1.430E 04	2.788E 04	1.068E 01
1	380h	24.	3.155E 02	7.091E-00	4.378E-00	8.792E 01	4.149E 02	1.419E 06	2.680E 06	7.237E 04	1.366E 05	2.380E 01
1	380h	32.	5.545E 02	1.117E 01	7.126E-00	1.542E 02	7.270E 02	4.474E 06	8.089E 06	2.283E 05	4.126E 05	4.174E 01
1	380h	40.	8.537E 02	1.495E 01	9.935E-00	2.367E 02	1.115E 03	1.087E 07	1.861E 07	5.553E 05	9.499E 05	6.408E 01

APPENDIX D

TABLE D1. - DIGITAL COMPUTER DATA - Concluded

M	RADIUS	TH	LENS WT	TORUS WT	INF SY WT	CANIST WT	TOTAL WT	X INRT ON	Z INRT ON	X INRT OFF	Z INRT OFF	VOL OF CNST
4	380c.	46.	1.207E 03	1.734E 01	1.243E 01	3.337E 02	1.571E 03	2.238E 07	3.590E 07	1.144E 06	1.833E 06	9.034E 01
4	380c.	56.	1.609E 03	1.803E 01	1.433E 01	4.432E 02	2.084E 03	4.101E 07	6.105E 07	2.097E 06	3.120E 06	1.200E 02
4	3747.	8.	2.606E 02	1.974E 01	1.179E 01	7.190E 01	3.640E 02	8.527E 05	1.694E 06	1.285E 05	2.553E 05	1.947E 01
4	3747.	16.	1.037E 03	7.515E 01	4.544E 01	2.852E 02	1.443E 03	1.363E 07	2.657E 07	2.055E 06	4.006E 06	7.722E 01
4	9747.	24.	2.315E 03	1.555E 02	9.604E 01	6.332E 02	3.200E 03	6.882E 07	1.300E 08	1.040E 07	1.963E 07	1.714E 02
4	9747.	32.	4.069E 03	2.450E 02	1.563E 02	1.105E 03	5.575E 03	2.167E 08	3.920E 08	3.280E 07	5.929E 07	2.991E 02
4	9747.	40.	6.265E 03	3.257E 02	2.179E 02	1.687E 03	8.495E 03	5.259E 08	9.009E 08	7.979E 07	1.365E 08	4.566E 02
4	9747.	48.	8.861E 03	3.803E 02	2.727E 02	2.363E 03	1.188E 04	1.081E 09	1.735E 09	1.644E 08	2.634E 08	6.396E 02
4	9747.	56.	1.180E 04	3.955E 02	3.144E 02	3.117E 03	1.563E 04	1.978E 09	2.947E 09	3.014E 08	4.483E 08	8.437E 02
4	20528.	8.	1.439E 03	2.273E 02	1.358E 02	3.884E 02	2.140E 03	2.123E 07	4.220E 07	6.563E 06	1.304E 07	1.052E 02
4	20528.	16.	5.726E 03	8.653E 02	5.233E 02	1.535E 03	8.650E 03	3.389E 08	6.611E 08	1.050E 08	2.046E 08	4.156E 02
4	20528.	24.	1.278E 04	1.771E 03	1.106E 03	3.386E 03	1.906E 04	1.709E 09	3.232E 09	5.311E 08	1.003E 09	9.168E 02
4	20528.	32.	2.246E 04	2.822E 03	1.800E 03	5.860E 03	3.294E 04	5.369E 09	9.727E 09	1.676E 09	3.028E 09	1.586E 03
4	20528.	40.	3.438E 04	3.750E 03	2.509E 03	8.856E 03	4.970E 04	1.300E 10	2.231E 10	4.075E 09	6.972E 09	2.397E 03
4	20528.	48.	4.891E 04	4.379E 03	3.141E 03	1.226E 04	6.869E 04	2.666E 10	4.288E 10	8.395E 09	1.346E 10	3.320E 03
4	20528.	56.	6.516E 04	4.554E 03	3.620E 03	1.598E 04	8.931E 04	4.868E 10	7.267E 10	1.539E 10	2.290E 10	4.326E 03
4	37668.	8.	6.652E 03	1.660E 03	9.919E 02	1.753E 03	1.106E 04	3.368E 08	6.694E 08	1.614E 08	3.207E 08	4.745E 02
4	37668.	16.	2.648E 04	5.320E 03	3.822E 03	6.896E 03	4.351E 04	5.370E 09	1.048E 10	2.582E 09	5.032E 09	1.867E 03
4	37668.	24.	5.909E 04	1.308E 04	8.076E 03	1.510E 04	9.535E 04	2.703E 10	5.115E 10	1.306E 10	2.466E 10	4.088E 03
4	37668.	32.	1.039E 05	2.061E 04	1.315E 04	2.587E 04	1.635E 05	8.471E 10	1.537E 11	4.120E 10	7.446E 10	7.004E 03
4	37668.	40.	1.549E 05	2.739E 04	1.833E 04	3.861E 04	2.442E 05	2.046E 11	3.517E 11	1.002E 11	1.714E 11	1.045E 04
4	37668.	48.	2.262E 05	3.196E 04	2.294E 04	5.271E 04	3.338E 05	4.185E 11	6.744E 11	2.064E 11	3.309E 11	1.427E 04
4	37668.	56.	3.013E 05	3.326E 04	2.644E 04	6.760E 04	4.266E 05	7.624E 11	1.140E 12	3.785E 11	5.631E 11	1.830E 04
4	62463.	8.	2.661E 04	8.678E 03	5.186E 03	6.865E 03	4.734E 04	3.761E 09	7.476E 09	2.320E 09	4.611E 09	1.859E 03
4	62463.	16.	1.059E 05	3.304E 04	1.998E 04	2.690E 04	1.858E 05	5.991E 10	1.169E 11	3.712E 10	7.235E 10	7.284E 03
4	62463.	24.	2.364E 05	6.836E 04	4.223E 04	5.854E 04	4.055E 05	3.011E 11	5.702E 11	1.878E 11	3.545E 11	1.585E 04
4	62463.	32.	4.154E 05	1.077E 05	6.873E 04	9.939E 04	6.913E 05	9.420E 11	1.711E 12	5.924E 11	1.071E 12	2.691E 04
4	62463.	40.	6.396E 05	1.432E 05	9.581E 04	1.466E 05	1.025E 06	2.270E 12	3.908E 12	1.441E 12	2.465E 12	3.970E 04
4	62463.	48.	9.046E 05	1.672E 05	1.199E 05	1.974E 05	1.389E 06	4.635E 12	7.480E 12	2.968E 12	4.757E 12	5.345E 04
4	62463.	56.	1.205E 06	1.739E 05	1.382E 05	2.493E 05	1.767E 06	8.426E 12	1.262E 13	5.442E 12	8.096E 12	6.749E 04
4	95931.	8.	9.260E 04	3.523E 04	2.105E 04	2.353E 04	1.724E 05	3.120E 10	6.203E 10	2.222E 10	4.415E 10	6.371E 03
4	95931.	16.	3.686E 05	1.341E 05	8.112E 04	9.197E 04	6.759E 05	4.967E 11	9.679E 11	3.555E 11	6.928E 11	2.490E 04
4	95931.	24.	8.227E 05	2.776E 05	1.714E 05	1.991E 05	1.471E 06	2.494E 12	4.726E 12	1.798E 12	3.395E 12	5.391E 04
4	95931.	32.	1.446E 06	4.374E 05	2.790E 05	3.358E 05	2.498E 06	7.793E 12	1.416E 13	5.673E 12	1.025E 13	9.090E 04
4	95931.	40.	2.226E 06	5.814E 05	3.890E 05	4.911E 05	3.688E 06	1.875E 13	3.232E 13	1.380E 13	2.360E 13	1.329E 05
4	95931.	48.	3.148E 06	6.786E 05	4.869E 05	6.541E 05	4.968E 06	3.823E 13	6.177E 13	2.842E 13	4.556E 13	1.771E 05
4	95931.	56.	4.195E 06	7.060E 05	5.612E 05	8.157E 05	6.277E 06	6.941E 13	1.041E 14	5.212E 13	7.753E 13	2.208E 05
4	120492.	8.	1.835E 05	7.411E 04	4.429E 04	4.634E 04	3.483E 05	9.802E 10	1.949E 11	7.374E 10	1.465E 11	1.755E 04
4	120492.	16.	7.306E 05	2.872E 05	1.706E 05	1.809E 05	1.364E 06	1.560E 12	3.046E 12	1.180E 12	2.299E 12	4.896E 04
4	120492.	24.	1.631E 06	5.839E 05	3.606E 05	3.907E 05	2.966E 06	7.828E 12	1.484E 13	5.967E 12	1.127E 13	1.058E 05
4	120492.	32.	2.866E 06	7.211E 05	5.870E 05	6.569E 05	5.030E 06	2.445E 13	4.444E 13	1.883E 13	3.402E 13	1.778E 05
4	120492.	40.	4.412E 06	1.223E 06	8.183E 05	9.569E 05	7.411E 06	5.880E 13	1.014E 14	4.579E 13	7.833E 13	2.591E 05
4	120492.	48.	6.240E 06	1.428E 06	1.024E 06	1.268E 06	9.961E 06	1.198E 14	1.936E 14	9.432E 13	1.512E 14	3.434E 05
4	120492.	56.	8.314E 06	1.485E 06	1.180E 06	1.573E 06	1.255E 07	2.173E 14	3.261E 14	1.729E 14	2.573E 14	4.257E 05

APPENDIX D

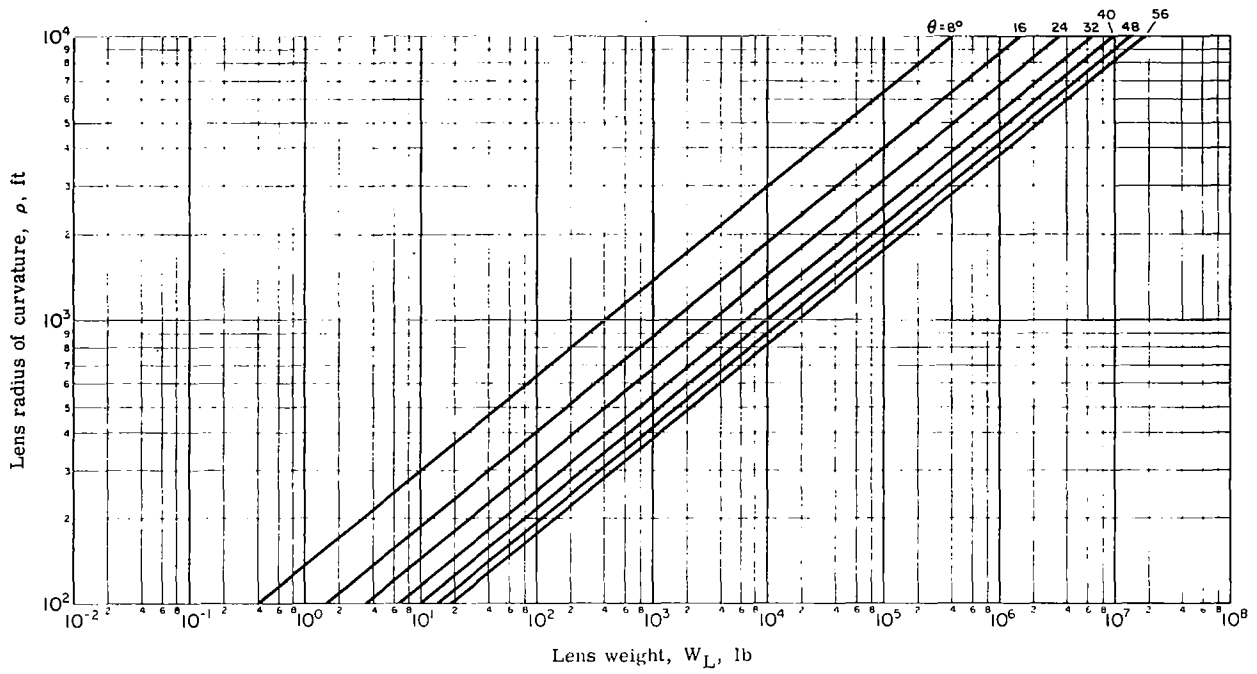


Figure D1. - Material I - lens weight versus lens radius of curvature.

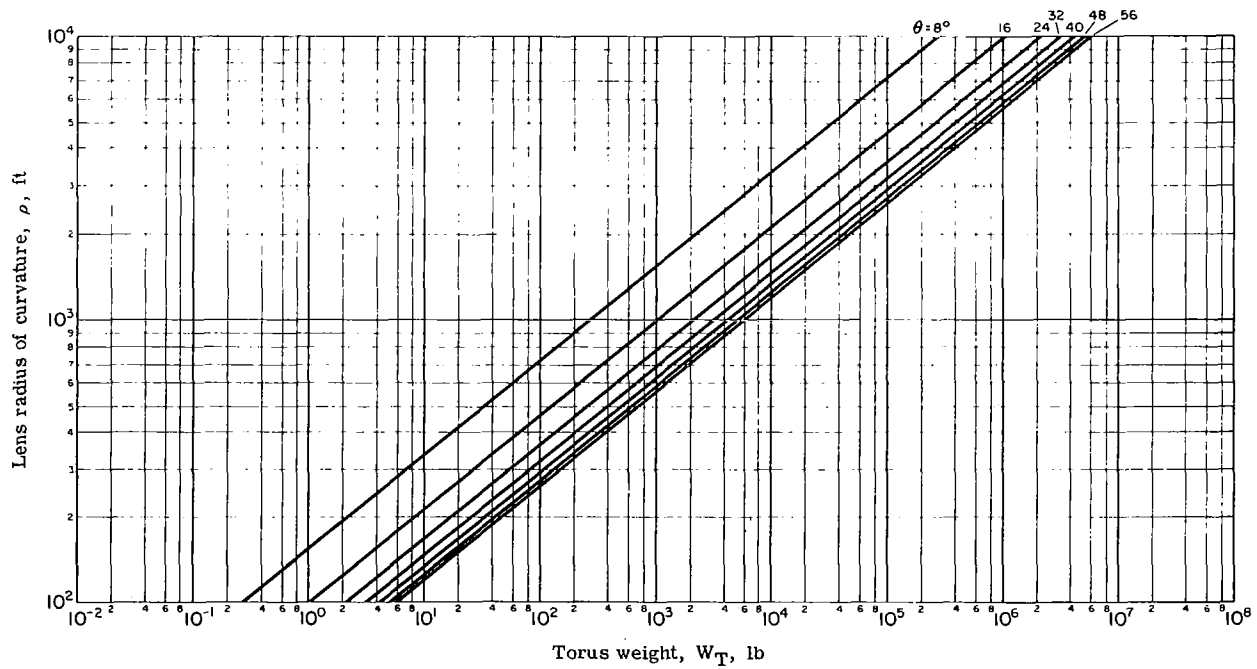


Figure D2. - Material I - torus weight versus lens radius of curvature.

APPENDIX D

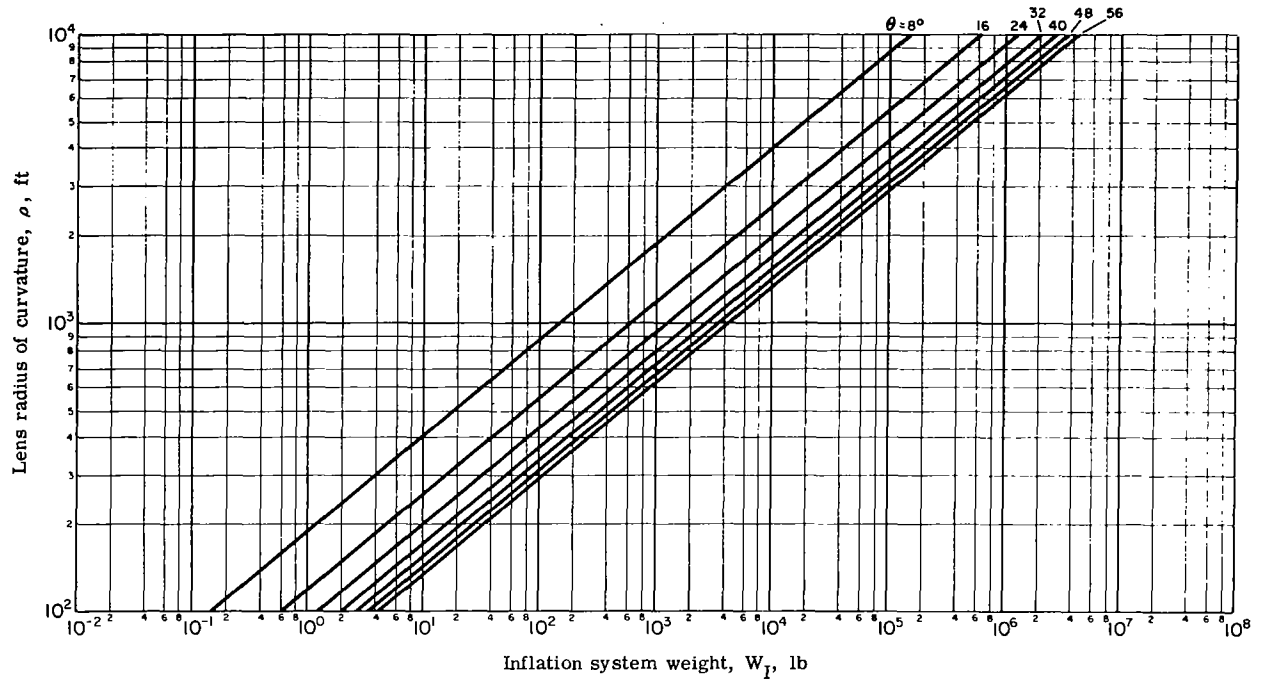


Figure D3. Material I - Inflation system weight versus lens radius of curvature.

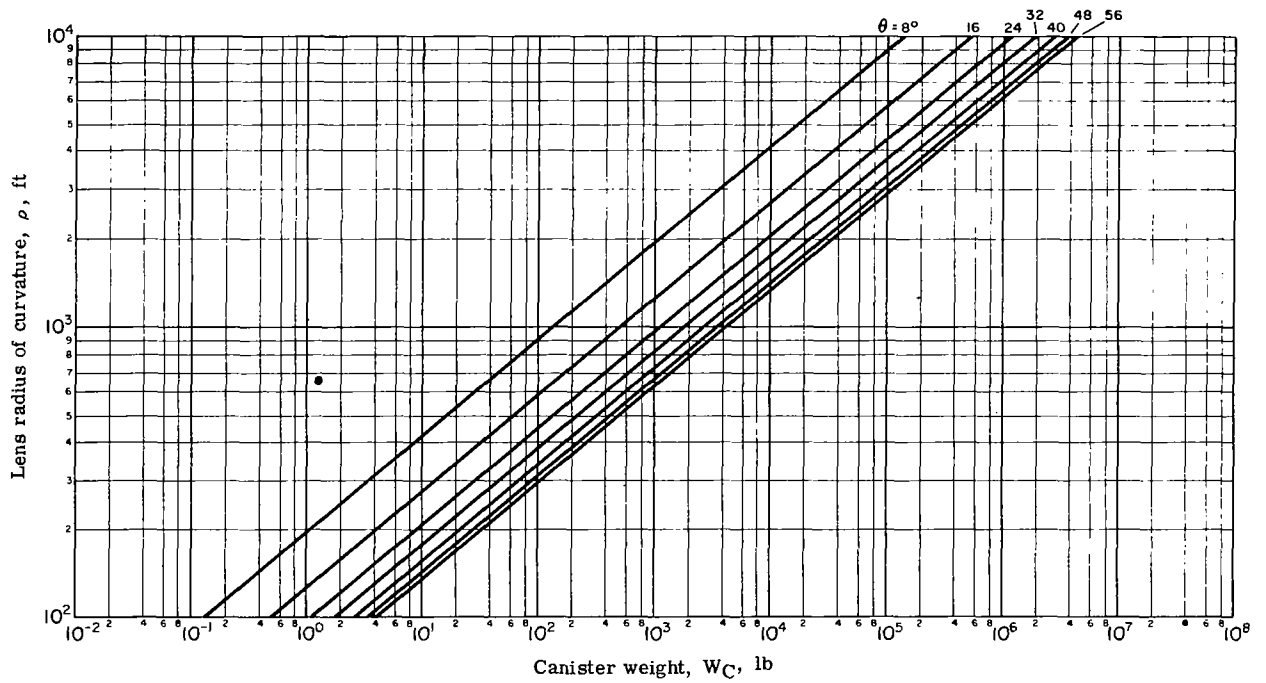


Figure D4. - Material I - canister weight versus lens radius of curvature.

APPENDIX D

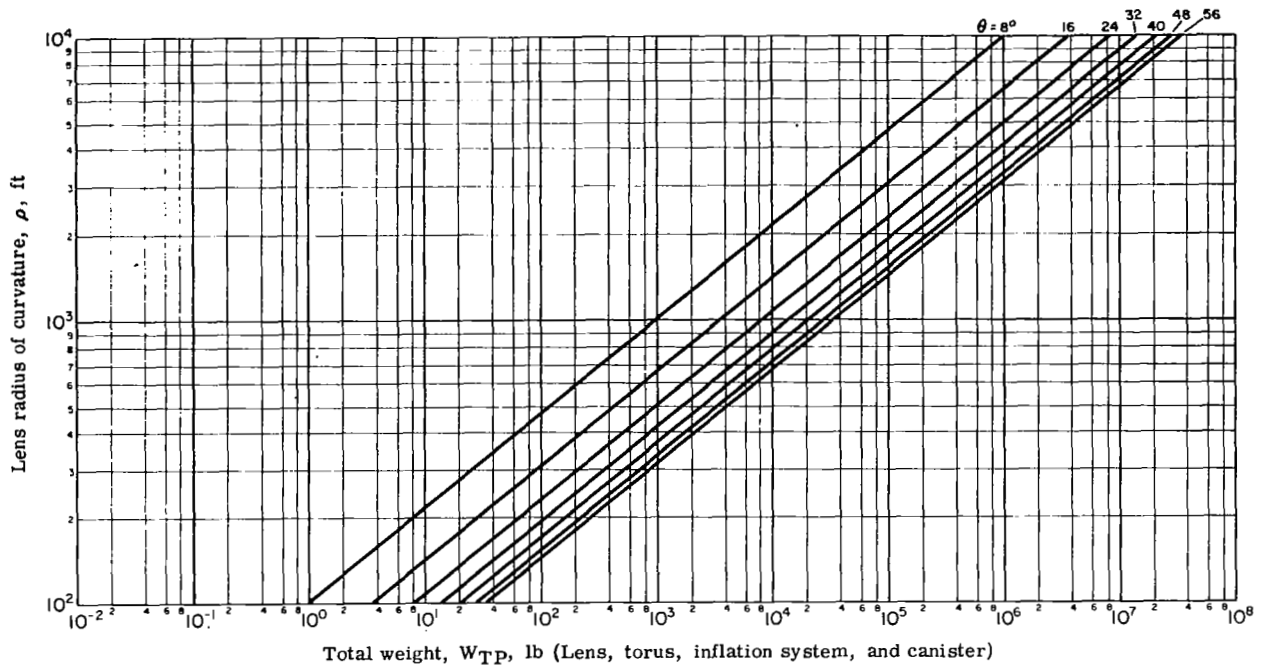


Figure D5. - Material I - total weight versus lens radius of curvature.

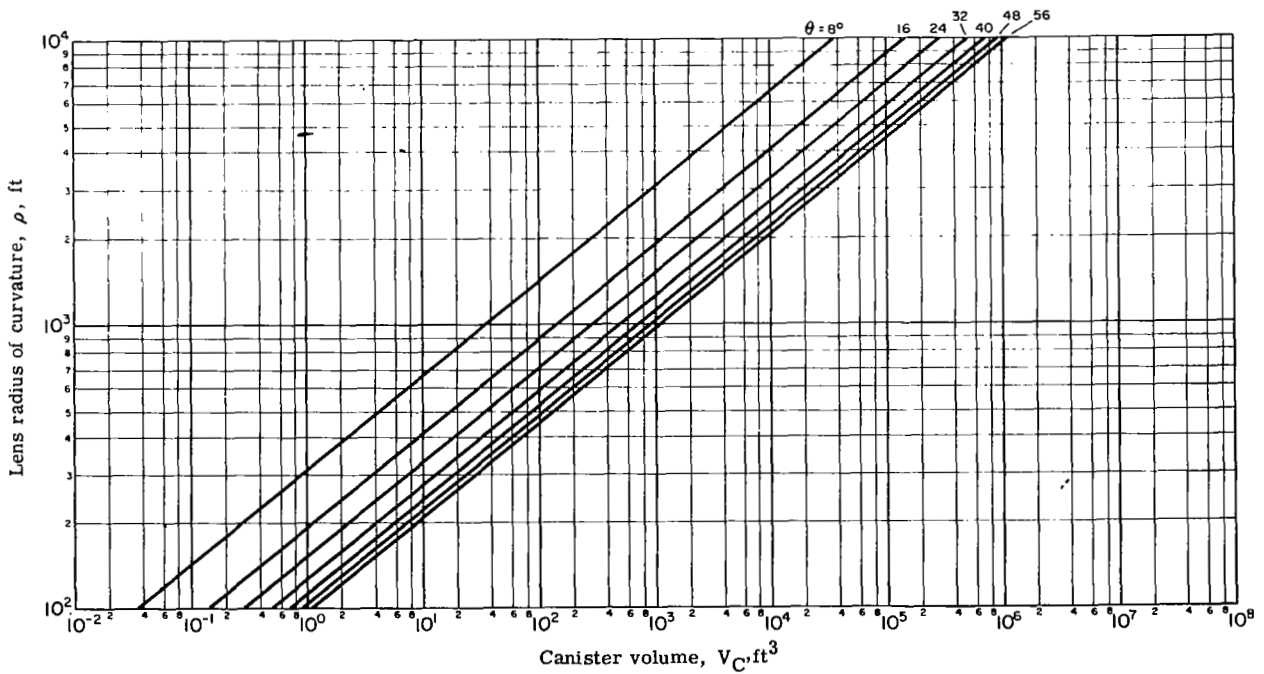


Figure D6. - Material I - canister volume versus lens radius of curvature.

APPENDIX D

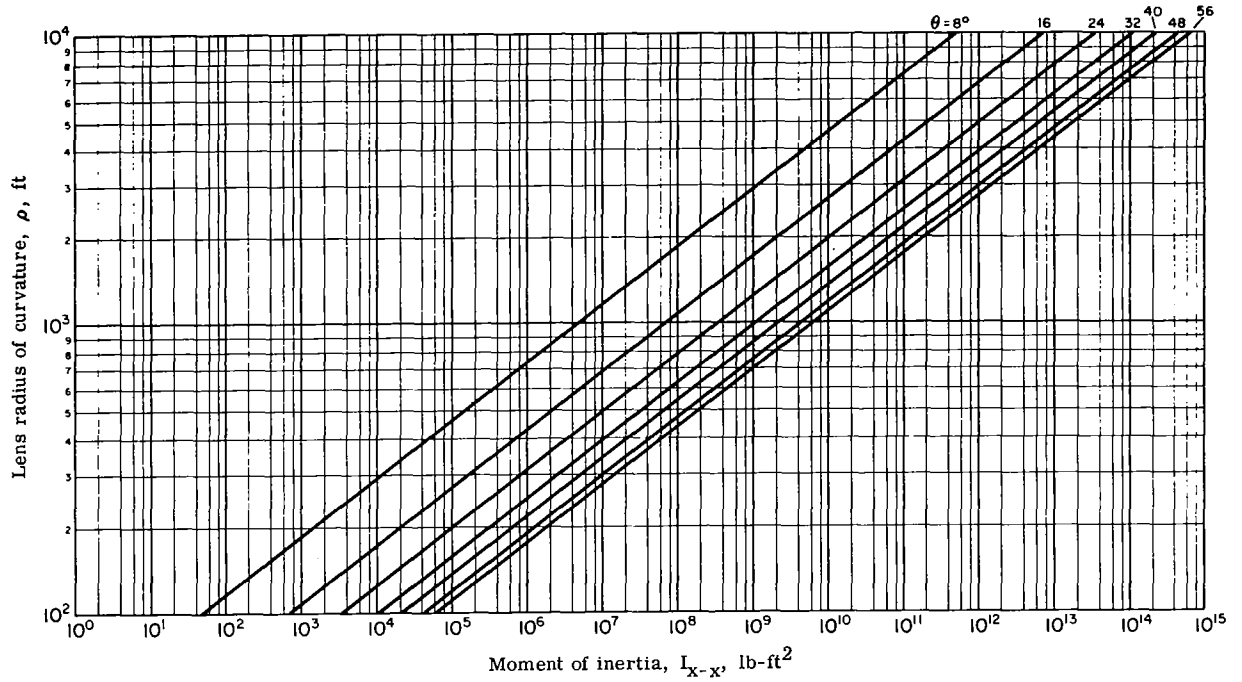


Figure D7. - Material I - moment of inertia I_{X-X} of lens and torus versus lens radius of curvature.

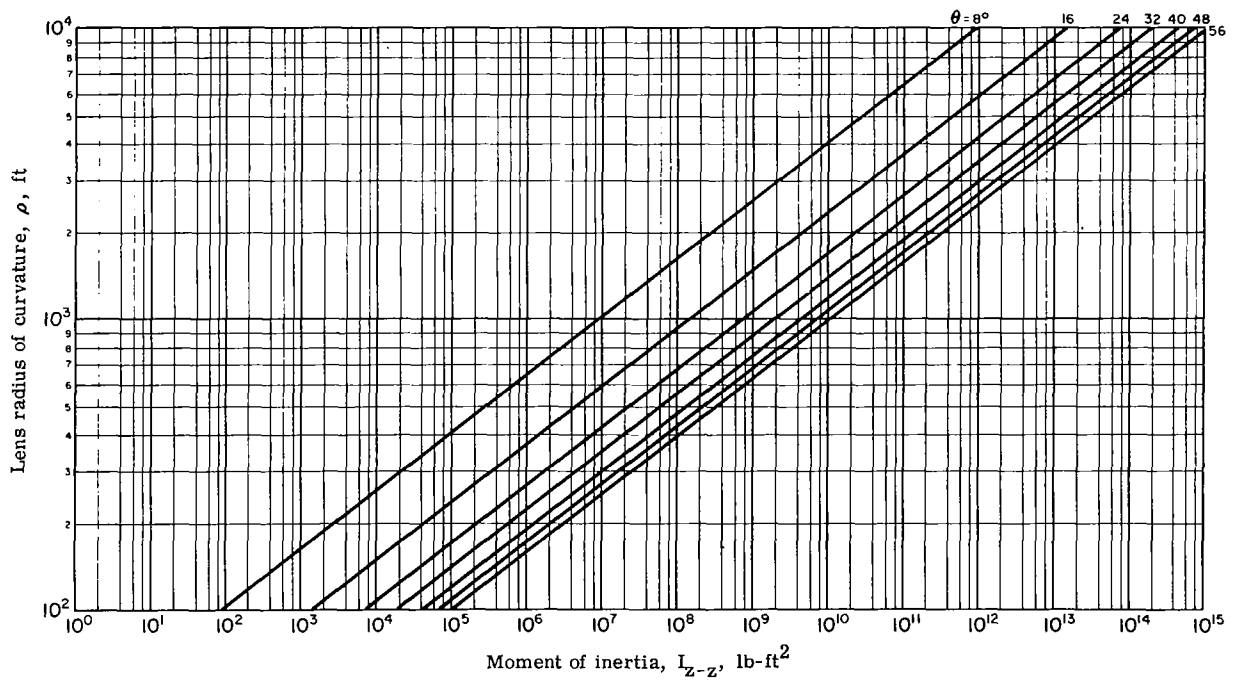


Figure D8. - Material I - moment of inertia I_{Z-Z} of lens and torus versus lens radius of curvature.

APPENDIX D

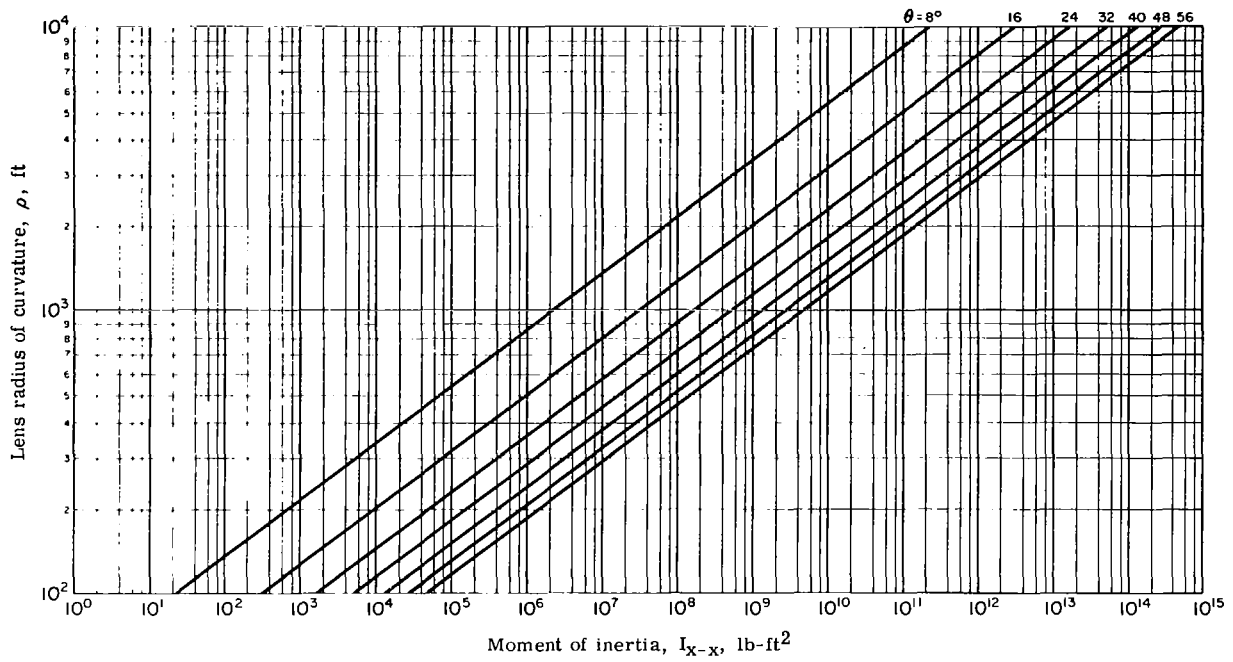


Figure D9. - Material I - moment of inertia I_{X-X} of lens versus lens radius of curvature.

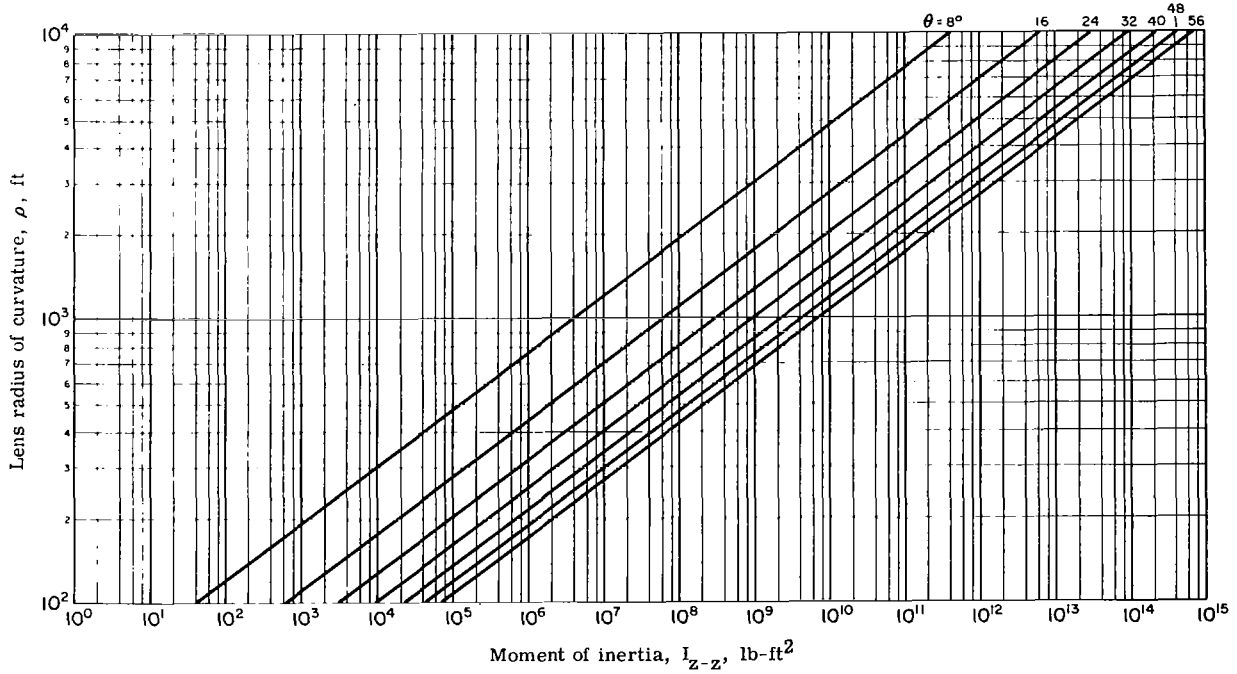


Figure D10. - Material I - moment of inertia I_{Z-Z} of lens versus lens radius of curvature.

APPENDIX D

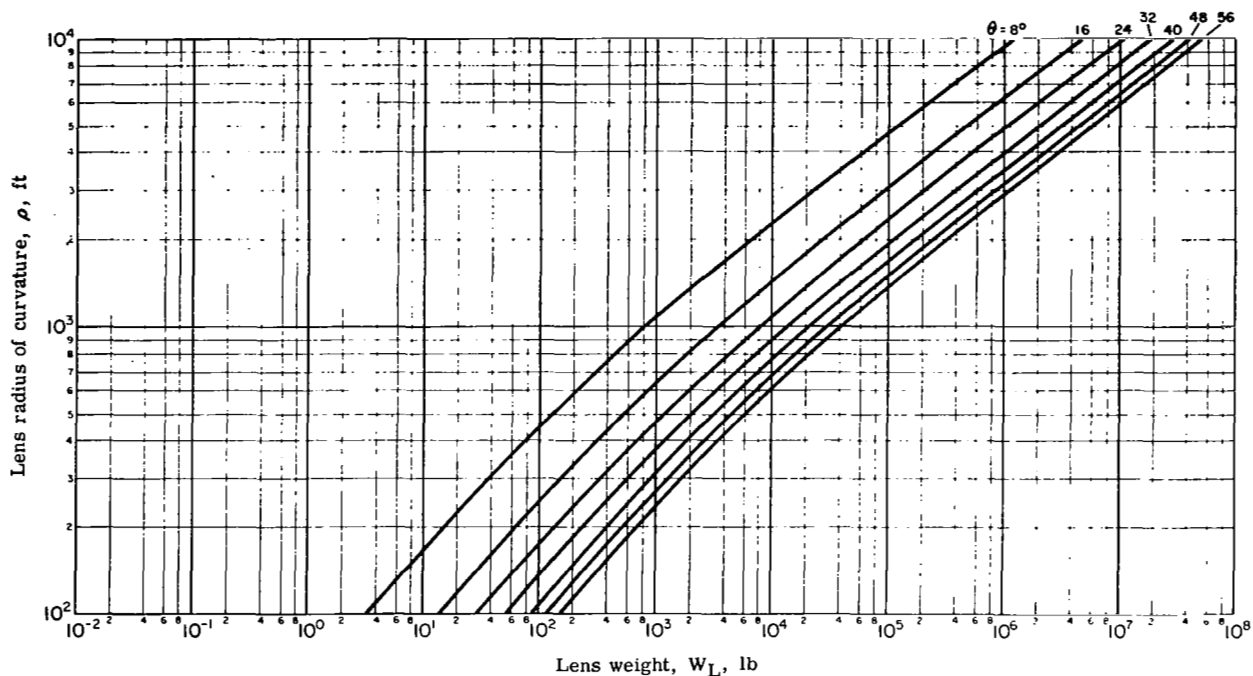


Figure D11. - Material II - lens weight versus lens radius of curvature.

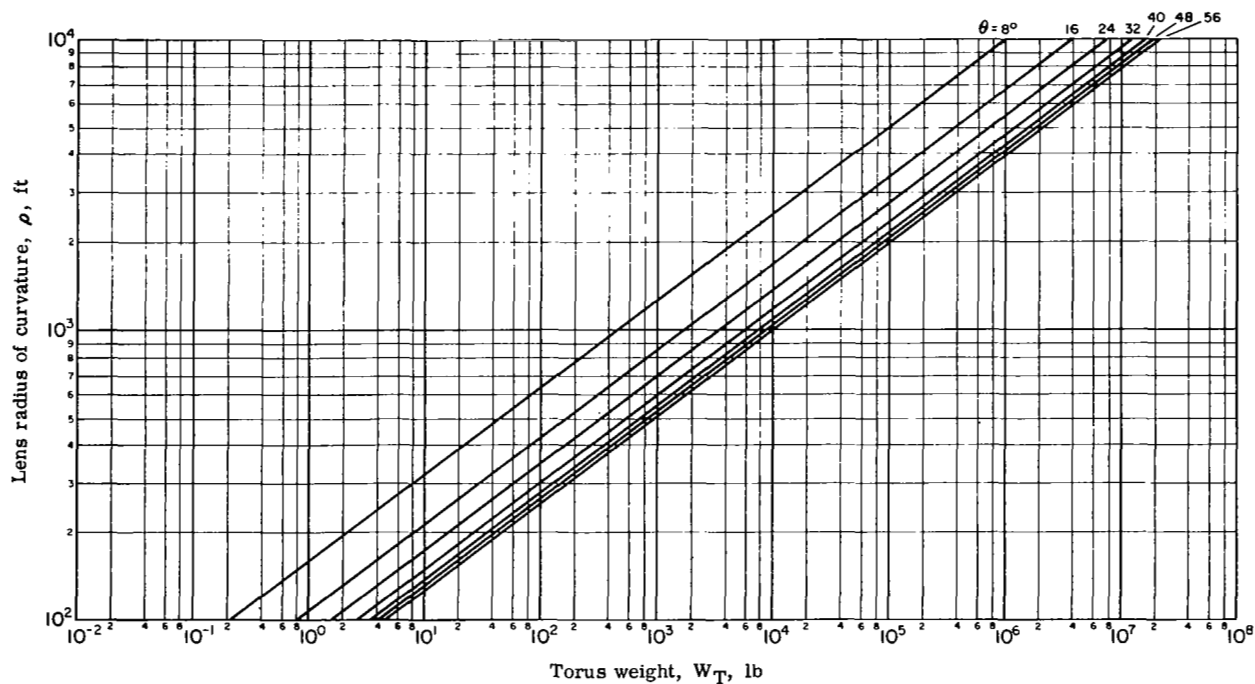


Figure D12. - Material II - torus weight versus lens radius of curvature.

APPENDIX D

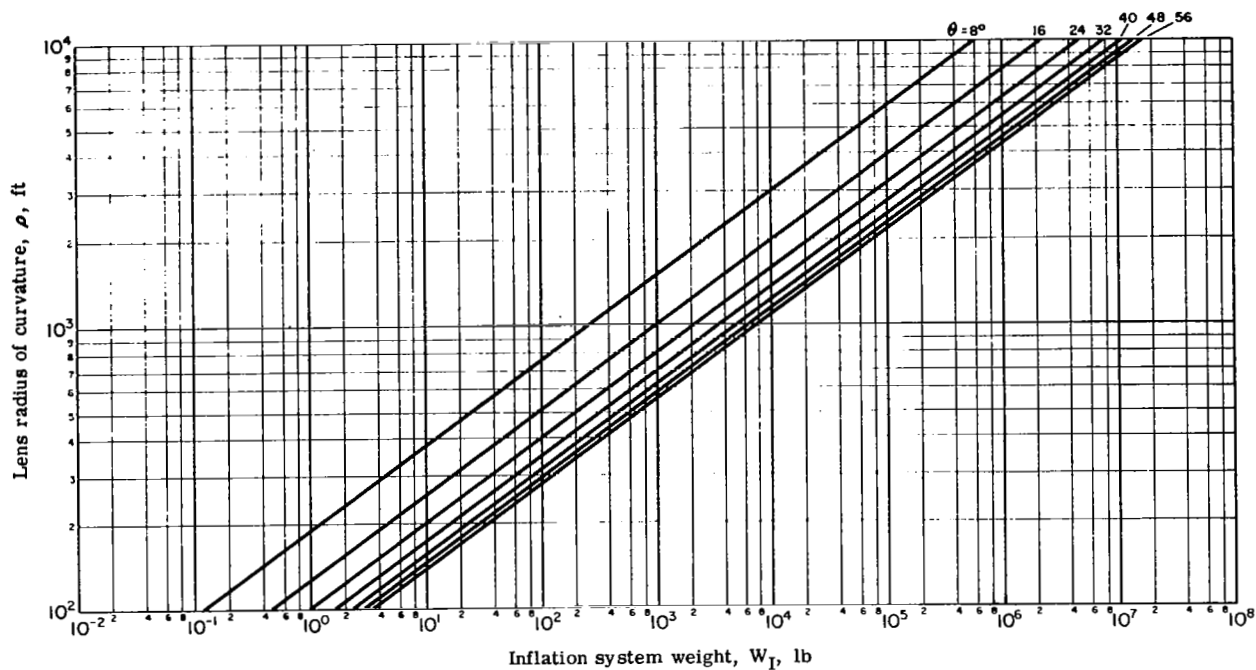


Figure D13. - Material II - inflation system weight versus lens radius of curvature.

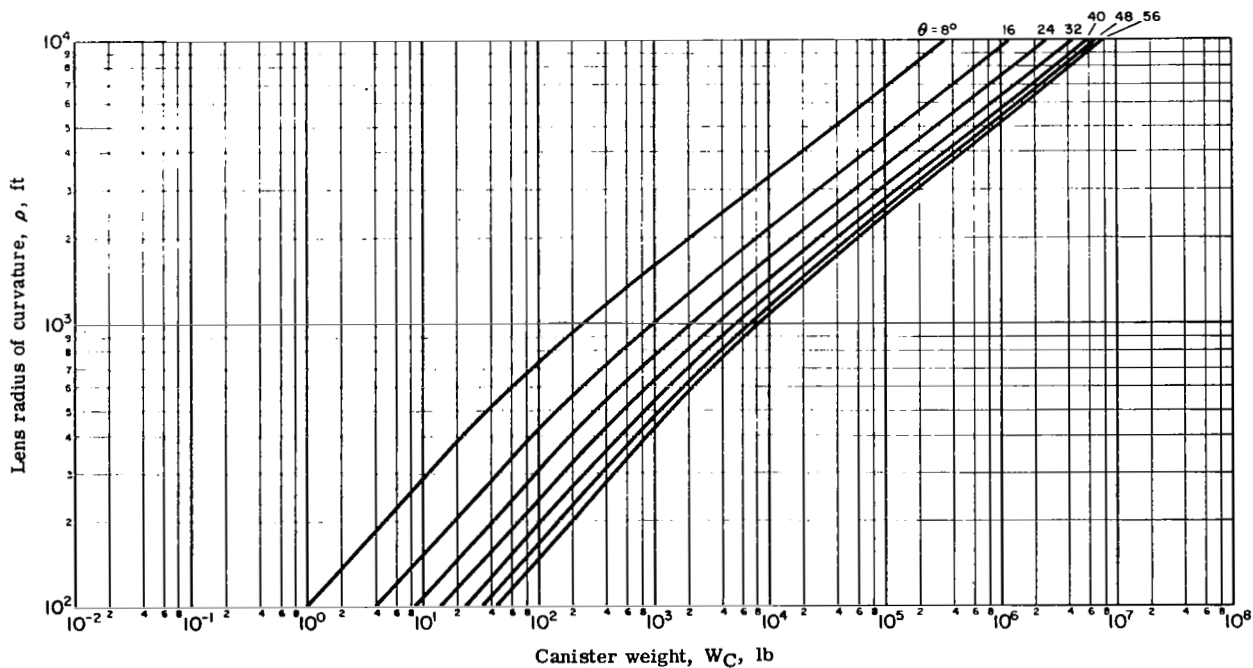


Figure D14. - Material II - canister weight versus lens radius of curvature.

APPENDIX D

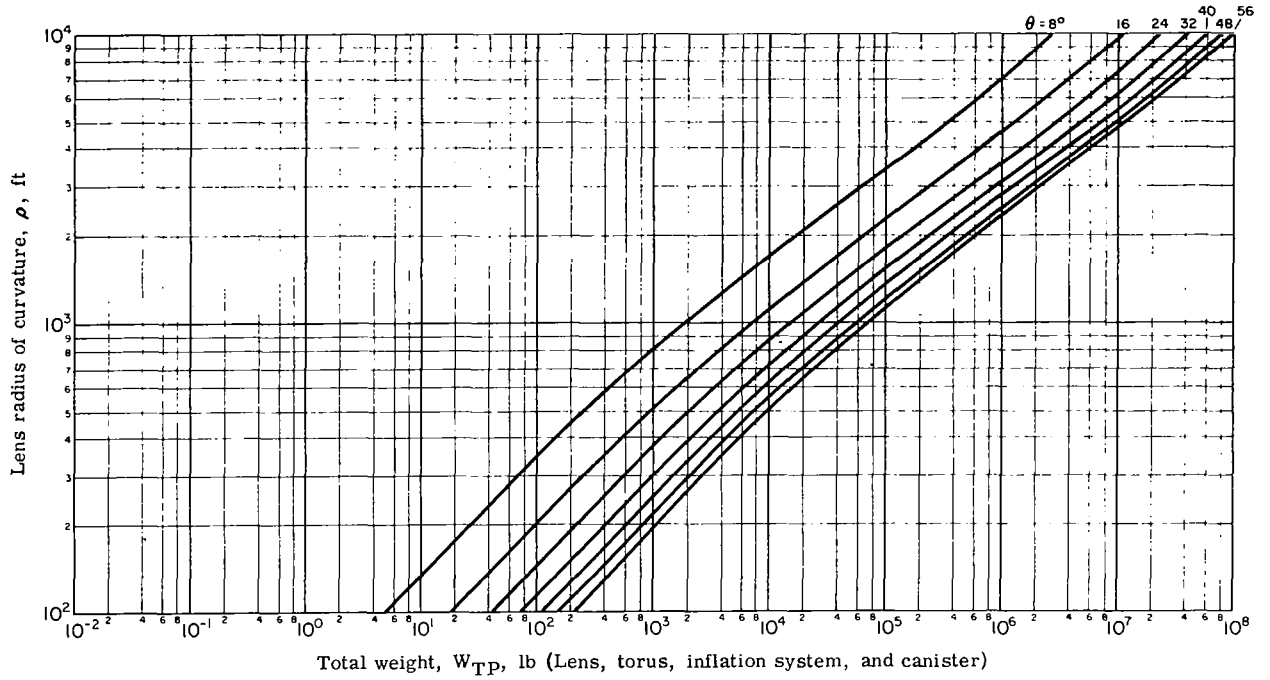


Figure D15. - Material II - total weight versus lens radius of curvature.

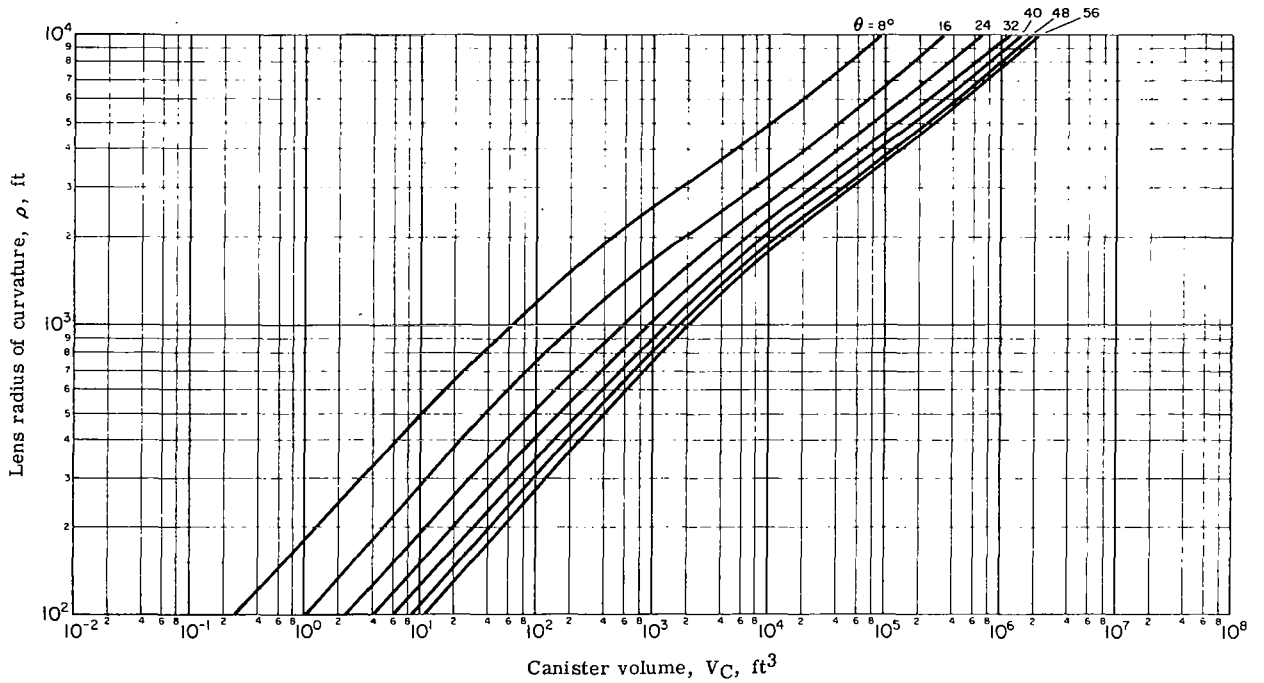


Figure D16. - Material II - canister volume versus lens radius of curvature.

APPENDIX D

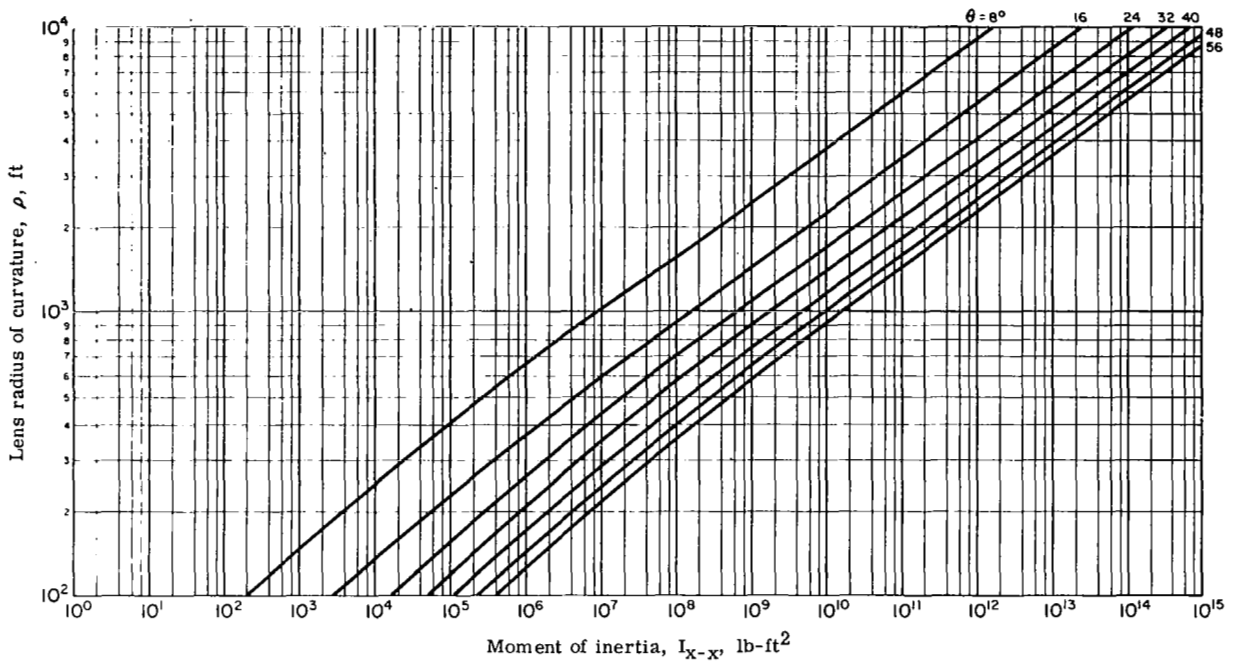


Figure D17. - Material II - moment of inertia I_{X-X} of lens and torus versus lens radius of curvature.

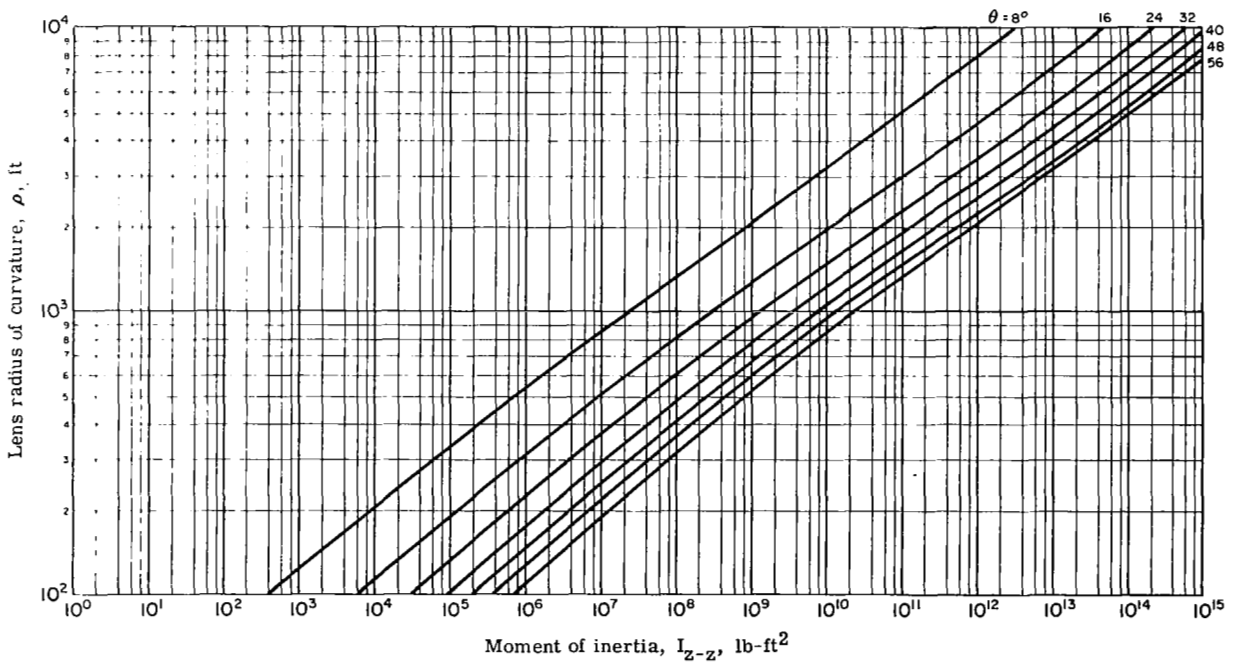


Figure D18. - Material II - moment of inertia I_{Z-Z} of lens and torus versus lens radius of curvature.

APPENDIX D

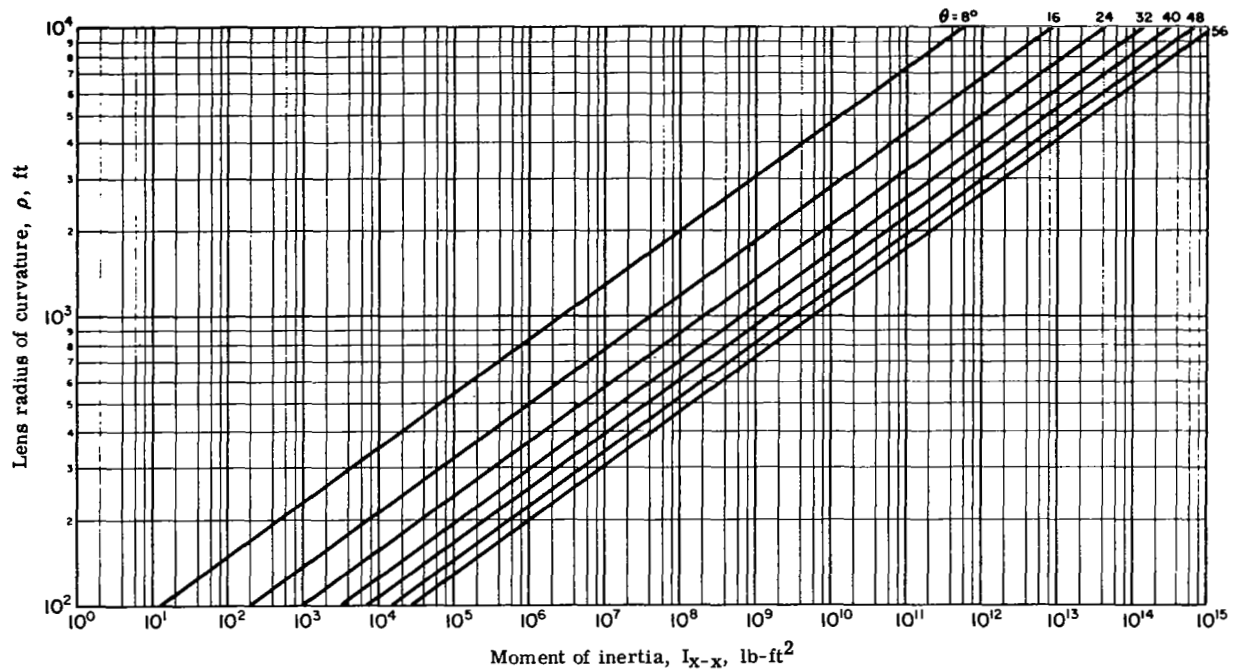


Figure D19. - Material II - moment of inertia I_{X-X} of photolyzed lens versus lens radius of curvature.

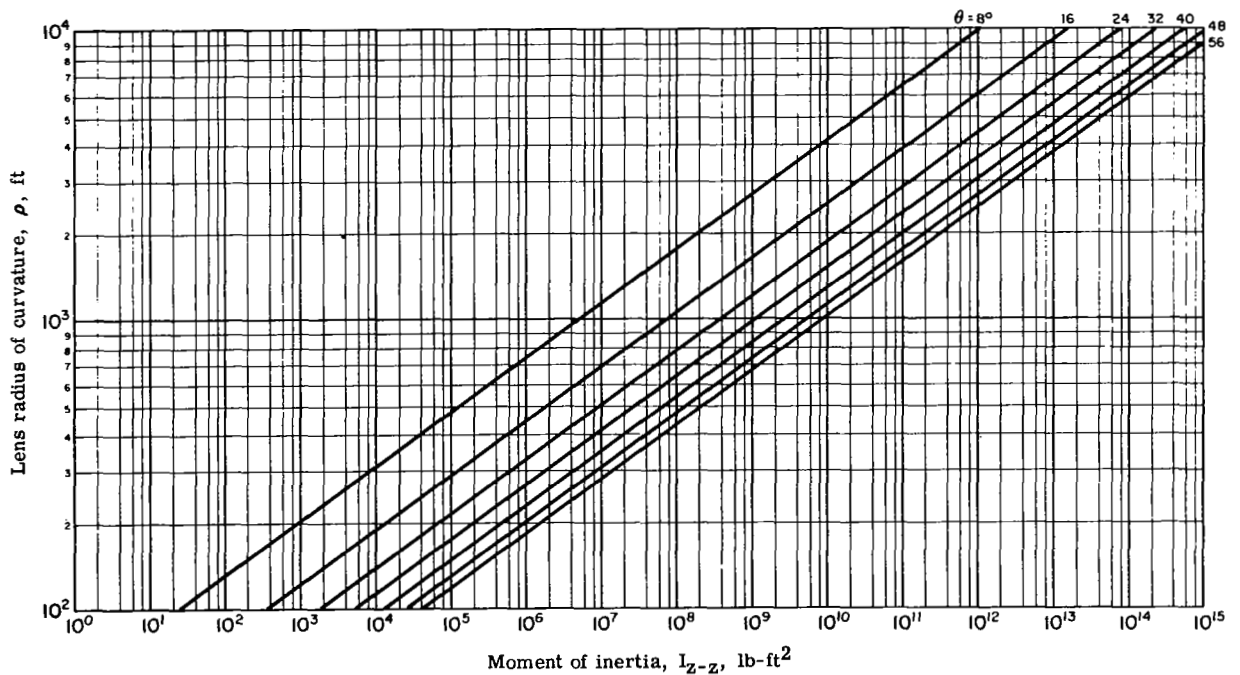


Figure D20. - Material II - moment of inertia I_{Z-Z} of photolyzed lens versus lens radius of curvature.

APPENDIX D

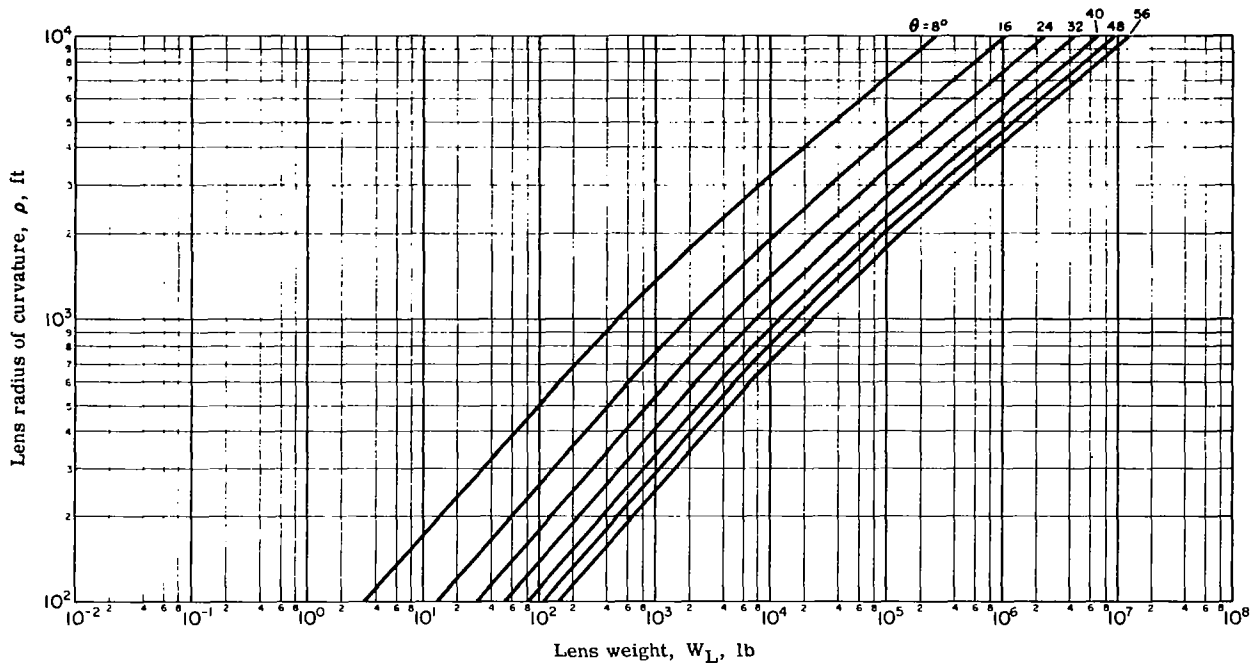


Figure D21. Material III - lens weight versus lens radius of curvature.

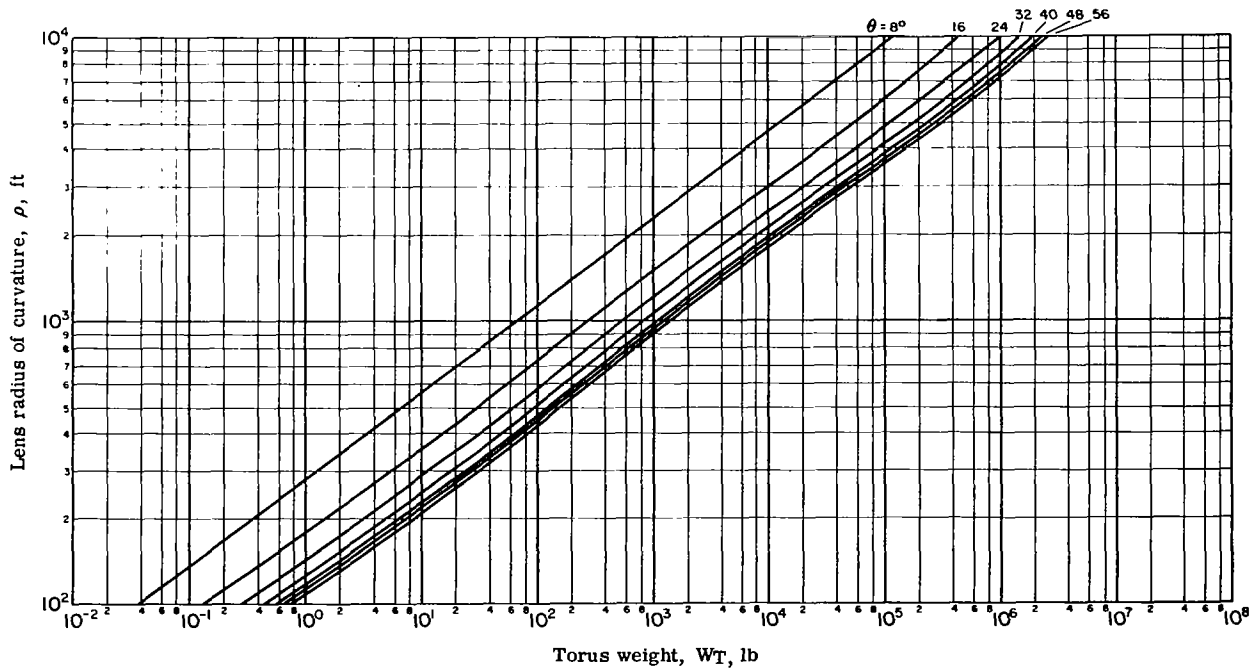


Figure D22. Material III - torus weight versus lens radius of curvature.

APPENDIX D

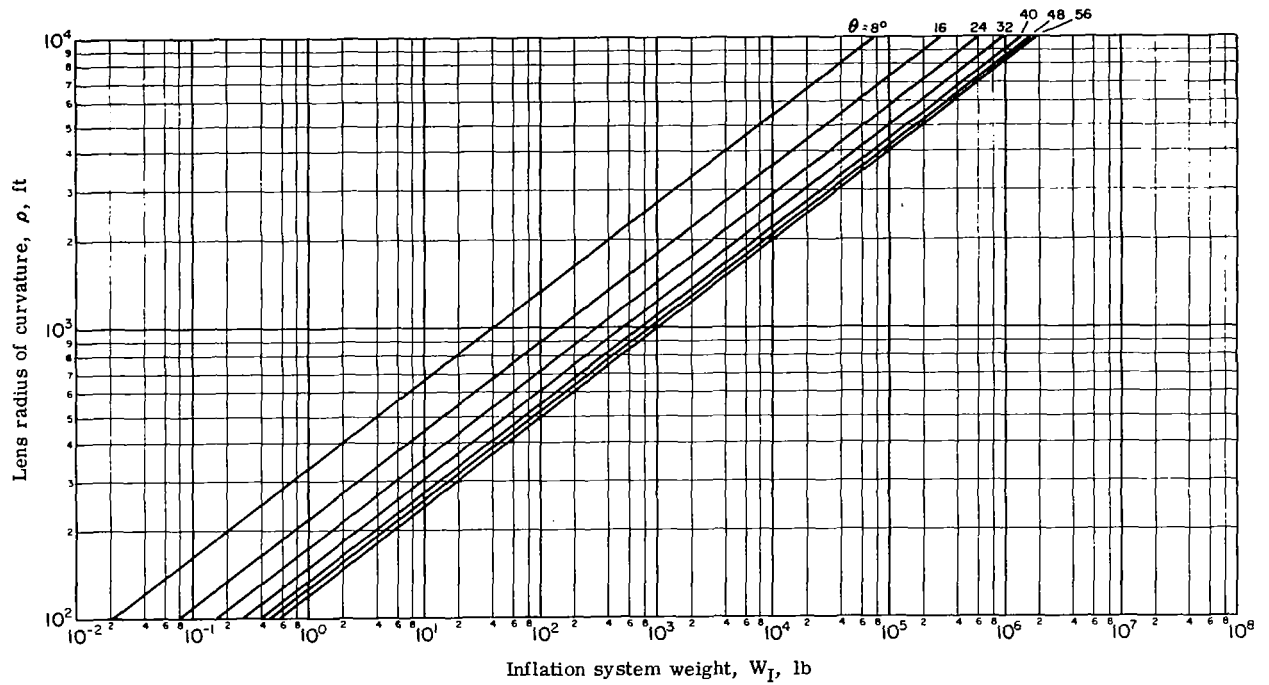


Figure D23. - Material III - inflation system weight versus lens radius of curvature.

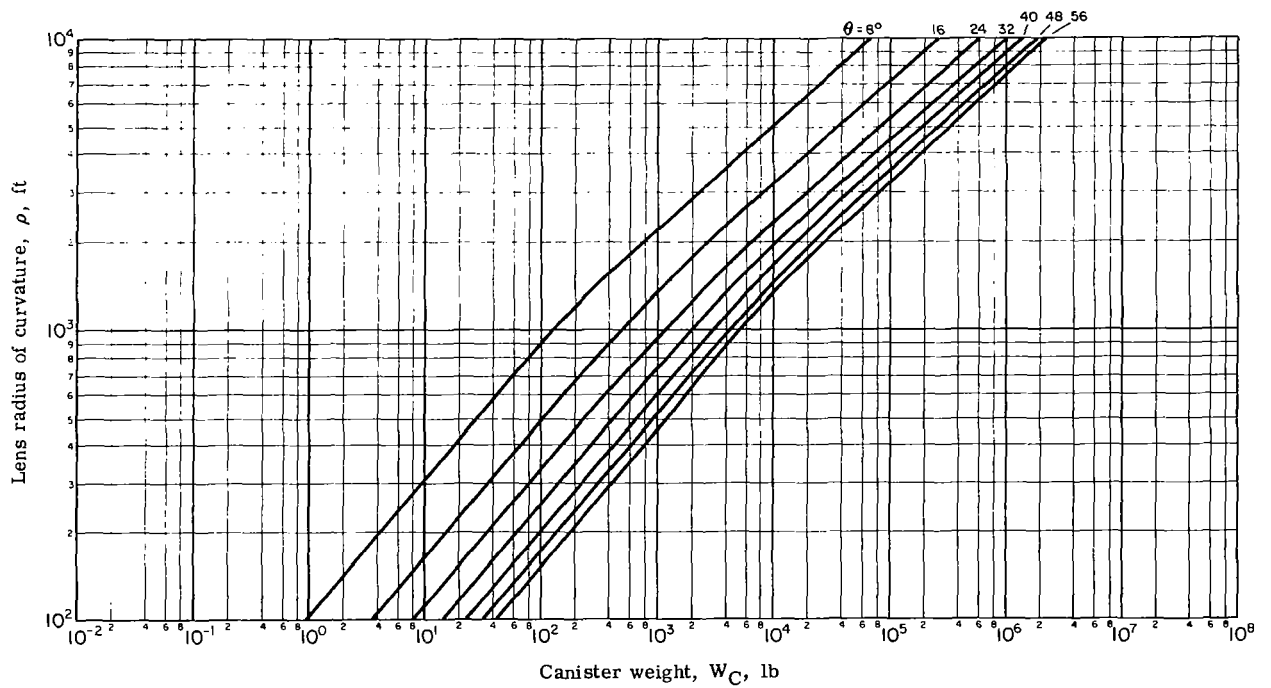


Figure D24. - Material III - canister weight versus lens radius of curvature.

APPENDIX D

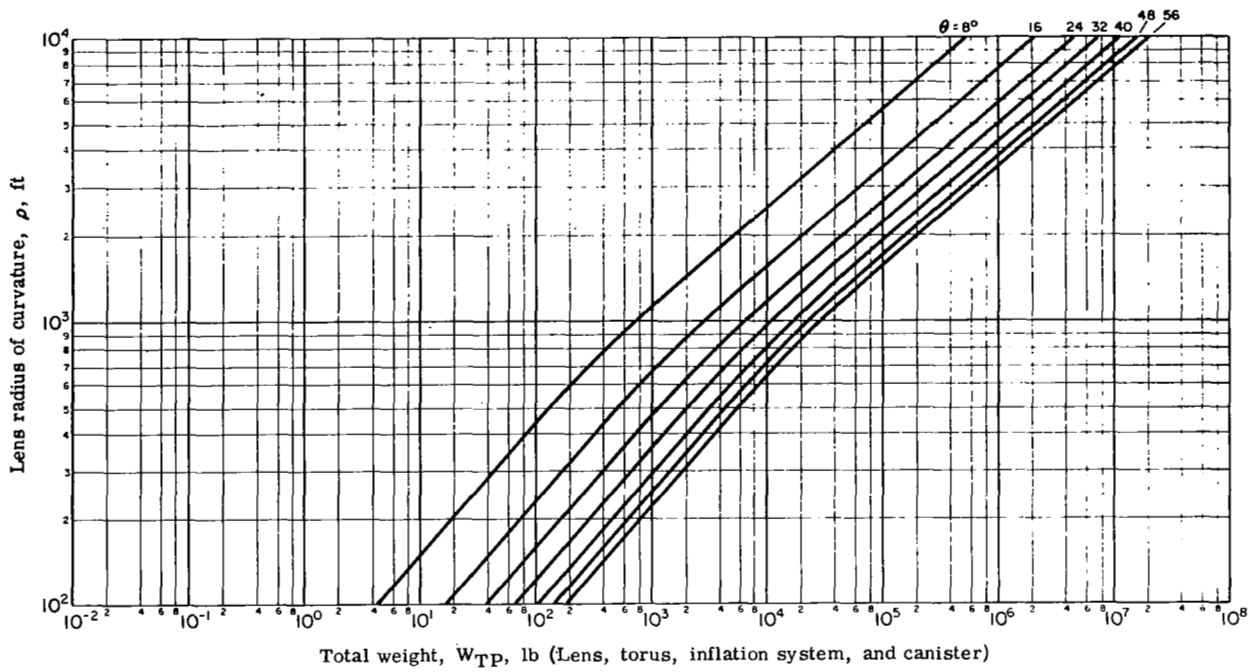


Figure D25. - Material III - total weight versus lens radius of curvature.

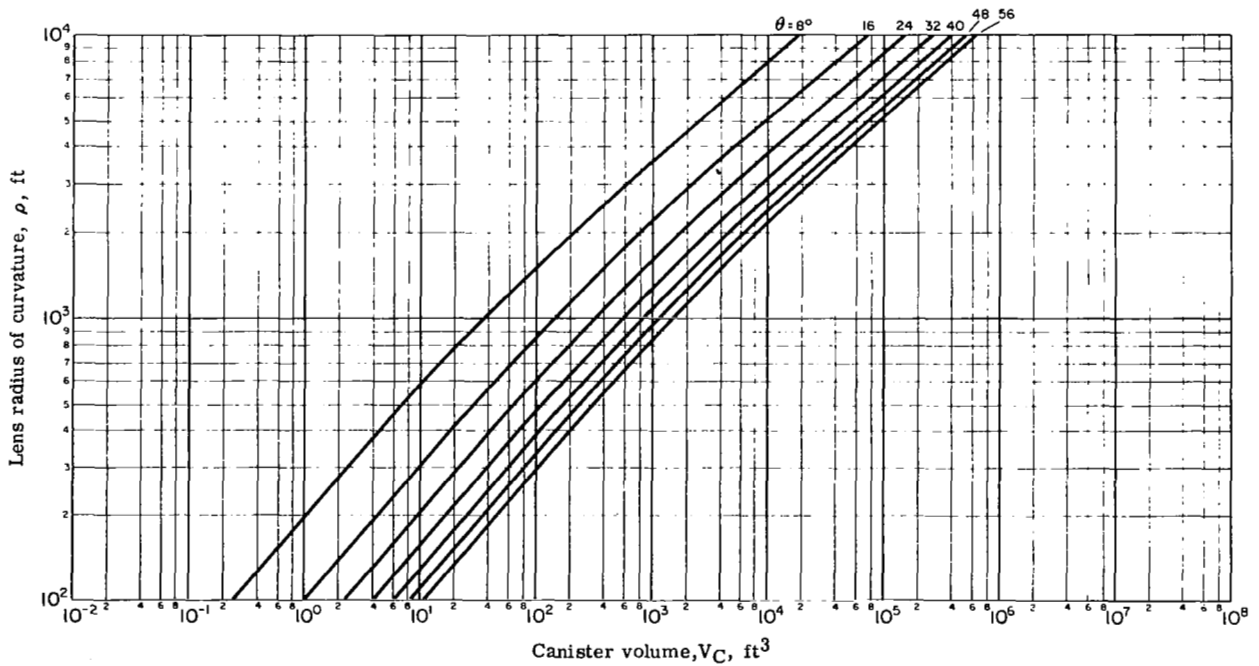


Figure D26. - Material III - canister volume versus lens radius of curvature.

APPENDIX D

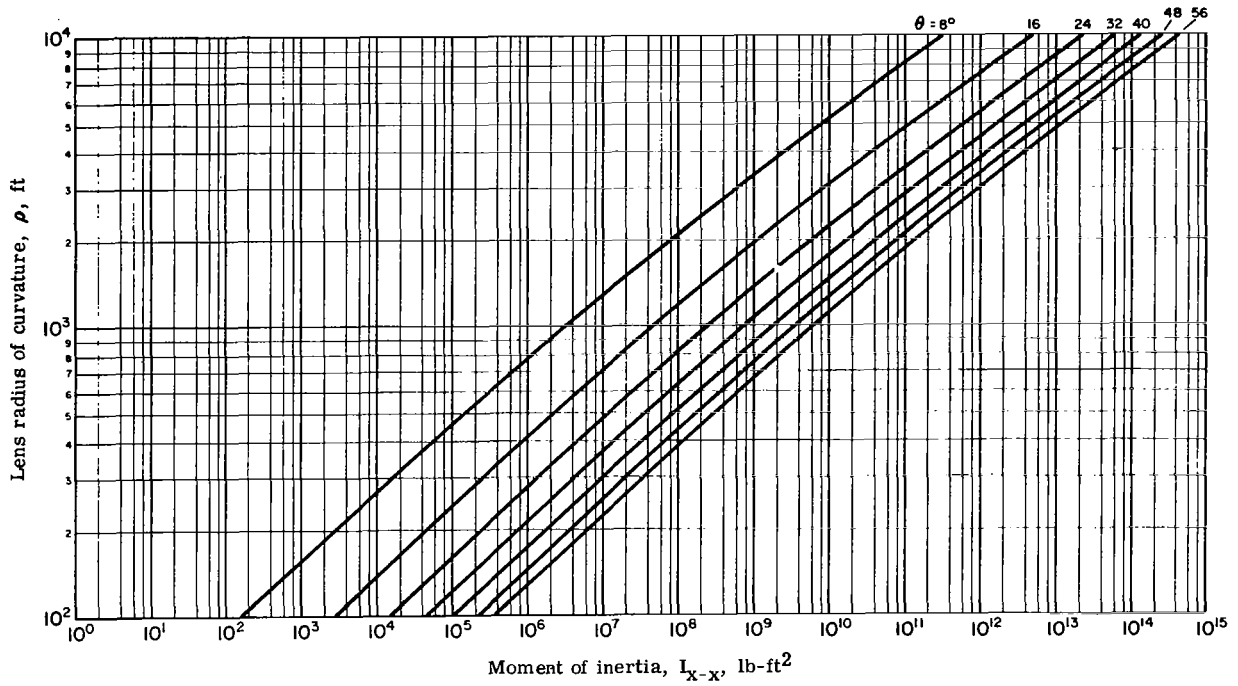


Figure D27. - Material III - moment of inertia I_{X-X} of lens and torus versus lens radius of curvature.

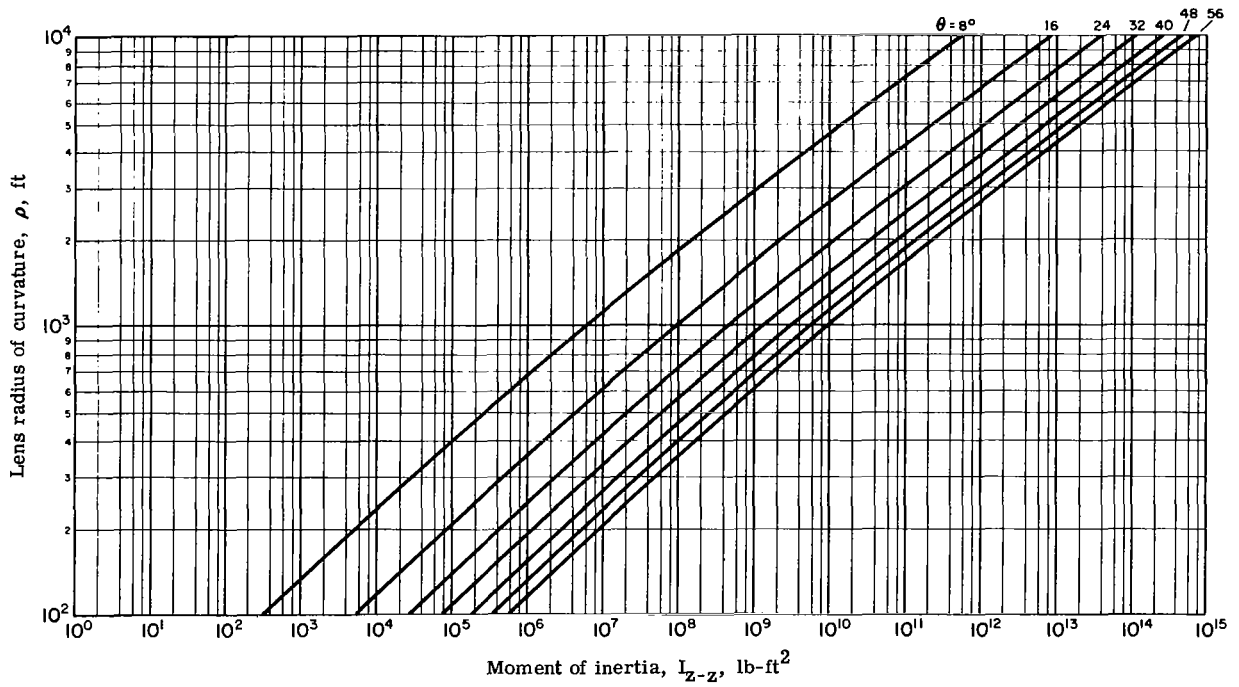


Figure D28. - Material III - moment of inertia I_{Z-Z} of lens and torus versus lens radius of curvature.

APPENDIX D

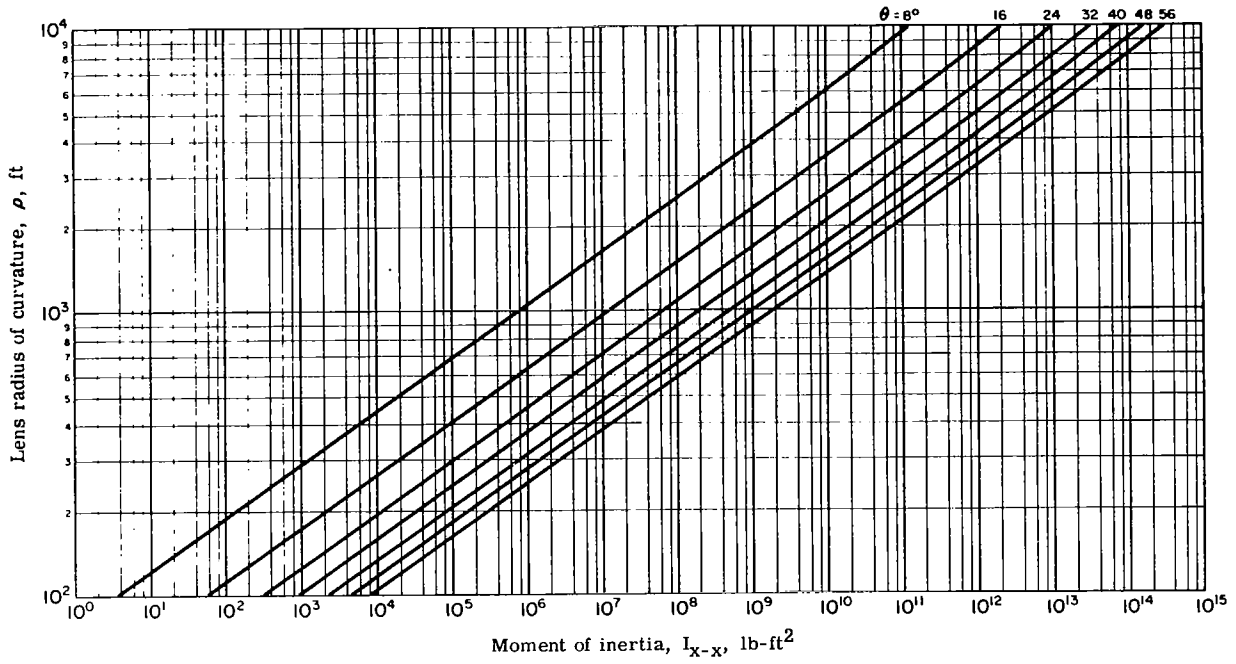


Figure D29. - Material III - moment of inertia I_{X-X} of photolyzed lens versus lens radius of curvature.

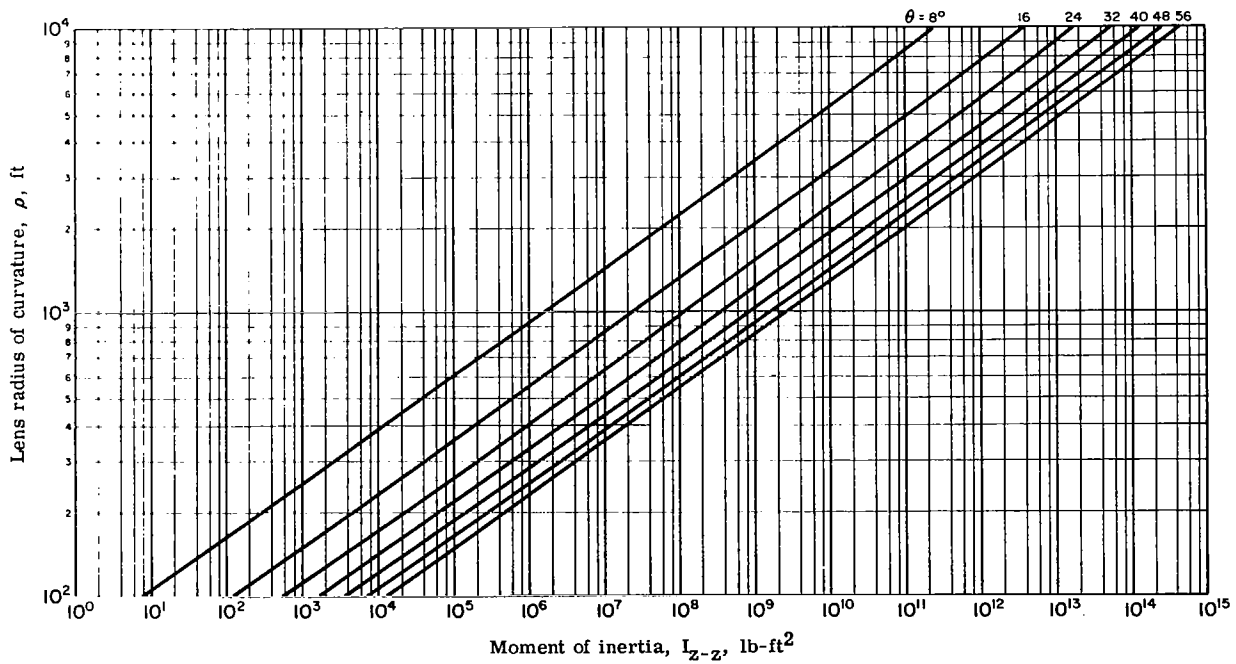


Figure D30. - Material III - moment of inertia I_{Z-Z} of photolyzed lens versus lens radius of curvature.

APPENDIX D

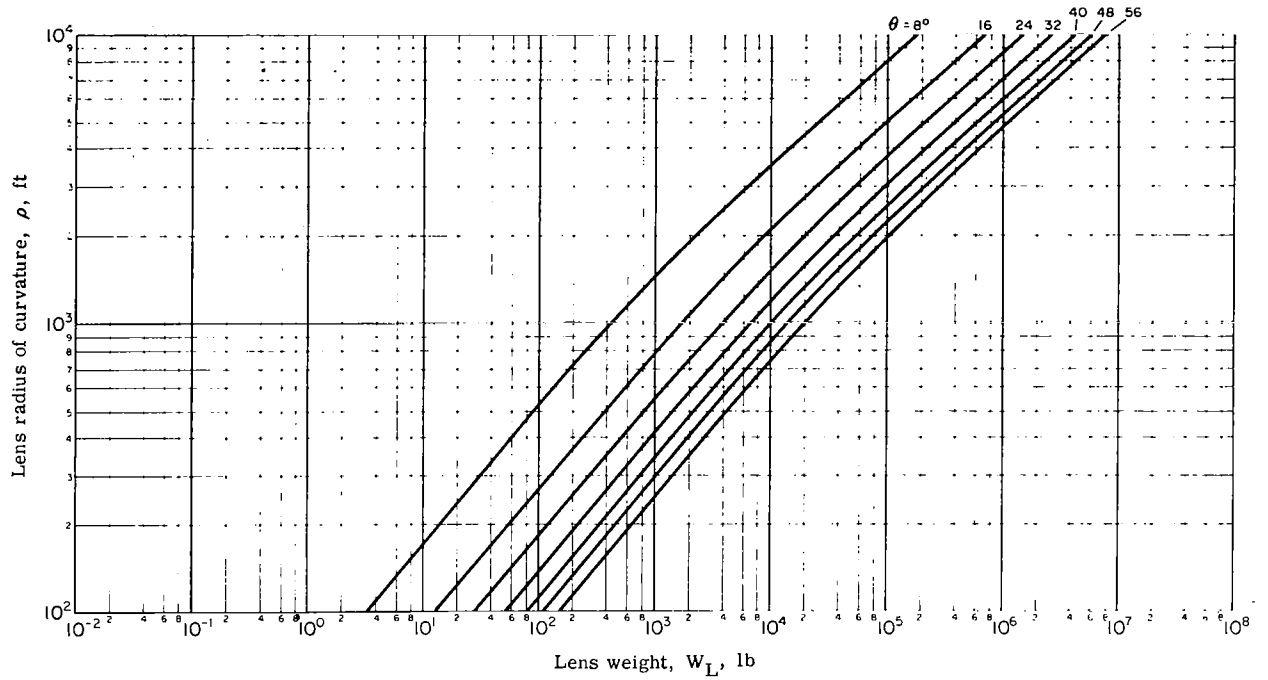


Figure D31. - Material IV - lens weight versus lens radius of curvature.

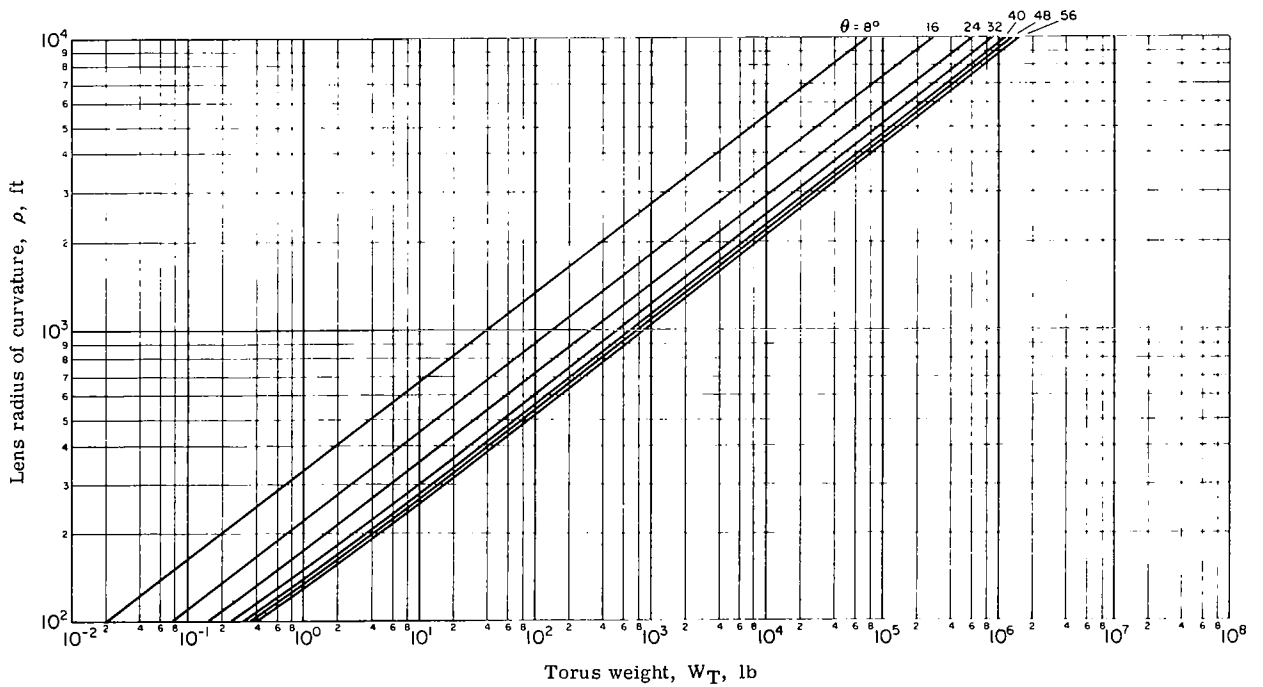


Figure D32. - Material IV - torus weight versus lens radius of curvature.

APPENDIX D

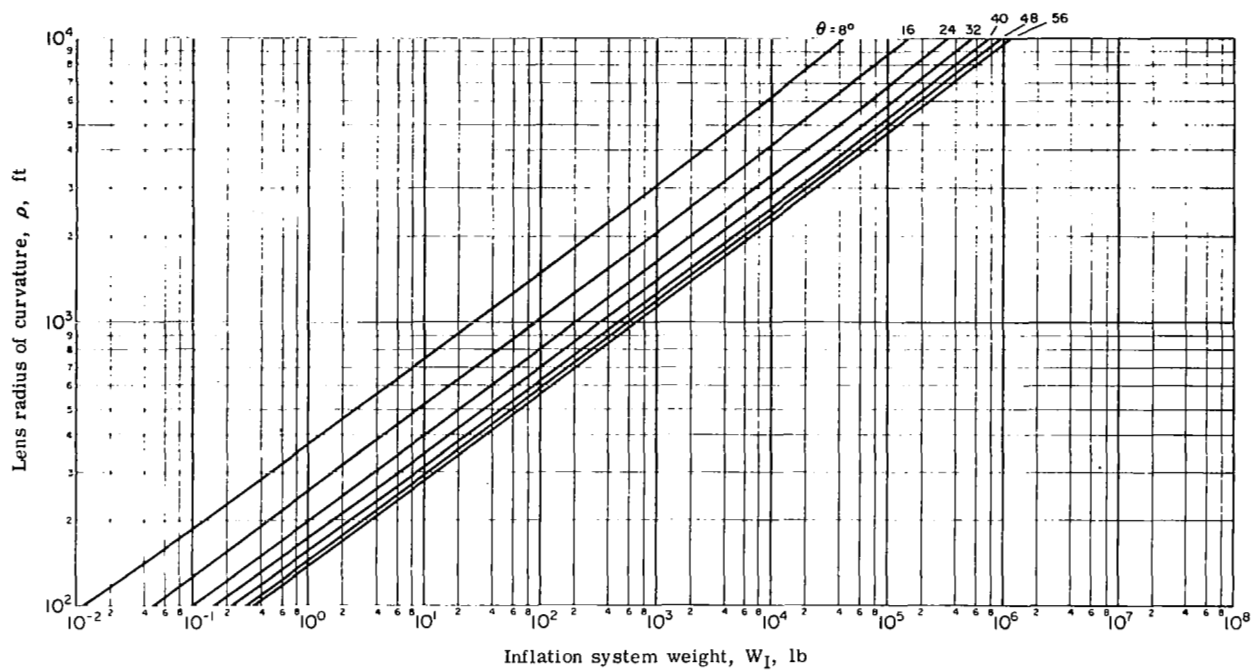


Figure D33. - Material IV - inflation system weight versus lens radius of curvature.

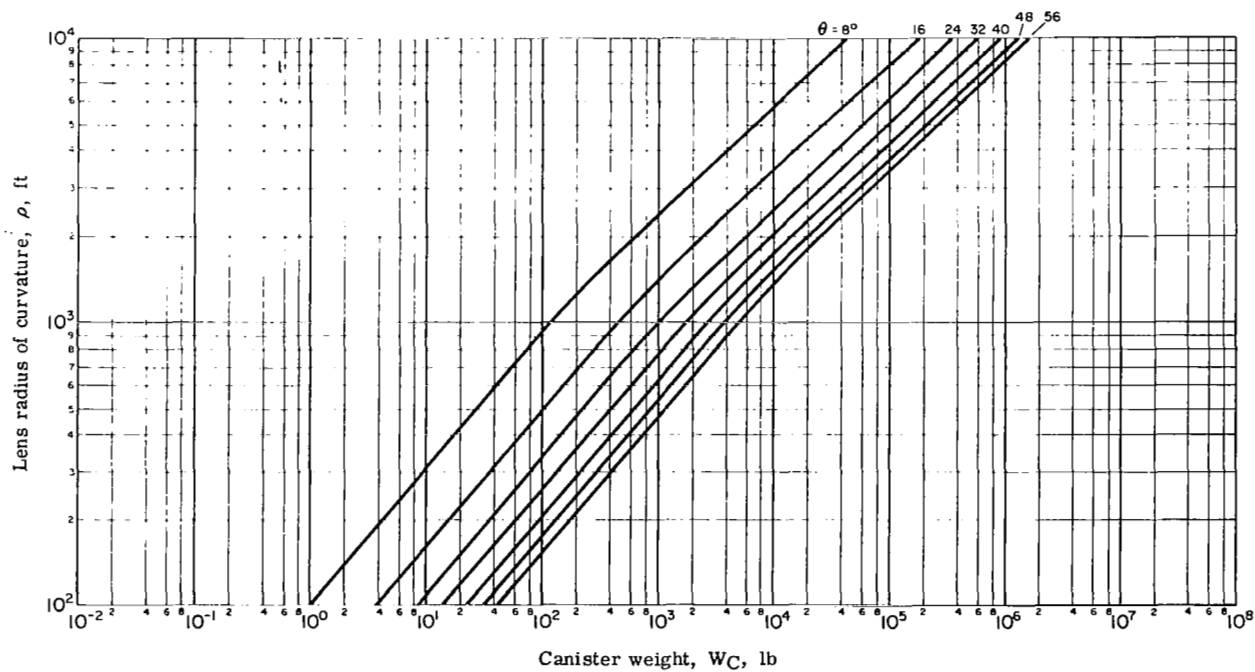


Figure D34. - Material IV - canister weight versus lens radius of curvature.

APPENDIX D

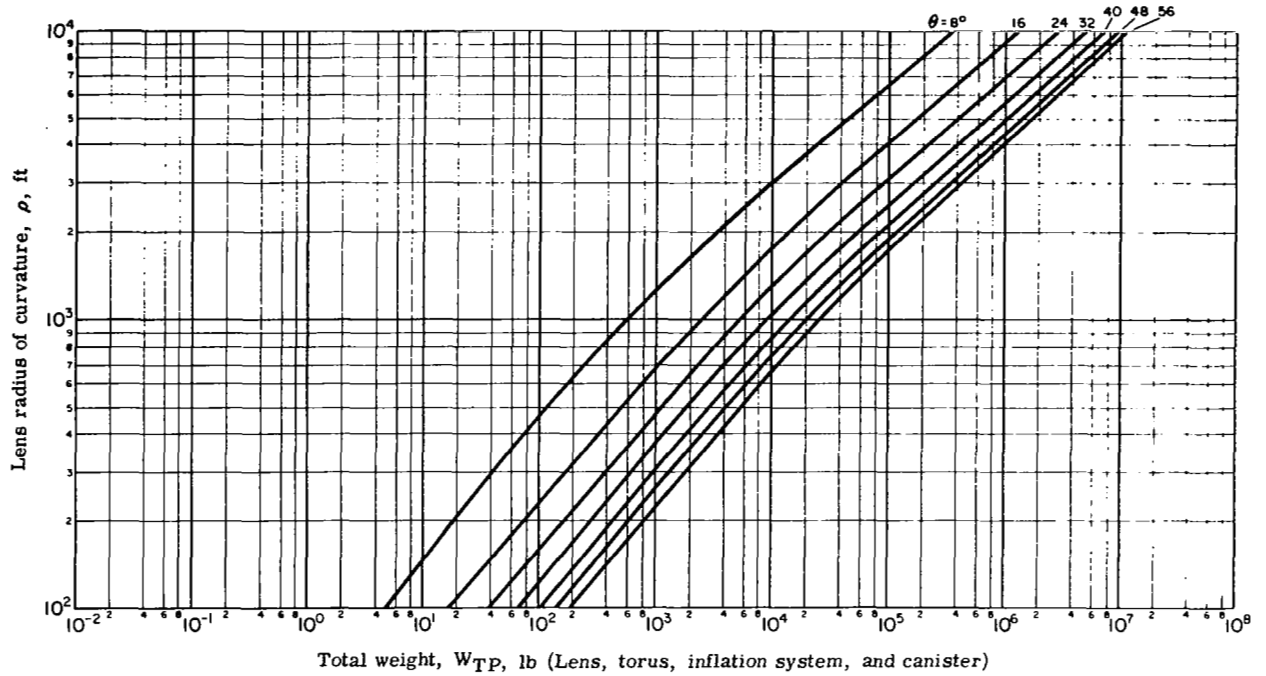


Figure D35. - Material IV - total weight versus lens radius of curvature.

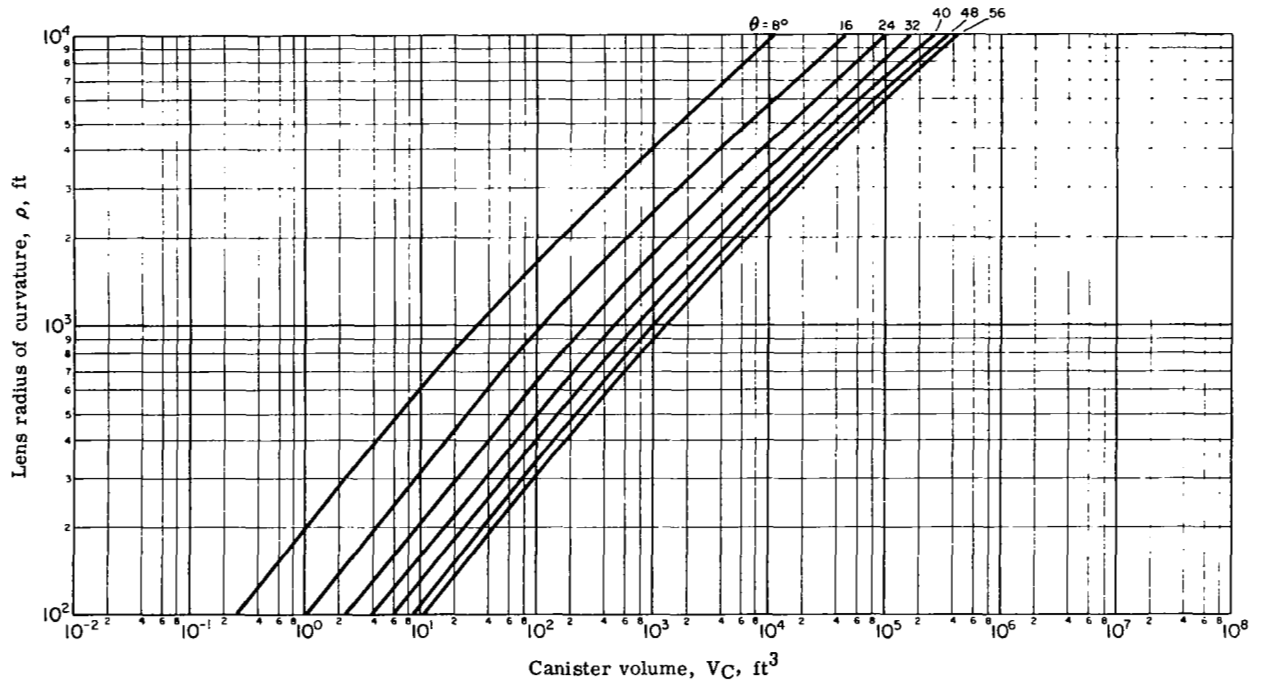


Figure D36. - Material IV - canister volume versus lens radius of curvature.

APPENDIX D

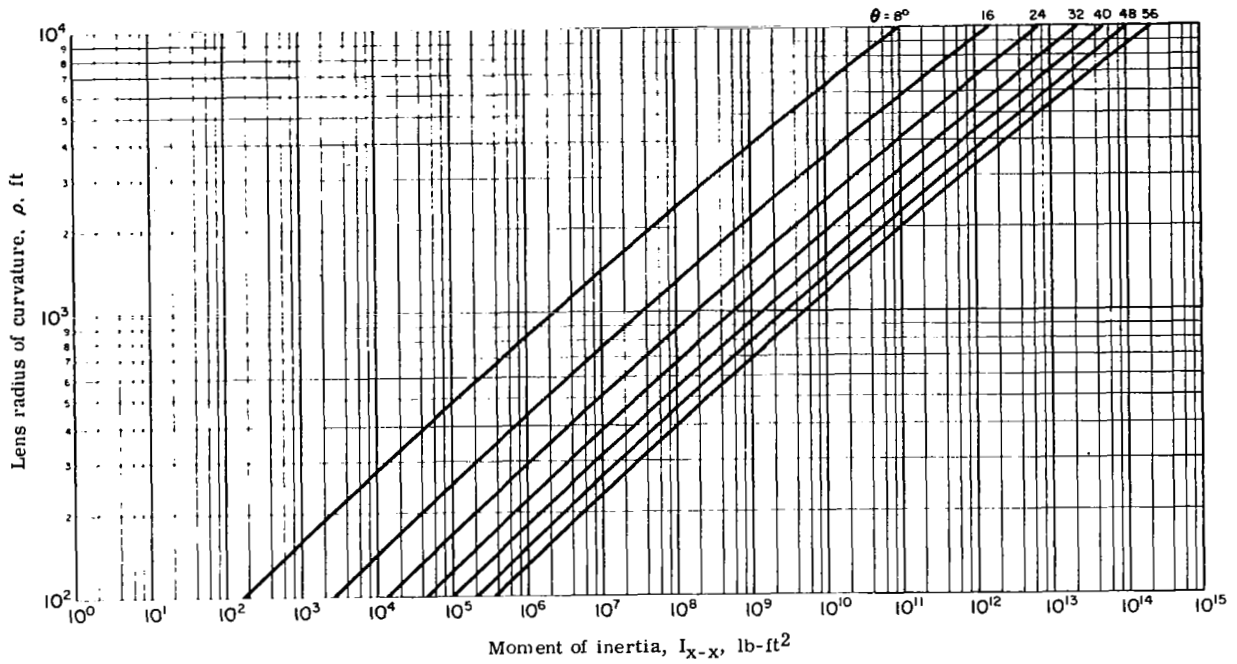


Figure D37. - Material IV - moment of inertia I_{X-X} of lens and torus versus lens radius of curvature.

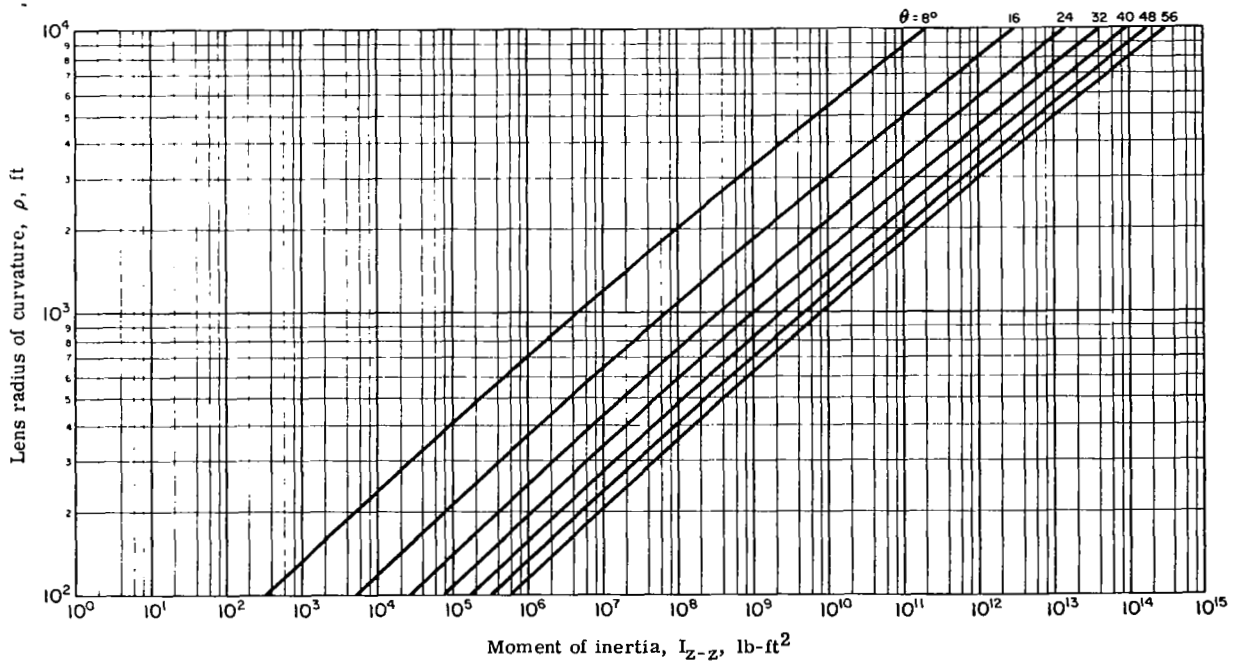


Figure D38. Material IV - moment of inertia I_{Z-Z} of lens and torus versus lens radius of curvature.

APPENDIX D

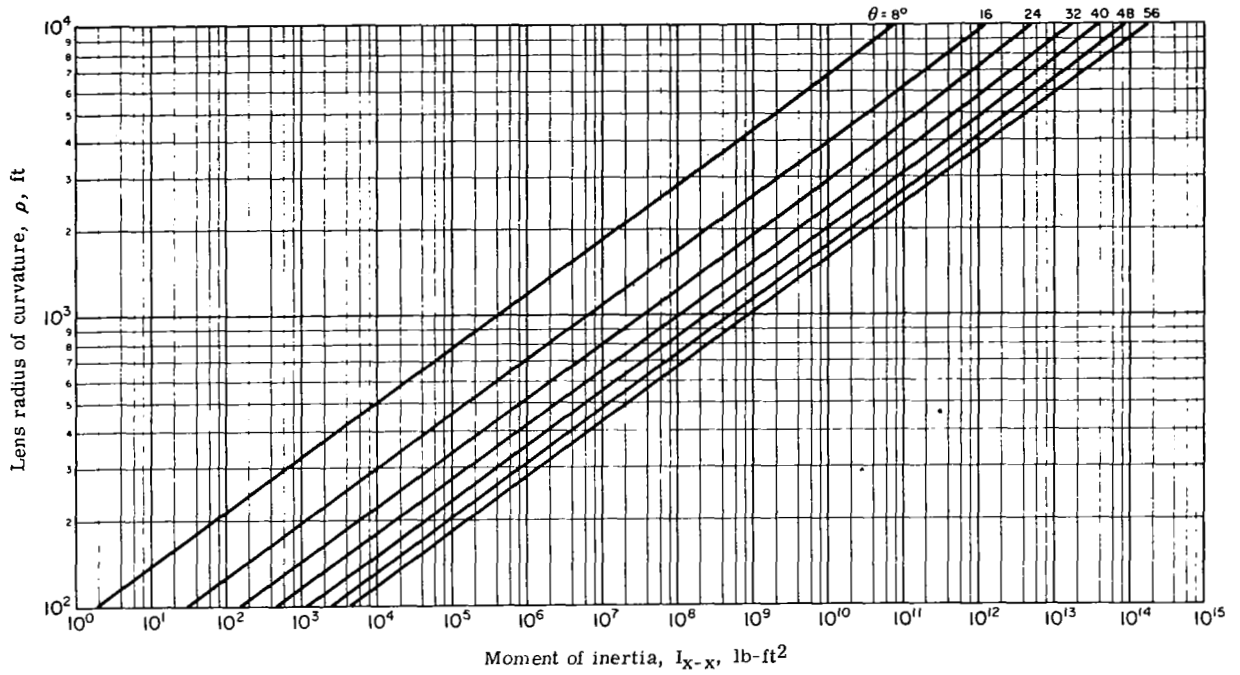


Figure D39. - Material IV - moment of inertia I_{X-X} of photolyzed lens versus lens radius of curvature.

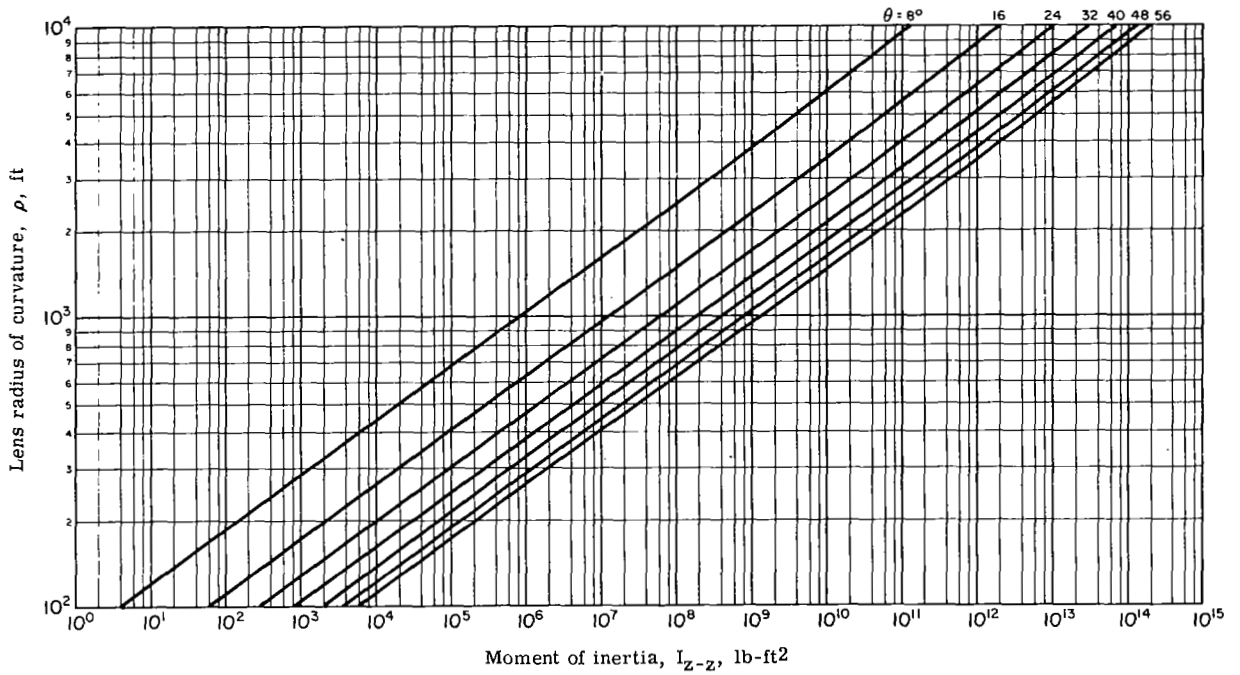


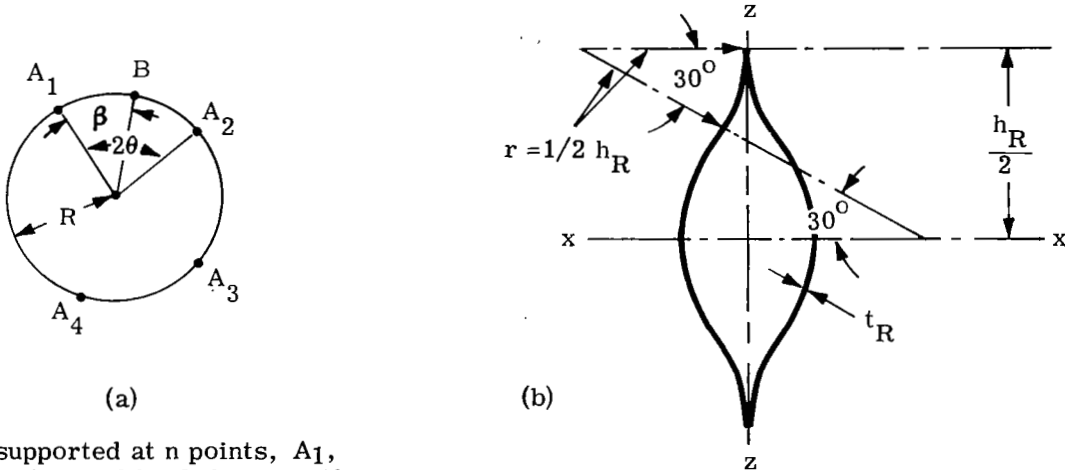
Figure D40. - Material IV - moment of inertia I_{Z-Z} of photolyzed lens versus lens radius of curvature.

APPENDIX E

CRITERIA FOR THE DETERMINATION OF THE SIZE OF RIM AND TETRAPOD BOOMS

Rim

Satellite components other than the lens, torus, inflation system and canister that significantly contribute to the launch weight are the rim, the tetrapod booms, and the stabilization system. Because the structural integrity of these components cannot be checked without knowing the final satellite configuration, in order to determine gravity gradient and other inertia loads, some criteria must be established in selecting these components. For the rim it was thought that a maximum out-of-plane deflection of one percent of the rim diameter would be an adequate design criterion. In reference 1, pages 108 to 112, the maximum rim deflection has been calculated under a critical loading condition for a tripod boom arrangement. Since the present study deals with a tetrapod boom arrangement, a comparison was made of rim deflections with tripod and tetrapod arrangements for the simple loading condition of uniformly distributed load normal to the rim plane, in order to establish the stiffening effect of the additional boom on the rim deflections. A brief discussion of this comparison is given below.



(a)

(b)

Rim supported at n points, A_1, A_2, \dots, A_n , and loaded by a uniform load q normal to its plane

Rim across section (see appendix B)

If B is any point at an angular distance β from A_1 , the deflection under B , from reference 9, is

$$\delta = C_1 \cos \beta + C_2 \sin \beta + C_3 + \frac{qR^4}{2} \left[\left(\frac{1}{EI} + \frac{1}{GJ} \right) \frac{\theta}{\sin \theta} \beta \sin (\theta - \beta) - \frac{(\theta - \beta)^2}{GJ} \right],$$

APPENDIX E

where

$$C_1 = -\frac{qR^4\theta^2}{2\sin^2\theta} \left[\frac{1}{EI} + \frac{1}{GJ} + \frac{\sin 2\theta}{2\theta} \left(\frac{1}{EI} + \frac{3}{GJ} \right) \right]$$

$$C_2 = -\frac{qR^4\theta}{2} \left(\frac{1}{EI} + \frac{3}{GJ} \right)$$

$$C_3 = \frac{qR^4\theta^2}{2\sin^2\theta} \left[\frac{1}{EI} + \frac{1+\sin^2\theta}{GJ} + \frac{\sin 2\theta}{2\theta} \left(\frac{1}{EI} + \frac{3}{GJ} \right) \right]$$

For the cross section shown in sketch (b) the moment of inertia about the x-axis and the torsional stiffness are respectively,

$$I = 0.17314 h_R^3 t_R \text{ and } J = 0.03429 h_R^3 t_R$$

Hence for a rim material with Poisson's ratio $\mu = 1/3$, the quantity EI/GJ is 13.464. Then for $\theta = \beta = \pi/3$, the above deflection equation yields

$$\delta_{\max} = 0.157 \frac{qR^4}{EI} \text{ (three supports),}$$

and for $\theta = \beta = \pi/4$, $\delta_{\max} = 0.037 \frac{qR^4}{EI}$ (four supports).

Consequently, δ_{\max} (for tetrapod) $\cong 0.25 \delta_{\max}$ (for tripod). (E1)

Another aspect to be considered is that the rim deflection is caused by gravity-gradient and inertia forces on the concentrated masses which are located at the tetrapod apices. These masses correspond to the canister, inflation system, and stabilization system weights; the gravity-gradient and inertia forces are therefore proportional to these masses in the gravity field $\omega^2 h$.

With the above remarks the maximum rim deflection can be written as follows:

$$\delta_{\max} = \alpha \frac{\omega^2 W R^2 h^2}{EI} \quad (E2)$$

The coefficient α can be found by using the dimensions of the rim configuration of reference 2, page 67, in which $\omega^2 = 0.39 \times 10^{-6}$, $h = 260.3$ ft, $R = 133.8$ ft, $W = 2 \times 184 = 368$ lb, $E = 18 \times 10^6$ psi, $I = 0.17730$ in.⁴ In order for the coefficient α to be valid for a tetrapod arrangement for one percent rim deflection, the $\delta_{\max}/2R$ value will be taken equal to $0.01 \times 0.25 \cong 0.0025$ (see equation E1). Substituting these numerical values in equation (E2) yields $\alpha = 0.007097 \text{ sec}^2/\text{in.}$ Noting that for the rim geometry of reference 1,

$$t_R = 0.00025 h_R, \quad (E3)$$

and letting $\delta_{\max}/R = 0.02$, $E = 18 \times 10^6$ psi (beryllium copper). Equation (E2) yields

$$h_R = 0.1461 \sqrt[4]{\omega^2 h^2 R W} \text{ in.} \quad (E4)$$

where W is the combined weight of canister, inflation system, and stabilization system (in pounds), and h , R are measured in inches.

APPENDIX E

Substituting equation (E4) into the mass moments of inertia of the rim, as given in appendix B, and simplifying yields

$$\left. \begin{aligned} I_{x,R} &= 10.429 \omega R^3 h \sqrt{WR} \times 10^{-6} \text{ lb-in.}^2 \\ I_{z,R} &= 20.858 \omega R^3 h \sqrt{WR} \times 10^{-6} \text{ lb-in.}^2 \end{aligned} \right\} \quad (\text{E5})$$

where R and h are measured in inches and W in pounds.

Tetrapod Booms

The criterion for the determination of the weight of the tetrapod booms is that the angle of twist of these booms should not exceed five degrees. Furthermore, the tetrapod should present a constant stiffness against the torque, M_z , which causes the booms to twist. The constant ratio M_z/I_z may be calculated from the full scale configuration of reference 10, appendixes C and E, where $I_z = 5.25 \times 10^6 \text{ lb-ft}^2$ and $M_z = 0.85 \text{ in-lb}$.

Hence,

$$\frac{M_z}{I_z} = \frac{0.85}{5.25 \times 144 \times 10^6} = 1.124 \times 10^{-9} \text{ in.}^{-1} \quad (\text{E6})$$

In equation (E6) the quantity I_z includes the lens, the rim, the stabilization system, and the tetrapod booms. Assuming that the latter two items are about 13 percent of the first two items, the ratio M_z/I_z may be written $M_z/1.13 I_z$, and equation (E6) solved for M_z yields

$$M_z = 1.27 I_z' \quad (\text{E7})$$

where I_z' is the yaw mass moment of inertia of lens and rim. Then the radius of the cross section of the tetrapod booms may be determined from equation

$$r_B = \frac{s_B}{\pi d_B} \sqrt[3]{\frac{5\pi \ell_B M_z}{12 d_B E \theta \cos \alpha_\mu}} \quad (\text{reference (ref. 10, p. C-4).}) \quad (\text{E8})$$

For $\theta_1 = 5^\circ = 0.08727$ radians, $\cos \alpha_\mu = h/\ell_B$, and by using equation (E7), equation (E8) results in

$$r_B = 3.946 \times 10^{-6} \left(\frac{s_B}{d_B} \right) \sqrt[3]{\frac{\ell_B^2 I_z'}{h d_B}} \quad (\text{E9})$$

Assuming that $s_B/d_B = 50$, and that 0.5-mil Mylar film can be constantly used, regardless of satellite configuration, the unit weight of the boom (wire-film material per square inch) can be optimized for minimum weight. This leads to an optimum wire diameter $d_B \cong 2.5$ mil and wire spacing (axially) $s_B = 0.125$ inch (see page 13). Then equation (E9) may be simplified as follows:

$$r_B = 0.0014537 \sqrt[3]{\frac{\ell_B^2 I_z'}{h}} \text{ in.}, \quad (\text{E10})$$

where I_z' is the combined yaw moment of inertia of lens and rim. The boom material weight

APPENDIX E

per square inch is

$$\begin{aligned} w_B &= 0.0005 \times 0.05 + \frac{3\pi}{4(0.125)} (0.0025)^2 (0.1) \\ &= 25 \times 10^{-6} + 11.78 \times 10^{-6} = 36.78 \times 10^{-6} \text{ lb/in.}^2 \end{aligned}$$

Then the total weight of eight booms (for two tetrapods) is

$$W_B = 8\ell_B (2\pi r_B) \times 36.78 \times 10^{-6} = 0.0018488 \ell_B r_B \text{ lb}, \quad (\text{E11})$$

where ℓ_B and r_B are measured in inches.

APPENDIX F

LENTICULAR LENS SURFACE AREA AND ENCLOSED VOLUME

Table F1 is the computer output for lenticular lens total surface area and volume for ranges of lens radius of curvature ρ from 100 feet to 10 000 feet and lens lenticular half angle θ from 8 to 56 degrees in the same increments as given in Table D1. Figures F1 and F2 are graphical representations of the numerical values from Table F1.

TABLE F1. - COMPUTER DATA FOR LENS AREA AND VOLUME

RADIUS	THETA	LENS SURF. AREA	VOLUME	RADIUS	THETA	LENS SURF. AREA	VOLUME
1200.	8.	1.7610E 05	1.0249E 06	20000.	8.	4.8917E 07	4.7449E 09
1200.	16.	7.0097E 05	1.6082E 07	20000.	16.	1.9471E 08	7.4452E 10
1200.	24.	1.5644E 06	7.8808E 07	20000.	24.	4.3455E 08	3.6485E 11
1200.	32.	2.7496E 06	2.3798E 08	20000.	32.	7.6377E 08	1.1017E 12
1200.	40.	4.2334E 06	5.4790E 08	20000.	40.	1.1760E 09	2.5366E 12
1200.	48.	5.9871E 06	1.0575E 09	20000.	48.	1.6631E 09	4.8956E 12
1200.	56.	7.9764E 06	1.7996E 09	20000.	56.	2.2157E 09	8.3315E 12
3000.	8.	1.1006E 06	1.6014E 07	40000.	8.	1.9567E 08	3.7959E 10
3000.	16.	4.3811E 06	2.5128E 08	40000.	16.	7.7886E 08	5.9562E 11
3000.	24.	9.7775E 06	1.2314E 09	40000.	24.	1.7382E 09	2.9188E 12
3000.	32.	1.7185E 07	3.7184E 09	40000.	32.	3.0551E 09	8.8140E 12
3000.	40.	2.6459E 07	8.5610E 09	40000.	40.	4.7038E 09	2.0293E 13
3000.	48.	3.7419E 07	1.6523E 10	40000.	48.	6.6523E 09	3.9165E 13
3000.	56.	4.9853E 07	2.8119E 10	40000.	56.	8.8627E 09	6.6652E 13
5000.	8.	3.0573E 06	7.4140E 07	80000.	8.	7.8267E 08	3.0368E 11
5000.	16.	1.2170E 07	1.1633E 09	80000.	16.	3.1154E 09	4.7650E 12
5000.	24.	2.7160E 07	5.7008E 09	80000.	24.	6.9529E 09	2.3351E 13
5000.	32.	4.7736E 07	1.7215E 10	80000.	32.	1.2220E 10	7.0512E 13
5000.	40.	7.3497E 07	3.9634E 10	80000.	40.	1.8815E 10	1.6234E 14
5000.	48.	1.0394E 08	7.6494E 10	80000.	48.	2.6609E 10	3.1332E 14
5000.	56.	1.3848E 08	1.3018E 11	80000.	56.	3.5451E 10	5.3322E 14
10000.	8.	1.2229E 07	5.9312E 08	120000.	8.	1.7610E 09	1.0249E 12
10000.	16.	4.8678E 07	9.3065E 09	120000.	16.	7.0097E 09	1.6082E 13
10000.	24.	1.0864E 08	4.5607E 10	120000.	24.	1.5644E 10	7.8808E 13
10000.	32.	1.9094E 08	1.3772E 11	120000.	32.	2.7496E 10	2.3798E 14
10000.	40.	2.9399E 08	3.1707E 11	120000.	40.	4.2334E 10	5.4790E 14
10000.	48.	4.1577E 08	6.1195E 11	120000.	48.	5.9871E 10	1.0575E 15
10000.	56.	5.5392E 08	1.0414E 12	120000.	56.	7.9764E 10	1.7996E 15

APPENDIX F

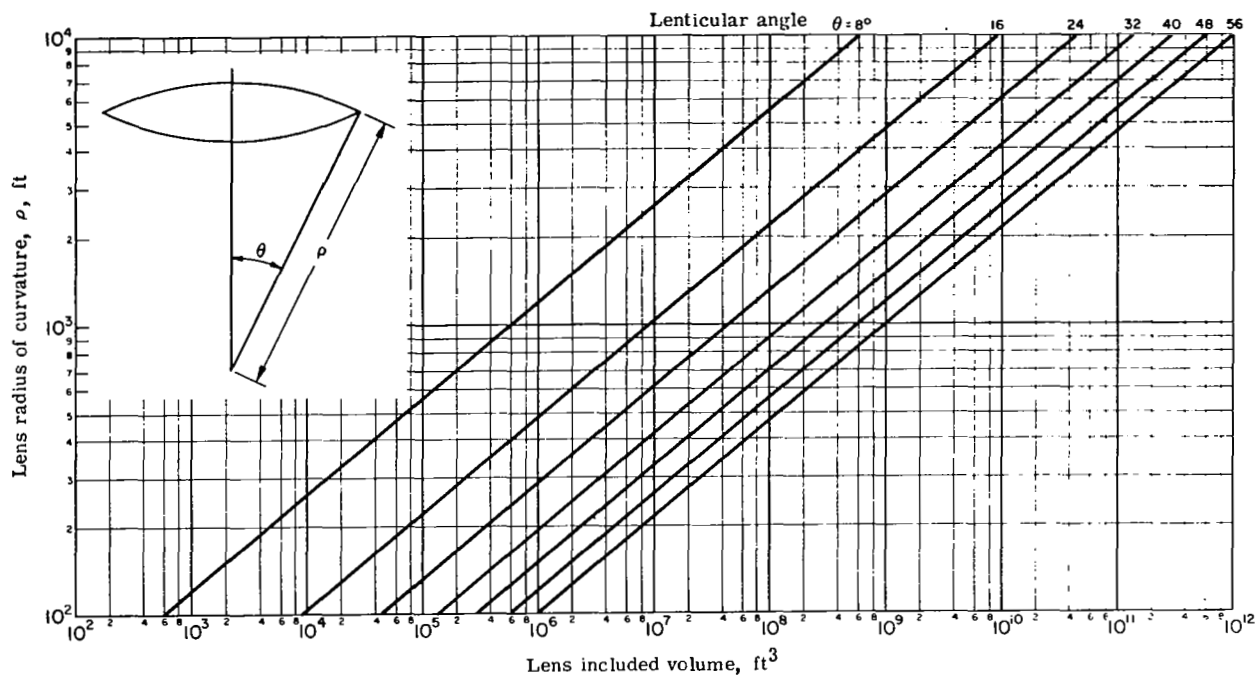


Figure F1. - Lenticular lens volume versus lens radius of curvature and lenticular angle.

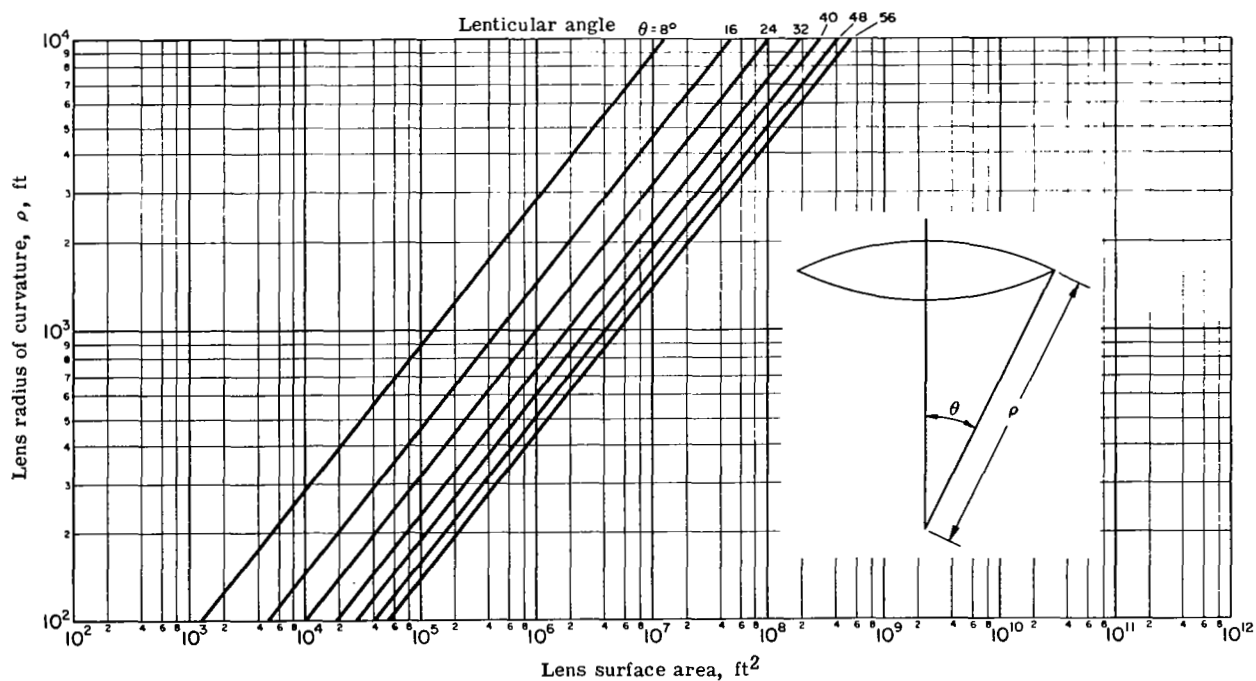


Figure F2. - Lenticular lens surface area versus lens radius of curvature and lenticular angle.

APPENDIX G

DERIVATION OF GRAVITY-GRADIENT STABILIZED LENTICULAR SATELLITE EQUATIONS OF MOTION, ORBITAL ECCENTRICITY FORCING FUNCTIONS, AND SOLAR TORQUE FORCING FUNCTIONS

General

The equations of motion and steady-state forcing functions related to the attitude control problem of the lenticular communication satellite are derived in this appendix. As described in the main body of the report, the satellite is equipped with a modified Ames damper. Two booms are employed, which have a common servo-driven degree of freedom about the nominal vertical axis, providing an adjustable yaw reference attitude needed for position keeping by solar sailing. One of the booms is of the Ames damper variety equipped with torsion bar suspension and dashpot.

The yaw reference drive moves at such a slow angular rate that the dynamics of this drive have been ignored in this study. The equations of motion for analytical purposes are therefore those of a four-degree-of-freedom system consisting of the pitch, roll, and yaw of the satellite and a single degree of freedom of the damper boom.

Stability characteristics were investigated by solution of the differential equations of rotational motion by analog and digital computer simulation. This report presents the derivation of those equations of motion. Modifications of the equations to include solar torques and orbital eccentricity effects are also presented.

The rotational equations of motion (four-degree) are derived assuming the satellite center-of-mass is in a circular orbit about a spherical earth. The center-of-mass of the satellite is assumed to be at the geometrical center of the lens. The satellite is considered a rigid body, except for one damper rod degree of freedom. For simplification, the equations are linearized in three degrees of freedom. The remaining variable (yaw) is not linearized because a steady-state yaw angle exists for this configuration. The energy method of LaGrange is used to accomplish the derivation, resulting in equations of motion in generalized coordinates.

The format followed in this presentation is first to define the coordinate systems used, and then the transformations between them. Derivation of the angular velocities is then made, followed by the derivation of the equations themselves.

Since the equations are derived under the idealized condition of a circular orbit, approximate forcing functions that simulate eccentricity are derived. Simplification of the forcing functions is accomplished by neglecting the damper boom degree of freedom and treating the satellite as a three-degree of freedom rigid body.

Solar torque forcing function expressions that are dependent on satellite attitude relative to the sun have been derived in reference 11. The expressions that relate satellite-sun attitude in functional form are derived herein. This permits use of the forcing functions in the equations of motion.

APPENDIX G

Coordinate Systems

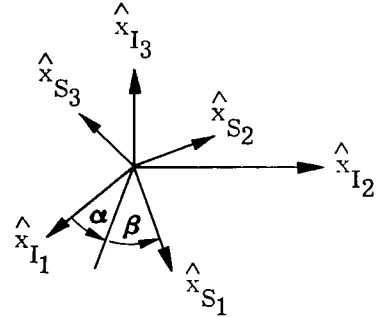
- X_I** Inertial system, centered in a non-rotating earth. $\hat{x}_{I1}, \hat{x}_{I2}, \hat{x}_{I3}$ the unit vectors forming a positive, orthogonal vector triple with \hat{x}_{I3} the north polar axis.
- X_S** Sun line system, centered commonly with the inertial system. $\hat{x}_{S1}, \hat{x}_{S2}, \hat{x}_{S3}$ the positive, orthogonal unit vector triple with \hat{x}_{S1} pointing toward the sun.
- X_O** Rotating orbital system, centered commonly with the inertial system. $\hat{x}_{O1}, \hat{x}_{O2}, \hat{x}_{O3}$ the positive, orthogonal unit vector triple with \hat{x}_{O1} pointing toward satellite center-of mass.
- X_T** Trajectory system, centered at the satellite center-of-mass. $\hat{x}_{T1}, \hat{x}_{T2}, \hat{x}_{T3}$, the positive, orthogonal unit vector triple with \hat{x}_{T1} coincident with local horizontal component of orbital velocity. \hat{x}_{T3} parallel to \hat{x}_{O1} (orbit radius vector).
- X_B** Body axis system, centered at the satellite center-of-mass and coincident with the principal axes. $\hat{x}_{B1}, \hat{x}_{B2}, \hat{x}_{B3}$ the positive, orthogonal unit vector triple with \hat{x}_{B1} out the nose (roll axis), \hat{x}_{B2} out the left side (pitch axis), \hat{x}_{B3} up (yaw axis).
- X_D** Damper axis system, centered at the damper unit center-of-mass and aligned with the damper principal axes. $\hat{x}_{D1}, \hat{x}_{D2}, \hat{x}_{D3}$ the positive, orthogonal unit vector triple defined by the coordinate transformation [E] .

Coordinate Transformations

The sun line-inertial coordinates are related by the transformation matrix [A] and illustrated by the accompanying sketch. The rotational order from \hat{x}_I to \hat{x}_S is α (about \hat{x}_{I2}), then β (about \hat{x}_{S3}).

$$\begin{bmatrix} \hat{x}_{S1} \\ \hat{x}_{S2} \\ \hat{x}_{S3} \end{bmatrix} = [A] \begin{bmatrix} \hat{x}_{I1} \\ \hat{x}_{I2} \\ \hat{x}_{I3} \end{bmatrix}$$

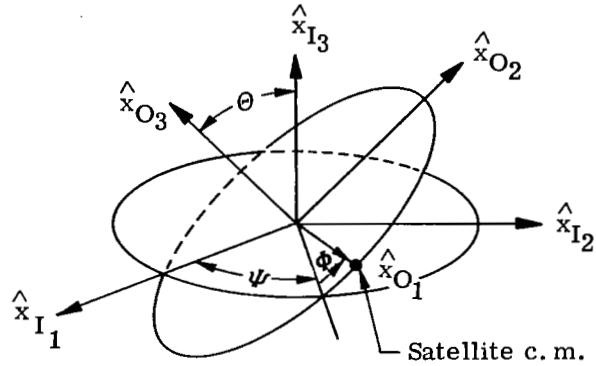
$$[A] = \begin{bmatrix} \cos \beta \cos \alpha & \sin \beta & -\sin \alpha \cos \beta \\ -\sin \beta \cos \alpha & \cos \beta & \sin \alpha \sin \beta \\ \sin \alpha & 0 & \cos \alpha \end{bmatrix}$$



APPENDIX G

The inertial-orbital coordinates are related through the matrix $[B]$. The rotational order from X_I to X_O is ψ , θ , ϕ .

$$\begin{bmatrix} \hat{x}_{O1} \\ \hat{x}_{O2} \\ \hat{x}_{O3} \end{bmatrix} = [B] \begin{bmatrix} \hat{x}_{I1} \\ \hat{x}_{I2} \\ \hat{x}_{I3} \end{bmatrix}$$

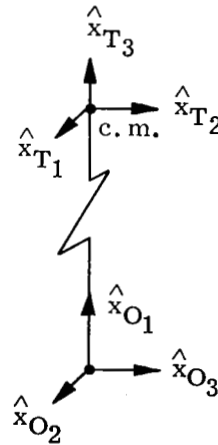


$$[B] = \begin{bmatrix} \cos \phi \cos \psi - \sin \phi \cos \theta \sin \psi & \cos \phi \sin \psi + \sin \phi \cos \theta \cos \psi & \sin \phi \sin \theta \\ -\sin \phi \cos \psi - \cos \phi \cos \theta \sin \psi & -\sin \phi \sin \psi + \cos \phi \cos \theta \cos \psi & \cos \phi \sin \theta \\ \sin \theta \sin \psi & -\sin \theta \cos \psi & \cos \theta \end{bmatrix}$$

The orbital-trajectory coordinates are related through the matrix $[C]$.

$$\begin{bmatrix} \hat{x}_{T1} \\ \hat{x}_{T2} \\ \hat{x}_{T3} \end{bmatrix} = [C] \begin{bmatrix} \hat{x}_{O1} \\ \hat{x}_{O2} \\ \hat{x}_{O3} \end{bmatrix}$$

$$[C] = \begin{bmatrix} 0 & 1 & 0 \\ 0 & 0 & 1 \\ 1 & 0 & 0 \end{bmatrix}$$



The trajectory-body coordinates are related through the matrix $[D]$. The $[D]$ matrix represents a standard Euler angle transformation (similar to the matrix $[B]$). However, the rotational sequence followed from X_T to X_B is pitch (θ), roll (ϕ), and yaw (ψ).

$$\begin{bmatrix} \hat{x}_{B1} \\ \hat{x}_{B2} \\ \hat{x}_{B3} \end{bmatrix} = [D] \begin{bmatrix} \hat{x}_{T1} \\ \hat{x}_{T2} \\ \hat{x}_{T3} \end{bmatrix}$$

APPENDIX G

$$[D] = \begin{bmatrix} \cos \theta \cos \psi + \sin \theta \sin \psi \sin \phi & \cos \phi \sin \psi & -\cos \psi \sin \theta + \sin \psi \cos \theta \sin \phi \\ -\cos \theta \sin \psi + \sin \theta \cos \psi \sin \phi & \cos \phi \cos \psi & \sin \psi \sin \theta + \cos \psi \cos \theta \sin \phi \\ \sin \theta \cos \phi & -\sin \phi & \cos \theta \cos \phi \end{bmatrix}$$

The damper-body coordinates are related through the matrix $[E]$. The rotational order from body to damper axes is yaw (ψ_D), then pitch (θ_D). There is no roll displacement between these axis systems.

$$\begin{bmatrix} \hat{x}_{D1} \\ \hat{x}_{D2} \\ \hat{x}_{D3} \end{bmatrix} = [E] \begin{bmatrix} \hat{x}_{B1} \\ \hat{x}_{B2} \\ \hat{x}_{B3} \end{bmatrix}$$

$$[E] = \begin{bmatrix} \cos \theta_D \cos \psi_D & \cos \theta_D \sin \psi_D & -\sin \theta_D \\ -\sin \psi_D & \cos \psi_D & 0 \\ \sin \theta_D \cos \psi_D & \sin \theta_D \sin \psi_D & \cos \theta_D \end{bmatrix}$$

Note that the above transformations relate orthogonal sets of coordinate axes and therefore the inverse is equal to the transpose of any of the above matrices, i.e., $A^{-1} = A^T$. Note also the general form of any matrix given in terms of its elements as demonstrated below.

$$[A] = \begin{bmatrix} a_{11} & a_{12} & a_{13} \\ a_{21} & a_{22} & a_{23} \\ a_{31} & a_{32} & a_{33} \end{bmatrix}$$

Angular Rates

The kinetic energy expression will contain the angular velocities of the satellite and the damper rods. This section will define and derive those angular rates. In general, an angular velocity may be expressed as follows:

$$\frac{\rightarrow X_O - X_I}{\omega_{X_O}} = \omega_{X_{O1}} \hat{x}_{O1} + \omega_{X_{O2}} \hat{x}_{O2} + \omega_{X_{O3}} \hat{x}_{O3} \quad (G1)$$

This notation defines angular velocity expressed in the orbital frame as indicated by the subscript. The superscript defines the angular velocity of the orbital frame relative to inertial space. This notation will be used throughout. Where necessary, the superscript notation will be applied to the scalar components.

The satellite angular velocity is given as follows:

$$\frac{\rightarrow X_B - X_I}{\omega_{X_B}} = \frac{\rightarrow X_B - X_T}{\omega_{X_B}} + \frac{\rightarrow X_T - X_I}{\omega_{X_B}} \quad (G2)$$

APPENDIX G

Assuming a circular orbit, and neglecting perturbations ($\dot{\theta} = \dot{\psi} = 0$):

$$\vec{\omega}_{X_O} - \vec{X}_I = \dot{\phi} \hat{x}_{O3} = \omega_O \hat{x}_{O3}, \quad (\omega_O = \text{orbital rate}) \quad (G3)$$

Transformation into the X_B system can be accomplished using [C] and [D].

$$\vec{\omega}_{X_B} - \vec{X}_I = [DC]^{-1} \vec{\omega}_{X_O} - \vec{X}_I$$

The body term ($\vec{\omega}_{X_B} - \vec{X}_I$) is obtained in terms of the Euler angle rates relating the body-trajectory sets. The scalar components are given as:

$$\omega_{X_{B1}} - X_I = \dot{\phi} \cos \psi + \dot{\theta} \cos \phi \sin \psi \quad (G5a)$$

$$\omega_{X_{B2}} - X_I = \dot{\theta} \cos \phi \cos \psi - \dot{\phi} \sin \psi \quad (G5b)$$

$$\omega_{X_{B3}} - X_I = \dot{\psi} - \dot{\theta} \sin \phi \quad (G5c)$$

Combining the velocity components provides the total satellite angular velocity in inertial space, expressed in body coordinates:

$$\vec{\omega}_{X_B} - \vec{X}_I = \omega_{X_{B1}} \hat{x}_{B1} + \omega_{X_{B2}} \hat{x}_{B2} + \omega_{X_{B3}} \hat{x}_{B3} \quad (G6)$$

where

$$\begin{bmatrix} \omega_{X_{B1}} \\ \omega_{X_{B2}} \\ \omega_{X_{B3}} \end{bmatrix} = [S] \begin{bmatrix} \dot{\phi} \\ \omega_O + \dot{\theta} \\ \dot{\psi} \end{bmatrix} \quad (G7)$$

and

$$[S] = \begin{bmatrix} \cos \psi & \cos \phi \sin \psi & 0 \\ -\sin \psi & \cos \phi \cos \psi & 0 \\ 0 & -\sin \phi & 1 \end{bmatrix}$$

Note that the matrix [S] does not transform orthogonal sets, and therefore

$$S^{-1} \neq S^T$$

APPENDIX G

The damper angular velocity will now be obtained from its components:

$$\frac{\rightarrow X_D - X_I}{\omega_{X_D}} = \frac{\rightarrow X_D - X_B}{\omega_{X_D}} + \frac{\rightarrow X_B - X_I}{\omega_{X_D}} \quad (G8)$$

The body rate component may be written in the damper frame with the help of the matrix [E].

$$\frac{\rightarrow X_B - X_I}{\omega_{X_D}} = [E] \frac{\rightarrow X_B - X_I}{\omega_{X_B}} \quad (G9)$$

The damper rate component is easily written under the constraint that damper motion is restricted to its own pitch plane only.

$$\frac{\rightarrow X_D - X_B}{\omega_{X_D}} = \dot{\theta}_D \hat{x}_{D2} \quad (G10)$$

The velocity components may now be combined to provide the total damper angular velocity in inertial space, expressed in damper coordinates:

$$\frac{\rightarrow X_D - X_I}{\omega_{X_D}} = \omega_{X_{D1}} \hat{x}_{D1} + \omega_{X_{D2}} \hat{x}_{D2} + \omega_{X_{D3}} \hat{x}_{D3} \quad (G11)$$

where

$$\omega_{X_{D1}} = e_{11} \omega_{X_{B1}} + e_{12} \omega_{X_{B2}} + e_{13} \omega_{X_{B3}} \quad (G12a)$$

$$\omega_{X_{D2}} = e_{21} \omega_{X_{B1}} + e_{22} \omega_{X_{B2}} + e_{23} \omega_{X_{B3}} + \dot{\theta}_D \quad (G12b)$$

$$\omega_{X_{D3}} = e_{31} \omega_{X_{B1}} + e_{32} \omega_{X_{B2}} + e_{33} \omega_{X_{B3}} \quad (G12c)$$

and the terms e_{11} , e_{12} ---- are the elements of the matrix [E].

Equations of Motion

The equations of angular motion are derived in terms of the generalized coordinates $(\phi, \theta, \psi, \theta_D)$, using the energy method (LaGrange). The assumption is made that relative motion takes place about the center-of-mass which is located at the center of the lens. The center-of-mass is constrained to move in a circular orbit about a spherical earth. The fixed damper rod is included as part of the main satellite body. The free damper rod is constrained to pitch motion only, relative to the main body. The system kinetic and potential energies will now be written, and the energy method applied to obtain the equations.

$$\text{Satellite body KE} = \frac{1}{2} \left(I_{X_{B1}} \omega_{X_{B1}}^2 + I_{X_{B2}} \omega_{X_{B2}}^2 + I_{X_{B3}} \omega_{X_{B3}}^2 \right) \quad (G13)$$

$$\text{Damper boom KE} = \frac{1}{2} \left(I_{X_{D1}} \omega_{X_{D1}}^2 + I_{X_{D2}} \omega_{X_{D2}}^2 + I_{X_{D3}} \omega_{X_{D3}}^2 \right) \quad (G14)$$

APPENDIX G

$$\text{Damper dissipation energy} = \frac{1}{2} K_B \dot{\theta}_D^2 \quad (\text{G15})$$

$$\begin{aligned} \text{Satellite body} &= \frac{3}{2} \omega_0^2 \left[I_{XB1} d_{13}^2 + I_{XB2} d_{23}^2 + I_{XB3} d_{33}^2 \right. \\ \text{potential energy} &\quad \left. - \frac{1}{3} (I_{XB1} + I_{XB2} + I_{XB3}) \right] \end{aligned} \quad (\text{G16})$$

$$\begin{aligned} \text{Damper boom} &= \frac{3}{2} \omega_0^2 \left[I_{XD1} f_{13}^2 + I_{XD2} f_{23}^2 + I_{XD3} f_{33}^2 \right. \\ \text{potential energy} &\quad \left. - \frac{1}{3} (I_{XD1} + I_{XD2} + I_{XD3}) \right] \end{aligned} \quad (\text{G17})$$

$$\text{Damper spring potential energy} = \frac{1}{2} K \theta_D^2 \quad (\text{G18})$$

$$\text{Matrix } [F] = [E] [D]$$

Before deriving the equations, the inertia terms are defined as follows. First, for simplification only, let:

$$\left. \begin{aligned} I_{XB1} &= I_{x-x} \\ I_{XB2} &= I_{y-y} \\ I_{XB3} &= I_{z-z} \end{aligned} \right\} \text{ by definition}$$

Now,

$$\begin{aligned} I_{x-x} &= I_{Xw/o \text{ booms}} + \mu h^2 \\ I_{y-y} &= I_{yw/o \text{ booms}} + \mu h^2 + I_F \\ I_{z-z} &= I_{zw/o \text{ booms}} + I_F \end{aligned}$$

where μ = mass of fixed boom + mass of damper boom.

The boom masses are located a distance, h , along the body z axis. The term I_F is the fixed boom inertia about its own axis system, which is oriented the same as the body axis systems but located at the boom center-of-mass. The fixed boom inertia is neglected about its own x -axis (the long, slender axis of the boom). The boom inertias about its own y and z axes are equal (by symmetry), and defined as I_F . Note that the satellite mass plus the boom masses define the system mass center. The system mass center is the origin of the body coordinates. Note also because of symmetry:

$$I_{Xw/o \text{ booms}} = I_{yw/o \text{ booms}}$$

and

$$\therefore I_{y-y} - I_{x-x} = (I_{yw/o \text{ booms}} + \mu h^2 + I_F) - (I_{xw/o \text{ booms}} + \mu h^2)$$

$$\therefore (I_{y-y} - I_{x-x}) = I_F = \Delta \text{ by definition.}$$

Note that all system inertias and masses have now been introduced into the kinetic energy of the satellite, with the exception of the damper boom inertia about its own axis system. This final damper boom inertia is introduced into the total kinetic energy through equation (G17).

The damper boom inertia about its own axis system is now defined. The long slender axis of the damper is X_D . The inertia about X_D is considered negligible. The boom is symmetrical about its own Y_D and Z_D axes, and therefore the inertias are equal. Now by definition:

$$I_{X_D1} = 0$$

$$I_{X_D2} = I_D$$

$$I_{X_D3} = I_D$$

The system equations of motion can now be written with the help of the angular rates previously derived. The equations are linearized on ϕ , θ , and θ_D . The yaw angle (ψ) is not linearized because the steady-state value can be large. Applying LaGrange under the above assumptions and with due consideration for the non-conservative forces, the partially linearized equations of rotation result:

(1) Pitch (θ)

$$\begin{aligned} & \left[I_{y-y} - \Delta \sin^2 \psi + I_D \cos^2 (\psi + \psi_D) \right] \ddot{\theta} + 3\omega_0^2 \left[I_{x-x} + \Delta \sin^2 \psi - I_{z-z} \right. \\ & \quad \left. - I_D \cos^2 (\psi + \psi_D) \right] \theta - \left[\Delta \sin \psi \cos \psi + I_D \sin (\psi + \psi_D) \cos (\psi + \psi_D) \right] \\ & \quad \left[\ddot{\phi} - 3\omega_0^2 \phi + 2\omega_0 \dot{\psi} \right] + I_D \cos (\psi + \psi_D) \left[\ddot{\theta}_D - 3\omega_0^2 \theta_D \right] = 0 \end{aligned} \quad (G19)$$

(2) Roll (ϕ)

$$\begin{aligned} & \left[I_{x-x} + \Delta \sin^2 \psi + I_D \sin^2 (\psi + \psi_D) \right] \ddot{\phi} + 4\omega_0^2 \left[I_{y-y} - \Delta \sin^2 \psi - I_{z-z} \right. \\ & \quad \left. - I_D \sin^2 (\psi + \psi_D) \right] \phi - \left[\Delta \sin \psi \cos \psi + I_D \sin (\psi + \psi_D) \cos (\psi + \psi_D) \right] \\ & \quad \left[\ddot{\theta} - 3\omega_0^2 \theta \right] + \left[I_{z-z} - \Delta \cos 2\psi + 2I_D \sin^2 (\psi + \psi_D) \right] \omega_0 \dot{\psi} - I_D \sin (\psi + \psi_D) \\ & \quad \left[\ddot{\theta}_D - 4\omega_0^2 \theta_D \right] = 0 \end{aligned} \quad (G20)$$

(3) Yaw (ψ)

$$\begin{aligned} & \left[I_{z-z} + I_D \right] \ddot{\psi} + \left[\Delta \sin \psi \cos \psi + I_D \sin (\psi + \psi_D) \cos (\psi + \psi_D) \right] \omega_0^2 \\ & \quad - \left[I_{z-z} + I_D - \Delta \cos 2\psi - I_D \cos 2 (\psi + \psi_D) \right] \omega_0 \dot{\phi} \\ & \quad + \left[\Delta \sin \psi \cos \psi + I_D \sin (\psi + \psi_D) \cos (\psi + \psi_D) \right] 2\omega_0 \dot{\theta} \\ & \quad + I_D \sin (\psi + \psi_D) 2\omega_0 \dot{\theta}_D = 0 \end{aligned} \quad (G21)$$

APPENDIX G

(4) Damper (θ_D)

$$I_D \ddot{\theta}_D + B \dot{\theta}_D + \left\{ K - I_D \omega_0^2 \left[3 + \sin^2(\psi + \psi_D) \right] \right\} \theta_D + I_D \cos(\psi + \psi_D) (\ddot{\theta} - 3\omega_0^2 \theta) - I_D \sin(\psi + \psi_D) (\ddot{\phi} - 4\omega_0^2 \phi + 2\omega_0 \dot{\psi}) = 0 \quad (G22)$$

The equations of motion will now be normalized to obtain results in parametric form. At the same time, further simplifications will be made by redefining terms to obtain a more compact notation. Therefore the following changes are made by definition:

$$\begin{aligned} \frac{d}{d\tau} &= \frac{1}{\omega_0} \frac{d}{dt} = S & T_y &= \text{external torque in pitch} \\ \frac{d^2}{d\tau^2} &= \frac{1}{\omega_0^2} \frac{d^2}{dt^2} = S^2 & T_x &= \text{external torque in roll} \\ B'' &= B/\omega_0 I_D & T_z &= \text{external torque in yaw} \\ K'' &= K/\omega_0^2 I_D & T_D &= \text{external torque in damper} \\ D &= I_D/I_x & T_y'' &= \frac{T_y}{I_{x-x} \omega_0^2} \\ F &= \Delta/I_{x-x} = I_F/I_{x-x} & T_x'' &= \frac{T_x}{I_{x-x} \omega_0^2} \\ J &= (I_{z-z} + I_F)/I_{x-x} & T_z'' &= \frac{T_z}{I_{z-z} \omega_0^2} \\ A &= F \sin^2 \psi + D \sin^2 \delta & T_D'' &= \frac{T_D}{I_D \omega_0^2} \\ E &= F \sin \psi \cos \psi + D \sin \delta \cos \delta \\ \delta &= \psi + \psi_D \end{aligned}$$

Under the above definitions, the final form of equations (G19) through (G22) become:

$$\begin{aligned} \begin{bmatrix} S^2 (1 + F + D - A) & -(S^2 - 3) E & -2SE & (S^2 - 3) D \cos \delta \\ +3(1 - J - D + A) & & & \end{bmatrix} \begin{bmatrix} \theta \\ \phi \\ \psi^* \\ \theta_D \end{bmatrix} &= \begin{bmatrix} T_y'' \\ T_x'' \\ T_z'' \\ T_D'' \end{bmatrix} \quad (G23) \\ \begin{bmatrix} -(S^2 - 3) E & S^2 (1 + A) & S(J - F + 2A) & -(S^2 - 4) D \sin \delta \\ +4(1 - J - A + F) & & & \end{bmatrix} \begin{bmatrix} \theta \\ \phi \\ \psi^* \\ \theta_D \end{bmatrix} &= \begin{bmatrix} T_y'' \\ T_x'' \\ T_z'' \\ T_D'' \end{bmatrix} \quad (G24) \\ \begin{bmatrix} 2ES & -S(J - F + 2A) & S^2(J + D) + E^{**} & 2SD \sin \delta \\ (S^2 - 3) \cos \delta & -(S^2 - 4) \sin \delta & -2S \sin \delta & S^2 + SB'' + K'' \end{bmatrix} \begin{bmatrix} \theta \\ \phi \\ \psi^* \\ \theta_D \end{bmatrix} &= \begin{bmatrix} T_y'' \\ T_x'' \\ T_z'' \\ T_D'' \end{bmatrix} \quad (G25) \\ \begin{bmatrix} & & & -(3 + \sin^2 \delta) \end{bmatrix} \begin{bmatrix} \theta \\ \phi \\ \psi^* \\ \theta_D \end{bmatrix} &= \begin{bmatrix} T_y'' \\ T_x'' \\ T_z'' \\ T_D'' \end{bmatrix} \quad (G26) \end{aligned}$$

Note that ψ is not linearized and $E^{**} = E$. Further note that $\psi^* = 1$ for the E^{**} term only. In other words,

$$E^{**} \psi^* = E.$$

APPENDIX G

To linearize ψ about the steady-state value γ , let $\psi = \gamma$ and $\therefore \delta = \gamma + \psi_D$. Then, $E^{**} = F \cos 2\gamma + D \cos 2\delta = F + D - 2A$ and $\psi^{**} = \psi$.

Orbital Eccentricity Forcing Functions

The effect of orbital eccentricity on the angular motion of the satellite is approximated in the form of forcing functions which can be applied to the previously derived equations of motion. The forcing functions are obtained by deriving the differential equations of motion of the satellite in an elliptic orbit of small eccentricity. The analysis is based on a spherical earth and negligible second order effects. The damper booms are neglected and the satellite is a rigid body. The technique of the previous section is applied with some minor changes.

Equation (G3) is now used in the following form:

$$\omega_{\dot{\mathbf{x}}_O} - \mathbf{x}_I = \dot{\phi} \hat{\mathbf{x}}_{O3} \quad (G27)$$

Equation (G7) is therefore changed to the following:

$$\begin{bmatrix} \omega_{\mathbf{x}_{B1}} \\ \omega_{\mathbf{x}_{B2}} \\ \omega_{\mathbf{x}_{B3}} \end{bmatrix} = [\mathbf{S}] \begin{bmatrix} \dot{\phi} \\ \dot{\phi} + \dot{\theta} \\ \dot{\psi} \end{bmatrix} \quad (G28)$$

Equations (G13) and (G16) are now used in the LaGrangian together with the redefined angular velocities above. This establishes new equations of motion in terms of the orbital parameters ϕ , $\dot{\phi}$, and μ/r^3 . The term μ/r^3 replaces ω_0^2 in equation (G16). The new equations are linearized on ϕ and θ to be compatible with the previous derivation, and are presented below:

(1) Pitch (θ)

$$\begin{aligned} & \left[(I_{x-x} - I_y) \sin^2 \psi + I_{y-y} \right] \ddot{\theta} + (I_{x-x} - I_{y-y}) \sin \psi \cos \psi \ddot{\phi} + 2\dot{\phi} \dot{\psi} \sin \psi \cos \psi (I_{x-x} - I_{y-y}) \\ & + \ddot{\phi} (I_{x-x} \sin^2 \psi + I_{y-y} \cos^2 \psi) + \frac{3\mu}{r^3} \left\{ \left[I_{x-x} - I_{z-z} + (I_{y-y} - I_{x-x}) \sin^2 \psi \right] \theta \right. \\ & \left. + \sin \psi \cos \psi (I_{y-y} - I_{x-x}) \phi \right\} = 0 \end{aligned} \quad (G29)$$

(2) Roll (ϕ)

$$\begin{aligned} & \left[I_{x-x} + (I_{y-y} - I_{x-x}) \sin^2 \psi \right] \ddot{\phi} - (I_{y-y} - I_{x-x}) \sin \psi \cos \psi \ddot{\theta} - 2\dot{\phi} \dot{\psi} \cos 2\psi (I_{y-y} - I_{x-x}) \\ & - (I_{y-y} - I_{x-x}) \sin \psi \cos \psi \ddot{\phi} + \dot{\phi}^2 \left[I_{y-y} - I_{z-z} - (I_{y-y} - I_{x-x}) \sin^2 \psi \right] \phi + I_{z-z} \dot{\phi} \dot{\psi} \\ & + \frac{3\mu}{r^3} \left\{ \left[I_{y-y} - I_{z-z} - (I_{y-y} - I_{x-x}) \sin^2 \psi \right] \phi + (I_{x-x} - I_{y-y}) \sin \psi \cos \psi \theta \right\} = 0 \end{aligned} \quad (G30)$$

APPENDIX G

(3) Yaw (ψ)

$$I_{Z-Z} [\ddot{\psi} - \dot{\phi} \dot{\phi} - \ddot{\phi} \phi] + \dot{\phi} \dot{\phi} (I_{Y-Y} - I_{X-X}) \cos 2\psi + \dot{\phi} (I_{Y-Y} - I_{X-X}) \sin \psi \cos \psi + 2 \dot{\phi} \dot{\phi} (I_{Y-Y} - I_{X-X}) \sin \psi \cos \psi = 0 \quad (G31)$$

Now the orbital parameters r , $\dot{\phi}$, and $\ddot{\phi}$ may be written in terms of eccentricity (ϵ), average orbital rate (ω_0), and time. This is accomplished by using Kepler's equations and ellipse geometry. The orbit is assumed to be two-dimensional (as before) and the initial point is perigee, therefore:

$$M = \omega_0 t = E - \epsilon \sin E \quad (G32)$$

$$r = a (1 - \epsilon \cos E) \quad (G33)$$

where (E) is the eccentric anomaly, (M) the mean anomaly, and (a) the semi-major axis of the ellipse. The orbital rates can now be written in terms of the momentum per unit mass (h):

$$\dot{\phi} = h/r^2 \quad (G34)$$

$$\ddot{\phi} = (-2\dot{r}/r)(h/r^2) \quad (G35)$$

and using equation (G33):

$$\frac{3\mu}{r^3} = \frac{3\mu}{a^3} \frac{1}{(1 - \epsilon \cos E)^3}$$

Assuming small eccentricity ($\epsilon \ll 1$), and following Sonabend (ref. 12), the equations may be approximated as:

$$\dot{\phi} \cong \omega_0 \quad (G36)$$

$$\ddot{\phi} \cong -2\omega_0^2 \epsilon \sin \omega_0 t \quad (G37)$$

$$3\mu/r^3 \cong 3\omega_0^2 \quad (G38)$$

These terms may now be substituted into equations (G29), (G30), and (G31). Comparison with the angular equations for a circular orbit then yields the effect of eccentricity in the form of forcing functions. They may then be applied to the equations of motion derived in the first section. Going through the above procedure, the forcing functions have the following form:

(1) Pitch (θ)

$$(2\omega_0^2 \epsilon \sin \omega_0 t) (I_{X-X} \sin^2 \psi + I_{Y-Y} \cos^2 \psi) \quad (G39)$$

(2) Roll (ϕ)

$$(-2\omega_0^2 \epsilon \sin \omega_0 t) (I_{Y-Y} - I_{X-X}) \sin \psi \cos \psi \quad (G40)$$

(3) Yaw (ψ)

$$-(2\omega_0^2 \epsilon I_{Z-Z} \sin \omega_0 t) \phi \quad (G41)$$

Note that these equations are derived in terms of the generalized coordinates ϕ , θ , and ψ . In this form the equations are restricted to the generalized coordinate system.

APPENDIX G

Comparing the relative magnitudes of the torques and their effect upon the resultant attitude errors, only the pitch function, equation (G39), is of any consequence. Equations (G40) and (G41) will therefore be neglected. The damper inertia will now be added into the pitch function by comparing with the form of the original pitch equation of motion (G19). Therefore equation (G39) will take the form:

$$(2 \omega_0^2 \epsilon \sin \omega_0 t) \left[I_{x-x} \sin^2 \psi + I_{y-y} \cos^2 \psi + I_D \cos^2 (\psi + \psi_D) \right] \quad (G42)$$

Equation (G42) can now be normalized and thus put in a form compatible with equation (G23). Note that this forcing function now has the form of an external torque T_y'' . Therefore:

$$T_y'' = 2 \epsilon (1 + F + D - A) \sin \omega_0 t \quad (G43)$$

Solar Torques

Torques about the body axes due to solar pressure have been derived in Section IV of reference 11. These torques arise from four satellite subsystems: lens, torus, booms, and canisters. Neglecting the booms and torus, the torque expressions have the following form:

$$M_x = \frac{P_i \pi}{4C} \left\{ -\mu_L^2 A^3 \sin 2\rho_{\max} + 2\mu_c^2 R_c^2 L \right\} \sin 2\alpha \cos \beta \quad (G44)$$

$$M_y = \frac{P_i \pi}{4C} \left\{ -\mu_L^2 A^3 \sin 2\rho_{\max} + 2\mu_c^2 R_c^2 L \right\} \sin 2\alpha \sin \beta \quad (G45)$$

$$M_z = 0 \quad (G46)$$

where the terms are defined as follows:

- P_i = incident radiation power per unit area
- C = speed of light
- μ_L = ratio of reflecting to total lens area (1 = 100 percent closed area)
- A = lens radius; ft
- ρ_{\max} = included lens angle, deg
- μ_c = canister reflectance coefficient (1 = 100 percent reflectance)
- R_c = canister radius, ft
- L = canister height above c. m., ft
- α & β = variables defining body orientation relative to the sun
- P_i/C = 9.649×10^{-8} lb/ft²

For a given satellite configuration, the equations reduce to:

$$M_x = C_1 \sin 2\alpha \cos \beta \quad (G47)$$

APPENDIX G

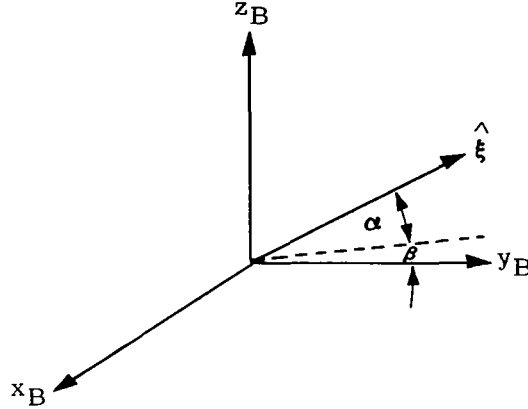
$$M_y = C_1 \sin 2\alpha \sin \beta \quad (G48)$$

$$M_z = 0 \quad (G49)$$

where the constant C_1 is defined assuming a canister reflectance coefficient of one.

$$C_1 = (7.58 \times 10^{-8}) \left(-\mu_L^2 A^3 \sin 2\rho_{\max} + 2R_C^2 L \right)$$

As shown in the sketch below (taken from reference 11), the variables α and β are seen to depend on satellite body axis orientation relative to the sun line ($\hat{\xi}$).



The sun line ($\hat{\xi}$) defined in reference 11 is the unit vector \hat{x}_{S1} defined in this report. Further, the body axes (x_B, y_B, z_B) are the axis system ($\hat{x}_{B1}, \hat{x}_{B2}, \hat{x}_{B3}$) defined herein. Therefore, the orientation angles (α and β) may now be defined as follows:

$$\alpha = \sin^{-1} \left[\frac{\hat{x}_{S1} \cdot \hat{x}_{B3}}{\hat{x}_{S1} \cdot \hat{x}_{S1}} \right] \quad (G50)$$

$$\beta = \tan^{-1} \left[-\frac{\hat{x}_{S1} \cdot \hat{x}_{B1}}{\hat{x}_{S1} \cdot \hat{x}_{B2}} \right] \quad (G51)$$

where \hat{x}_{S1} is obtained from:

$$\begin{bmatrix} \hat{x}_{S1} \\ \hat{x}_{S2} \\ \hat{x}_{S3} \end{bmatrix} = [A] [B^{-1}] [C^{-1}] [D^{-1}] \begin{bmatrix} \hat{x}_{B1} \\ \hat{x}_{B2} \\ \hat{x}_{B3} \end{bmatrix} \quad (G52)$$

Two specific cases will now be analyzed. Case I assumes that the sun lies in the orbital plane. Case II has the sun at 45 degrees to the orbital plane. Note that the matrix $[A]$ uses the angles α and β , which are not the same angles defined in reference 12 and equations (G50) and (G51). However, no confusion should result. For Case I, the matrix angles α and β are equal to zero. Since the earth is assumed spherical, the angles θ and ψ may be taken as zero. Equation (G52) then becomes:

APPENDIX G

$$\begin{aligned}\hat{x}_{S1} = & (-d_{11} \sin \phi + d_{13} \cos \phi) \hat{x}_{B1} + (-d_{21} \sin \phi + d_{23} \cos \phi) \hat{x}_{B2} \\ & + (-d_{31} \sin \phi + d_{33} \cos \phi) \hat{x}_{B3}\end{aligned}\quad (G53)$$

and therefore

$$\hat{x}_{S1} \cdot \hat{x}_{B1} = (-d_{11} \sin \phi + d_{13} \cos \phi) \quad (G54)$$

$$\hat{x}_{S1} \cdot \hat{x}_{B2} = (-d_{21} \sin \phi + d_{23} \cos \phi) \quad (G55)$$

$$\hat{x}_{S1} \cdot \hat{x}_{B3} = (-d_{31} \sin \phi + d_{33} \cos \phi) \quad (G56)$$

$$\hat{x}_{S1} \cdot \hat{x}_{S1} = 1$$

where

$$\phi = \phi_0 + \omega_0 t \text{ (circular orbit)} \quad (G57)$$

These equations, (G47) through (G51) and (G54) through (G57) now completely define solar torques in the body axis system for Case I.

For Case II, where the sun is at 45 degrees to the orbital plane, the matrix angle α may be taken as 45 degrees. The matrix angle β is equal to zero, and the angles θ and ψ are again zero. Letting $\sin 45^\circ$ equal $\cos 45^\circ$ equal C_2 , equation (G52) is obtained and the defining dot products become:

$$\hat{x}_{S1} \cdot \hat{x}_{B1} = C_2 (-d_{11} \sin \phi - d_{12} + d_{13} \cos \phi) \quad (G58)$$

$$\hat{x}_{S1} \cdot \hat{x}_{B2} = C_2 (-d_{21} \sin \phi - d_{22} + d_{23} \cos \phi) \quad (G59)$$

$$\hat{x}_{S1} \cdot \hat{x}_{B3} = C_2 (-d_{31} \sin \phi - d_{32} + d_{33} \cos \phi) \quad (G60)$$

$$\hat{x}_{S1} \cdot \hat{x}_{S1} = 1 \quad (G61)$$

Now, equations (G47) through (G51) and (G57) through (G61) completely define solar torques in the body axis system for Case II.

Now the torque equations (G47) through (G49) may be used as forcing functions in the equations of motion, (G19) through (G21), after a conversion to generalized coordinates. This is accomplished using the expression for rotational power, and the matrix transformation [S].

Define:

$$\begin{aligned}T_{\dot{\phi}} &= \text{solar torque about the generalized coordinate } \phi \\ T_{\dot{\theta}} &= \text{solar torque about the generalized coordinate } \theta \\ T_{\dot{\psi}} &= \text{solar torque about the generalized coordinate } \psi\end{aligned}$$

APPENDIX G

Therefore:

$$\begin{bmatrix} T_{\dot{\phi}} & T_{\dot{\theta}} & T_{\dot{\psi}} \end{bmatrix} \begin{bmatrix} \dot{\phi} \\ \dot{\theta} \\ \dot{\psi} \end{bmatrix} = \begin{bmatrix} M_x & M_y & M_z \end{bmatrix} \begin{bmatrix} \omega_{xB_1} \\ \omega_{xB_2} \\ \omega_{xB_3} \end{bmatrix} \quad (G62)$$

Using equation (G7), the solar torques may now be written in generalized coordinates:

$$T_{\dot{\phi}} = M_x \cos \psi - M_y \sin \psi \quad (G63)$$

$$T_{\dot{\theta}} = M_x \cos \phi \sin \psi + M_y \cos \phi \cos \psi - M_z \sin \phi \quad (G64)$$

$$T_{\dot{\psi}} = M_z \quad (G65)$$

The solar torque forcing functions will now be simplified for Cases I and II.

Assume:

$$\theta = 0$$

$$\phi = 0$$

$$\psi = \gamma \text{ (const)}$$

$$\Phi = 0 \text{ (in equation G57)}$$

Then:

$$[D] \cong \begin{bmatrix} \cos \gamma & \sin \gamma & 0 \\ -\sin \gamma & \cos \gamma & 0 \\ 0 & 0 & 1 \end{bmatrix} \quad (G66)$$

and for Case I, therefore:

$$\tan \beta = \cot \gamma = \tan (90 - \gamma)$$

$$\beta = (90 - \gamma)$$

$$\sin \alpha = \cos \omega_0 t = \sin (90 - \omega_0 t)$$

$$\sin 2\alpha = \sin 2\omega_0 t$$

Substituting into equations (G63) through (G65), by way of equations (G47) through (G49), the solar torques become:

$$T_{\dot{\phi}} = 0 \quad (G67)$$

$$T_{\dot{\theta}} = C_1 \sin 2\omega_0 t \quad (G68)$$

$$T_{\dot{\psi}} = 0 \quad (G69)$$

APPENDIX G

Note that $T_{\dot{\theta}}$ is an external pitch torque, T_y , in the equations of motion previously derived. We may therefore normalize to obtain the final form of the Case I solar torque forcing function as follows:

$$T_y'' = \frac{T_y}{I_{x-x} \omega_0^2} = \frac{C_1 \sin 2 \omega_0 t}{I_{x-x} \omega_0^2} \quad (G70)$$

For Case II, using equation (G66),

$$\tan \beta = \frac{\cos \gamma \sin \omega_0 t + \sin \gamma}{\sin \gamma \sin \omega_0 t - \cos \gamma}$$

using the identities:

$$\tan \beta = \sqrt{\sec^2 \beta - 1}$$

$$\cos \beta = 1/\sec \beta$$

$$\sin \beta = \cos \beta \tan \beta$$

then:

$$\sin \beta = \frac{\cos \gamma \sin \omega_0 t + \sin \gamma}{\sqrt{1 + \sin^2 \omega_0 t}}$$

$$\cos \beta = \frac{\sin \gamma \sin \omega_0 t - \cos \gamma}{\sqrt{1 + \sin^2 \omega_0 t}}$$

and for α , first let

$$C_2 = 1/\sqrt{2}$$

then

$$\sin \alpha = \frac{\cos \omega_0 t}{\sqrt{2}}$$

$$\cos \alpha = \sqrt{1 - \sin^2 \alpha}$$

therefore:

$$\sin 2\alpha = \cos \omega_0 t \sqrt{1 + \sin^2 \omega_0 t}$$

Substituting into Equations (G63) through (G65) by way of equations (G47) through (G49), the solar torques become:

$$T_{\dot{\phi}} = C_1 \cos \omega_0 t \quad (G71)$$

$$T_{\dot{\theta}} = \frac{C_1}{2} \sin 2\omega_0 t \quad (G72)$$

$$T_{\dot{\psi}} = 0 \quad (G73)$$

APPENDIX G

Note that $T_{\dot{\theta}}$ is the torque T_x , and $T_{\dot{\phi}}$ is the torque T_y in the equations of motion previously derived. We may therefore normalize to obtain the final form of the Case II solar torque forcing functions as follows:

$$T_x'' = \frac{T_x}{I_{x-x} \omega_0^2} = \frac{C_1 \cos \omega_0 t}{I_{x-x} \omega_0^2} \quad (G74)$$

$$T_y'' = \frac{T_y}{I_{x-x} \omega_0^2} = \frac{C_1 \sin 2\omega_0 t}{2I_{x-x} \omega_0^2} \quad (G75)$$

Fixed and Damper Boom Solar Torques

Boom solar torques are derived by obtaining the force on each boom due to solar pressure, and then multiplying by the respective moment arms to the satellite center-of-mass. Both the fixed and damper booms have the same configuration and coincident mass centers. This permits the derivation of solar force to be made for one boom and applied to both. Since boom force is the integral of pressure acting over the area, the resultant solar force, due to symmetry, acts at the boom mass centers.

The solar force on the booms is derived for one specified pair of booms and three specific positions of the sun relative to the satellite's orbit. The force is then broken down into components and plotted as a function of satellite orbital position. These forces are then generalized into forcing functions for use with the equations of motion.

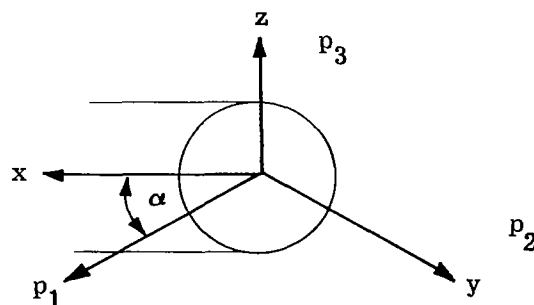
For purposes of deriving the solar force, the following assumptions will be made:

- (1) The sun is at infinity and therefore all rays are parallel.
- (2) All solar radiation is specularly reflected.
- (3) Vehicle motion is negligible (sun line orientation is constant relative to the booms).

The expression for force on the booms due to solar pressure will now be derived. First the coordinate systems as shown in the sketches below are defined.

$\hat{x}, \hat{y}, \hat{z}$ The unit vectors aligned with the cylinder.

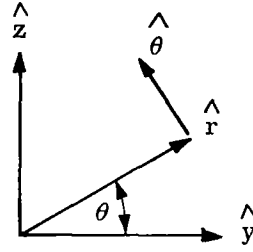
$\hat{p}_1, \hat{p}_2, \hat{p}_3$ The unit vectors with \hat{p}_1 aligned with the sun.



Boom coordinates for solar pressure

APPENDIX G

$\hat{r}, \hat{\theta}, \hat{x}$ Unit vectors aligned with the cylinder, \hat{r} the normal, $\hat{\theta}$ the tangent.



Boom cylindrical coordinate unit vectors

The transformations are written as follows:

$$\begin{bmatrix} \hat{p}_1 \\ \hat{p}_2 \\ \hat{p}_3 \end{bmatrix} = [A] \begin{bmatrix} \hat{x} \\ \hat{y} \\ \hat{z} \end{bmatrix}, \quad [A] = \begin{bmatrix} \cos \alpha & \sin \alpha & 0 \\ -\sin \alpha & \cos \alpha & 0 \\ 0 & 0 & 1 \end{bmatrix}$$

$$\begin{bmatrix} \hat{x} \\ \hat{y} \\ \hat{z} \end{bmatrix} = [B] \begin{bmatrix} \hat{r} \\ \hat{\theta} \\ \hat{\phi} \end{bmatrix}, \quad [B] = \begin{bmatrix} 1 & 0 & 0 \\ 0 & \cos \theta & -\sin \theta \\ 0 & \sin \theta & \cos \theta \end{bmatrix}$$

In terms of the above defined coordinate systems, the force on an element of area due to specularly reflected solar radiation is given as:

$$d\vec{F} = -\mu_2 \frac{P_i}{C} dA (\hat{p}_1 \cdot \hat{r})^2 \hat{r} \quad (G76)$$

where

$$P_i/C = 9.65 \times 10^{-8} \text{ lb/ft}^2$$

$$\mu = 1 \text{ (assuming total reflectance)}$$

$$dA = r d\theta dx$$

and evaluating $(\hat{p}_1 \cdot \hat{r})$ using the transformations defined above:

$$(\hat{p}_1 \cdot \hat{r}) = \sin \alpha \cos \theta.$$

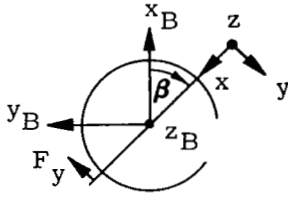
The total force in the y direction (cylinder normal force) can now be obtained using the transformations above:

$$F_y = \vec{F} \cdot \hat{y} = - \int_0^l \int_{-\pi/2}^{\pi/2} (2\mu P_i/C) (r d\theta dx) (\sin \alpha \cos \theta)^2 \cos \theta \quad (G77)$$

$$F_y = - \left(2\mu \frac{P}{C} \right) (r l) \frac{4}{3} \quad (G78)$$

The force (F_y) can now be expressed in satellite body coordinates through the use of the sketch on the following page.

APPENDIX G



$$\left. \begin{aligned} F_{yB} &= F_y \sin \beta \\ F_{xB} &= F_y \cos \beta \end{aligned} \right\} \quad (G79)$$

Equations (G78) and (G79) are now used to evaluate the boom solar forces for three conditions. Case I assumes the sun is in the orbital plane. The results are presented in figure G1 along with the specified boom dimensions and attitudes. Note that the sun may be broken down into components, and each component evaluated separately. Note also that F_{zB} is omitted because it contributes no moment.

Case II assumes that the sun is inclined 45 degrees to the orbital plane. The results are presented in figure G2. Again, the solar force is obtained from equations (G78) and (G79) and resolving of the sun components.

Case III assumes the sun is normal to the orbital plane. The results are constant around the orbit and are tabulated below:

$$F_{xB} = -0.0009 \times 10^{-4} \text{ lb}$$

$$F_{yB} = 0.1416 \times 10^{-4} \text{ lb}$$

A generalized forcing function will now be derived for use in the equations of motion. Note that the forces (F_y and F_x) shown in figures G1 and G2 may be written as:

$$\left. \begin{aligned} F_{yB} &= F_{y0} + F_{y1} \sin \omega_0 t \\ F_{xB} &= F_{x0} + F_{x1} \sin \omega_0 t \end{aligned} \right\} \quad \text{where the phase angles are negligible.}$$

The torques may now be written as:

$$T_{xB} = h (F_{y0} + F_{y1} \sin \omega_0 t) \quad (G80)$$

$$T_{yB} = h (F_{x0} + F_{x1} \sin \omega_0 t) \quad (G81)$$

where h is the moment arm from boom c. m. to satellite c. m. Equations (G80) and (G81) are for a specific boom length of 1200 ft and a radius of one-half inch. The equations may be generalized for any boom length and diameter by the following corrections:

$$T_{yB} = h (F_{y0} + F_{y1} \sin \omega_0 t) (L/600) (2r) \quad (G82)$$

$$T_{xB} = h (F_{x0} + F_{x1} \sin \omega_0 t) (L/600) (2r) \quad (G83)$$

where L is the new boom semi-length in feet and r is the new boom radius in inches. It only remains to resolve the torques equations, (G82) and (G83), into the pitch and roll axes used in the equations of motion, and to normalize. Since the assumption was made originally that the torques may be treated as steady-state, the transformation to the generalized coordinates is written in final normalized form:

$$T_{yB}'' = (T_{xB} \sin \gamma + T_{yB} \cos \gamma) \frac{1}{\omega_0^2 I_{x-x}} \quad (G84)$$

$$T_{xB}'' = (T_{xB} \cos \gamma - T_{yB} \sin \gamma) \frac{1}{\omega_0^2 I_{x-x}} \quad (G85)$$

where T_{yB} and T_{xB} are given in equations (G82) and (G83). Note now for a fixed γ we may write $\sin \gamma$ and $\cos \gamma$ as constants. Therefore, the final form of the torque equations is written:

$$T_{yB}'' = \frac{h}{I_{x-x} \omega_0^2} \left(\frac{Lr}{300} \right) (F_{y0}' + F_{y1}' \sin \omega_0 t)$$

$$T_{xB}'' = \frac{h}{I_{x-x} \omega_0^2} \left(\frac{Lr}{300} \right) (F_{x0}' + F_{x1}' \sin \omega_0 t)$$

where the primed terms contain both F_x and F_y terms.

Summary

The derivation of the linearized rotational equations of motion for the lenticular satellite with a modified Ames damper system has been completed. The equations are valid for the satellite in a circular orbit and include the torques due to gravity gradient. The orientation of the satellite relative to an attitude reference frame, and the damper attitude relative to the satellite, may be obtained by integrating equations (G23) through (G26). The integration provides the transient response when the torques are set equal to zero. The steady-state response to external forces may be analyzed by applying the proper torque expressions that simulate specific torque inputs.

A torque input (forcing function) that simulates the effect of orbital eccentricity has been derived. When equation (G43) is used in the equations of motion, the steady-state response to eccentricity may be evaluated.

Torque inputs simulating the effect of solar pressure have been derived for specific cases. For the sun at 0 and 45 degrees to the orbital plane, the expressions for the effect of solar pressure on the basic satellite are derived. Solar pressure on the damping booms is also derived for the sun at 0 and 45 degrees to the orbital plane. In addition, the booms are expected to produce the largest hang-off error when the sun is at 90 degrees to the orbital plane. This torque has also been derived. Use of these solar torque expressions will permit the evaluation of steady-state response due to solar pressure.

This appendix has covered the derivation of the linearized equations of motion, and certain of the important disturbing torques. These equations were used in the simulation of the rotational dynamics of the gravity-gradient stabilized lenticular satellite.

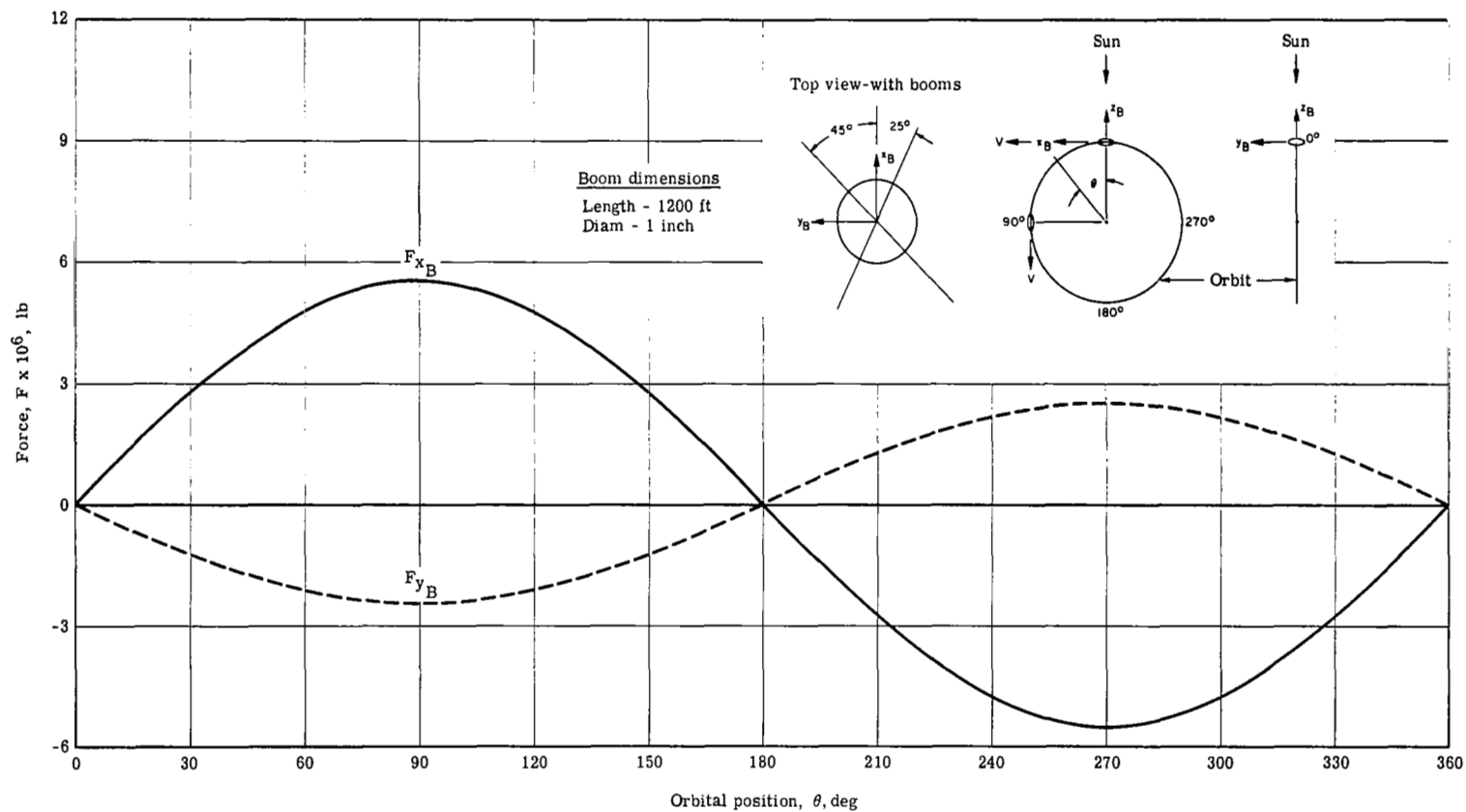


Figure G1. - Solar pressure force on damper booms with sun line in orbital plane

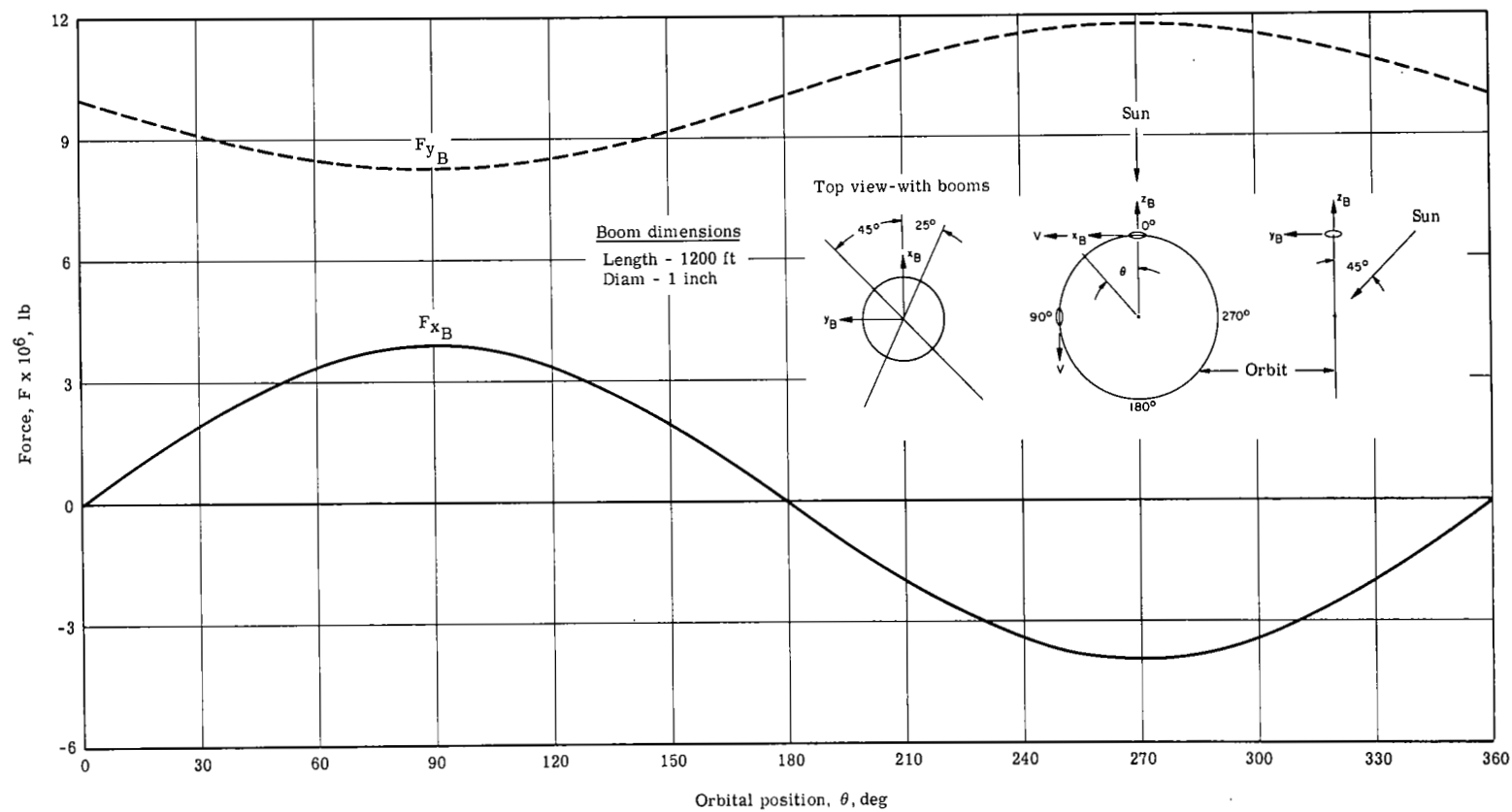


Figure G2. - Solar pressure force on damper booms with sun line 45° to orbital plane

APPENDIX H

DERIVATION OF REALIZABLE DAMPER BOOM MASS MOMENT OF INERTIA

General

The damper boom is one of the two booms of the X arrangement in the Ames stabilization system. The DeHavilland tube scheme has been considered, with General Electric's Consil 995 material with 160° nominal overlap. This material consists of 99.5 percent silver, 0.3 percent magnesium, and 0.2 percent nickel. For convenience the physical and mechanical properties of this material are given below (ref. 13):

Ultimate strength, $F_{TU} = 60\,000$ psi

Yield strength, $F_{TY} = 50\,000$ psi

Young's modulus, $E = 13 \times 10^6$ psi

Solar absorptivity, $\alpha = 0.09$

Thermal conductivity, $K = 155$ Btu/hr-ft-°F

Coefficient of thermal expansion, $\mu = 10 \times 10^{-6}$ in./in.-°F

Density, $w = 0.380$ lb/in.³

In order for the damper to operate efficiently and reliably, the maximum tip deflection should be held as low as possible. Furthermore, for maximum utilization of the damper weight the distribution of rod mass and tip mass should be such that for a prescribed tip deflection the mass moment of inertia of the damper about its midpoint be a maximum.

Critical Conditions

Critical condition for the damper boom deflections are

- (1) Solar heating
- (2) Static condition due to normal flight (gravity-gradient and inertia loads)
- (3) Tumbling of the satellite at the rate of five times per orbit.

Since solar heating can be present with either the second or third conditions listed above, the following two cases have been considered:

- (1) Solar heating and static condition
- (2) Solar heating and tumbling at the rate of 5ω

For each of these two cases, maximum tip deflection equations are derived below.

APPENDIX H

Solar heating and static condition. - The temperature differential across the diameter of the boom is given by the equation

$$\Delta T = \frac{\alpha S r^2}{K t} \sin \psi \quad (\text{ref. 13})$$

where $S = 440 \text{ Btu/hr-ft}^2$ (solar radiation constant). Substituting numerical values $K = 155$, $\psi = 90^\circ$, $\alpha = 0.09$ yields

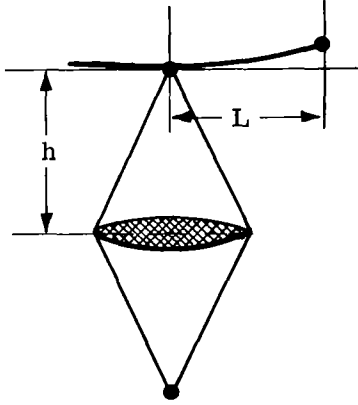
$$\Delta T = \frac{0.09(440)}{155 \times 12} \frac{r^2}{t} = 0.0213 \frac{r^2}{t} \quad (\text{H1})$$

The optimum relationship between r and t is $F_{TY} = \frac{Et}{2r}$ from which ($F_{TY} = 50\,000$, $E = 13 \times 10^6 \text{ psi}$)

$$t = \frac{r}{130} \quad (\text{H2})$$

Substituting equation (H1) into equation (H2) yields

$$\Delta T = 2.77r \text{ } [^\circ\text{F}] \quad (r \text{ in inches}) \quad (\text{H3})$$



The thermal tip deflection δ_T is given by

$$\delta_T \cong \frac{\mu \Delta T L^2}{4 r} = \frac{10^{-5} (2.77) L^2}{4}$$

or

$$\delta_T \cong 0.6925 \times 10^{-5} L^2 \quad (\text{H4})$$

An upper limit for the damper boom half-length, L , can be determined from equation (H4),

$$L_{\max} = 1.444n \times 10^5 \text{ in.}, \quad (\text{H5})$$

where n is the ratio $\delta_{T(\max)}/L$. Let W_T = weight of concentrated tip mass and W_R = weight of half rod. Then the total weight W of the damper is given by the equation

$$W = 2 (W_T + W_R) \quad (\text{H6})$$

With the damper boom normal to the orbital plane, the tip deflection due to gravity-gradient forces is

$$\delta_B = \left(\frac{W_T L^3}{3EI} + \frac{W_R L^3}{8EI} \right) \frac{3\omega^2 h}{g} \quad (\text{H7})$$

where ω is the orbit angular velocity of the satellite, h is the height of the tetrapod, and $g = 386 \text{ in./sec}^2$ (ref. 14, page 7). The total tip deflection, δ , expressed as a multiple of L , is

$$\delta = nL = 0.6925L^2 \times 10^{-5} + \frac{3\omega^2 h L^3}{gEI} \left(\frac{W_T}{3} + \frac{W_R}{8} \right) \quad (\text{H8})$$

Weight of half-rod W_R :

$$W_R = \frac{360 + 160}{360} 2\pi r t (0.380)L = \frac{52}{36} (2\pi)(0.38) \frac{r^2 L}{130}$$

APPENDIX H

or

$$W_R = 0.02653 r^2 L \quad (H9)$$

Substituting equation (H9) into equation (H6) and solving for W_T yields

$$W_T = \frac{W}{2} - 0.02653 r^2 L. \quad (H10)$$

Substituting equations (H9) and (H10) into equation (H8), and noting that $E = 13 \times 10^6$,

$$I \cong \pi r^3 t = \frac{\pi}{130} r^4.$$

Simplifying yields

$$n - 0.6925 \times 10^{-5} L - 0.02474 \times 10^{-6} \frac{\omega^2 h L^2}{r^4} \left(\frac{W}{6} - 0.005527 r^2 L \right) = 0$$

or

$$F(L, r) = 10^6 n r^4 - 6.925 r^4 L - 0.02474 \omega^2 h L^2 \left(\frac{W}{6} - 0.005527 r^2 L \right) = 0 \quad (H11)$$

Equation (H11) can be thought of as a constraint between L and r , when n (see eq. H8) and W (see eq. H6) are given quantities.

The problem now is to determine the maximum value of the quantity

$$\begin{aligned} I_d &= 2 \left(W_T L^2 + \frac{1}{3} W_R L^2 \right) = L^2 \left(W - \frac{4}{3} W_R \right) \\ &= 2L^2 \left(\frac{W}{2} - 0.01769 r^2 L \right) \end{aligned} \quad (H12)$$

with the quantities L and r subjected to the constraint (eq. H11).

Hence,

$$\frac{dI_d}{dL} = 0 = 2LW - 6L^2 r^2 (0.01769) - 4L^3 r (0.01769) \frac{dr}{dL}$$

or

$$\frac{W}{2} - 0.02653 r^2 L - 0.01769 r L^2 \frac{dr}{dL} = 0 \quad (H13)$$

where

$$\frac{dr}{dL} = - \frac{\frac{\partial F(r, L)}{\partial L}}{\frac{\partial F(r, L)}{\partial r}} = \frac{6.925 r^4 + 0.02474 \omega^2 h \left(\frac{WL}{3} - 0.016581 r^2 L^2 \right)}{4r^3 n \times 10^6 - 27.7 r^3 L + 0.0002734 \omega^2 h L^3 r} \quad (H14)$$

Substituting equation (H14) into (H13) yields

$$\frac{W}{2} - 0.02653 r^2 L - 0.01769 r L^2 \left[\frac{6.925 r^4 + 0.02474 \omega^2 h \left(\frac{WL}{3} - 0.016581 r^2 L^2 \right)}{4r^3 n \times 10^6 - 27.7 r^3 L + 0.0002734 \omega^2 h L^3 r} \right] = 0 \quad (H15)$$

APPENDIX H

For $n = 1/10$ (tip deflection to boom semi-length ratio), equations (H11) and (H15) solved for r and W yield

$$r^2 = L^3 \omega^2 h \frac{4.335 - 0.0001738L + \sqrt{(4.335 - 0.0001738L)^2 + 6.2882(1 - 0.00006925L)^2}}{(10^5 - 6.925L)^2}$$

$$W = \frac{10^5 r^4 + 13.67 \times 10^{-5} r^2 L^3 \omega^2 h - 6.925 r^4 L}{0.004123 L^2 \omega^2 h}$$

Table H1 is the digital computer output for corresponding values of L , r , $\omega^2 h$, W and $I_d(\max)$. The numerical values of Table H1 have been graphically represented in figures H1, H2, and H3. Figure H3 has been crossplotted from figures H1 and H2.

Solar heating and tumbling about pitch axis at the rate of 5ω . - With the damper boom in the orbital plane and normal to the axis of the satellite, when the latter is along the local vertical the forces of a tumbling satellite are (from ref. 10, appendix C, pp. C-2 and C-3):

$$dF_x = \left[-3\omega^2 (z \sin \alpha \cos \alpha - x \sin^2 \alpha) + \omega_0^2 x - 2\omega \omega_0 x + \frac{3}{2} \omega^2 \lambda x \sin 2\alpha \right] dm$$

$$dF_y = -\omega^2 y dm$$

$$dF_z = \left[-3\omega^2 (x \sin \alpha \cos \alpha - z \cos^2 \alpha) + \omega_0^2 z - 2\omega \omega_0 z - \frac{3}{2} \omega^2 \lambda x \sin 2\alpha \right] dm$$

where

$$\lambda = (I_y - I_z)/I_z \text{ and } \alpha = 0^\circ, y = 0, z = h.$$

For $\omega_0 = -4\omega$ (tumbling angular velocity about the pitch axis equal to 5ω . i.e., ω required for proper orientation of satellite with respect to the local vertical, plus additional 4ω) and with the above numerical values for α , y , and z , the above equations become:

$$dF_x = x (16\omega^2 + 8\omega^2) dm = 24 \omega^2 x dm$$

$$dF_y = 0$$

$$dF_z = h (3\omega^2 + 16 \omega^2 + 8\omega^2) = 27\omega^2 h dm.$$

Neglecting the straightening effect of the forces dF_x , the damper boom is subjected to uniformly distributed (due to rod's own weight) and concentrated tip loads (end masses) described by equation $dF_z = 27\omega^2 h dm$. The optimization of the damper rod coincides with the case previously considered, with the only difference in the coefficient in $\omega^2 h$, which here is 27 instead of 3 as in the previous analysis. As a consequence, the only difference between the solution of the present problem and the previous one is that here the quantity $\omega^2 h$ should be read as $9\omega^2 h$. Therefore for $n = 0.1$,

$$r^2 = 9L^3 \omega^2 h \frac{4.335 - 0.0001738L + \sqrt{(4.335 - 0.0001738L)^2 + 6.2882(1 - 0.00006925L)^2}}{(10^5 - 6.925L)^2}$$

$$W = \frac{10^5 r^4 + 123.03 \times 10^{-5} r^2 L^3 \omega^2 h - 6.925 r^4 L}{0.037107 L^2 \omega^2 h}$$

$$I_d = 2L^2 \left(\frac{W}{2} - 0.01769 r^2 L \right)$$

APPENDIX H

$$W_R = 0.02653r^2L \text{ (half rod weight)}$$

$$W_T = \frac{W}{2} - W_R = \frac{W}{2} - 0.02653r^2L \text{ (tip mass weight)}$$

The quantities r , W , W_R , W_T , and I_d were determined for $w^2h = 10^{-5}$, 10^{-4} , 10^{-3} , and 10^{-2} , and $L = 600, 1200, 1800, 2400, \dots, 9000$ inch and the computer output is given in table H2. Figures H4 through H6 are graphical representations of the numerical values of table H2.

TABLE H1. - COMPUTER DATA FOR THE SOLAR HEATING AND STATIC CONDITION

LENGTH L, in	ω^2h in./sec ²	ROD RADIUS r, in.	DAMPER WT W, lb	HALF ROD WT W _R , lb	TIP MASS WT W _T , lb	MAX INERT MO I _{d(max)} , lb-in. ²
600.	1.00000E-05	1.46249E-03	7.20907E-05	3.40468E-C5	1.99856E-C6	9.60711E-C0
600.	1.00000E-04	4.62481E-03	7.20907E-04	3.40468E-C4	1.99856E-05	9.60711E 01
600.	1.00000E-02	1.46249E-02	7.20907E-03	3.40468E-C3	1.99856E-04	9.60711E 02
600.	1.00000E-07	4.62481E-02	7.20907E-02	3.40468E-C2	1.99856E-03	9.60711E 03
1200.	1.00000E-05	4.26508E-03	1.23479E-03	5.79125E-C4	3.82705E-C5	6.65969E 02
1200.	1.00000E-04	1.34874E-02	1.23479E-02	5.79125E-C3	3.82705E-04	6.65969E 03
1200.	1.00000E-03	4.26508E-02	1.23479E-01	5.79125E-C2	3.82705E-03	6.65969E 04
1200.	1.00000E-02	1.34874E-01	1.23479E-00	5.79125E-C1	3.82705E-02	6.65969E 05
1800.	1.00000E-05	8.09254E-03	6.71875E-03	3.12737E-C3	2.32004E-04	8.25596E 03
1800.	1.00000E-04	2.55909E-02	6.71875E-02	3.12737E-C2	2.32004E-03	8.25596E 04
1800.	1.00000E-03	8.09254E-02	6.71875E-01	3.12737E-C1	2.32004E-02	8.25596E 05
1800.	1.00000E-02	2.55909E-01	6.71875E-00	3.12737E-C0	2.32004E-01	8.25596E 06
2400.	1.00000E-05	1.28922E-02	2.29248E-02	1.05828E-C2	8.79585E-04	5.07555E 04
2400.	1.00000E-04	4.07686E-02	2.29248E-01	1.05828E-C1	8.79585E-03	5.07555E 05
2400.	1.00000E-03	1.28922E-01	2.29248E-00	1.05828E-C0	8.79585E-02	5.07555E 06
2400.	1.00000E-02	4.07686E-01	2.29248E 01	1.05828E 01	8.79585E-01	5.07555E 07
3000.	1.00000E-05	1.86822E-02	6.07248E-02	2.77788E-C2	2.58356E-03	2.13114E 05
3000.	1.00000E-04	5.90783E-02	6.07248E-01	2.77788E-C1	2.58356E-02	2.13114E 06
3000.	1.00000E-03	1.86822E-01	6.07248E-00	2.77788E-C0	2.58356E-01	2.13114E 07
3000.	1.00000E-02	5.90783E-01	6.07248E 01	2.77788E C1	2.58356E-00	2.13114E 08
3600.	1.00000E-05	2.55239E-02	1.37385E-01	6.22204E-C2	6.47201E-03	7.05136E 05
3600.	1.00000E-04	8.07136E-02	1.37385E-00	6.22204E-C1	6.47201E-02	7.05136E 06
3600.	1.00000E-03	2.55239E-01	1.37385E 01	6.22204E-C0	6.47201E-01	7.05136E 07
3600.	1.00000E-02	8.07136E-01	1.37385E 02	6.22204E C1	6.47201E-00	7.05136E 08
4200.	1.00000E-05	3.35159E-02	2.79460E-01	1.25166E-C1	1.45635E-02	1.98520E 06
4200.	1.00000E-04	1.05986E-01	2.79460E-00	1.25166E-C0	1.45635E-01	1.98520E 07
4200.	1.00000E-03	3.35159E-01	2.79460E 01	1.25166E C1	1.45635E-00	1.98520E 08

APPENDIX H

TABLE H1. - COMPUTER DATA FOR THE SOLAR
HEATING AND STATIC CONDITION - Concluded

LENGTH L, in.	$\omega^2 h$ in./sec ²	ROD RADIUS r, in.	DAMPER WT W, lb	HALF ROD WT W _R , lb	TIP MASS WT W _T , lb	MAX INRT MO I _{d(max)} , lb-in. ²
4200.	1.00000E-02	1.05986E-00	2.79460E 02	1.25166E C2	1.45635E 01	1.98520E 09
4800.	1.00000E-05	4.27966E-02	5.27238E-01	2.33237E-C1	3.03820E-C2	4.98117E 06
4800.	1.00000E-04	1.35335E-01	5.27238E-00	2.33237E-C0	3.03820E-01	4.98117E 07
4800.	1.00000E-03	4.27966E-01	5.27238E 01	2.33237E C1	3.03820E-C0	4.98117E 08
4800.	1.00000E-02	1.35335E-00	5.27238E 02	2.33237E C2	3.03820E 01	4.98117E 09
5400.	1.00000E-05	5.35521E-02	9.41723E-01	4.10851E-C1	6.00101E-02	1.14837E 07
5400.	1.00000E-04	1.69347E-01	9.41723E-00	4.10851E-C0	6.00101E-01	1.14837E 08
5400.	1.00000E-03	5.35521E-01	9.41723E 01	4.10851E C1	6.00101E-00	1.14837E 09
5400.	1.00000E-02	1.69347E-00	9.41723E 02	4.10851E C2	6.00101E 01	1.14837E 10
6000.	1.00000E-05	6.60296E-02	1.61588E-00	6.94011E-C1	1.13932E-01	2.48531E 07
6000.	1.00000E-04	2.08804E-01	1.61588E 01	6.94011E-C0	1.13932E-C0	2.48531E 08
6000.	1.00000E-03	6.60296E-01	1.61588E 02	6.94011E C1	1.13932E 01	2.48531E 09
6000.	1.00000E-02	2.08804E-00	1.61588E 03	6.94011E C2	1.13932E 02	2.48531E 10
6600.	1.00000E-05	8.05584E-02	2.69332E-00	1.13633E-C0	2.10335E-01	5.13109E 07
6600.	1.00000E-04	2.54748E-01	2.69332E 01	1.13633E C1	2.10335E-C0	5.13109E 08
6600.	1.00000E-03	8.05584E-01	2.69332E 02	1.13633E C2	2.10335E 01	5.13109E 09
6600.	1.00000E-02	2.54748E-00	2.69332E 03	1.13633E C3	2.10335E 02	5.13109E 10
7200.	1.00000E-05	9.75822E-02	4.40026E-00	1.81891E-C0	3.81220E-C1	1.02363E 08
7200.	1.00000E-04	3.08582E-01	4.40026E 01	1.81891E C1	3.81220E-C0	1.02363E 09
7200.	1.00000E-03	9.75822E-01	4.40026E 02	1.81891E C2	3.81220E C1	1.02363E 10
7200.	1.00000E-02	3.08582E-00	4.40026E 03	1.81891E C3	3.81220E 02	1.02363E 11
7800.	1.00000E-05	1.17710E-01	7.10258E-00	2.86719E-C0	6.84099E-C1	1.99491E 08
7800.	1.00000E-04	3.72231E-01	7.10258E 01	2.86719E C1	6.84099E-C0	1.99491E 09
7800.	1.00000E-03	1.17710E-00	7.10258E 02	2.86719E C2	6.84099E 01	1.99491E 10
7800.	1.00000E-02	3.72231E-00	7.10258E 03	2.86719E 03	6.84099E 02	1.99491E 11
8400.	1.00000E-05	1.41795E-01	1.14120E 01	4.48062E-C0	1.22540E-C0	3.83617E 08
8400.	1.00000E-04	4.48395E-01	1.14120E 02	4.48062E C1	1.22540E C1	3.83617E 09
8400.	1.00000E-03	1.41795E-00	1.14120E 03	4.48062E C2	1.22540E 02	3.83617E 10
8400.	1.00000E-02	4.48395E-00	1.14120E 04	4.48062E C3	1.22540E 03	3.83617E 11
9000.	1.00000E-05	1.71073E-01	1.83952E 01	6.98781E-C0	2.20976E-C0	7.35181E 08
9000.	1.00000E-04	5.40979E-01	1.83952E 02	6.98781E C1	2.20976E 01	7.35181E 09
9000.	1.00000E-03	1.71073E-00	1.83952E 03	6.98781E C2	2.20976E 02	7.35181E 10
9000.	1.00000E-02	5.40979E-00	1.83952E 04	6.98781E C3	2.20976E 03	7.35181E 11

APPENDIX H

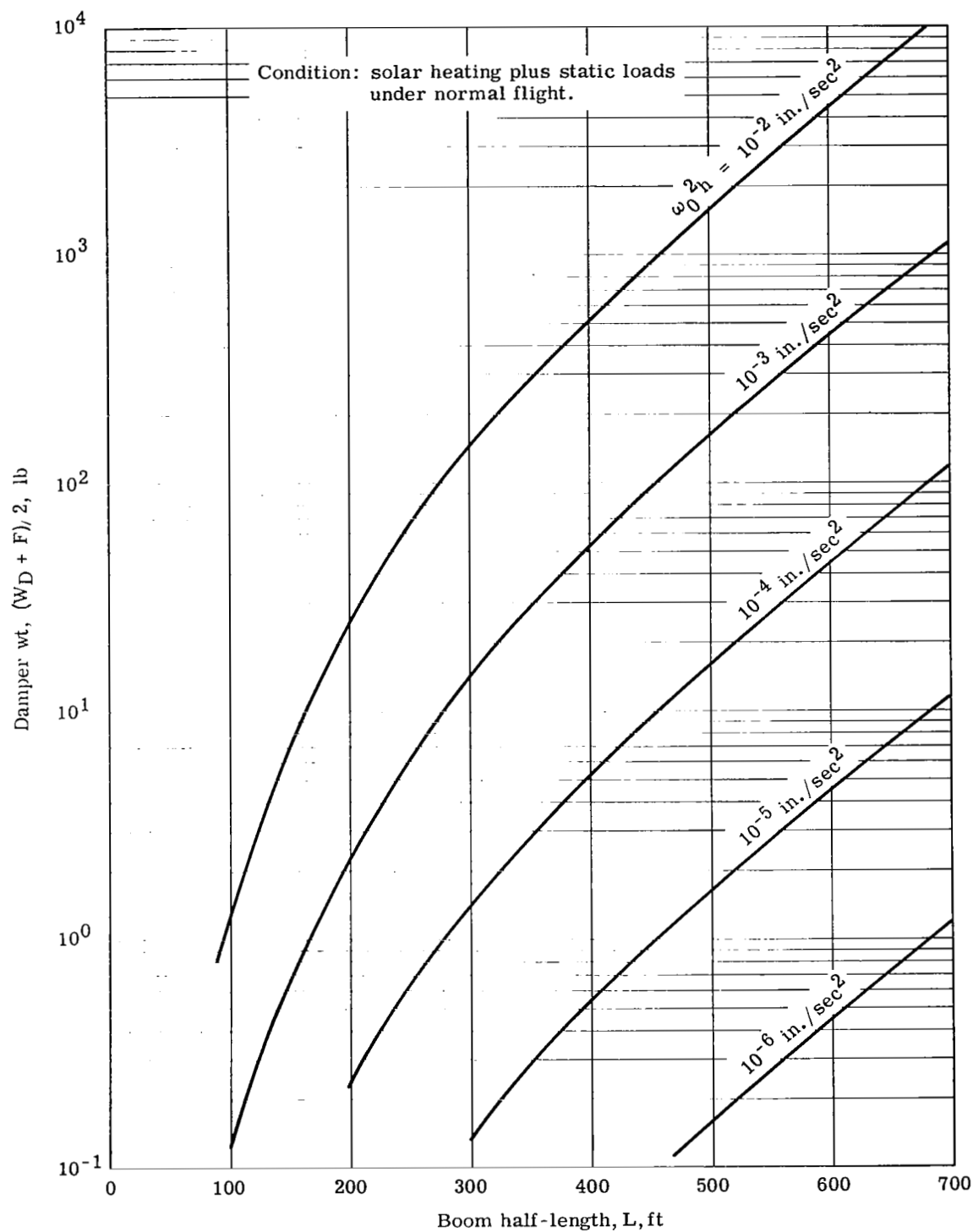


Figure H1. - Damper boom weight versus boom half-length for maximum mid-point mass moment of inertia for case 1.

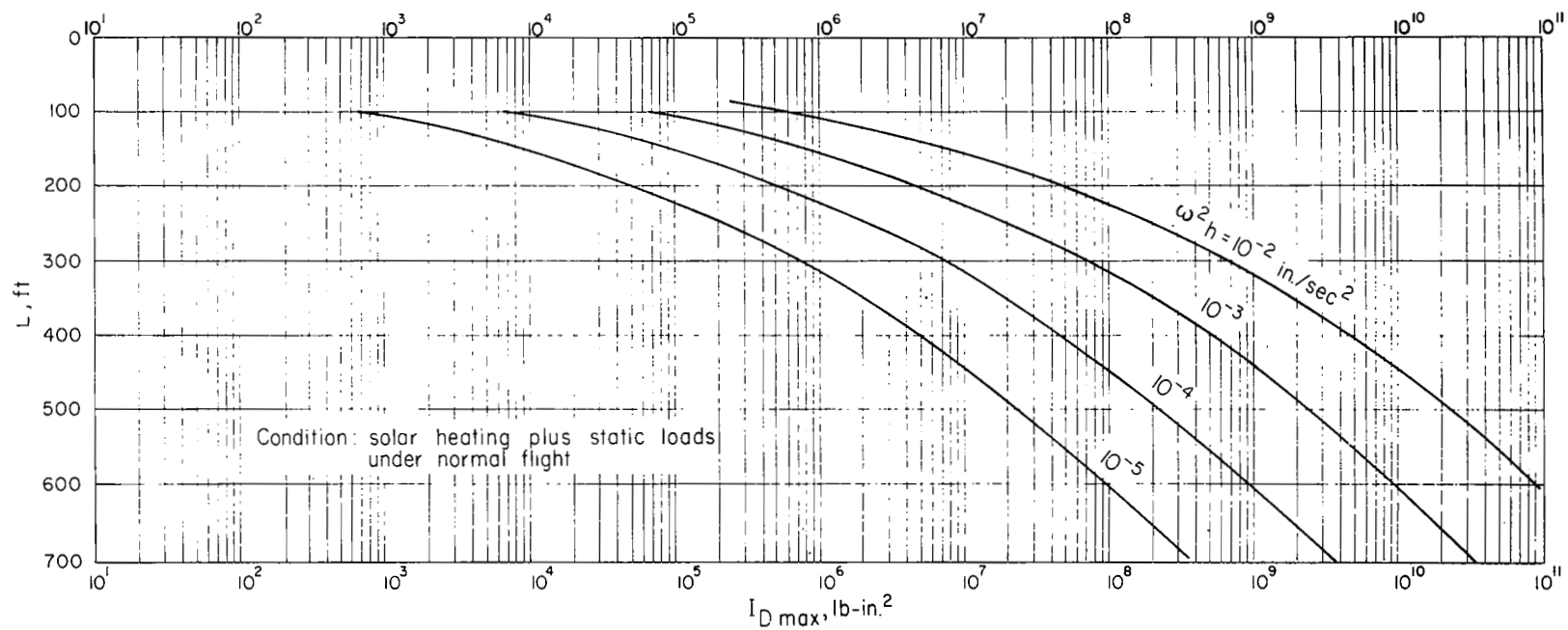


Figure H2. - Optimum mid-point mass moment of inertia of damper boom versus boom half-length - static condition,

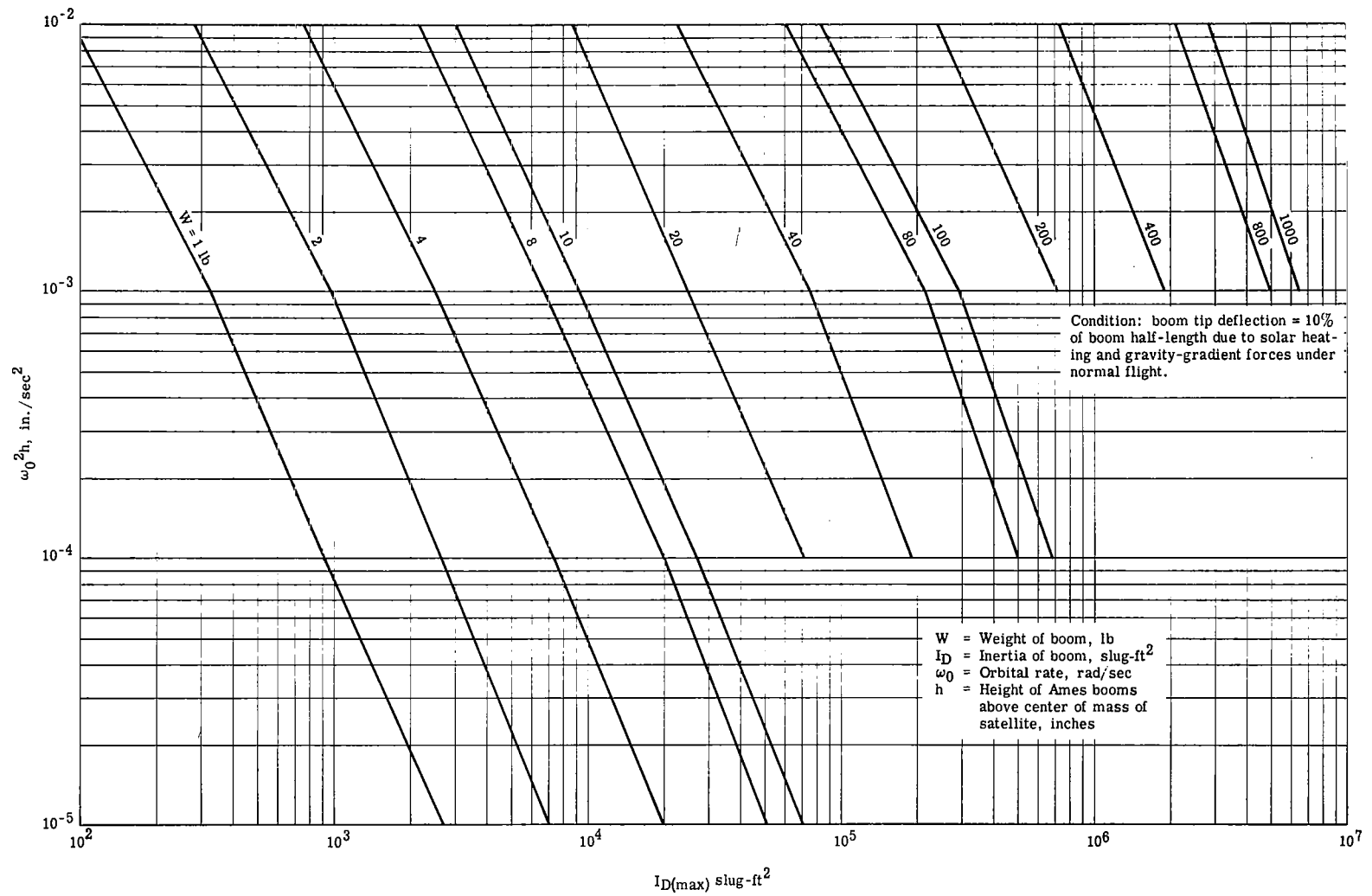


Figure H3. - Maximum moment of inertia of damper boom about its mid-point for case 1.

APPENDIX H

TABLE H2. - COMPUTER DATA FOR THE SOLAR HEATING AND
TUMBLING ABOUT THE PITCH AXIS CONDITION

LENGTH L, in.	$\omega^2 h$ in./sec ²	ROD RADIUS r, in.	DAMPER WT W, lb	HALF ROD WT W _R , lb	TIP MASS WT W _T , lb	MAX INRT MO I _{d(max)} , lb-in. ²
600.	1.00000E-05	4.38748E-03	6.48816E-04	3.06421E-04	1.79871E-05	8.64640E 01
600.	1.00000E-04	1.38744E-02	6.48816E-03	3.06421E-03	1.79871E-04	8.64640E 02
600.	1.00000E-03	4.38748E-02	6.48816E-02	3.06421E-02	1.79871E-03	8.64640E 03
600.	1.00000E-02	1.38744E-01	6.48816E-01	3.06421E-01	1.79871E-02	8.64640E 04
1200.	1.00000E-05	1.27952E-02	1.11131E-02	5.21212E-03	3.44434E-04	5.99372E 03
1200.	1.00000E-04	4.04621E-02	1.11131E-01	5.21212E-02	3.44434E-03	5.99372E 04
1200.	1.00000E-03	1.27952E-01	1.11131E-00	5.21212E-01	3.44434E-02	5.99372E 05
1200.	1.00000E-02	4.04621E-01	1.11131E 01	5.21212E-00	3.44434E-01	5.99372E 06
1800.	1.00000E-05	2.42776E-02	6.04687E-02	2.81463E-02	2.08804E-03	7.43036E 04
1800.	1.00000E-04	7.67726E-02	6.04687E-01	2.81463E-01	2.08804E-02	7.43036E 05
1800.	1.00000E-03	2.42776E-01	6.04687E-00	2.81463E-00	2.08804E-01	7.43036E 06
1800.	1.00000E-02	7.67726E-01	6.04687E 01	2.81463E 01	2.08804E-00	7.43036E 07
2400.	1.00000E-05	3.86765E-02	2.06323E-01	9.52452E-02	7.91626E-03	4.56799E 05
2400.	1.00000E-04	1.22306E-01	2.06323E-00	9.52452E-01	7.91626E-02	4.56799E 06
2400.	1.00000E-03	3.86765E-01	2.06323E 01	9.52452E-00	7.91626E-01	4.56799E 07
2400.	1.00000E-02	1.22306E-00	2.06323E 02	9.52452E 01	7.91626E-00	4.56799E 08
3000.	1.00000E-05	5.60466E-02	5.46523E-01	2.50009E-01	2.32520E-02	1.91803E 06
3000.	1.00000E-04	1.77235E-01	5.46523E-00	2.50009E-00	2.32520E-01	1.91803E 07
3000.	1.00000E-03	5.60466E-01	5.46523E 01	2.50009E 01	2.32520E-00	1.91803E 08
3000.	1.00000E-02	1.77235E-00	5.46523E 02	2.50009E 02	2.32520E 01	1.91803E 09
3600.	1.00000E-05	7.65716E-02	1.23646E-00	5.59984E-01	5.82480E-02	6.34622E 06
3600.	1.00000E-04	2.42141E-01	1.23646E 01	5.59984E-00	5.82480E-01	6.34622E 07
3600.	1.00000E-03	7.65716E-01	1.23646E 02	5.59984E 01	5.82480E-00	6.34622E 08
3600.	1.00000E-02	2.42141E-00	1.23646E 03	5.59984E 02	5.82480E 01	6.34622E 09
4200.	1.00000E-05	1.00548E-01	2.51514E-00	1.12650E-00	1.31071E-01	1.78668E 07
4200.	1.00000E-04	3.17959E-01	2.51514E 01	1.12650E 01	1.31071E-00	1.78668E 08
4200.	1.00000E-03	1.00548E-00	2.51514E 02	1.12650E 02	1.31071E 01	1.78668E 09
4200.	1.00000E-02	3.17959E-00	2.51514E 03	1.12650E 03	1.31071E 02	1.78668E 10
4800.	1.00000E-05	1.28390E-01	4.74514E-00	2.09913E-00	2.73438E-01	4.48305E 07
4800.	1.00000E-04	4.06004E-01	4.74514E 01	2.09913E 01	2.73438E-00	4.48305E 08
4800.	1.00000E-03	1.28390E-00	4.74514E 02	2.09913E 02	2.73438E 01	4.48305E 09

APPENDIX H

**TABLE H2. - COMPUTER DATA FOR THE SOLAR HEATING AND
TUMBLING ABOUT THE PITCH AXIS CONDITION - Concluded**

LENGTH L, in.	$\omega^2 h$ in./sec ²	ROD RADIUS r, in.	DAMPER WT W, lb	HALF ROD WT W _R , lb	TIP MASS WT W _T , lb	MAX INRT MO I _{d(max)} , lb-in. ²
4800.	1.00000E-02	4.06004E-00	4.74514E 03	2.09913E 03	2.73438E 02	4.48305E 10
5400.	1.00000E-05	1.60656E-01	8.47550E-00	3.69766E-00	5.40092E-01	1.03354E 08
5400.	1.00000E-04	5.08040E-01	8.47550E 01	3.69766E 01	5.40092E-00	1.03354E 09
5400.	1.00000E-03	1.60656E-00	8.47550E 02	3.69766E 02	5.40092E 01	1.03354E 10
5400.	1.00000E-02	5.08040E-00	8.47550E 03	3.69766E 03	5.40092E 02	1.03354E 11
6000.	1.00000E-05	1.98089E-01	1.45430E 01	6.24610E-00	1.02539E-00	2.23678E 08
6000.	1.00000E-04	6.26412E-01	1.45430E 02	6.24610E 01	1.02539E 01	2.23678E 09
6000.	1.00000E-03	1.98089E-00	1.45430E 03	6.24610E 02	1.02539E 02	2.23678E 10
6000.	1.00000E-02	6.26412E-00	1.45430E 04	6.24610E 03	1.02539E 03	2.23678E 11
6600.	1.00000E-05	2.41675E-01	2.42399E 01	1.02269E 01	1.89302E-00	4.61798E 08
6600.	1.00000E-04	7.64244E-01	2.42399E 02	1.02269E 02	1.89302E 01	4.61798E 09
6600.	1.00000E-03	2.41675E-00	2.42399E 03	1.02269E 03	1.89302E 02	4.61798E 10
6600.	1.00000E-02	7.64244E-00	2.42399E 04	1.02269E 04	1.89302E 03	4.61798E 11
7200.	1.00000E-05	2.92747E-01	3.96024E 01	1.63702E 01	3.43099E-00	9.21265E 08
7200.	1.00000E-04	9.25746E-01	3.96024E 02	1.63702E 02	3.43099E 01	9.21265E 09
7200.	1.00000E-03	2.92747E-00	3.96024E 03	1.63702E 03	3.43099E 02	9.21265E 10
7200.	1.00000E-02	9.25746E-00	3.96024E 04	1.63702E 04	3.43099E 03	9.21265E 11
7800.	1.00000E-05	3.53129E-01	6.39232E 01	2.58047E 01	6.15689E-00	1.79541E 09
7800.	1.00000E-04	1.11669E-00	6.39232E 02	2.58047E 02	6.15689E 01	1.79541E 10
7800.	1.00000E-03	3.53129E-00	6.39232E 03	2.58047E 03	6.15689E 02	1.79541E 11
7800.	1.00000E-02	1.11669E 01	6.39232E 04	2.58047E 04	6.15689E 03	1.79541E 12
8400.	1.00000E-05	4.25385E-01	1.02708E 02	4.03256E 01	1.10286E 01	3.45256E 09
8400.	1.00000E-04	1.34519E-00	1.02708E 03	4.03256E 02	1.10286E 02	3.45256E 10
8400.	1.00000E-03	4.25385E-00	1.02708E 04	4.03256E 03	1.10286E 03	3.45256E 11
8400.	1.00000E-02	1.34519E 01	1.02708E 05	4.03256E 04	1.10286E 04	3.45256E 12
9000.	1.00000E-05	5.13218E-01	1.65556E 02	6.28903E 01	1.98879E 01	6.61663E 09
9000.	1.00000E-04	1.62294E-00	1.65556E 03	6.28903E 02	1.98879E 02	6.61663E 10
9000.	1.00000E-03	5.13218E-00	1.65556E 04	6.28903E 03	1.98879E 03	6.61663E 11
9000.	1.00000E-02	1.62294E 01	1.65556E 05	6.28903E 04	1.98879E 04	6.61663E 12

APPENDIX H

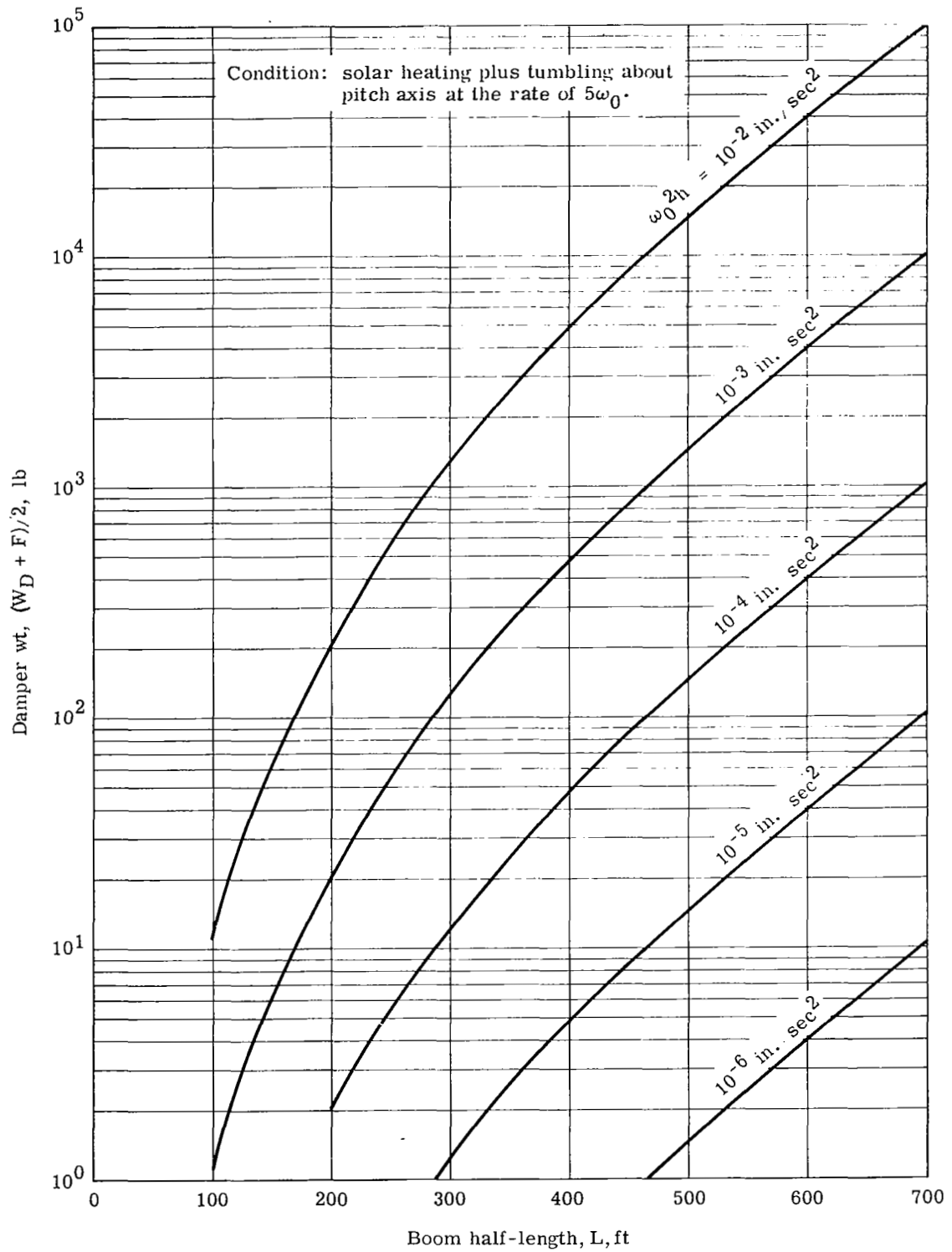


Figure H4. - Damper boom weight versus boom half-length for maximum mid-point moment of inertia for case 2.

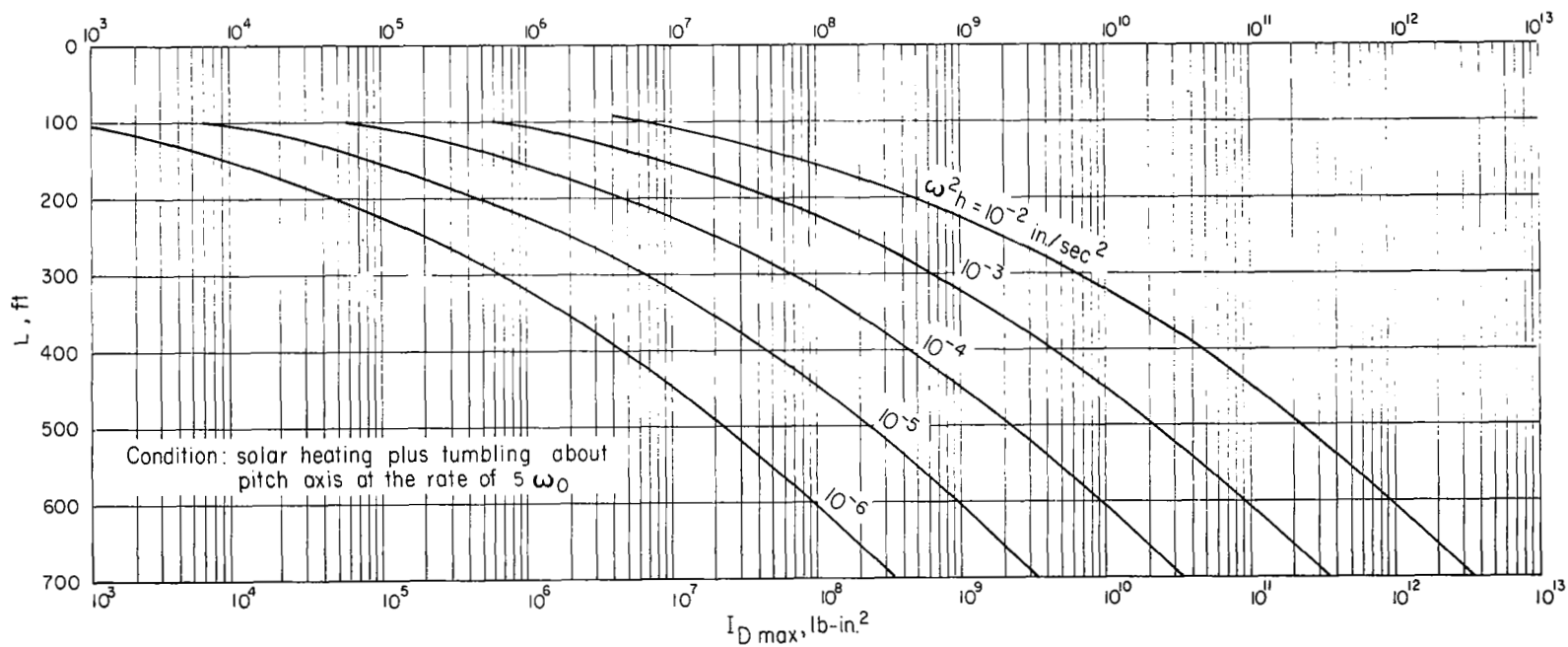


Figure H5. - Optimum mid-point mass moment of inertia of damper boom versus boom half-length - tumbling at $5\omega_0$.

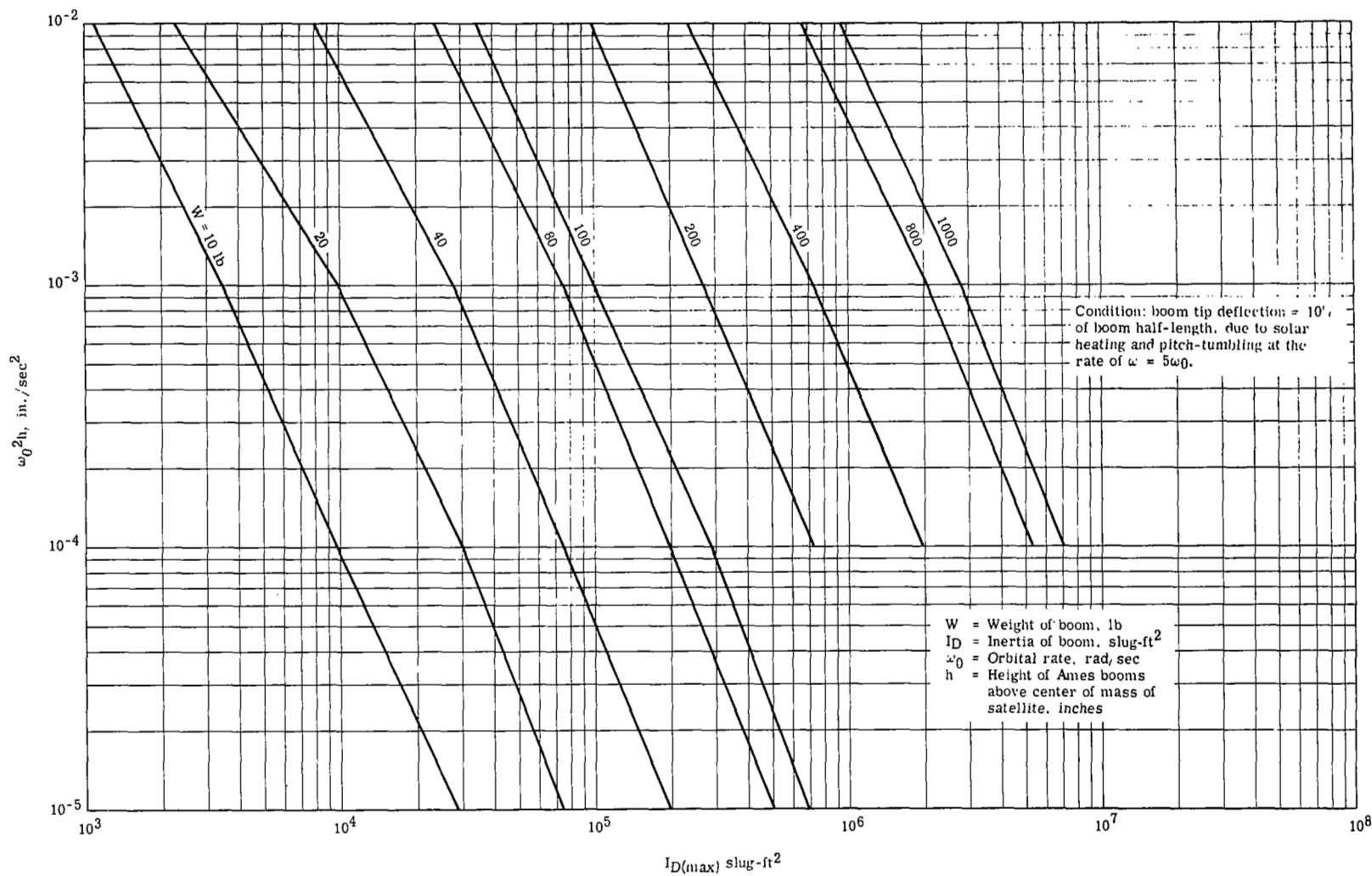


Figure H6. - Maximum moment of inertia of damper boom about its mid-point for case 2.

REFERENCES

1. Anon.: Feasibility Study and Preliminary Design of Gravity-Gradient-Stabilized Lenticular Test Satellite. Interim Technical Report, GER 11502 (Contract NAS 1-3114), Goodyear Aerospace Corp., June 1964.
2. Anon.: Study of a Passive Communication Gravity-Gradient-Stabilized Lenticular Satellite. Interim Summary Report, Goodyear Aerospace Corp., January 1965.
3. Timoshenko, S. P.; and Gere, J. M.: Theory of Elastic Stability. Second ed., McGraw Hill Book Company, Inc., 1961.
4. Anon.: Study of Methods of Structurally Evaluating Expandable Structures Having Potential Space Applications. GER 10938, Quarterly Progress Report No. Two (Contract NAS W-471), Goodyear Aerospace Corp., Feb. 1963.
5. Tinling, Bruce E.; and Merrick, Vernon K.: Exploitation of Inertial Couplings in Passive Gravity Gradient Stabilized Satellites. AIAA No. 63-342, 1963.
6. Delisle, J. F.; Olgeltree, E. G.; and Hildenbrant, B. M.: Applications of Gyrostabilizers to Satellite Attitude Control. MIT Instrumentation Lab. AIAA Guidance and Control Conf. Paper No. 63-325, Aug. 12 through 14, 1963.
7. Anon.: Collected Papers on Instability of Shell Structures. Technical Note D-1510, Langley Research Center, December 1962.
8. Anon.: Monthly Progress Reports for Feasibility Study and Preliminary Design for a Gravity-Gradient-Stabilized Lenticular Test Satellite. GER 11189 (Contract NAS 1-3114), Goodyear Aerospace Corp.
9. Anon.: Cone and Column Solar Concentrator Model. GER 12114, Interim Summary Progress Report, Goodyear Aerospace Corp., Feb. 1965.
10. Anon.: Advanced Passive Communications Lenticular Satellite Studies. GER 11891, Summary Report, Phase III (Contract NAS 1-3114, Amendment No. 6), Goodyear Aerospace Corp., Dec. 1964.
11. Anon.: Application of Rice/Wilberforce Gravity-Gradient Damper to NASA Lenticular Communication Satellite. GER 11790, Goodyear Aerospace Corp., 3 Nov. 1965.
12. Sonnabend, D.: The Dumbbell Effect Ad Rigorum. LMSD-445247, 3 Feb. 1960.
13. Anon.: Study of Thermal Effects on Gravity-Gradient Rods. Final Report (Contract NAS 7-234), General Electric Spacecraft Dept, Document No. 63SD851, Oct. 1963.
14. Rottmayer, E.; and Marketos, J. D.: Study of Orbital Design Conditions for a Gravity-Gradient Stabilized Lenticular Satellite. GER 11277, Goodyear Aerospace Corp., Oct. 1963.